31 May 2013 | $10

Science

India
Science for All

AAAS

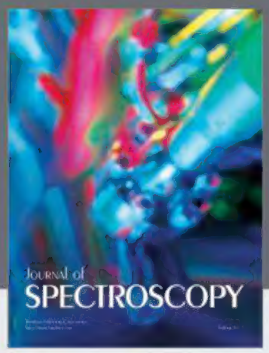

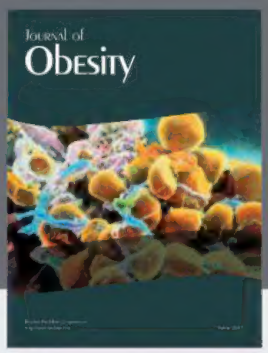

Hindawi

Submit your manuscripts at
http://www.hindawi.com

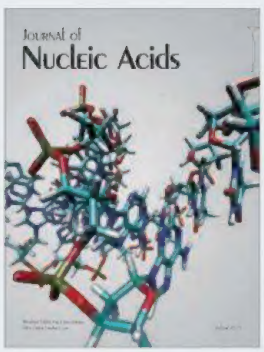

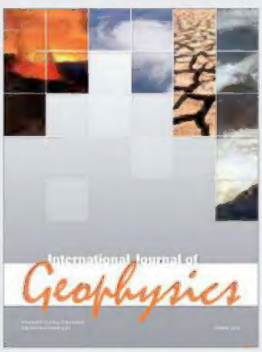

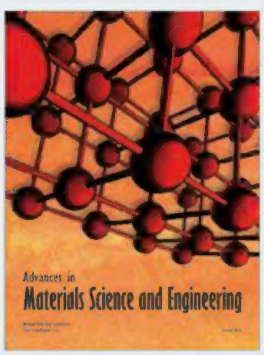

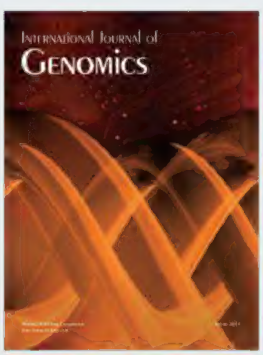

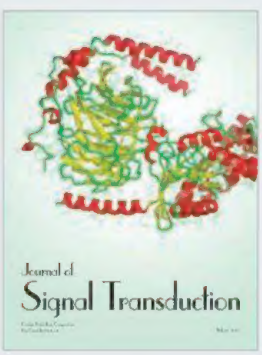

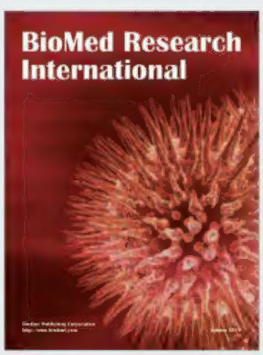

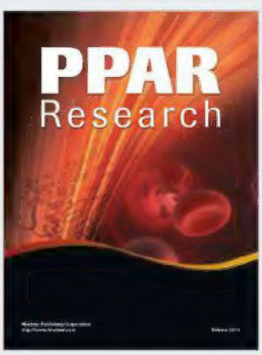

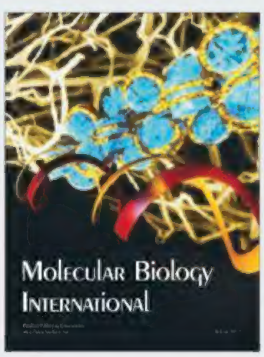

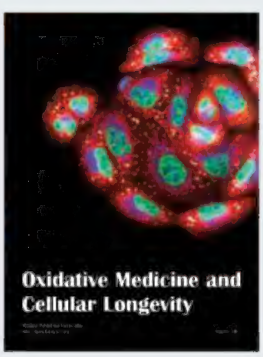

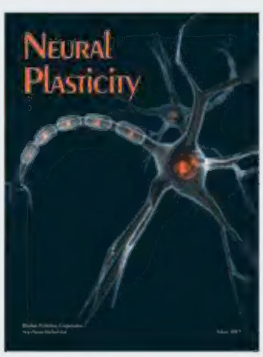

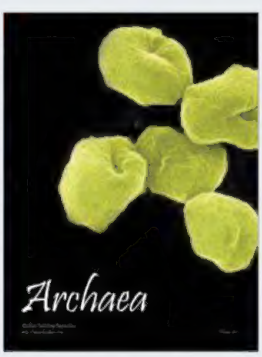

abcam®
discover more

What can RabMAbs® do for you?

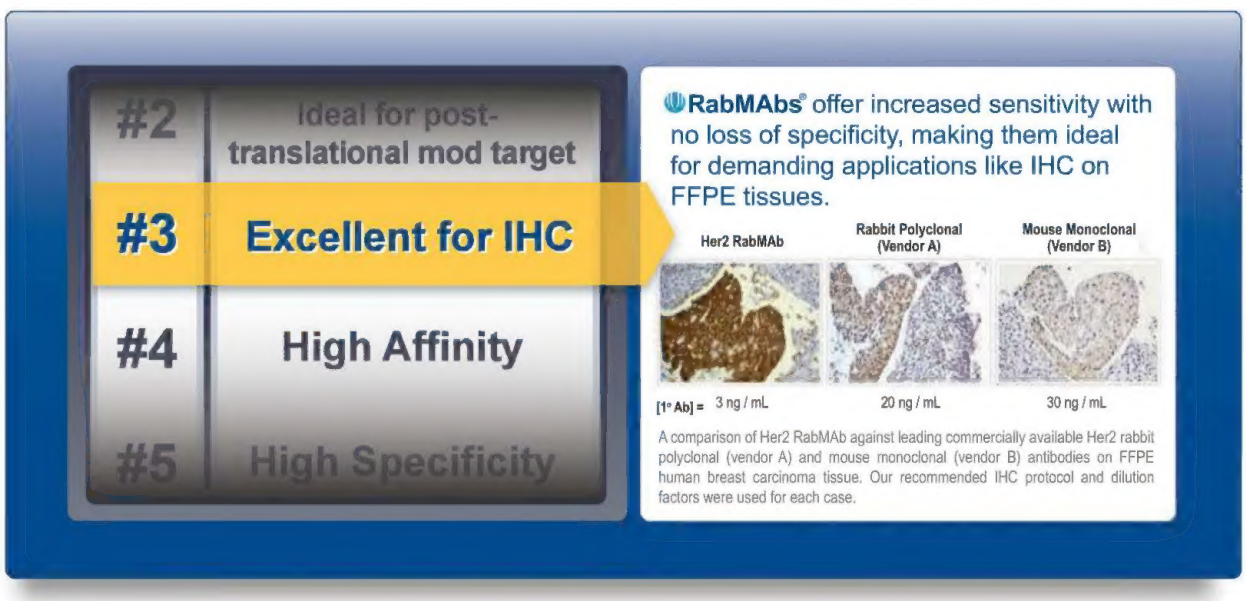

RabMAbs® High Quality Antibodies

Rabbit Monoclonal Antibodies (RabMAbs®) offer multiple advantages to bring you the highest quality antibody possible.

Discover more at abcam.com/RabMAbs

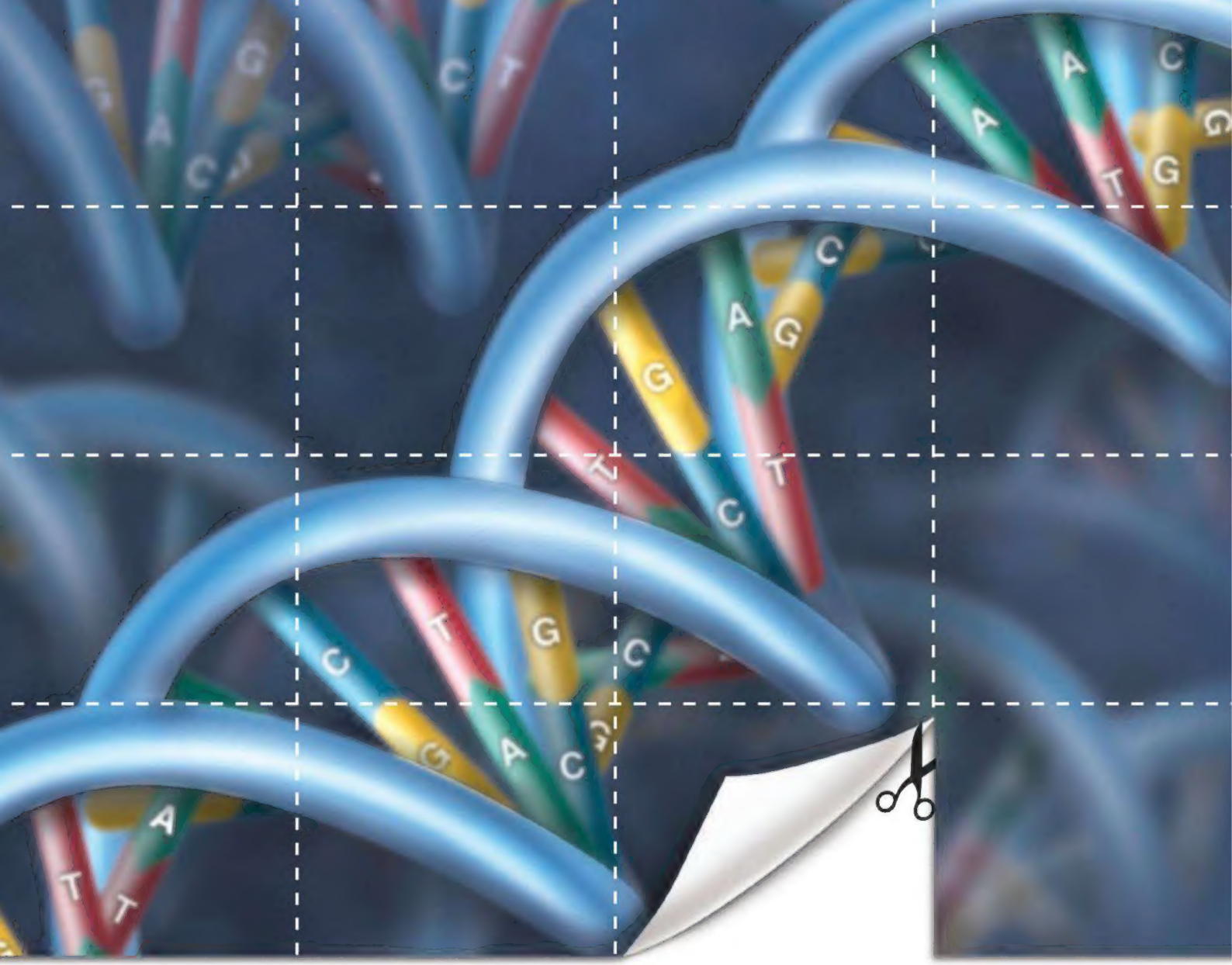

Cut smarter.

Restriction enzymes from NEB – now with CutSmart™ Buffer

You make smart choices every day. Why stop there? The choice to use restriction enzymes from New England Biolabs is now even easier.

- Choose from > 200 restriction enzymes supplied with a single buffer
- Simplify your double digest reactions
- Reduce your pipetting steps by no longer having to add BSA

Now, that's **Smart!**

Explore the smarter choice at
NEBCutSmart.com

NEW ENGLAND BioLabs® Inc.
enabling technologies in the life sciences

CONTENTS continued >>

page 1037

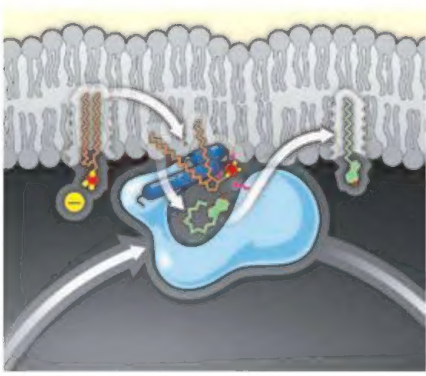

pages 1051 & 1106

ON THE WEB THIS WEEK

>> Policy Podcast
Listen to an interview with outgoing *Science* Editor-in-Chief Bruce Alberts.

>> Find More Online
Check out *Science* Express, our podcast, videos, daily news, our research journals, and *Science* Careers at **www.sciencemag.org**.

COVER

Can science do more to help the world's poor? India is a test bed for innovative approaches to poverty reduction. India's wheat crop is critical to the nation's food security. Farmers across the country now use their cell phones to send pest sightings and growing conditions to the Directorate of Wheat Research in Karnal, headed by Indu Sharma (pictured). See the Editorial on page 1015 and the News story on page 1032.

Photo: Pallava Bagla

DEPARTMENTS

Reagent Proteins

Discover the Source

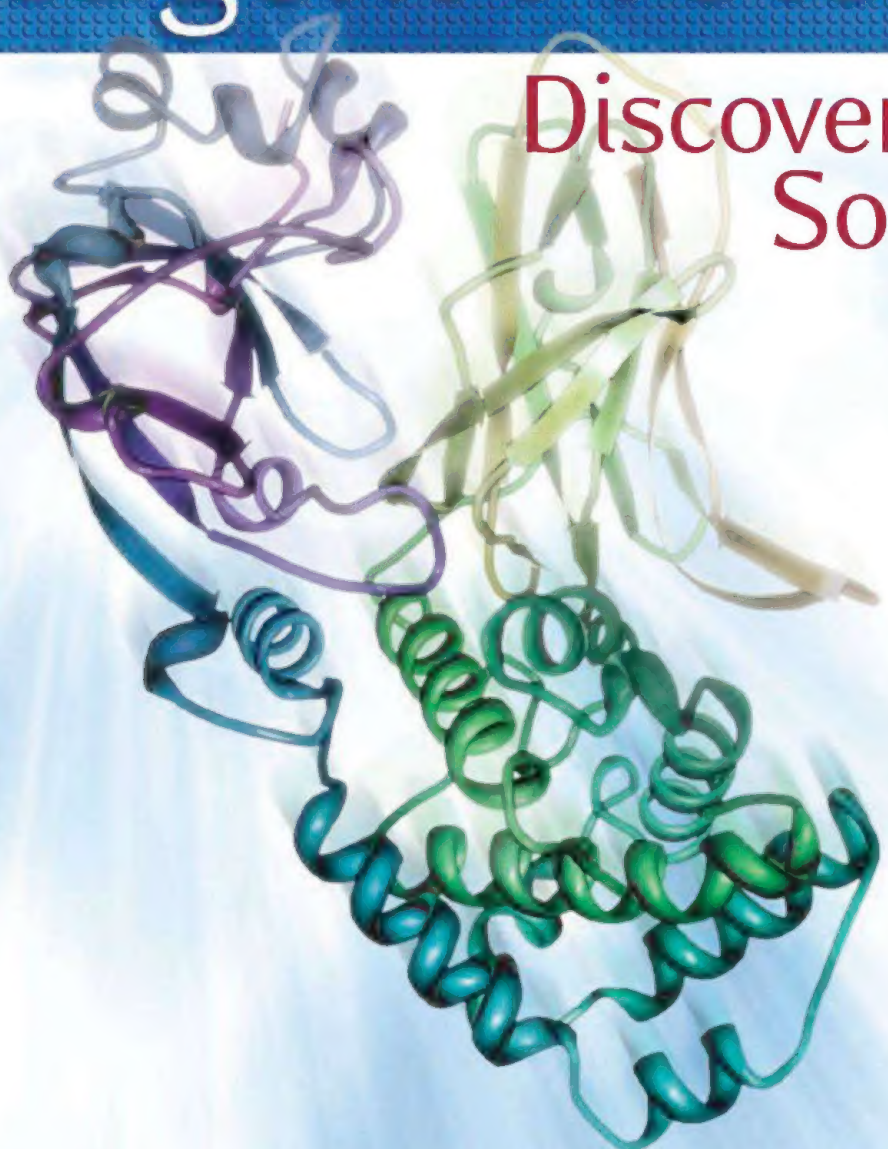

Reagent Proteins is the source

With over 5,000 recombinant proteins available, *Reagent* Proteins provides seamless access to the highest quality reagent, pre-clinical and cGMP grade proteins for research purposes.

Reagent Proteins
A DIVISION OF Pfenex Inc.

phone 858 · 352 · 4400 **reagentproteins.com** fax 858 · 352 · 4602

REVIEW

RESEARCH ARTICLES

REPORTS

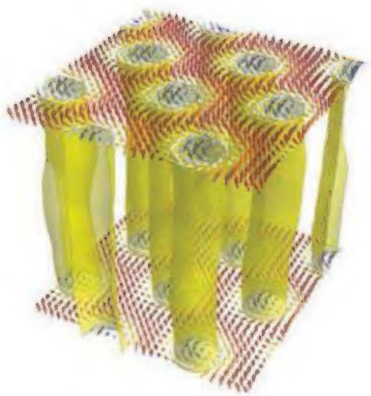

page 1076

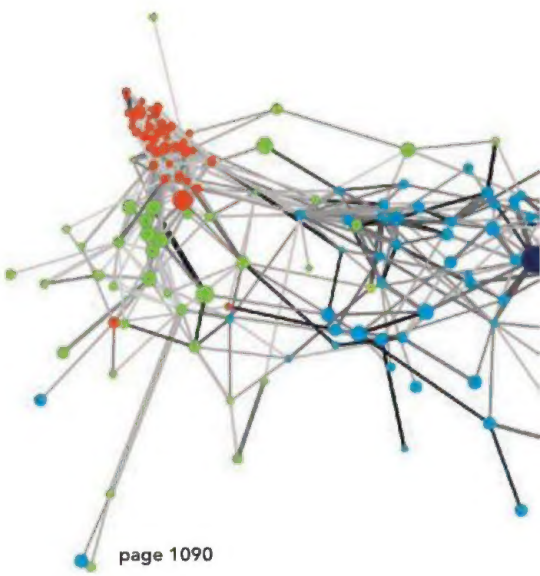

page 1090

SCIENCE (ISSN 0036-8075) is published weekly on Friday, except the last week in December, by the American Association for the Advancement of Science, 1200 New York Avenue, NW, Washington, DC 20005. Periodicals Mail postage (publication No. 484460) paid at Washington, DC, and additional mailing offices. Domestic individual membership and subscription (51 issues): $149 ($74 allocated to subscription). Domestic institutional subscription (51 issues): $990; Foreign postage extra: Mexico, Caribbean (surface mail) $55; other countries (air assist delivery) $85. First class, airmail, student, and emeritus rates on request. Canadian rates with GST available upon request, GST #1254 88122. Publications Mail Agreement Number 1069624. **Printed in the U.S.A.**

Change of address: Allow 4 weeks, giving old and new addresses and 8-digit account number. **Postmaster:** Send change of address to AAAS, P.O. Box 96178, Washington, DC 20090–6178. **Single-copy sales:** $10.00 current issue, $15.00 back issue prepaid includes surface postage; bulk rates on request. **Authorization to photocopy** material for internal or personal use under circumstances not falling within the fair use provisions of the Copyright Act is granted by AAAS to libraries and other users registered with the Copyright Clearance Center (CCC) Transactional Reporting Service, provided that $30.00 per article is paid directly to CCC, 222 Rosewood Drive, Danvers, MA 01923. The identification code for *Science* is 0036-8075. *Science* is indexed in the *Reader's Guide to Periodical Literature* and in several specialized indexes.

cOmplete His-Tag Purification Resin
Truly compatible with EDTA and DTT

Try it in your lab!

Test to see if your protein's optimal buffer will cause nickel loss in cOmplete His-Tag Purification Resin – request a free sample today at ***http://go.roche.com/his3***

Purify proteins that you couldn't previously purify by choosing **cOmplete His-Tag Purification Resin**, which is compatible with a broad range of buffer conditions and additives, including chelators (*e.g.,* EDTA) and reducing agents (*e.g.,* DTT).

- **Let your protein — not the purification resin — determine buffer conditions.**
- **Protect your protein and lab from toxic nickel.**
- **Spend time studying your protein — not purifying it.**

Visit **www.proteomics.roche.com** or call **800 262 4911** to learn more.

For life science research only.
Not for use in diagnostic procedures.

COMPLETE is a trademark of Roche.

Roche Diagnostics Corporation
Roche Applied Science
Indianapolis, Indiana

Roche

EDITED BY STELLA HURTLEY

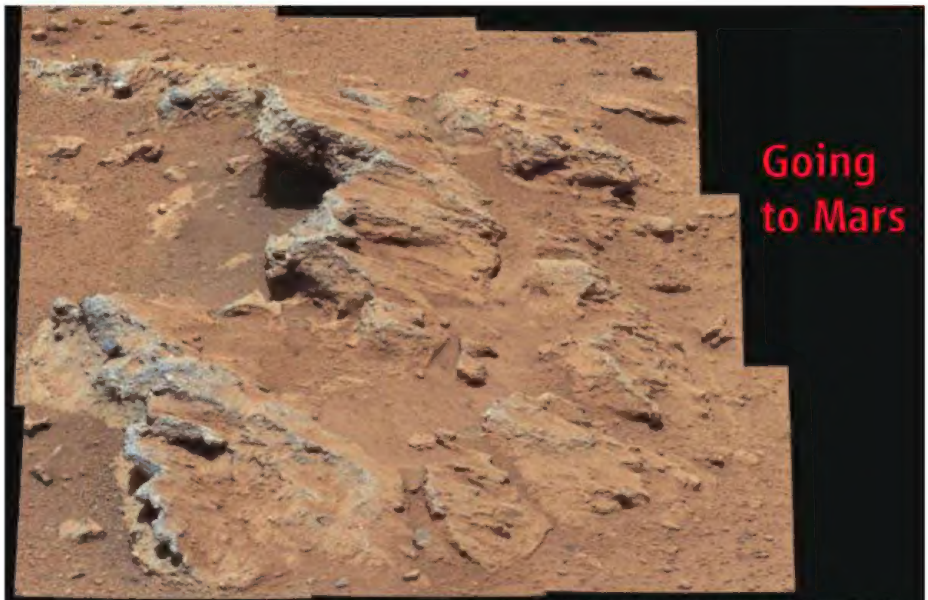

The Mars Science Laboratory spacecraft containing the Curiosity rover, was launched from Earth in November 2011 and arrived at Gale crater on Mars in August 2012. **Zeitlin *et al.*** (p. 1080) report measurements of the energetic particle radiation environment inside the spacecraft during its cruise to Mars, confirming the hazard likely to be posed by this radiation to astronauts on a future potential trip to Mars. **Williams *et al.*** (p. 1068, see the Perspective by **Jerolmack**) report the detection of sedimentary conglomerates (pebbles mixed with sand and turned to rock) at Gale crater. The rounding of the rocks suggests abrasion of the pebbles as they were transported by flowing water several kilometers or more from their source.

Building Better Vaccines

Vaccines are one of the most effective tools to protect against infectious diseases. Unfortunately, vaccines for diseases with the highest global health burdens, such as HIV, malaria, and tuberculosis, are not yet available. **Koff *et al.*** (p. 1064) review the latest advances in vaccine development and why these particular diseases remain such a challenge. Respiratory syncytial virus (RSV) is a serious cause of morbidity and mortality in infants and young children worldwide. Although a prophylactic antibody is available for children at high risk, a vaccine is much needed. As a potential step toward this goal, **McLellan *et al.*** (p. 1113, published online 25 April) solved the cocrystal structure of a neutralizing antibody (D25) bound to the prefusion F protein of RSV. Knowledge of the structure of the prefusion protein should help to guide vaccine design and the development of additional therapeutics.

Independent Chiral Catalysts

Synthetic catalysts can be prepared in their mirror-image form and thereby furnish the mirror-image (enantiomer) of the reaction product. In practice, however, this versatility is largely limited to products featuring a single stereocenter that accounts for the dissymmetry. **Krautwald *et al.*** (p. 1065; see the Perspective by **Schindler and Jacobsen**) now report a pair of chiral catalysts—an iridium complex and an amine—that operate in concert to facilitate carbon-carbon bond formation, while retaining independent stereoselectivity toward their respective sides of the bond.

Multiple Inputs to Flowering

Perennial plants need to cycle through an extended vegetative phase, in a process known as vernalization, before they initiate flowering. **Bergonzi *et al.*** (p. 1094) and **Zhou *et al.*** (p. 1097) studied how molecular signals translate environmental information—such as exposure to a winter season or changes in daylength and physiological information, such as age of the plant—into signals that promote flowering. In both *Arabis alpina* and *Cardamine flexuosa*, age and vernalization pathways are integrated through the regulation of microRNAs miR156 and miR172.

It's an Ant's Life

Eusocial insects live in highly organized societies where groups of individuals carry out specific tasks; for example, caring for the eggs, cleaning the nest, or foraging, which might suggest the presence of an advanced form of organization, similar to what might be expected from more cognitively advanced species. **Mersch *et al.*** (p. 1090, published online 18 April) tracked individual ant movements and interactions to show that their precise social organization results from temporal changes in the spatial location of workers. As they aged, ants largely progressed from being nurses located near the queen, to nest cleaners who move throughout the colony, and finally to foragers moving in and out at the colony edges.

Graphene Staying Strong

Although exfoliated graphene can be extremely strong, it is produced on too small a scale for materials application. Graphene can be produced on a more practical scale by chemical vapor deposition, but the presence of grain boundaries between crystallites apparently weakens the material. **Lee *et al.*** (p. 1073) show that postprocessing steps during the removal of the graphene sheets can oxidize the grain boundaries and weaken them. If these steps are avoided, the material is comparable in strength to exfoliated graphene.

The Birds and the Seeds

When species are lost from ecosystems through local extinction, the pattern of ecological interactions changes. **Galetti *et al.*** (p. 1086) show how the loss of large fruit-eating birds from tropical forest fragments in Brazil affects the reduction of seed size in a palm species. A data set was compiled that consisted of >9000 seeds measured in 22 populations over a large area of Atlantic rainforest, including seven areas where large-seed dispersers (toucans, cracids, and large cotingas) were extinct and 15 areas where they are still common.

Hedgehogs, Whirls, and Zippers

Topologically ordered materials at certain ranges of temperature and magnetic field can form a regular lattice of magnetic whirls called skyrmions. **Milde *et al.*** (p. 1076) studied the destruction of a skyrmion lattice with varying magnetic fields by imaging the surface magnetic structure. Magnetic force microscopy revealed a pairwise merging of skyrmions on the surface. Furthermore, in the bulk, a hedgehog-like spin structure with the properties of the elusive magnetic monopole was needed to "zip" together the corresponding skyrmion lines.

CREDITS (TOP TO BOTTOM): NASA/JPL-CALTECH/MALIN SPACE SCIENCE SYSTEMS; EDSON ENDRIGO AND LINDOLFO SOUTO

Finally, one application that syncs your **PDF articles**, your lab group, and your next manuscript.

ACS ChemWorx is a free, single-source solution designed to increase productivity in research management, collaboration, and publishing.

Find out how you can spend less time organizing and more time researching.

Search. Import. Annotate. Collaborate. Store. Publish.

Import your reference library using your existing file structure.

Login today at www.acschemworx.org

ACS ChemWorx
RESEARCH. COLLABORATE. PUBLISH.

Available on the App Store

GET IT ON Google play

ACS Publications
MOST TRUSTED. MOST CITED. MOST READ.

Bruce Alberts is Editor-in-Chief of *Science*.

After 5 Years at *Science*

THIS EDITORIAL, WRITTEN AS I COMPLETE MY TERM AS EDITOR-IN-CHIEF OF *SCIENCE*, PROVIDES AN opportunity to reflect on the role of science in human societies. As the president of the U.S. National Academy of Sciences from 1993 to 2005, I came to realize that science is much more important for the world than most scientists suspect.* The scientific values of honesty, respect for evidence, openness, and tolerance are critical for every nation. And scientific approaches to problem-solving are essential everywhere for meeting a huge range of societal challenges. Those challenges have formed the basis for many special issues of *Science* magazine, including those published in the past few years on Science Education, Working with Waste, Disease Prevention, H5N1, Human Conflict, Food Security, and Population.†

It is fitting that these reflections coincide with the current issue on India: Science for All. India's first prime minister, Jawaharlal Nehru, wisely worked to create both the strong base for science and technology and the "scientific temper" that he believed necessary to ensure the success of his populous, highly diverse democracy. Through many visits to India, I have become aware of the large number of innovative experiments under way aimed at harnessing science and technology to improve the livelihoods of the more than 400 million Indians who live in extreme poverty—one-third of the world's poor. Several of India's most prestigious scientific institutions have long been engaged in projects targeting sustainable technologies, including the Indian Institute of Science in Bangalore. And in a visit last month with our News team, I learned about promising projects pioneered by the Indian Institute of Technology Madras, the M.S. Swaminathan Research Foundation, and others (see p. 1032).

Similar experiments are attempting to harness science and technology for poverty reduction in other nations. As in India, some have been successful, but many others have failed. It is unfortunate that the world lacks efficient mechanisms for learning from these experiments—especially from failures, where perhaps the most can be learned—so as to create the type of ever-improving knowledge base that underlies the sciences. Instead, those in charge of projects aimed at benefiting the poor often feel forced to claim victory. Thus, the failures that should generate profound learning experiences are often hidden in ways that prevent any honest analysis.

Online

sciencemag.org

Podcast interview with author Bruce Alberts (http://scim.ag/ed_6136).

The good news is that new centers are emerging that focus on "science and technology for poverty" on the campuses of some of the leading U.S. universities. These reflect a strong interest of outstanding young scientists and engineers, as well as many prominent faculty, in confronting these challenges. How might such institutions in industrialized nations help connect everyone with similar goals across the globe to create a new "science of sustainable poverty reduction"? What roles might scientific societies and academies play in such a movement? How could scientific journals contribute?

Science provides a powerful approach to cooperative problem-solving. There is an enormous amount yet to be discovered, and it is energizing to be faced with such great opportunities for further progress. Personally, I shall focus on some of the opportunities for invigorating science education that have been featured in *Science* throughout my term as Editor.‡

I am extremely pleased to leave *Science* in the hands of Dr. Marcia McNutt, an outstanding geophysicist and institution builder who becomes the new Editor-in-Chief next month. She inherits a very talented and dedicated staff, whom I sincerely thank for all that they have done over the past 5 years to advance our common mission of spreading the knowledge and spirit of science around the globe.

– Bruce Alberts

10.1126/science.1240945

*http://biochemistry.ucsf.edu/labs/alberts/nas.html. †www.sciencemag.org/site/collections/online/special. ‡www.sciencemag.org/site/extra/education/ (this site is open access, not requiring a subscription to *Science*).

EDITED BY KRISTEN MUELLER AND MARIA CRUZ

ECOLOGY

Secrets of Long Life

The accumulation of reactive oxygen species (ROS) causing oxidative stress is well known as one of the factors associated with senescence, particularly in animals. Oxidative stress has also been shown to be associated with senescence in plant organs (leaves and flowers). However, much less is known about its potential for affecting the senescence of whole plants, especially longer-lived perennials. To address this gap, Morales *et al.* studied photo-oxidative stress markers in an exceptionally long-lived herbaceous species, *Borderia pyrenaica*, which inhabits scree slopes in the Pyrenees and reaches ages of more than three centuries. The markers of oxidative stress were measured in both male and female plants over an age range of 1 to 245 years. None of the markers showed any signs of deterioration in older plants and were even enhanced in some aged female plants. Though it is possible that intrinsic physiological stress mechanisms exert their effects at even greater ages beyond those addressed in this study, mortality in this species—and perhaps in other small, long-lived perennials—may ultimately depend more on extrinsic factors such as pathogens, physical disturbances, and climatic extremes. — AMS

J. Ecol. **101**, 555 (2013).

DEVELOPMENTAL NEUROSCIENCE

To Fold or Not to Fold

The surface of the normal human brain is characterized by deep and complex folds. Ferret brains are similarly gyrencephalic, whereas mouse brains are smooth-surfaced, or lissencephalic. During development, proliferation of different subtypes of stem and progenitor cells

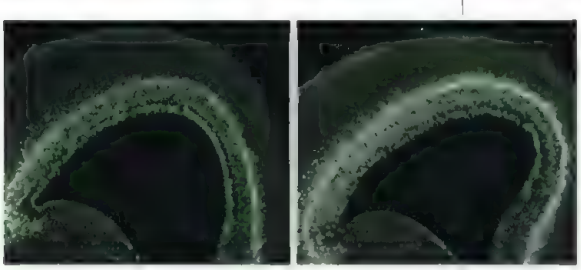

shapes the brain surface. In order to understand the relative contributions of these different progenitor cell types, Nonaka-Kinoshita *et al.* manipulated the proliferation of these cells at different times during the brain development of mice and ferrets. Mice with an excess of basal progenitors had thicker brain layers but, despite an increase in brain surface area, the surface remained smooth. In contrast, ferrets with excess progenitor activity developed more brain folds than control mice. In both species, neuronal specification and the structure of brain layers remained normal. Thus, the brain's surface area and the amount of folding may be regulated by progenitor activity, but the distinction between lissencephalic or gyrencephalic brains is not simply due to the number of progenitors. — PJH

EMBO J. 10.1038/emboj.2013.96 (2013).

ASTRONOMY

A New River in the Sky

Stellar streams are found throughout the outskirts of our galaxy. They are thought to be disrupted dwarf satellite galaxies or clusters of stars and are proof that the Milky Way formed in part by accreting smaller collections of stars. Based on data from two different all-sky surveys, Grillmair *et al.* have found a new, 24°-long, stellar stream running through the southern constellations of Phoenix, Eridanus, Hydrus, and Tucana. Named Alpheus, after the river in Homer's *Iliad*, this stream is estimated to be about 6200 light-years away—much closer than the stellar streams found so far in our galaxy. It is likely that Alpheus is associated with the globular cluster NGC 288, a family of stars that is thought to be in the process of breaking apart. If this is the case, further characterization of the stream will enable better modeling of the orbit of NGC 288. — MJC

Astrophys. J. **769**, L23 (2013).

NEUROSCIENCE

Lingering Pain

Neuropathic pain results from injury or disease in the nervous system and is estimated to affect more than 2 million people in the United States. The pain can linger, but the mechanisms for such persistence are not well defined. Qiu *et al.* studied a mouse model in which injury to a peripheral nerve caused behavioral effects that lasted for weeks, in which mechanical stimuli that were normally not noxious would cause pain. They looked for effects of this treatment in a brain region called the insular cortex. This region is implicated in pain sensation, and direct stimulation of the insular cortex in humans causes pain sensation. The authors found that signaling responses to neurotransmitters were altered in animals that had experienced the nerve injury. Neurotransimitter receptors activated by NMDA (*N*-methyl-D-aspartate) were phosphorylated on tyrosine residues and accumulated in synapses of the insular cortex. The injection of inhibitors of NMDA receptor signaling into the insular cortex decreased the hypersensitivity to pain in the treated mice. Such insights may help direct new therapeutic approaches to managing neuropathic pain. — LBR

Sci. Signal. **6**, ra34 (2013).

OCEAN SCIENCE

Mysterious Rise

The concentration of atmospheric carbon dioxide (CO_2) rose from about 180 parts per million by volume (ppmv) to 280 ppmv between the end of the Last Glacial Maximum and the Holocene. It is widely believed, largely based on measurements of the ^{14}C in the CO_2 of air trapped in polar ice and of forams from marine sediments, that the atmospheric CO_2 rise was caused in large part by ventilation of old, CO_2-rich water from the deep Southern Ocean. Tessin and Lund analyzed another isotope of carbon, ^{13}C, to show that the mid-depth waters along the Brazil Margin

underwent an abrupt change in their inventories of ^{13}C during the initial 30-ppmv increase in CO_2 between about 17,000 and 16,000 years ago. These data, collected from analyses of planktonic forams in marine sediments, in conjunction with data on the oxygen isotopic composition of these waters, suggest that two distinct water masses must have influenced the mid-depth Atlantic Ocean during that interval and that a previously unrecognized source of carbon outside of the ocean-atmosphere system may have been involved. The authors also inferred that the release of carbon into the atmosphere from a reservoir depleted in ^{13}C must have been a key trigger of the last deglaciation. — HJS

Paleoceanography 10.1002/palo.20026 (2013).

CHEMISTRY

Tiny Cocktails

The effective treatment of many diseases, especially cancer and AIDS, requires the synergistic interaction of several drugs; their delivery is often referred to as a "cocktail." Although several drugs can be combined into one delivery agent, the different rates of systemic uptake, solubility, and clearance make it challenging to deliver all of the drugs simultaneously. Windbergs *et al.* have used a microfluidic platform to create core-shell particles in which a hydrophobic drug (paclitaxel) forms the shell and a hydrophilic drug (doxorubicin hydrochloride) is carried in the core. The particles, which have an overall diameter of less than 100 μm, were made with two glass capillaries drawn to fine tips inside a microfluidic channel. The finer capillary (with an ~20-μm opening) held an aqueous solution of the core drug on the inside, and the fluid outside this capillary carried the shell drug dissolved in a food-grade lipid. This capillary tip pointed toward the opening of a wider tip (with an ~100-μm opening) facing the opposite direction. The action of a third solvent (a solution of polyvinyl alcohol in water) on the outside of the larger capillary drew in both fluids from the smaller one and created the core-shell droplets. The particles were stable upon drying and could be processed to form free-flowing powders. The viability of the drugs was confirmed in testing on immortalized human cervical cancer cell lines. Delivery in the body can be tuned by using a lipid that melts near body temperature or by relying on lipid degradation in the gastrointestinal tract. — PDS

J. Am. Chem. Soc. 10.1021/ja401422r (2013).

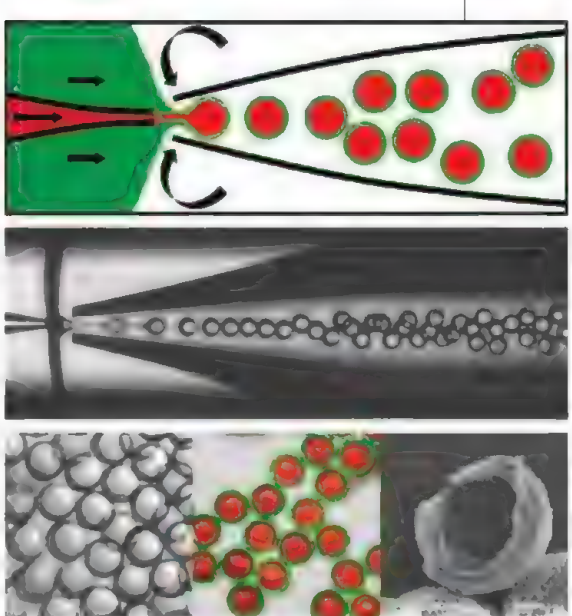

CREDIT: M. WINDBERGS *ET AL.*, *JOURNAL OF THE AMERICAN CHEMICAL SOCIETY* (30 APRIL 2013) © 2013 AMERICAN CHEMICAL SOCIETY

NEUROSCIENCE

Fasting Protects the Brain

Fasting has been shown to slow aging in a number of species. Caloric restriction acts on many different cell types and tissues and, importantly, also on the brain. There, it leads to a slowing-down of age-associated pathologies, such as brain atrophy or loss of synaptic plasticity. Moreover, in several animal models, a reduced consumption of calories seems to protect against cognitive deficits such as memory loss. However, it is not known whether caloric restriction can delay the beginning of neurodegeneration. The mechanisms underlying these observations are also largely unclear. In experiments using genetically modified mice, Gräff *et al.* found that caloric restriction effectively delayed the onset of neurodegeneration and preserved structural and functional synaptic plasticity as well as memory capacities. Fasting activated the expression and activity of the nicotinamide adenine dinucleotide (NAD)–dependent protein deacetylase SIRT1, a known promoter of neuronal life span. Surprisingly, this effect of reduced consumption of calories could be mimicked by a small-molecule SIRT1-activating compound. Mice treated with this substance recapitulated the beneficial effects of caloric restriction against neurodegeneration-associated pathologies. If this mechanism also applies to humans, SIRT1 may represent an appealing pharmacological target against neurodegeneration. — PRS

J. Neurosci. **33**, 8951 (2013).

life technologies™

life technologies™

www.sciencemag.org

Science

1200 New York Avenue, NW
Washington, DC 20005
Editorial: 202-326-6550, FAX 202 289-7562
News: 202-326-6591, FAX 202-371-9227
Bateman House, 82-88 Hills Road
Cambridge, UK CB2 1LQ
+44 (0) 1223 326500, FAX +44 (0) 1223 326501

Subscription Services For change of address, missing issues, new orders and renewals, and payment questions: 866-434-AAAS (2227) or 202-326-6417, FAX 202-842-1065. Mailing addresses: AAAS, P.O. Box 96178, Washington, DC 20090-6178 or AAAS Member Services, 1200 New York Avenue, NW, Washington, DC 20005

Institutional Site Licenses please call 202-326-6755 for any questions or information

Reprints: Author Inquiries 800-635-7181
Commercial Inquiries 803-359-4578

Permissions 202-326-6765, permissions@aaas.org

Member Benefits AAAS Travels: Betchart Expeditions 800-252-4910; Apple Store www.store.apple.com/us/go/eppstore/aaas; NASA Federal, 1-888-NASA-FCU (1-888-627-2328) or www.nasafcu.com; Cold Spring Harbor Laboratory Press Publications www.cshlpress.com/affiliates/aaas.htm; GEICO Auto Insurance www.geico.com/landingpage/go51.htm?logo=17624; Hertz 800-654-2200 CDP#343457; Office Depot https://bsd.officedepot.com/portalLogin.do; Seabury & Smith Life Insurance 800-424 9883; Subaru VIP Program 202-326-6417; VIP Moving Services www.vipmayflower.com/domestic/index.html; Other Benefits: AAAS Member Services 202-326-6417 or www.aaasmember.org.

science_editors@aaas.org	(for general editorial queries)
science_letters@aaas.org	(for queries about letters)
science_reviews@aaas.org	(for returning manuscript reviews)
science_bookrevs@aaas.org	(for book review queries)

Published by the American Association for the Advancement of Science (AAAS), *Science* serves its readers as a forum for the presentation and discussion of important issues related to the advancement of science, including the presentation of minority or conflicting points of view, rather than by publishing only material on which a consensus has been reached. Accordingly, all articles published in *Science*—including editorials, news and comment, and book reviews—are signed and reflect the individual views of the authors and not official points of view adopted by AAAS or the institutions with which the authors are affiliated.

AAAS was founded in 1848 and incorporated in 1874. Its mission is to advance science, engineering, and innovation throughout the world for the benefit of all people. The goals of the association are to: enhance communication among scientists, engineers, and the public; promote and defend the integrity of science and its use; strengthen support for the science and technology enterprise; provide a voice for science on societal issues; promote the responsible use of science in public policy; strengthen and diversify the science and technology workforce; foster education in science and technology for everyone; increase public engagement with science and technology; and advance international cooperation in science.

Information for Authors
See pages 716 and 717 of the 8 February 2013 issue or access www.sciencemag.org/about/authors

EDITOR-IN-CHIEF **Bruce Alberts**
EXECUTIVE EDITOR **Monica M. Bradford**
NEWS EDITOR **Colin Norman**
MANAGING EDITOR, RESEARCH JOURNALS **Katrina L. Kelner**
DEPUTY EDITORS **Barbara R. Jasny, Andrew M. Sugden, Valda J. Vinson**

Editorial senior editors/commentary Lisa D. Chong, Brad Wible; **senior editors** Gilbert J. Chin, Pamela J. Hines, Paula A. Kiberstis (Boston), Marc S. Lavine (Toronto), Beverly A. Purnell, L. Bryan Ray, Guy Riddihough, H. Jesse Smith, Phillip D. Szuromi (Tennessee), Jake S. Yeston, Laura M. Zahn (San Diego); **associate editors** Melissa R. McCartney (Education Projects), Kristen L. Mueller, Jelena Stajic, Sacha Vignieri (Oregon), Nicholas S. Wigginton (Michigan); **book review editor** Sherman J. Suter; **associate letters editor** Jennifer Sills; **editorial manager** Cara Tate; **senior copy editors** Jeffrey E. Cook, Cynthia Howe, Harry Jach, Lauren Kmec, Barbara P. Ordway, Trista Wagoner; **copy editor** Chris Filiatreau; **senior editorial coordinators** Carolyn Kyle, Beverly Shields; **editorial coordinators** Ramatoulaye Diop, Joi S. Granger, Lisa Johnson, Anita Wynn; **publications assistants,** Aneera Dobbins, Jeffrey Hearn, Dona Mathieu, Le-Toya Mayne Flood, Shannon McMahon, Scott Miller, Jerry Richardson, Teresa R. Sakon, Brian White; **editorial assistant** Patricia M. Moore; **executive editorial assistant** Yolanda O'Bannon (San Francisco); **executive assistant** Alison Crawford; **administrative support** Maryrose Madrid

Editorial director, web and new media Stewart Wills; **senior web editor** Sarah Crespi; **web editor** Kerry Klein; **web development manager** Martyn Green; **web developer** Corinna Cohn

News deputy news editors Robert Coontz, Elizabeth Culotta, David Grimm (Online), Eliot Marshall, Jeffrey Mervis, Leslie Roberts, Richard Stone, John Travis; **contributing editor** Polly Shulman; **news writers** Yudhijit Bhattacharjee, Adrian Cho, Jennifer Couzin-Frankel, Carolyn Gramling, Jocelyn Kaiser, Richard A. Kerr, David Malakoff, Elizabeth Pennisi, Robert F. Service (Pacific NW), Erik Stokstad, Emily Underwood; **web developer** Daniel Berger; **social media strategist** Meghna Sachdev; **intern** Lizzie Wade; **contributing correspondents** John Bohannon, Jon Cohen (San Diego, CA), Ann Gibbons, Sam Kean, Eli Kintisch, Andrew Lawler, Mitch Leslie, Charles C. Mann, Virginia Morell, Gary Taubes; **copy editors** Melissa Raimondi, Kara Estelle; **administrative support** Scherraine Mack; **bureaus** San Diego, CA: 760-942-3252, FAX 760-942-4979; Pacific Northwest: 503-963-1940

Production director Wendy K. Shank; **assistant manager** Rebecca Doshi; **senior specialists** Steve Forrester, Anthony Rosen; **Preflight director** David M. Tompkins; **manager** Marcus Spiegler; **specialists** Jason Hillman, Tara Kelly

Art director Yael Fitzpatrick; **associate art director** Laura Creveling; **senior illustrators** Chris Bickel, Katharine Sutliff; **senior art associates** Holly Bishop, Preston Huey; **art associates** Kay Engman, Garvin Grullón, Chrystal Smith; **photo editor** Leslie Blizard

***Science* International**

Europe (science@science-int.co.uk) **editorial: international managing editor** Andrew M. Sugden; **senior editor/commentary** Julia Fahrenkamp-Uppenbrink; **senior editors** Caroline Ash, Stella M. Hurtley, Ian S. Osborne, Peter Stern; **associate editor** Maria Cruz; **contributing editor** Helen Pickersgill; **editorial support** Rachel Roberts, Alice Whaley; **administrative support** Janet Clements, Sarah Stephenson; **news: deputy news editor, u.k.** Daniel Clery; **contributing editor, europe** Martin Enserink; **contributing correspondents** Michael Balter (Paris), Kai Kupferschmidt (Berlin), Gretchen Vogel (Berlin)

Asia Japan Office: Asca Corporation, Tomoko Furusawa, Rustic Bldg. 7F, 77 Tenjin-cho, Shinjuku-ku, Tokyo 162-0808, Japan; +81 3 6802 4616, FAX +81 3 6802 4615, inquiry@sciencemag.jp; **contributing editor, asia** Mara Hvistendahl [China: mhvisten@aaas.org]; **contributing correspondents** Dennis Normile [Japan: +81 (0) 3 3391 0630, FAX +81 (0) 3 5936 3531; dnormile@gol.com]; Hao Xin [China: cindyhao@gmail.com]; Pallava Bagla [South Asia: +91 (0) 11 2271 2896; pbagla@vsnl.com]

EXECUTIVE PUBLISHER **Alan I. Leshner**
PUBLISHER **Beth Rosner**

Fulfillment Systems and Operations (membership@aaas.org); **customer service supervisor** Pat Butler; **specialists** LaToya Casteel, Michelle Ofordire, April Marshall; **manager, data entry** Mickie Napoleoni; **data entry specialists** JJ Regan, Jaimee Wise, Fiona Giblin

Business Operations and Administration director Deborah Rivera-Wienhold; **business systems and financial analysis director** Randy Yi; **manager of fulfillment systems** Neal Hawkins; **systems analyst** Nicole Mehmedovich; **manager, business analysis** Eric Knott; **manager, business operations** Jessica Tierney; **business analysts** Cory Lipman, Cooper Tilton, Celeste Troxler; **financial analyst** Jeremy Clay; **rights and permissions: assistant director** Emilie David; **associate** Elizabeth Sandler; **marketing director** Ian King; **marketing managers** Alison Chandler, Julianne Wielga, Justin Sawyers; **marketing associates** Mary Ellen Crowley, Elizabeth Sattler, Rebecca Riffkin; **senior marketing executive** Jennifer Reeves; **director, site licensing** Tom Ryan; **director, corporate relations** Eileen Bernadette Moran; **senior publisher relations specialist** Kiki Forsythe; **publisher relations manager** Catherine Holland; **publisher relations, eastern region** Keith Layson; **publisher relations, western region** Ryan Rexroth; **customer relations manager** Iquo Edim; **customer relations analysts** Simon Chong, Lana Guz; **marketing manager** Christina Schlecht; **marketing associates** Paulina Curto, Mitchell Edmund; **electronic media: director** Lizabeth Harman; **assistant manager** Lisa Stanford; **production specialists** Antoinette Hodal, Nichele Johnston, Lori Murphy, Kimberly Oster; **web and new media: senior project manager** Trista Smith, **project leader** Luke Johnson **computer specialists** Walter Jones, Kai Zhang, **web developer** Chris Coleman; **program director, aaas member central** Peggy Mihelich

director, global collaboration, custom publications, advertising Bill Moran
editor, custom publishing Sean Sanders: 202-326-6430
assistant editor, custom publishing Tianna Hicklin 202-326-6463
sponsored content specialist Candice Nulsen 202-256-1528
associate director, collaboration, custom publications/china/taiwan/korea/singapore Ruolei Wu +86-1367-101-5294

Product (science advertising@aaas.org); **midwest** Rick Bongiovanni: 330-405-7080, FAX 330-405-7081; **east coast/e. canada** Laurie Faraday: 508-747-9395, FAX 617-507-8189; **west coast/w. canada** Lynne Stickrod: 415-931-9782, FAX 415-520-6940; **uk europe/asia** Roger Goncalves: TEL/FAX +41 41 243 1358; **japan**, Makiko Hara: +81 (0) 3 6802 4616, FAX +81 (0) 3 6802 4615; ads@sciencemag.jp; **china/taiwan** Ruolei Wu: +86 1367 1015 294 rwu@aaas.org

worldwide associate director of *Science* Careers Tracy Holmes: +44 (0) 1223 326525, FAX +44 (0) 1223 326532

Classified (advertise@sciencecareers.org); **u.s./canada/south america** Tina Burks: 202-326-6577; **u.s. corporate** Candice Nulsen 202-256-1528; **sales administrator** Marci Gallun; **europe/row sales** Axel Gesatzki, Lucy Nelson; **sales assistant** Kelly Grace; **japan** Yuri Kobayashi +81 (0)90-9110-1719; careerads@sciencemag.jp; **china/taiwan** Ruolei Wu: +86 1367 1015 294 rwu@aaas.org; **advertising support manager** Karen Foote: 202-326-6740; **advertising production operations manager** Deborah Tompkins; **senior production specialist/graphic designer** Amy Hardcastle; **production specialist** Yuse Lajiminmuhip; **senior traffic associate** Christine Hall; **sales coordinator** Shirley Young; **marketing manager** Allison Pritchard; **marketing associate** Aimee Aponte

AAAS Board of Directors retiring president, chair William H. Press; **president** Phillip A. Sharp; **president-elect** Gerald R. Fink; **treasurer** David Evans Shaw; **chief executive officer** Alan I. Leshner; **board** Bonnie L. Bassler, May R. Berenbaum, Claire M. Fraser, Elizabeth Loftus, Stephen L. Mayo, Raymond Orbach, Sue V. Rosser, Inder M. Verma

AAAS
ADVANCING SCIENCE, SERVING SOCIETY

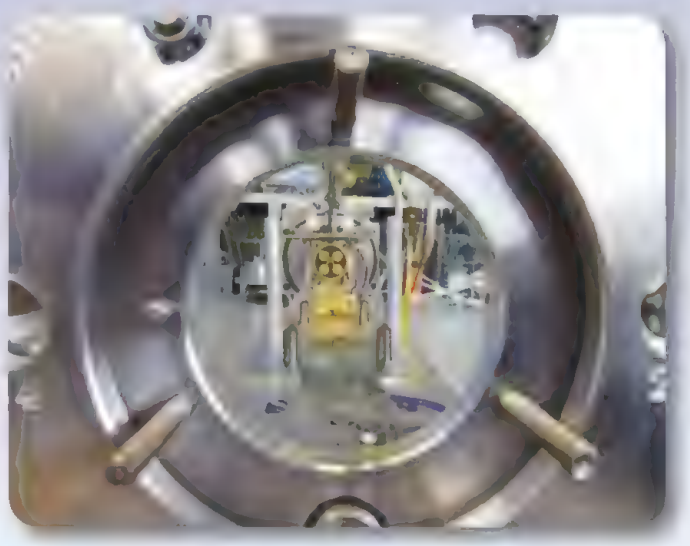

Mass Spec Imaging: From Bench to Bedside

There's a lot of high-tech equipment in today's clinical laboratory. Microscopes and histology stains are sharing bench-space with flow cytometers and microfluidic processors, DNA sequencers, and microarray readers—and mass spectrometers. Long the province of chemists and proteomicists, mass spectrometry has more recently established itself as a bona fide clinical tool. Now a new application is heading to the clinic, mass spec imaging.

See the full story on page 1119.

Upcoming Features

Data Management: Cloud-Based—June 14

Separation Techniques—July 12

Genomics—October 11

AROUND THE WORLD

Geneva, Switzerland 1

New Biotech Center on Merck Site

Billionaires Hansjörg Wyss and Ernesto Bertarelli—ranked by *Forbes* as the richest men in Switzerland—have bought the former building of drug company Merck Serono in Geneva, where they plan to set up a biotech research center with two local universities. The announcement, made on 22 May, was welcomed by Swiss scientists as a boon for the Geneva area. It comes about a year after Merck Serono said that it would close down its Geneva headquarters and relocate R&D activities to Germany, the United States, and China.


Wyss


Bertarelli

On 28 June, Merck Serono will hand over the property to a consortium called Campus Biotech, made up of the Bertarelli family, the Wyss Foundation, the University of Geneva (UNIGE), and the Swiss Federal Institute of Technology in Lausanne (EPFL). The Campus Biotech project includes the creation of Wyss Institute for Bio- and Neuro-Engineering, which will receive $103 million from the Wyss Foundation and will be modeled after a similar center for biologically inspired engineering that Wyss funded at Harvard University. (On 21 May, that institute announced that Wyss had doubled his gift, from $125 million to $250 million.)
http://scim.ag/Swissbiotech

Los Angeles, California 2

Brain Imaging Lab Leaves UCLA for USC

Over 80 neuroscientists at the University of California, Los Angeles (UCLA), will pack up their sophisticated brain scanners and hefty portfolio of private and public grants this fall when the $12 million Laboratory of Neuro Imaging moves across town to the University of Southern California (USC) Keck Medical Center. Led by neuroscientists Arthur Toga and Paul Thompson, who announced their decision to leave UCLA last week, the lab will get powerful new neuroimaging tools; larger, customized laboratory space; and more financial support from the well-heeled private university.

Statewide financial troubles, which have plagued the University of California system for years, combined with waning federal funding for "big" neuroscience research projects, influenced Toga's decision to move the lab to USC, he says. "You have to consider that when you protect your program."

Toga and Thompson did not provide UCLA an opportunity to make a counteroffer. UCLA Chancellor Gene Block expressed pride in the lab's accomplishments and disappointment about its departure, but stressed his university's continued investment in neuroscience. "The departure of one lab will not diminish our impact."

Geneva, Switzerland 3

No Coronavirus Hoarding, Scientists Say

At last week's World Health Assembly, the annual meeting of the world's health ministers, Saudi Deputy Health Minister Ziad Memish complained that intellectual prop-

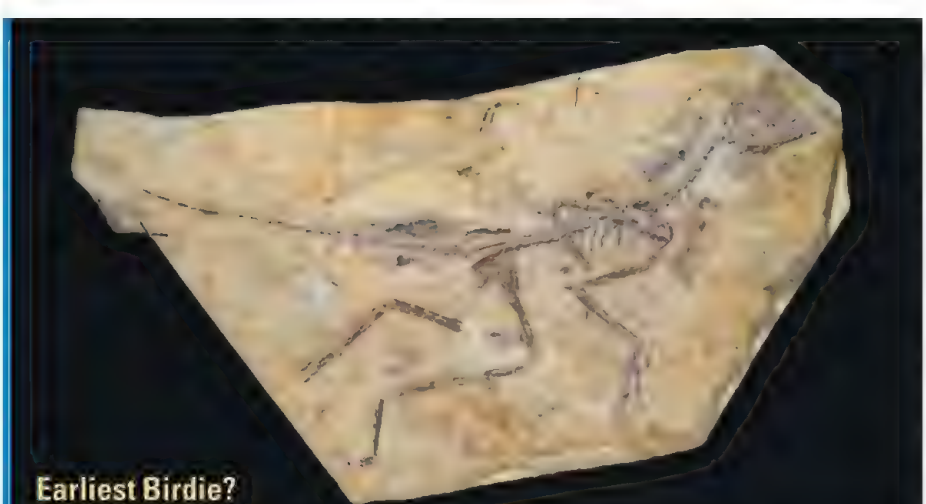

Earliest Birdie?

Nearly all paleontologists agree that birds descended from dinosaurs, but spotting that crucial evolutionary transition in the fossil record has been difficult—especially because the ancestors of the earliest birds were feathered dinosaurs, some of which could even fly. Researchers, reporting in this week's issue of *Nature*, now claim that this beautifully preserved, 170-million-year-old skeleton from China's fossil-rich Liaoning province, dubbed *Aurornis xui*, is the earliest known-for-sure bird. If that's correct, its discovery also could help resolve the controversial evolutionary heritage of several other claimed early birds, including the famous *Archaeopteryx*, whose avian status has recently been challenged (*Science*, 29 July 2011, p. 511).

CREDITS (COUNTER CLOCKWISE FROM TOP LEFT): RUBEN SPRICH/REUTERS/NEWSCOM; LAURENT GILLIERON/EPA/NEWSCOM; THIERRY HUBIN/IRSNB

Random Sample

Teachable Science in Popcorn SciFi

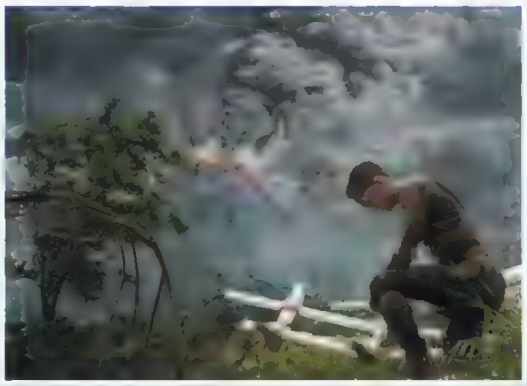

In the new Will Smith flick *After Earth,* 60 years from now human activities have altered the planet's climate to the point where Earth is uninhabitable, prompting the remaining humans to flee to a distant world. It's a storyline that might appeal to scientists—an ecological fable with a stark moral about humans' impact on the planet.

But from a scientific standpoint, *After Earth* quickly goes off the rails. Fast forward 1000 years, when Will and son Jaden crash-land on Earth and find that it has become not only uninhabitable but downright hostile. "Everything on Earth has evolved to kill humans," note the *After Earth* press materials. Cue the eye-rolls from scientists at that evolutionary "goal." Other eye-rolling opportunities include radical day-night temperature shifts in a rainforest ("You literally see the jungle freeze over," says *After Earth* writer Gary Whitta), and plate tectonics gone mad (in just 1000 years, Africa and South America have *recollided*).

"What we're presenting in the movie is grossly exaggerated," Whitta acknowledges. Science fiction, he says, requires "healthy doses" of both science and fiction.

But Whitta also points to the movie's ecological message—and yes, thinking about it that way, the movie has teachable moments, says biologist and science educator Joseph Levine of the Organization for Tropical Studies in Costa Rica. Levine, at the behest of Sony Pictures, devised an *After Earth*–inspired educational curriculum that delves into the actual science behind human impacts on the planet, including climate change, biodiversity, and land-use changes (http://www.lifeafterearthscience.com).

"Obviously, scientists are not going to agree that there is going to be a sudden crisis," Levine says. But like the much-maligned *The Day After Tomorrow*, which increased public awareness of climate change, he notes, any movie with a scientific premise is an opportunity for scientists to grab an interested audience's attention to counter the wealth of misinformation online.

erty considerations were slowing down the development of diagnostic tests for Middle East respiratory syndrome coronavirus. The virus has sickened 49 people and killed 24 since it surfaced last year. "No IP intellectual property should stand in the way of you, the countries of the world, to protect your people," agreed Margaret Chan, director-general of the World Health Organization, according to Agence France-Presse.

But scientists working with the virus say the criticism is unjustified. Virologist Ron Fouchier's group at Erasmus MC in Rotterdam, the Netherlands, identified the coronavirus last June after receiving a sample from Ali Zaki, an Egyptian doctor at the Dr. Soliman Fakeeh Hospital in Jeddah, Saudi Arabia. Fouchier's group has shared the virus with labs that sign a "fairly standard" material transfer agreement (MTA), says David Fidler, a legal scholar at Indiana University, Bloomington. "There is nothing here … that's unusual or highly restrictive." **http://scim.ag/coronhoard**

NEWSMAKERS

Cycles, Stats Earn Shaw Prizes

Rhythms, instabilities, and statistics are the focus of this year's Shaw prizes. The discovery of the molecular mechanisms

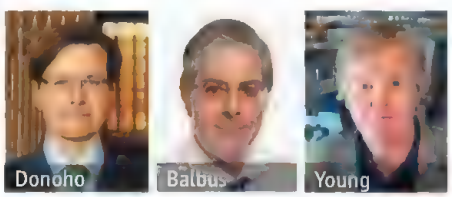

underlying circadian rhythms nets the prize in life science and medicine for Jeffrey Hall of the University of Maine, Orono; Michael Rosbash of Brandeis University; and Michael Young of the Rockefeller University. Steven Balbus of the University of Oxford and John Hawley of the University of Virginia are sharing the astronomy award for their work on magnetorotational instability, a concept describing the turbulence of astrophysical accretion disks. Stanford University's David Donoho earns the mathematical sciences award for the development of optimal algorithms for statistical estimation. Hong Kong media entrepreneur and philanthropist Run Run Shaw established the Shaw Prize in 2002. Each prize carries a $1 million award. **http://scim.ag/Shaw2013**

FINDINGS

Fighting Flu With Ready-Made Antibodies

When faced with a pandemic, is there a way to sidestep the time-consuming process of influenza vaccine development and delivery? Gene therapy pioneer James Wilson and co-workers have an idea: Squirt genes for the antibodies up people's noses.

Wilson, who works at the University of Pennsylvania, describes in the 29 May issue of *Science Translational Medicine* how he and his team engineered a harmless adeno-associated virus (AAV) to carry a gene for an unusual antibody that attacks many variants of the influenza virus. When they delivered the AAV into the noses of mice and ferrets, it infected epithelial cells and produced "broadly neutralizing antibodies." The team then exposed the animals to a range of flu viruses—and in most cases, they did not develop disease. "It's an excellent study," says immunologist Antonio Lanzavecchia, whose group at the Institute for Research in Biomedicine in Bellinzona, Switzerland, isolated the antibody used in the experiment.

Lanzavecchia, who notes that Wilson's work builds on studies done by AIDS researchers, says a critical limitation is that the vector seems capable of producing high levels of antibodies for only a month or two. That means protection against an influenza pandemic could require multiple doses.

Science LIVE

Join us on Thursday, 6 June, at 3 p.m. EDT for a live chat **with astronaut Buzz Aldrin on Mars travel. http://scim.ag/science-live**

BIOMEDICINE

Review of Cloning Paper Prompts Questions

Nearly 8 years after a massive fraud perpetrated by South Korean stem cell researchers, the embryo cloning breakthrough they claimed was back in the news this month. A different group published a paper reporting that they had cloned human embryos and derived stem cells from them. But incredibly, the new paper has come under scrutiny itself for duplicated images.

So far there's no indication that the recent work, by a well-respected Oregon-based team that studies primate cloning, is fraudulent or even wrong. "It was just an honest mistake," says the study's senior author, Shoukhrat Mitalipov of the Oregon National Primate Research Center in Beaverton, speaking of a pair of image mix-ups. The first author, lab member Masahito Tachibana, is "devastated," Mitalipov says. But he and his colleagues are confident that the work will stand up to scrutiny, he says. The cell lines that his team derived are being distributed to other labs, which he expects will soon confirm the results.

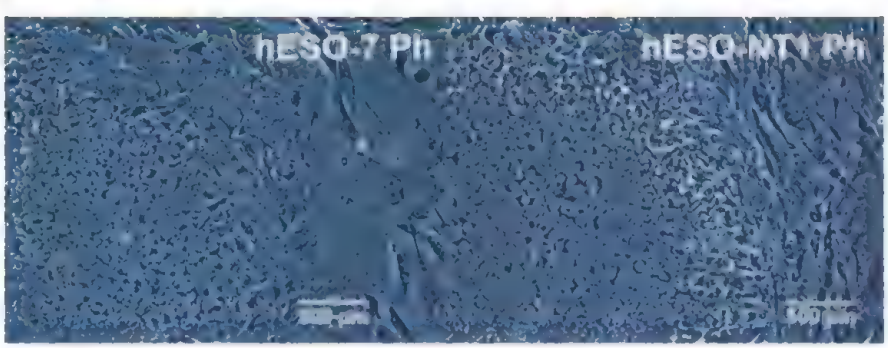

Double trouble. Several images were used twice, and one set (*below*) was mislabeled in a paper describing human cloned embryos by Shoukhrat Mitalipov (*left*) and his colleagues.

Mitalipov's paper, published online on 15 May by *Cell*, used cloning to create personalized human embryonic stem (ES) cells from human skin cells (*Science*, 17 May, p. 795).

The errors—several images in the paper appeared more than once under different labels—are another black mark on how high-profile papers are vetted, or not, before being published. They raise troubling questions that have dogged scientific publishing for years. For instance, how much responsibility do journals and reviewers bear for detecting problematic images in papers, whether honest errors or not? How is it possible that the very same result that unraveled so spectacularly in 2005 was not exhaustively reviewed when it was submitted for publication a second time?

Cell issued a statement the day after an anonymous commentor posted about the problem. The journal admitted to "some minor errors made by the authors." And it defended its unusually quick review; the research was formally submitted on 30 April and accepted on 3 May. In an e-mail to *Science*, the editor-in-chief of *Cell*, Emilie Marcus, writes that "the reviewers returned their comments quite rapidly and given their recommendations for acceptance, with our focus on author service and because of the interest and importance of the work, we then decided to take special efforts to keep the delay between acceptance and publication to a minimum to reduce the likelihood that the findings would come out first in the popular press."

That desire to snag the hottest of hot papers, and bask in their limelight, is often at odds with what it takes to fact-check them as thoroughly as possible. "These things happen," says Robin Lovell-Badge, a stem cell researcher at the MRC National Institute for Medical Research in London, though he notes that time pressure raises the chance that mistakes will slip through. "I think the fault lies with the combination of the authors, the editors, and the reviewers. It's been missed by three sets of people," Lovell-Badge says.

Inconsistencies in the Mitalipov paper first surfaced on 22 May on PubPeer, a site for postpublication peer review where commenters can describe concerns about a paper and authors can respond. Although it's hardly the first time that anonymous voices on the Internet have proven critical, "I don't think we should be relying on the crowd to be policing" research papers, says Hany Farid, a computer scientist at Dartmouth College who is working to commercialize software that can detect duplicated images and other manipulations. Reviewers are already "overburdened," and Farid believes it's the journals that must take this on.

At *Science*, which in 2004 and 2005 published the stem cell work by South Korean scientist Woo-Suk Hwang that turned out to be fraudulent, Executive Editor Monica Bradford says that she empathizes with her counterparts at *Cell*. "I know what position they're in. You go from this amazing high … to 'Oh my God.' … You feel like, 'How did we make these mistakes?' "

Bradford was at *Science* during the Hwang debacle and was interviewed at the time by the authors of this article about the journal's response. The Hwang fraud, she says now, had a lasting impact. *Science* commissioned an external report led by Stanford University chemist John Brauman to examine what it might do differently in the future. "It is essential to develop a process by which papers that have the likelihood of attracting attention are examined particularly closely for errors, misrepresentation, deception, or outright fraud," wrote the authors of the Brauman report, as it was called.

After the Hwang case, which involved deliberate image manipulations, *Science* began checking all figures in papers at the revision stage and launched previously planned routine analysis of images using Photoshop software. "My level of trust is way different than when I started this job," Bradford says. "In the area of stem cells we've been very cautious, maybe too cautious." But other papers that later were dis-

CREDITS (TOP TO BOTTOM): COURTESY OF OREGON HEALTH & SCIENCE UNIVERSITY; M. TACHIBANA *ET AL. CELL* (ADVANCED ONLINE EDITION)

credited have continued to slip through, such as work claiming that a virus called XMRV causes chronic fatigue syndrome. It was later retracted. "It's like whack-a-mole. We keep trying," Bradford says, "but we are far from perfect, so that's why I really have sympathy for *Cell*."

The software that *Science* and some other journals use isn't designed to detect duplicated images, although it can make them easier to spot. Rather, it reveals various inappropriate modifications made to an image to enhance it. Marcus declined to say whether *Cell* uses image analysis technology. In 2006, she expressed reluctance to cast blanket suspicions in a story in *The New York Times* about screening images. "Why say, 'We trust you, but not in this one domain?' And I don't favor saying, 'We don't trust you in any,' " Marcus told the *Times* reporter.

Stem cell scientists expressed dismay that their field is again under scrutiny. Some say that they are working hard to replicate Mitalipov's results. Even if the image duplications and mislabelings are quickly corrected—as *Cell* and the authors say they're working to do—Farid warns that cases like this one can ripple well beyond the labs parsing the cells. "Suddenly the public starts wondering what the hell we're doing," he says. It's important and natural for science to move slowly, he says, perhaps especially so when the results seem remarkable. After all, Farid says, "This isn't cable news."

–JENNIFER COUZIN-FRANKEL AND GRETCHEN VOGEL

U.S. IMMIGRATION POLICY

Visa Reform Advances in Senate as House Offers STEM Ideas

Efforts to overhaul U.S. immigration policy often generate more show than substance. Last week, they produced both: a three-ring circus of activity that pushed reform ahead without deciding what Congress ultimately will do.

Most attention focused on the U.S. Senate, where a committee last week won bipartisan agreement on a path to citizenship for some 11 million undocumented immigrants. By a 13 to 5 vote, the panel on 21 May approved a bill that also makes it easier for foreign-born scientists and engineers to live and work in the United States and taps visa fees to create new funding streams for STEM (science, technology, engineering, and mathematics) education and training programs aimed at providing more domestic workers with STEM skills. But members of the U.S. House of Representatives also shared the limelight. Republican leaders demonstrated their piecemeal approach to immigration reform with a bill that would ease the entry of skilled foreign labor in ways that paralleled the Senate legislation. And a bipartisan group of House members continued work on a broader immigration proposal that is expected to include STEM provisions.

"We're seeing a convergence on some policies that try to … retain skilled STEM immigrants and improve STEM education," says Scott Corley, executive director of Compete America, a coalition of business and academic groups that backs many of the proposals.

The overhaul effort faces numerous obstacles, however. Some labor specialists, for example, worry that the Senate bill does too little to protect U.S. STEM workers from immigrant competition. Provisions allowing more high-skill guest workers will "depress wages in STEM fields and put U.S. workers at a disadvantage," predicts economist Hal Salzman of Rutgers University in New Brunswick, New Jersey.

Such complaints got limited traction as the Senate Judiciary Committee spent 5 days considering hundreds of proposed changes to a bipartisan proposal released last month (*Science*, 26 April, p. 415). In one move, the panel weakened rules designed to encourage U.S. high-tech companies to hire U.S. workers before turning to foreign guest workers on temporary visas known as H-1Bs. Senator Orrin Hatch (R–UT), siding with high-tech companies in his state, said that the changes in hiring temporary workers—the bill would raise the annual H-1B ceiling from 65,000 to 110,000—were needed to win his support in committee. But he said that he will take a fresh look when the measure comes before the full Senate.

The deal that Hatch struck with Senator Charles Schumer (D–NY) displeased groups representing U.S. engineers and other skilled workers, who would prefer fewer H-1Bs. But STEM advocates welcomed another Hatch amendment adopted by the panel that steers more visa fees—potentially tens of millions of dollars annually—to STEM programs funded by the U.S. Department of Education and run by states. They were also glad that senators didn't tinker with provisions that would automatically give a green card to a foreign student who earns an advanced degree from a U.S. university in all STEM fields.

A narrower high-skill immigration bill introduced on 24 May by senior House Republicans includes similar provisions. Two differences are that it would allow more H-1Bs—155,000—and cap the number of green cards for foreign-born STEM graduates at 55,000.

Such a standalone Republican bill has little chance of winning Senate approval, however. But it could help a bipartisan House group shape a more comprehensive immigration bill that might fly. But that draft is still under wraps, and months of negotiations have yielded only broad principles. The group says that it might have a bill ready next month, when the Senate is expected to act.

–DAVID MALAKOFF

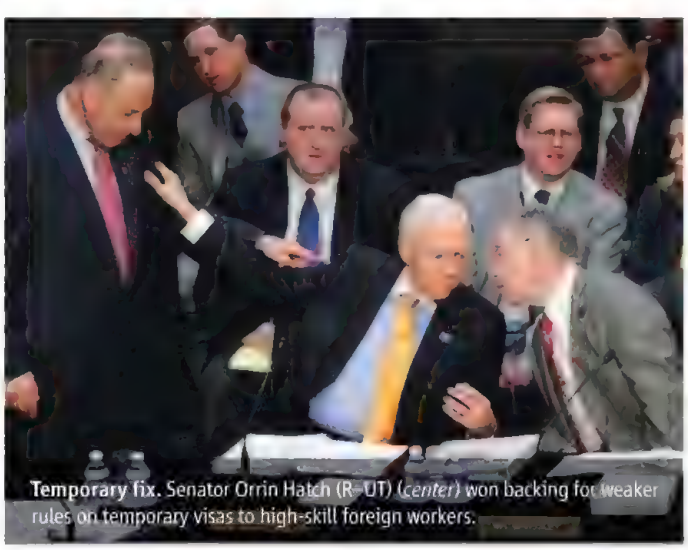

Temporary fix. Senator Orrin Hatch (R–UT) (*center*) won backing for weaker rules on temporary visas to high-skill foreign workers.

CREDIT: WIN MCNAMEE/GETTY IMAGES

Making their case. Pro-Stamina rally in Rome.

CREDIT: JPEG FOTOSERVIZI

STEM CELLS

Italian Parliament Orders €3 Million Trial of Disputed Therapy

ROME—The Italian Parliament has decided that the administration of a controversial stem cell treatment for neurodegenerative diseases, provided by the Stamina Foundation in Turin, can continue—although on only a small scale. Lawmakers also ordered a formal clinical trial of the therapy and allocated €3 million to pay for it. The law, opposed by many stem cell scientists, became official after it was approved by Italy's Chamber of Deputies on 20 May and by the Senate 2 days later.

Although some patients say that they have benefited from the treatment, researchers contend that the Stamina Foundation's therapy hasn't been properly described, let alone shown to be effective; a 15 March open letter signed by 13 stem cell scientists compared it to "snake oil." Spending millions on a trial is "a waste of money," contends Massimo Dominici of the University of Modena and Reggio Emilia, who is president-elect of the International Society for Cellular Therapy.

But critics are relieved that the Italian government's original proposal to make the therapy widely available has been amended (*Science*, 29 March, p. 1504). Under the new law, the therapy can be given to some 90 patients already receiving it at a hospital in Brescia, but new patients must enroll in the trial. Cells used in the study must be produced under good manufacturing practice (GMP) standards; presently, they're not.

Scientific details about the treatment are hard to come by. The only available document is a 2010 U.S. patent application in which Stamina scientists describe how to transform mesenchymal stem cells, extracted from bone marrow, into neurons by culturing them and soaking them in retinoic acid and ethanol. The U.S. Patent and Trademark Office rejected the application because the method was not described clearly enough and because it was "unclear" how the chemical bath could coax stem cells to become neurons.

Davide Vannoni, president of the Stamina Foundation and a psychology professor at the University of Udine, tells *Science* that the treatment is based on in vitro and preclinical studies by other groups using similar compounds, published in Russian and Chinese journals in the early 2000s. (He sent *Science* one paper on the condition that its details not be revealed.) Vannoni says that the cells can't be produced under GMP standards because the companies that Stamina employs to provide the culture media don't adhere to GMP.

Under existing Italian law, which complies with E.U. regulations, unproven stem cell therapies can be administered on a case-by-case basis to patients with untreatable, severe illnesses—but only in hospitals and under stringent conditions. Since 2011, Stamina has treated patients at the Spedali Civili, a public hospital in Brescia.

But in May 2012, the Italian Medicines Agency (AIFA) halted the work after an investigation identified irregularities. AIFA's confidential report, which *Science* has obtained, says that at the time, 12 patients at the hospital, including four children, had received the treatment for diseases such as spinal muscular atrophy, Alzheimer's, and Parkinson's. The report states that doctors who prescribed and injected the cells didn't know exactly what the treatment consisted of; they believed that the information was proprietary. "The administration of an unknown compound would not be admissible in a hospital if this is what has happened," says Francesca Pasinelli, director-general of Telethon, a nonprofit foundation for research on genetic diseases.

The report also states that the hospital's ethical committee approved the therapies without making a proper risk-benefit assessment, as required by law—a characterization that Vannoni disputes—and that treatment protocols were unclear: Apparently, Stamina used the patients' own bone marrow cells in some cases, but in others, it took those of a family member, a nonrelated donor, or even another patient, the report says. Treatment outcomes have not been published; parents of some patients told an Italian TV show that their children's conditions had improved.

At AIFA's request, Dominici tried to replicate Stamina's recipe for producing neurons using cells seized by AIFA and Italian police during the lab inspection and following the methodology in the patent application. "We did not see any differentiation of those cells into neurons," he says. One of the two seized samples contained a significant number of immune cells, he says, which could trigger dangerous reactions if injected into someone other than the donor. Vannoni says that the cells had yet to undergo a second procedure to remove contaminants. "The treatment is safe and does not trigger immune reactions," he claims. Spedali Civili officials declined to comment.

The hospital and Stamina have appealed the decision to halt the treatments to Brescia's Administrative Court, arguing that AIFA's investigation wasn't properly conducted; a ruling is expected in November. Meanwhile, however, patients have pressured the government and Parliament to step in.

The clinical trial, to be conducted regardless of the outcome of the court case, will be led by AIFA and two other government institutes. Designing a protocol will be tricky, says Paolo Bianco of the Sapienza University of Rome. "One must assume that there is no Stamina method," he says, because "there's no published account."

The case highlights a problem in the E.U. regulation on stem cells and other advanced therapies, Dominici says. European rules allow the "hospital exemption" used by Stamina in Brescia; a European Commission consultation, published last week, shows that countries have implemented the exemption in different ways. This is almost an invitation to "dodgy stem cell companies" to operate in countries where hospital exemption rules are lacking or unclear, Dominici says. "This has to be prevented." **–LAURA MARGOTTINI**

Laura Margottini is a writer in Rome.

CHINA

Divided Loyalties Land Scientists in Hot Water

BEIJING—As the old saying goes, it's hard to serve two masters. Three Chinese researchers at New York University (NYU) were charged last week with taking bribes from a company and a government-funded lab in China. One of them was also accused of falsifying records in an application for a $3 million grant from the U.S. National Institutes of Health (NIH). A U.S. attorney labeled the defendants at NYU "foxes in the henhouse." But many in the Chinese scientific community think that the three scientists may instead be guilty of a lesser offense of foolishly trying to two-time their employer.

On 20 May, the U.S. Federal Bureau of Investigation and the U.S. Attorney in Manhattan filed charges of "commercial bribery conspiracy" against Yudong Zhu, 44, an accomplished electrical engineer, and Xing Yang and Ye Li, both 31 and research engineers in Zhu's lab. The trio, who studied ways to enhance the imaging capabilities of MRI technology, are accused of obtaining "financial benefits" from a Chinese company in exchange for acquiring "certain research and non-public information at the US-based university that employed them," charged FBI Special Agent Michael J. Weniger in the unsealed complaint. NYU Langone Medical Center, where the three worked, issued a statement saying that it was "deeply disappointed" by the news but could not comment because the investigation is ongoing.

The case highlights the pitfalls of what Chinese call "attempting to straddle two boats." Thanks in large part to China's stepped-up recruitment efforts, it's increasingly common for scientists like Zhu to hold dual posts, says Cong Cao, an expert on Chinese science policy at the University of Nottingham in the United Kingdom. In such arrangements, he says, "sooner or later there are going to be conflicts."

Zhu was a rising star in 2008 when the NYU center recruited him from General Electric's Global Research Center in Niskayuna, New York, to work on parallel MRI technology, a way to increase the speed of image acquisition. A 2008 press release announcing his appointment boasted, "NYU Langone Medical Center continues to attract the best and brightest faculty from around the world." But around 2011, Zhu took up "undisclosed affiliations" in China, according to the FBI complaint. He allegedly did not inform the university that he was involved with the Chinese medical imaging company United Imaging Healthcare in Shanghai and the Shenzhen Institutes of Advanced Technology (SIAT).

Zhu's troubles began in 2010, when he won a 5-year NIH grant to advance MRI capabilities by using higher magnetic field strengths. In the first 3 years, Zhu and his team received $2.1 million for the research, which the FBI alleges directly "impacted" the value of a U.S. patent that he holds on an MRI technology. The U.S. attorney charged Zhu with "falsification of records" over his failure to disclose his patent to NYU. The Chinese lab and company, meanwhile, were pursuing similar research with Chinese government funding.

In 2011 and 2012, Zhu arranged for Yang and Li to move from China to New York to assist with his research, according to the FBI complaint. Soon after, the complaint continues, an executive at United Imaging Healthcare affiliated with SIAT reimbursed Yang for roughly $20,000 in graduate school tuition payments and paid Li's rent. Yang also allegedly conveyed information about his and Zhu's research to United Imaging Healthcare. Li, meanwhile, worked simultaneously for SIAT and the Chinese company. Zhu, Li, and Yang all maintained e-mail accounts with the domain name "united-imaging.com" while at NYU, according to the complaint.

In late 2012 or early 2013, NYU began to investigate the research team. The evidence that the university turned over to the FBI this spring included video footage of Yang photographing lab equipment, the complaint states.

The NYU case is the latest in a string of charges brought against Chinese scientists working in the United States for funneling raw or nonpublic research and information to institutions in China. Allegations are often characterized as economic espionage. The phenomenon "is not unique to China, but I think the majority of cases have been from China," says Adam Segal, a senior fellow at the Council on Foreign Relations in New York City who studies intellectual property and innovation.

The spate of incidents may be partly blamed on Chinese government talent recruitment programs that tacitly allow—and sometimes even encourage—holding dual appointments in China and in the West. As a result, Chinese scientists may unwittingly violate U.S. institutions' conflict-of-interest rules, says Jian Han, a faculty investigator at HudsonAlpha Institute for Biotechnology in Huntsville, Alabama. Some may think playing both sides "is a win-win situation—but it's not," he says. Another attraction to overseas Chinese researchers may be the ease of receiving government funding in China, Segal notes: "There are very clear avenues for funding and support back in China if a scientist is tempted to take intellectual property and strike out on their own." Professors at U.S. universities with China-based labs, grad students, and Chinese government grants are "not uncommon," says Denis Simon, a vice provost at Arizona State University and an expert on science and innovation in China: "It's very amorphous territory."

Indeed, those recruited by the Chinese government's Recruitment Program of Global Experts, commonly known as 1000 Talents (*Science*, 31 July 2009, p. 534),

Here today, gone tomorrow. Photos of innovation team members were deleted from SIAT's website soon after the FBI brought charges against Zhu (*top row, center*).

CREDIT: COURTESY OF JIAN HAN

eppendorf & Science

PRIZE FOR NEURO BIOLOGY

2012 Winner
Dr. Marlene R. Cohen
Assistant Professor
University of Pittsburgh

Application Deadline
June 15, 2013

Call for Entries

Eppendorf & Science Prize for Neurobiology
The annual Eppendorf & Science Prize for Neurobiology, an international award, honors young scientists for their outstanding contributions to neurobiological research. The winner and finalists are selected by a committee of independent scientists, chaired by Science's Senior Editor, Dr. Peter Stern. To be eligible, you must be 35 years of age or younger.

You could be next to win this prize and to receive
> Prize money of US$25,000
> Publication of your work in Science
> Full support to attend the Prize Ceremony held in conjunction with the Annual Meeting of the Society for Neuroscience in the USA
> An invitation to visit Eppendorf in Hamburg, Germany

It's easy to apply!

Learn more at: www.eppendorf.com/prize

eppendorf

Science
AAAS

receive up to hundreds of thousands of dollars in startup funds and a $163,000 relocation subsidy. Following the central government's lead, provinces launched their own recruitment programs. Zhu was recruited by Guangdong, a province in southern China, to be a core member of an innovation team focused on advanced MRI technology, the complaint states. In 2011, the Guangdong government recruited 20 innovation teams and provided them with about $80 million total, according to Chinese news reports.

Meanwhile, Chinese scientists working overseas worry that the allegations against Zhu could cast them in a negative light. The case will be "followed carefully by Chinese scientists both in China and in the U.S.," Han says. Wei Jia, a researcher at the University of North Carolina, Greensboro, fears that the Zhu case could harm perceptions among U.S. employers and federal funding agencies.

Two scientists in the case have been arrested. The third, Li, returned to China before charges were filed, according to the FBI press release. After news of the arrests broke, SIAT deleted photos of and information about Zhu and Li from its website and is reportedly considering legal action to shield its reputation. A United Imaging Healthcare official told *The Wall Street Journal* that it's "impossible that our company would get involved in this kind of thing."

At the very least, the case against the three scientists should alarm others attempting to straddle two boats. Ying Xu, a bioinformatics researcher at the University of Georgia in Athens, says, "I hope those with full positions in the U.S. and [who] consult in China can learn a lesson from this incident."

–CHRISTINA LARSON AND HAO XIN

Christina Larson writes for *Science* in Beijing.

PLANETARY EXPLORATION

Radiation Will Make Astronauts' Trip to Mars Even Riskier

Most robotic missions to Mars have failed, but future astronauts headed for the Red Planet will have more than an imagined martian jinx to worry about. Measurements that the Curiosity rover made en route to its touchdown on Mars last August show that radiation in deep space could pose a significant—if poorly understood—threat to human space travelers.

The radiation levels that Curiosity measured "are in line with the kind we expect," says astrobiologist Lewis Dartnell of the University of Leicester in the United Kingdom. "That's in a way reassuring. But traveling Earth to Mars, you're getting a fairly large portion of [the allowed] exposure." And even with good measurements in hand, he adds, much about radiation's effects on the human body remains unknown.

The measurements—from the Radiation Assessment Detector (RAD) piggybacking on Curiosity—provide the best hard numbers gauging the radiation that astronauts will encounter as they voyage beyond Earth's protective magnetic field. The spacecraft that carried Curiosity to Mars provided much the same radiation shielding as the Crew Exploration Vehicle that NASA is building to carry astronauts beyond low Earth orbit. So RAD's counts of the energetic charged particles that make up space radiation should give a reasonable idea of what humans will be up against, says physicist Cary Zeitlin of Southwest Research Institute in Boulder, Colorado, lead author on the RAD paper on page 1080.

Those energetic charged particles come in two sorts. Protons flung off the sun in solar flares or in great blobs of plasma called coronal mass ejections caused a spike in RAD readings five times from December 2011 into July 2012. The protons' energies tend to range up to a few hundred megaelectron volts. Astronauts caught outside with nothing but a spacesuit to protect them from those surges could become acutely ill, but shielding like RAD's can stop much although not all of such radiation. Then there are the cosmic rays—atomic nuclei ranging from lone protons up to iron nuclei—blasting in from the galaxy with energies of a few hundred to many thousands of megaelectron volts. Most of them passed right through RAD's shielding or even shattered atoms in the protective material, creating showers of damaging fragments.

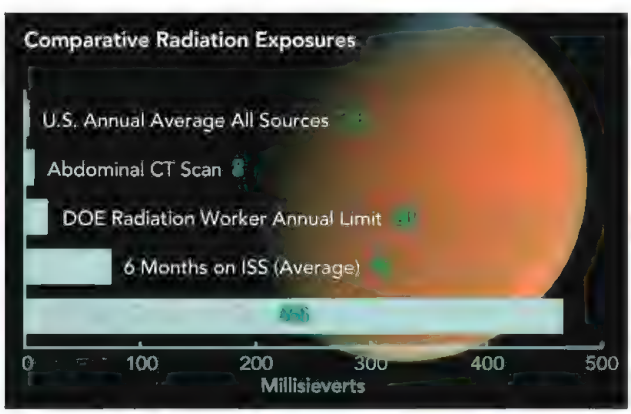

CREDIT: CARY ZEITLIN/SOUTHWEST RESEARCH INSTITUTE, BOULDER

RAD's bottom line was that a round trip to Mars would give an astronaut a hefty dose of damaging radiation. Zeitlin and colleagues converted RAD measurements of energetic particle abundances, energies, and masses into a measure of biological damage called sieverts, which is related to lifetime cancer risk. During a 360-day round trip, an astronaut would receive a dose of about 662 millisieverts (mSv), according to RAD measurements. National space agencies limit exposure to about 1000 mSv or less during an astronaut's entire career; NASA's limit corresponds to a 3% risk of exposure-induced death from cancer.

"These results show that cosmic rays are not a showstopper," says Robert Zubrin, a trained nuclear engineer and president of The Mars Society headquartered in Lakewood, Colorado. "This confirms what you might expect: The radiation risk is quite acceptable. Frankly, it's a modest portion of the risks on a Mars mission."

Dartnell is less sanguine. He notes that RAD traveled to Mars during a quieter part of what is turning out to be a relatively quiet solar cycle. Future astronauts might well encounter more and bigger solar events, he says. And RAD team members have yet to report radiation levels from the surface of Mars, where astronauts could well spend a year or more.

But Dartnell's biggest reservation is the uncertainty of it all. "It's the things we don't know that are the biggest concern," he says. "We don't know how dangerous [the observed radiation] would be." The conversion from charged-particle energies and masses to biological damage involves "a high degree of uncertainty," Zeitlin says, especially when it comes to the heavy nuclei of galactic cosmic rays.

So more work looms for both space physicists and radiation biologists. "Radiation is one of many risks in space travel," Zeitlin says. But when flesh-and-blood explorers start to travel between planets, "How much risk?" will be as much an ethical as a technical question.

–RICHARD A. KERR

Science for All

With 400 million people earning less than $1.25 per day, India is home to a staggering one-third of the world's poor. Can scientists do more to lift people out of poverty?

CHENNAI, INDIA—In March 2012, Ashok Jhunjhunwala invited 45 young hotshots in India's electronics industry to this southern Indian city to brainstorm on a challenge: Could they design a tablet computer with Internet connectivity that would sell for 2500 Indian rupees—about $50—and still allow their companies to turn a profit on the device? To Jhunjhunwala, an electrical engineer here at the Indian Institute of Technology (IIT), Madras, it wasn't merely the fortunes of India's Silicon Valley that hung in the balance. India's future was at stake.

India has made strides in extending education to all strata of society. According to the Ministry of Human Resources Development, in 2010, 50% of children attended school through grade 12—up from 37% just 8 years ago. Equality is taking root in higher education as well. "The poorest children are getting into engineering colleges. That was inconceivable a decade back," says Jhunjhunwala, who serves on a science advisory council to Prime Minister Manmohan Singh. But India is failing, Jhunjhunwala says, in what it offers up to those young minds in the classroom. "We have made zero progress, even negative progress, in the quality of education," he asserts. Steering away from rote instruction and raising the bar, he says, "is our biggest challenge."

Jhunjhunwala didn't expect a cure-all from the computer jocks he coaxed to Chennai. But he knew that an inexpensive tablet, purchased en masse by the government and distributed to students, would be a powerful teaching aid. Two previous attempts had not lived up to their promise, and half the companies represented in the room, Jhunjhunwala knew, "were dead opposed to the idea" of a cheap tablet. It was hard to erase memories of the first cut-rate handheld alternative to laptops developed in India: the Simputer, which flopped a decade ago. The industry needed a reboot. But after huddling with the group all day, Jhunjhunwala recalls, "we felt confident that we could do something."

Unlike in past efforts, competition is the name of the game this time. As *Science* went to press, a dozen companies were racing to refine prototypes of a $50 tablet. These are undergoing dozens of performance tests here at IIT Madras's research park. Based on the benchmarking outcome, the Indian government is considering making an initial purchase this fall of 5 million tablets from the five top-performing manufacturers;

CREDIT: PALLAVA BAGLA

Homespun innovation. A new rotavirus vaccine developed in India could be a boon to public health.

all of their machines will be marketed under the name "Aakash 4." The price for each unit: Twenty-five hundred rupees, plus taxes. With educational applications that will initially enhance and someday possibly even supplant printed textbooks, the Aakash 4, Jhunjhunwala predicts, "will be an integral part" of India's effort to raise education standards.

The Aakash 4 is at the vanguard of India's drive to use science and technology to raise millions of people out of poverty. The aim is to bypass hidebound approaches and link talent and ideas in a push for rapid economic growth. S. Shankar Sastry, dean of engineering at the University of California, Berkeley, and colleagues envision the emergence of a new academic discipline—development engineering—aimed to assemble a toolkit of methods to find sustainable solutions to poverty. India, where 833 million of the country's 1.21 billion people live in villages sorely deficient in health care, sanitation, electricity, and educational opportunities, is a natural crucible for such experiments.

In this impoverished landscape, Singh, an academic at heart, is sowing the seeds of an intellectual revolution. Last week, speaking about his vision of inclusive growth, Singh said: "The glass was almost empty when we started. The important point to note is that it is being filled." High on the agenda are plans to extend a $1.2 billion National Knowledge Network—a high-speed Internet backbone now linking 1000 agencies and research institutions—to every one of India's 630,000 villages.

Another push is coming from the National Innovation Fund, established last year with a $50 million pot of money to bankroll promising technological solutions for societal woes. "The fund is built on the principle that innovative enterprise can engage citizens at the bottom of the economic pyramid," says Sam Pitroda, chair of India's National Innovation Council, which helps oversee the fund. For example, using a grant from the fund, villagers coping with periodic droughts spawned by deforestation in the Himalayan state of Uttarakhand are teaming up with scientists from the Bhabha Atomic Research Centre in Mumbai to identify where ground water is more readily recharged in the watershed. The nuclear scientists are mapping underground water flow using isotopes of oxygen and tritium, enabling villagers to pinpoint locations to build recharge ponds.

Other initiatives that promise to transform India include agricultural extension services that use cell phones to broadcast best practices and prevailing market prices for crops to farmers and fishers; a national ID program that will extend the welfare safety net to the nation's poorest corners; and vaccines against diseases whose toll is highest among the most deprived. All told, experts say, India in 2013 will spend about $6 billion on science-based efforts to raise living standards: half of its total R&D budget.

Online
sciencemag.org
Podcast interview with Pallava Bagla (http://scim.ag/pod_6136).

In a nation known for its prowess in rockets and atomic bombs, poverty alleviation is not something that most researchers gravitate to, says nuclear scientist Rajagopala Chidambaram, principal scientific adviser to the Government of India. "Active scientists are not the best suited for grassroots intervention," he argues. The lion's share of work, he says, should be left to nongovernmental organizations led by scientists. Others feel differently. "We have a moral responsibility to help the poor," Pitroda says. For years, Pitroda, who helped establish India's modern telecom industry in the 1990s, doubted whether significant inroads were feasible. "The problems of poverty weren't drawing talented researchers," he says, and the government approach was at times piecemeal, at times negligent. However, India's rapid economic development is rewriting the script. "I didn't think it was possible to do much to help," Pitroda says. "Until now."

Leading the charge. Ashok Jhunjhunwala, holding an Aakash tablet, hopes the cut-rate computer will transform Indian education.

CREDIT: PALLAVA BAGLA

Vaccinations for all

To Krishna Ella, Indian science is a study in contradictions. For decades, he notes, India has excelled in basic research in chemistry and a few other fields. But many of the nation's most pressing needs have lain neglected. Particularly deserving of opprobrium, he argues, is India's track record in disease research. Thousands of Indians die of malaria each year, he notes, yet, "Why have we not developed a single good antimalaria drug?" Typhoid, cholera, dengue: "Nobody was touching these poor man's diseases," Ella says.

His father was a farmer in the southern state of Tamil Nadu, so Ella knew how hard it can be to scratch out a living from the land. After earning a doctorate in plant pathology from the University of Wisconsin, Madison, in 1993, Ella spent a brief period as a research assistant professor at the Medical University of South Carolina in Charleston before heeding the wishes of his wife, Suchitra, and his mother, and returning with his family to India in 1996. In a lab that he set up in Hyderabad, Ella developed a hepatitis B vaccine by inserting genes for viral surface proteins into yeast. With seed funding from the Industrial Development Bank of India, Ella and Suchitra in 1996 founded Bharat Biotech International Ltd. The company scored its first triumph just 2 years later, when India's president, A. P. J. Abdul Kalam, came to Hyderabad to unveil Revac-B+, a recombinant hepatitis B vaccine that Bharat put on the market for about $1 per dose—a fraction of the price of hepatitis vaccines made by Western firms.

Over the next decade, Bharat Biotech built a portfolio of cheap vaccines against scourges such as polio, typhoid, and rabies,

and the company anchored a high-tech enclave in Hyderabad that Krishna christened "Genome Valley."

The company stumbled in September 2011, when the World Health Organization, in an audit of Bharat Biotech's production plant in Hyderabad, found "deficiencies in the implementation of good manufacturing practices and in the quality management system of the company," WHO said in a statement that December. WHO, which noted that Bharat Biotech's vaccines on the market were deemed safe, asked for the audit in response to the company's applications to include two vaccines on a roster of products approved by WHO for bulk purchase by the U.N. Children's Fund and other U.N. agencies. Ella insists that the problem is merely about documentation and that quality was never an issue. Company officials are in discussions now with WHO on getting their firm approved as an authorized vaccine supplier.

In the meantime, Bharat Biotech achieved a milestone earlier this month when the Indian government announced that the company's homegrown vaccine against rotavirus had scored high marks in clinical trials. In the United States, the virus is a public health nuisance, causing severe diarrhea in infants and young children, but few deaths. In India, rotavirus is a menace that easily spreads through contaminated food and water. It infects some 20 million children in India every year, claiming more than 100,000 lives. Most of those deaths are preventable—children become dehydrated and fail to receive adequate treatment.

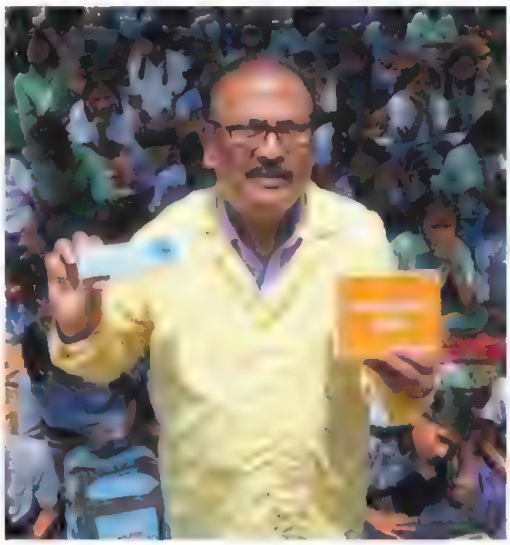

Mass appeal. Bharat Biotech, led by Krishna Ella (*left*), has made cheap vaccines a profitable venture. Indian telecom pioneer Sam Pitroda (*right*) believes scientists have a moral responsibility to help the poor.

At a press conference in New Delhi earlier this month, K. Vijayraghavan, secretary of the Department of Biotechnology, announced that ROTAVAC, Bharat Biotech's vaccine against the predominant rotavirus strain circulating in India, had compiled an "excellent safety and efficacy profile" in phase III clinical trials—the first time such trials were conducted in India for any vaccine. In a statement, Anthony S. Fauci, director of the National Institute of Allergy and Infectious Diseases (NIAID) in Bethesda, Maryland, hailed the results as "a significant victory for India's scientific community." (A partner in the collaboration, NIAID provided one of the strains tested in the ROTAVAC trial.)

This effort originated at the All India Institute of Medical Sciences in New Delhi, where Maharaj Kishan Bhan, a vaccine researcher, in 1985 identified a nonpathogenic strain of rotavirus. Thirteen years later, the Indo-U.S. Vaccine Action Program selected Bharat Biotech to develop the vaccine. Since then,

A Role for Science in Poverty Alleviation?

NEW DELHI—With more than 400 million people in India earning less than $1.25 a day, poverty reduction in this sprawling nation is an urgent task. Perhaps that's why the ruling United Progressive Alliance turned to one of its deep thinkers to tackle the intransigent problem. In July 2011, Jairam Ramesh was tapped to lead the Ministry of Rural Development, an $18 billion agency focused on the plight of the 70% of India's 1.2 billion people who live in the countryside.

Ramesh, 59, is no stranger to India's scientific community. He garnered headlines in January 2010, when, as environment minister, he imposed an indefinite moratorium on the introduction of genetically modified eggplant (*Science*, 12 February 2010, p. 767). A mechanical engineer by training who's known for his wit and biting remarks, Ramesh is also a China expert; in 2005 he published a book on the relationship between the two Asian powers, *Making Sense of Chindia: Reflections on China and India.*

Reaching out. Jairam Ramesh's main task now is helping rural poor.

Last month, *Science* spoke with Ramesh in his office here about the role of science in poverty alleviation. His remarks were edited for brevity and clarity. **–P. B. AND R. S.**

Q: Is science in India helping the poor?

J.R.: People are coming out of poverty because of agricultural growth, better wages, and better infrastructure. Science played an important role in creating new varieties of rice and wheat; that has lifted farmers out of poverty. Science has created mobile phones that are giving farmers and wage seekers links with markets. But if you are asking me if there is a direct relationship between investment in science in India and rural development, my answer is no.

Q: How would you get scientists more involved in poverty alleviation?

J.R.: Almost 60% of all open defecations in the world are in India. And open defecation and poor sanitation has a direct link with malnutrition and stunted growth. But we've had no innovation whatsoever in the field of toilets. So when Mr. Bill Gates came to meet me a couple of months ago, we said, why don't we collaborate together and have a global challenge? Challenge the world's inventors to come up with low-cost toilets for use in trains, for use in our homes. You take four or five crucial areas and certainly you can throw the market open for ideas.

CREDITS (TOP TO BOTTOM): PALLAVA BAGLA (3)

the Indian government and foreign partners, including the Bill & Melinda Gates Foundation, have poured about $100 million into the project. ROTAVAC is expected to be on the market in early 2014, priced at about $1 per oral dose for a three-dose series. Two Western-manufactured vaccines now on the market in India each cost about $40 per dose.

Toward total inclusion

In his 2008 book *Imagining India*, Nandan Nilekani, a tycoon who co-founded the Bangalore-based software and information technology giant Infosys in 1981, made an intriguing proposition. Biometrics technology had become reliable and cheap enough to deploy nationwide in India; Nilekani proposed entering people living below the poverty line into a database that would help them access benefits. "Millions of people become adults in India without an identity document," and they are unable to tap into the country's welfare system, Nilekani says. "We had to find a way to make society more inclusive." Toward this end, he argued, biometrics could be a powerful tool.

Prime Minister Singh threw his weight behind the venture, and in July 2009 the Unique Identification Authority of India (UIDAI) was formed. Its ambitions have since grown: UIDAI is now striving to assign a random 12-digit "Aadhaar" ID number to every resident of India, based on photos, iris scans, and a full set of 10 fingerprints. Some critics blast the program as far too ambitious to succeed. Others say it feels like Big Brother; they point out that security agents will have access to the database. Nevertheless, 300 million people have received Aadhaar numbers since the authority's enrollment centers, scattered across the country, opened in September 2010.

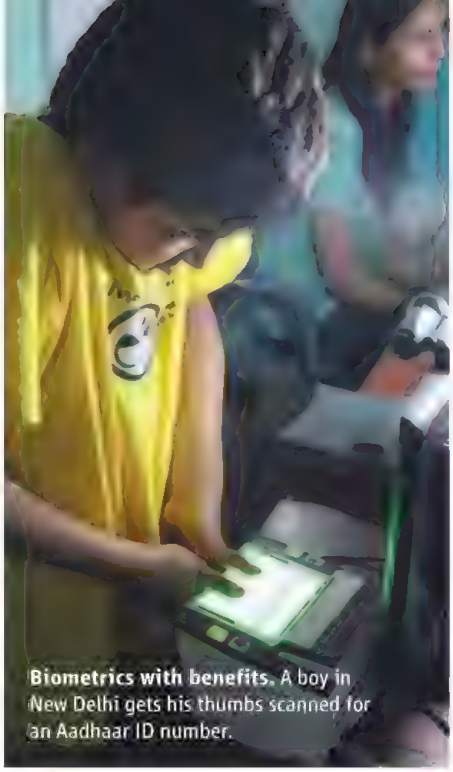

Biometrics with benefits. A boy in New Delhi gets his thumbs scanned for an Aadhaar ID number.

The system's raison d'etre is authentication: Biometrics offers a simple and more reliable way to verify a person's identity. With corporate partners, UIDAI is now rolling out a micro-ATM system in which welfare payments and other government benefits are directly paid into the ID holder's account, rather than getting routed through leaky and often corruption-ridden government channels. Beneficiaries will be able to receive their payments at shops equipped with fingerprint or iris scanners. And students may be required to have Aadhaar numbers when sitting for nationwide tests.

Nationwide connectivity is transforming India in other ways as well. Today, the country has 900 million cell phones. "Only about 35% of Indian homes have toilets. About 60% have mobile phones," says Jairam Ramesh, who as India's minister for rural development is searching for innovative solutions for poverty alleviation (see p. 1034).

Text messaging services now alert farmers to prevailing market prices, enabling them to decide how and where to sell commodities before leaving the farm. In the past, they would have to lug their wares to a market and hope for the best. Fishers, too, are reaping the benefits of technology. Using data gathered by its satellite fleet, the Indian Space Research Organisation maps plankton-rich zones within 20 nautical miles of India's coast where fish are likely to congregate. It then feeds daily fishing forecasts, as well as wave height and other data, to Village Resource Centers pioneered by the M. S. Swaminathan Research Foundation (MSSRF) here. "We're getting a lot of feedback from fisher folk," says MSSRF information specialist Nancy J. Anabel. "Now

Q: Why is poverty so entrenched in India?

J.R.: It has nothing to do with science. It is the failure of land reform. We have not ensured equal access to land. We've had a horrendously iniquitous caste system, which is still very much prevalent in our country. Public health successes in India have reduced mortality rates drastically, but we've had a tripling of our population since independence. So the causes of poverty are complex, and the causes of poverty are not linked to the availability or nonavailability of science and technology.

One shouldn't make the mistake of giving science and technology more power than it actually has to alleviate poverty. Sure, it has a place to reduce drudgery, for example, if you can develop improved cookstoves. But how do you disseminate 150 million cookstoves?

Q: What about a McDonald's of cookstoves?

J.R.: McDonaldization has taken place in a few areas. Mobile telephones are the most ubiquitous instrument of rural transformation today. But in other areas, we have not been very successful. Cookstoves is a classic example. We've been at this cookstove game for almost 40 years. But whether improved stoves have actually penetrated rural households, I find no convincing answer.

Q: Will the universal ID (see p. 1032) make a major difference?

J.R.: It is a very big technological intervention that will have a major transformative effect in rural areas. All pension payments will be delivered electronically to the doorstep of the beneficiaries.

Q: How long will it take for everyone in India to have a universal ID?

J.R.: It is a huge priority issue. We hope that by the end of 2014, all subsidy payments, whether it is a kerosene subsidy or cooking gas or whatever subsidy, will be through this route, through micro-ATMs.

Q: So you need 600,000 micro-ATM machines, one for every village?

J.R.: At least. From a rural point of view, this is a game changer. It gives you a channel for delivery: cash benefits in a relatively hassle-free environment.

Q: India helped find water on the moon. But it struggles to provide clean drinking water to its people. Why?

J.R.: Water is a good example of where science is coming to our rescue. In 1987, there were about 50,000 villages in India without drinking water sources. Satellites helped locate sources for these villages within 1.5 kilometers. This was one of the earliest examples of a quick win for science in rural development.

I am not a worshipper of science. I realize the potential of science and the power of science. But I also realize that there is more to life than science itself. And the constraints to the diffusion of knowledge, the societal barriers, those have to be addressed.

CREDIT: PALLAVA BAGLA

they are even asking for species-specific forecasts." Communities see the resource centers "as a source of empowerment," adds V. Selvam, program director of MSSRF's coastal systems research.

A more efficient information flow to farms should also help safeguard the gains of the Green Revolution. In the 1960s, millions of Indians lived from "ship to mouth," surviving on boatloads of wheat imported from the United States. Thanks to the introduction of high-yield dwarf varieties about 40 years ago, India has since become a net exporter of wheat, but there are concerns that a strain of wheat rust called Ug99 could devastate harvests. Wheat farmers across the country now use their cell phones to send pest sightings and general growing conditions to the Directorate of Wheat Research in Karnal. So far, Ug99 has not been seen in India, says Indu Sharma, the directorate's head.

The essential role of farmers in crop disease surveillance underscores the point that knowledge flow goes both ways. In Ahmedabad, the National Innovation Foundation gathers local wisdom in "people registers": local technologies honed over centuries or millennia. One recent find is a nonstick surface for cookware developed by the Bhils, a tribal community in Madhya Pradesh state. They coat earthenware pots with a resin secreted by insects that infect certain plants. The nontoxic preparation is being commercialized; profits will flow back to the Bhil. It's an example of how "minds on the margins are not marginal minds," says Anil Gupta, the foundation's executive vice president.

Knowledge flows both ways. Anil Gupta (*left*) of the National Innovation Foundation points to the Bhils tribal community's nonstick cookware as a technology worthy of wide dissemination.

Crucibles of ideas

Two young blackbuck antelope lock their twisting horns in a violent clatter. Several meters away, placidly grazing, a rare albino blackbuck seems to pay no heed to the sparring match. IIT Madras students in the vicinity are also blasé: They get to experience a cervid safari every day. A half century ago, IIT Madras's 2.5-square-kilometer campus was carved from Guindy National Park. Although the institution's coexistence with nature hasn't always been harmonious—a troop of bonnet macaques that prowls the leafy grounds has tested the administration's tolerance—it has nevertheless helped IIT Madras stand out in Indian academia.

No single institution in India can lay claim to the mantle of doing the most to help the neediest. Indeed, as Pitroda and others have pointed out, academia's track record at tackling societal ills is spotty at best. But as awareness of the need for action grows, IIT Madras and a handful of other centers have become test beds of new ideas. "Our focus today is on transformation research," says IIT Madras Director Bhaskar Ramamurthi.

One area in which they hope to make a difference is affordable housing. "We have a huge housing shortage in India," says Devdas Menon, an IIT Madras civil engineer. In the center of campus, Menon's team last month finished putting up a model house divided into four apartments built from glass fiber-reinforced gypsum. It took a mere 29 days to erect, at a cost of $2000. The technology is not new. Australia pioneered the concept more than 20 years ago, in which gypsum, a common waste in industries such as fertilizer production, is milled with glass fibers to form water- and fire-resistant paneling. Despite the fact that the paneling is much lighter than concrete or other traditional building materials, it can be used to construct earthquake-resistant structures up to 10-stories tall, Menon says. A several-story building would take less than 6 months to build, he says: about one-fifth the time it would take to put up a steel and concrete building.

The model home will also accommodate a pie-in-the-sky idea: village-level direct current (DC) electricity supplies. One half of the model home will run on AC, the way power is commonly supplied from a grid, and the other half will run on DC: how batteries generate power and how communities across India were supplied with electricity several decades ago.

Energy is a critical limiting factor in efforts to boost rural livelihoods. "Energy demand is rising dramatically. People throughout India are buying air conditioners so fast, it's scary to think where we're heading," says Ramamurthi, an electrical engineer by training. Solar and other renewable energies have "great potential in the countryside," he says, but they are hard to stably feed into a power grid. Thus, he and Jhunjhunwala are working on a prototype in which villages can run off-grid, on solar-powered DC power stations. They say that they will know within 6 months whether their concept is feasible.

A more pressing concern for Jhunjhunwala is the Aakash 4 debut. If the tablets can meet performance standards on 151 benchmark tests, "the project will be successful," predicts computer scientist Rajat Moona, director general of the Centre for Development of Advanced Computing in Pune. "The project is headed in the right direction now," he says. Even more bullish is Kannan Mani Moudgalya, a chemical engineering professor at IIT Bombay. "Aakash is a great idea," he says. As software applications for Aakash mature, he predicts, the tablet, "without any doubt," will help give Indian children a richer, higher quality education.

Just beyond the walls of IIT Madras's research park, where the Aakash 4 prototypes are being put through their paces, a sprawl of tenements is haphazardly strung with laundry drying in the sun on a steamy day. It's the sort of scene that Jhunjhunwala and his colleagues hope to transform through education, as fast as they possibly can. "We're racing against time," he says.

–PALLAVA BAGLA AND RICHARD STONE

CREDITS: PALLAVA BAGLA (2)

Street cred. A researcher gathers data on household income in a rural area of Shandong Province.

SOCIAL SCIENCE

The Numbers Game

In China, statistics have long been skewed by their use in rewarding performance; social scientists say they are beginning to remove those distortions

SHANGHAI, CHINA—When economist Gan Li set out in 2009 to survey thousands of Chinese households on income and assets, he had a modest goal: Expand the nation's scant information about its economic life. No detailed household survey data were available that could offer a fair picture of the situation nationwide. Everything from household wealth to the percentage of Chinese owning multiple homes was unknown. China had—and still has—"very little knowledge about its baseline," says Gan, who splits his time between Texas A&M University, College Station, and Southwestern University of Finance and Economics in Chengdu. His project, called the China Household Finance Survey, got little direct support from China's National Bureau of Statistics (NBS), effectively the only source of household income information then, Gan says. But the bureau didn't try to block his work.

Gan's ability to quietly research vanished, however, when he and colleagues used their data to estimate China's Gini coefficient, a common index of income inequality. It runs on a scale from 0 to 1, with 1 being severe inequality. Accepted wisdom held that a Gini coefficient above 0.4 yields societal instability, and Gan had assumed that anything above 0.6 would be "maybe revolutionary." NBS had last released a Gini value in 2000, when it was 0.41. In findings released last December, Gan and colleagues calculated it at 0.61.

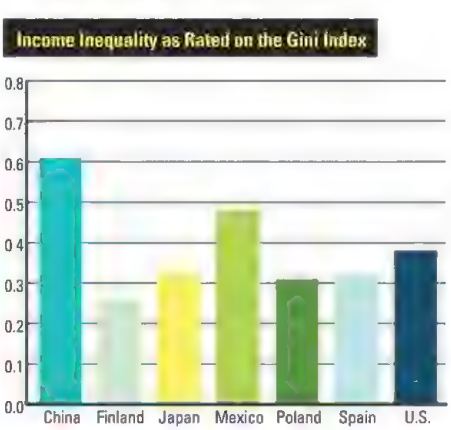

High on disparity. A 2012 study placed China among the nations with the largest income differences.

CREDITS: CHINA HOUSEHOLD FINANCE SURVEY (2)

NBS officials countered Gan's research by pointing to his small sample size and the fact that he employed novice student interviewers. (Gan says that his sample has an error of only 1%, and the surveyors underwent 56 hours of training.) A mere month after Gan and colleagues published their findings, NBS released its own, lower estimate for China's Gini coefficient: 0.47. At a press conference in January, bureau Director Ma Jiantang explained that although it was high, inequality in China had been declining since 2008—a claim that is impossible to check because NBS did not release its sample selection method, complete data at the individual respondent level, or the nonresponse rate for the surveys underlying the calculations.

The bureau's attempt to steal the spotlight flopped. Chinese media seized on Gan's number, prompting an outcry online. The reported yawning income gap caused a big sensation, says Yu Xie, a sociologist at the University of Michigan, Ann Arbor, and Peking University, who is not affiliated with the survey. The controversy highlights just how volatile a reaction to new data can be in China. And it shows how difficult it is to derive accurate statistics when reports are distorted by government incentives and cloaked in secrecy. "The research community is really starving for data," says Zhao Yaohui, an economist with Peking University's China Center for Economic Research.

The accuracy and availability of data in China vary by field. But some themes crop up again and again: Cases are under- or overreported, data are obtained but not released, and definitions and methodologies shift from one use to the next. These problems are more pressing now, as fields like sociology and economics are rapidly developing. The lack of access to good data, Zhao says, has become a "major hindrance to the advancement of the social sciences in China."

Deconstructing the data

The roots of China's problems are partly systemic; statistics get both too little and too much respect. A numbers-driven country, China has an "old, centralized administration that collects data on everything," says Carsten Holz, an economist who specializes in Chinese statistics at Hong Kong University of Science and Technology. Government officials are evaluated on indicators such as environmental protection rather than on their overall performance. Under the *yi piao fou-*

Reaching out. In rural Henan Province, a survey on household income sent interviewers out to gather data from a broad sample of citizens.

jue, or "one-vote down," system introduced in 1991, local officials who poorly perform in one of several key areas can face wage cuts or dismissal. As the saying goes, *shuzi chu guan*: "Numbers make leaders."

As a result, notes Liu Junguo, a hydrologist at Beijing Forestry University, the inverse is also true: *guan chu shuzi*, or "leaders make numbers." Scholars say that outright cooking of the books is rare, perhaps because it's a red flag: With data released consistently every month or every year, says Yong Cai, a demographer at the University of North Carolina, Chapel Hill, "it's very difficult to fake something in a systematic way without being caught." Instead, officials may change definitions so that one year's data are not comparable to previous years'. "Local officials are manipulating a little of the gray area rather than outright fabricating," says Kam Wing Chan, a geographer at the University of Washington, Seattle. But for scholars seeking accurate figures, this can be infuriating. As a result of political incentives, "all indicators of well-being" are suspect, Xie says.

For instance, in determining per capita gross domestic product (GDP) or the unemployment rate, a mayor may conveniently exclude millions of struggling migrant workers. Because they lack an urban residence permit, migrants are not counted in a city's population. When they are included, a city's report card can change dramatically, says Chan, who studies migration in China. With migrants excluded from the population of Shenzhen, a booming industrial city near Hong Kong, the city had a per capita GDP of about $21,700 in 2000. When migrants were counted, Chan found in a paper for the July 2007 issue of *Eurasian Geography and Economics*, the figure plummeted to $3900.

Challenger. Gan Li's group found significant income disparity in China.

Compounding China's data woes are policies that encourage concealing information. Because of limits imposed by the one-child policy, some parents do not register births of second and third children, complicating attempts by demographers to track population changes. "If you want to get a timely number you have to rely on local numbers, and everyone knows those numbers are not reliable," Cai says. For a more accurate birthrate, demographers often wait a few years to see if unreported children crop up at the age when school enrollment begins.

NBS makes corrections to aggregate data for such misreporting. "They are aware of the limitations of data," Xie says. But because the bureau does not typically release complete data sets or detailed methodology, it is impossible for scholars to check how the numbers are modified. "They don't tell you how they got to where they got," says Avraham Ebenstein, an economist at the Hebrew University of Jerusalem who studies China. "So you don't know if the data are good and bad." An NBS spokesperson wrote in an e-mail that the bureau publishes information about the "subjects, survey methods, [and] statistical range" of its data.

NBS occasionally releases household income microlevel data, or data at the individual respondent level, but it does so only for a handful of provinces at once, according to several scholars—a tactic that prevents independent calculations of the Gini coefficient from official statistics. "The government is tremendously tight-fisted with these data," Ebenstein says. "It's as if, 'We want you to do research, but we don't want it to be too good.'"

Global repercussions

Statistics are hardly the only research tool that Chinese officials view as dangerous in the wrong hands. Detailed topographic maps and GPS devices are tightly controlled as well (*Science*, 25 January, p. 384). But holding back data has a broader impact by tainting research not exclusively focused on China. Because global indices compiled by the United Nations and World Bank often incorporate figures furnished by Chinese government agencies, misleading statistics can skew global comparisons.

China's birthrate is a case in point. To correct for underreporting by parents and local officials, Cai says, NBS adjusts its estimate of the crude birthrate, but "we never know the mechanism." China's National Population and Family Planning Commission, which was recently combined with the health ministry, issues separate population projections that are even sketchier. Working backward from the figures, demographers can derive a total fertility rate, or the number of children the average woman is expected to have over her lifetime—and they contend that officials deliberately overestimate the rate. A high birthrate keeps the family planning commission in business: "High fertility is the very foundation of its existence," Cai says.

In 2008, the population commission's estimates sparked a debate when the United Nations Population Division (UNPD) released its biannual *World Population Prospects* report, with projections to 2050. Cai and demographer Gu Baochang of Renmin University of China in Beijing noticed that UNPD's estimates put China's total fertility rate for 2000 to 2005 at 1.77, close to the family planning commission's estimate of 1.73—and predicted that fertility would increase from there. The two demographers suspect that UNPD relied on a 2006 population commission survey that scholars widely consider biased. Invited to comment, they suggested lowering the estimate to about 1.5.

The appeal may have had some impact. Projections in UNPD's revised *World Population Prospects* in 2010 imply a total fertility rate of 1.70 for 2000 to 2005 and shows births declining after that. The shift is significant: The difference between the two reports' esti-

CREDITS: CHINA HOUSEHOLD FINANCE SURVEY (2)

mates for global population in 2010 is 12.81 million people. "That can almost entirely be attributed to the adjustment of the Chinese population," Cai says.

Inside China, drama surrounding Chinese statistics extends beyond numbers. In 2006, NBS head Qiu Xiaohua was removed from his post after being investigated for involvement in a pension fund scandal. A Chinese Communist Party commission expelled him from the party for accepting bribes and keeping multiple wives, issuing a statement saying he had exerted "vile social and political influence." In recent years, NBS has become a favorite target of Chinese social media users. In one popular online jibe, commentators referred to the bureau as *tongji ju*, a homonym for its official name that means "the Bureau of Dicking Around."

Such jabs at the government's lack of transparency are gradually yielding change. Much as Gan's study appears to have provoked NBS to release its own Gini coefficient, outcry over incomplete air pollution data prompted the government in January to begin measuring concentrations of harmful particulate matter less than 2.5 micrometers in diameter for many Chinese cities (*Science*, 11 January, p. 124). "The government is under more and more pressure to release data of public interest," Xie says. In 2009, China introduced a regulation stipulating punishment for concocting statistics or encouraging others to do so (*Science*, 7 August 2009, p. 675). NBS also now regularly sends teams to check the methods of its local branch offices.

Some scholars say that data quality in their fields is improving. Liu notes that in recent years, when China's environment ministry was strictly monitoring water quality—boosting the incentive for local officials to clean up polluted rivers and lakes—official data nonetheless show a deterioration. For China-oriented researchers accustomed to reading the tea leaves, such depressing statistics are actually an encouraging sign that "the quality of statistics is improving," Liu says. Certain economic calculations are progressing as well, says Holz, who is editing an upcoming special issue of the *China Economic Review* focused on Chinese statistics. China has long been accused of doctoring its national GDP figures to maintain the impression of continued high economic growth. But although no evidence so far definitively shows that the NBS figures are correct, "nobody so far has been able to prove the NBS data wrong," Holz says.

But Chinese agencies are still a far cry from their U.S. counterparts, many of which employ scholars on rotation and staff liaisons to facilitate use of government data by outside experts. Ebenstein says that China is "just much more cautious" about letting results fall where they may. It doesn't help that intense pressure to publish makes many Chinese scholars reluctant to share what they have. "Traditionally," Zhao says, "people collect data and hold on to it—and don't let others use it." Xie agrees: "There is no norm for data sharing."

Playing the numbers. Critics say data-driven goals—such as China's one child policy touted in a poster have fueled statistical errors.

CREDIT: © BETTMANN/CORBIS

Upstart surveys

A growing number of scholars hope to change that culture by challenging what Xie calls NBS's "monopoly." The China Household Finance Survey is just one of several notable efforts to generate independent microlevel data. In the past 5 years, a number of similar longitudinal, nationally representative surveys have cropped up in China to fill the vast data holes. Among them are the Chinese General Social Survey, a project spearheaded by Renmin University's National Survey Research Center in Beijing that queries respondents on questions like religion, social inequality, and health; the Chinese University Student Learning and Development Follow-Up Research project, a survey tracking university students throughout their lives led by Tsinghua University in Beijing; the Chinese Family Panel Studies, a survey of 60,000 respondents on everything from child care to election participation run out of Peking University in Beijing (*Science*, 30 April 2010, p. 554); and the China Health and Retirement Longitudinal Study (CHARLS), also overseen by researchers at Peking University, which aims to shed light on issues faced by China's rapidly aging population.

Increased funding for social science research, both at universities and at China's government science institutions, is behind the new wave of surveys, says Zhao, a co–principal investigator for CHARLS. Her survey, which covers 17,500 respondents over age 45, is modeled in part after the University of Michigan's Health and Retirement Study. It benefited from an $813 million grant from a program launched by the National Natural Science Foundation of China in 2012 to fund research that generates large data sets. CHARLS aims to release data within a year after a survey round, which is faster than many similar surveys in other countries. The independent surveys can be "used to either validate or check against government statistics," says Xie, who helped design the Chinese Family Panel Studies survey.

Officials need not instinctively fear the emergence of such upstart fact checkers, says Gan, who is planning to launch a new survey round for the China Household Finance Survey in July that expands his sample size by 50%. When he and colleagues arrived at a high Gini coefficient, he went back to find the study that, years ago, determined that 0.4 is the threshold for instability—and came up with no published papers on the topic. Instead, he found numerous studies suggesting that it is opportunity inequality, and not simply income inequality, that sparks instability. Although Gan believes that China should redistribute wealth, the explanation for its stability, he says, is that people in China "believe that they can move up, and there are also institutions helping them move up." For the moment, at least, "there is this mobility" in China.

Numbers like the Gini coefficient are not inherently threatening, Gan contends. It all depends on their interpretation.

–MARA HVISTENDAHL

LETTERS

edited by Jennifer Sills

Education Guidelines Fail to Inspire

SELDOM IN THE SPECIAL SECTION ON GRAND CHALLENGES IN SCIENCE Education (19 April, p. 290) do I see the words "inspiration" or "excitement."

The News story "Transformation is possible if a university really cares" (J. Mervis, p. 292) suggests starting "by asking what the faculty member wants students to know how to do at the end of the course" and approves of applying "basic concepts to real-life situations." That is suitable for an engineering course or for basic physics, but what if your goal for nonscience students is to foster inspiration, excitement about what they have learned, and enthusiasm for supporting science by reading newspaper or magazine articles on STEM topics or by voting for candidates who demonstrate scientific experience or understanding?

The Review "Physical and virtual laboratories in science and engineering education" (T. de Jong *et al.*, p. 305) acknowledges the importance of enthusiasm by suggesting that actual labs are more successful than virtual ones in creating "young people who are skillful in and enthusiastic about science," but the article is aimed at those "who view science as their future career field."

Meanwhile, the Review "Outside the pipeline: Reimagining science education for nonscientists" (N. W. Feinstein *et al.*, p. 314) describes the goal of "nonscientists who can access and make sense of science relevant to their lives." I agree that we want nonscientists to "judge the credibility of scientific claims," but I contend that teaching about exciting, mind-bending, and current results can inspire students to do better in all their studies, not just those in science courses.

I suggest adding several components to the list of Next Generation Standards listed in the Venn diagram in "Opportunities and challenges in next generation standards" (E. K. Stage *et al.*, Education Forum, p. 276). Students should recognize that many scientific questions are currently unsolved. They should study current trailblazers and the sequence of discovery. Courses should emphasize the importance of current research. Each topic should end with a summary of some outstanding questions.

Without context, students may leave school thinking that physical science ended with Newton and that it isn't important to support our current research efforts. They may believe that scientific problems have been solved and can all be dealt with in classroom-quality laboratories.

JAY M. PASACHOFF

Department of Astronomy, Williams College, Williamstown, MA 01267, USA. E-mail: eclipse@williams.edu

Self-Medication: A Learning Process?

WE WELCOME THE RECOGNITION THAT SELF-medication in animals is widespread ("Self-medication in animals," J. C. de Roode *et al.*, Perspectives, 12 April, p. 150). However, we disagree with the assumption that learning is only a valid explanation of self-medication for animals with high cognitive abilities and the ability to make "conscious decisions." This assumption underestimates the power and pervasiveness of learning.

Conditioned flavor aversions provide a flexible and effective mechanism for all animals to assemble balanced, nutritious, and safe diets and have been demonstrated in vertebrates, insects, and mollusks (*1*–*3*). Even slime molds can adjust their diets to meet specific nutritional needs (*4*). Animals continually adjust and refine their diet preferences to achieve a state of nutritional and neurological homeostasis in the face of perturbation by nutritional deficits and excesses, ingestion of toxic compounds, and also, we suggest, infection by pathogens and parasitoids (*5*). Simple animals can be guided by limited experience toward diets that achieve homeostasis through therapeutic self-medication, without cognitive awareness.

De Roode *et al.* suggest that to convincingly demonstrate that a behavior is an adaptive form of therapeutic medication, it must be shown to be relevant in the host's natural environment. Although this is necessary to demonstrate a behavior's adaptive significance, studies with novel therapeutic substances can test the flexibility of therapeutic self-medication strategies and establish the true roles of learning and of hard-wired responses. We urge researchers not to overlook the myriad fascinating processes that may underlie self-medication by any organisms.

BEN D. MOORE,[1]* WILLIAM J. FOLEY,[2] JENNIFER S. FORBEY,[3] JANE L. DEGABRIEL[4]

[1]Hawkesbury Institute for the Environment, University of Western Sydney, Penrith, NSW 2751, Australia. [2]Research School of Biology, The Australian National University, Acton, ACT 0200, Australia. [3]Department of Biological Sciences, Boise State University, Boise, ID 83725–1515, USA. [4]Office of Environment and Heritage, Sydney, NSW 1232, Australia.

*Corresponding author. E-mail: b.moore@uws.edu.au

References

1. R. Sugai *et al.*, *J. Exp. Biol.* **209**, 826 (2006).
2. J. J. Villalba *et al.*, *Anim. Behav.* **71**, 1131 (2006).
3. G. A. Wright *et al.*, *Curr. Biol.* **20**, 2234 (2010).
4. A. Dussutour, T. Latty, M. Beekman, S. J. Simpson, *Proc. Natl. Acad. Sci. U.S.A.* **107**, 4607 (2010).
5. J. S. Forbey *et al.*, *Integr. Compar. Biol.* **49**, 314 (2009).

Response

WE AGREE WITH MOORE *ET al.* that learning is widespread among organisms of vastly different cognitive abilities, providing the potential to adjust diet to combat agents of disease. However, the key word here is "potential." None of the articles cited by Moore *et al.* on insects (*1*), mollusks (*2*), or slime molds (*3*) actually presents evidence of learned medication behavior. Instead, they provide evidence that learning can adjust the behavior of organisms in response to the palatability or nutritional content of food. We certainly agree that learned responses to food quality should influence aspects of disease susceptibility in a much wider variety of organisms than only vertebrates (*4*), but evidence for it remains poor at present. Rather, our Perspective describes documented examples of medication behavior against agents of disease.

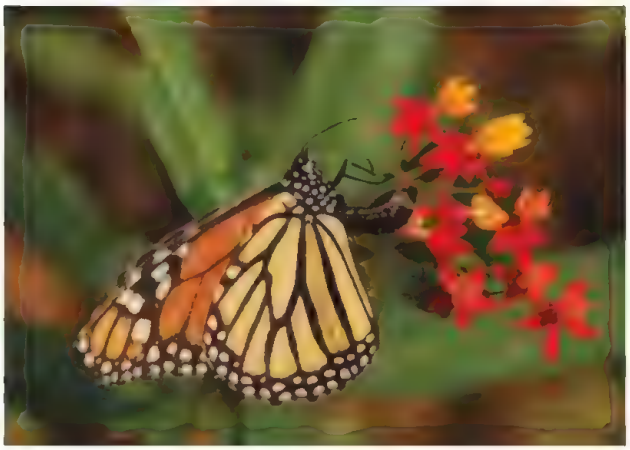

A monarch butterfly lays an egg on milkweed.

While we agree that assessing the role of learning in medication behavior is an important goal across taxa, we also suggest that an overemphasis on learning is not helpful because it can exclude important alternative mechanisms. For example, the emerging studies of medicating kin that we describe in our Perspective (*5*, *6*) are unlikely to be "guided by limited experience toward diets that achieve homeostasis." Diseased monarch butterflies preferentially oviposit on medicinal milkweed, which reduces disease in their offspring (*5*). This behavior does not involve ingestion of the plants and thus is not regulated by internal homeostasis. In general, medicating kin appears to result from innate behaviors rather than individual learning.

We also agree that artificial diets can be useful for exploring the flexibility of medication behavior. Experiments with artificial diets allow researchers to evaluate how dietary choices enable hosts to offset the costs of disease resistance (*7*, *8*). Nonetheless, the evolutionary and ecological consequences of medication that we describe in detail in our Perspective can only emerge when medication behaviors take place beyond the simplified universe of the laboratory.

JACOBUS C. DE ROODE,[1]* THIERRY LEFÈVRE,[2] MARK D. HUNTER[3]

[1]Department of Biology, Emory University, Atlanta, GA 30322, USA. [2]Maladies Infectieuses et Vecteurs: Écologie, Génétique, Évolution et Contrôle, UM1-UM2-CNRS 5290-IRD 224, Institut de Recherche pour le Développement, Montpellier 34394, France. [3]Department of Ecology and Evolutionary Biology, University of Michigan, Ann Arbor, MI 48109–1048, USA.

*Corresponding author. E-mail: jderood@emory.edu

References

1. G. A. Wright *et al.*, *Curr. Biol.* **20**, 2234 (2010).
2. R. Sugai *et al.*, *J. Exp. Biol.* **209**, 826 (2006).
3. A. Dussutour, T. Latty, M. Beekman, S. J. Simpson, *Proc. Natl. Acad. Sci. U.S.A.* **107**, 4607 (2010).
4. J. S. Forbey, M. D. Hunter, in *The Ecology of Plant Secondary Metabolites: From Genes to Global Processes*, G. R. Iason, M. Dicke, S. E. Hartley, Eds. (Cambridge Univ. Press, Cambridge, 2012), pp. 78–100.
5. T. Lefèvre, L. Oliver, M. D. Hunter, J. C. de Roode, *Ecol. Lett.* **13**, 1485 (2010).
6. B. Z. Kacsoh, Z. R. Lynch, N. T. Mortimer, T. A. Schlenke, *Science* **339**, 947 (2013).
7. K. P. Lee, J. S. Cory, K. Wilson, D. Raubenhaimer, S. J. Simpson, *Proc. R. Soc. London Ser. B Biol. Sci.* **273**, 823 (2006).
8. S. Povey, S. C. Cotter, S. J. Simpson, K. P. Lee, K. Wilson, *J. Anim. Ecol.* **78**, 437 (2009).

CORRECTIONS AND CLARIFICATIONS

Reports: "Enantioselective synthesis of pactamycin, a complex antitumor antibiotic" by J. T. Malinowski *et al.* (12 April, p. 180). Reference 31 should be "R. Shen, C. T. Lin, E. J. Bowman, B. J. Bowman, J. A. Porco, *Org. Lett.* **4**, 3103 (2002)." Also, this reference should be referred to in the text as "Shen *et al.*" The HTML and PDF versions online have been corrected.

News Focus: "The deep Earth machine is coming together" by R. A. Kerr (5 April, p. 22). The global map was incomplete. Due to a production error, 24 of the 25 Large Igneous Provinces (LIPs) had been deleted. In the corrected map (shown here), 23 of the 25 LIPs fall near the edges of LLSVPs—the two piles of material on the bottom of the mantle—suggesting that rising plumes connect LLSVPs to volcanic centers on the surface. The image has been corrected in the HTML and PDF versions online.

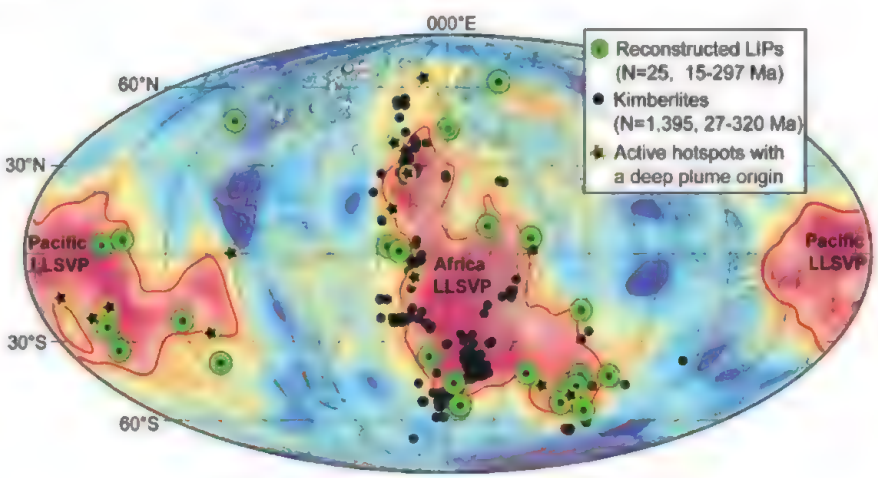

Perspectives: "The perfect hypnotic?" by E. Mignot (5 April, p. 36). Chloral hydrate, meprobamate, and barbiturates were touted as nonaddictive miracle tranquilizers at the beginning of the 20th century, not at the beginning of the 19th century as indicated in the first line of the second paragraph. The HTML and PDF versions online have been corrected.

News: "The downside of diversity" by J. Kaiser (special section of Cancer Genomics, 29 March, p. 1543). The article incorrectly attributed "punctuated evolution" to Darwin. The concept comes from the hypothesis of "punctuated equilibrium" proposed by Niles Eldredge and Stephen Jay Gould in 1972. The HTML and PDF versions online have been corrected.

News Focus: "Pollutants capture the high ground in the Himalayas" by J. Qiu (1 March, p. 1030). In the map on p. 1031, the relative locations of Mt. Everest and the Nepal Climate Observatory at Pyramid are inaccurate. The correct coordinates for Pyramid station are 27.95 N, 86.82 E, and for Mt. Everest are 27.99 N, 86.93 E.

Letters to the Editor

Letters (~300 words) discuss material published in *Science* in the past 3 months or matters of general interest. Letters are not acknowledged upon receipt. Whether published in full or in part, Letters are subject to editing for clarity and space. Letters submitted, published, or posted elsewhere, in print or online, will be disqualified. To submit a Letter, go to www.submit2science.org.

Little Genius

BLItz

BLItz brilliantly packs the power of Dip and Read™ label-free analysis into a personal assay system. Give BLItz a drop of your sample and it does the rest!

- Protein presence/absence in seconds
- Binding kinetics assays at your bench
- Protein quantitation in seconds
- Develop immunoassays in minutes
- Easily analyze crude samples

Cleverly priced under $20K so you can have your own little genius.

Want to try BLItz in your lab? Visit BlitzMeNow.com or call 855.BLITZ.ME.

fortéBIO
A Division of Pall Life Sciences

PALL Life Sciences

SOCIAL SCIENCES

A (Science-Based) Poor Kids' Manifesto

Samuel Bowles

James Heckman opens his compelling essay with "The accident of birth is a principal source of inequality in America today. American society is dividing into skilled and unskilled. … [B]irth is becoming fate." To counter that trend, Heckman argues for a "strategy that works," based on the following logic: "[B]oth cognitive and socioemotional skills develop in early childhood, and their development depends on the family environment." Growing up poor deprives children of opportunities to develop these skills, and "family environments in the United States have deteriorated." In response, Heckman advocates early interventions such as the enriched preschool environments and home visits by professionals to assist parents that his research shows can "produce positive and lasting effects on children in disadvantaged families."

The take-home message is that the kids of poor parents often grow up to be poor, that this fact has little to do with genetics and everything to do with the socioemotional behaviors associated with growing up poor, and that something can be done to break this cycle of poverty. If you are losing patience with overblown claims and rhetoric by policy advocates, read this book: It's not every day that you get a pro-poor manifesto written by an econometrician whose Nobel prize was awarded for advances in the quantitative evaluation of the effectiveness of public policy.

Giving Kids a Fair Chance is remarkable for the scientific advances that it represents, in good part due to Heckman and his co-authors. When Lyndon Johnson launched his War on Poverty 50 years ago, most economists would have objected to the book's first two claims: that economic success and failure run in the family and that nongenetic and noncognitive aspects of behavior are central to this process. As recently as the late 1980s, Heckman's colleague at the University of Chicago and fellow Nobel laureate Gary Becker could affirm the "land of opportunity" moniker for the United States: "Aside from families victimized by discrimination … [a]lmost all earnings advantages and disadvantages are wiped out in three generations" (*1*). In his presidential address, Becker reassured the members of the American Economic Association that "low earnings as well as high earnings are not strongly transmitted from fathers to sons." (*2*).

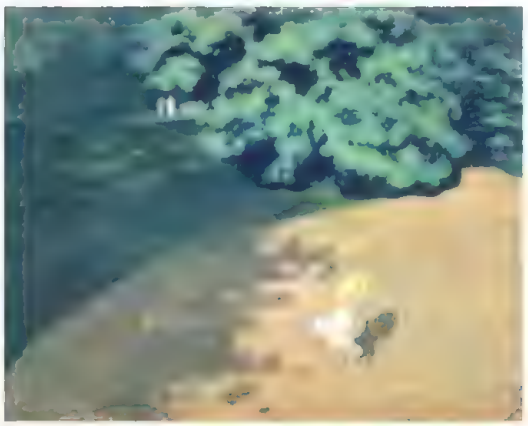

Felix Edouard Vallotton, *The Ball* (1899).

The third claim—that we can do something to help poor kids succeed—was the hope animating Johnson's War on Poverty, but it was based on no convincing evidence. Arthur Jensen began a celebrated 1969 paper "Compensatory education has been tried, and apparently it has failed" (*3*), and he pointed to genetic limits to raising the cognitive skills of poor kids.

But we now know that Becker's optimism was based on a statistical lapse: what appeared to be high levels of intergenerational mobility in his data resulted from a failure to take into account measurement errors that reduce the statistical association between indicators of parental and offspring economic status (*4*–*7*). Much of what looked to Becker like mobility turned out to be statistical noise. The corrected data reveal the United States as a global leader in the extent to which economic success is passed on within families (*8*). And although subsequent years have witnessed many failed attempts to significantly raise the cognitive performance of poor children, convincing evidence for a number of highly effective interventions (*9*, *10*) has challenged Jensen's pessimism on this score.

Giving Kids a Fair Chance
(A Strategy That Works)
by James J. Heckman et al.
MIT Press, Cambridge, MA, 2013. 147 pp. $14.95
ISBN 9780262019132
A *Boston Review* Book.

The reviewer is at the Behavioral Sciences Program, Santa Fe Institute,1399 Hyde Park Road, Santa Fe, NM 87501, USA. E-mail: samuel.bowles@gmail.com

Moreover, what counts as an effective intervention on behalf of the children of the poor has changed. Extending earlier work by Herbert Gintis (*11*), Heckman's own research has overturned the once-dominant notion that effective schooling opens the doors of economic opportunity simply by improving cognitive skills (*12*). Commenting on an intervention whose long-term effects he has closely studied, Heckman notes: "The Perry Preschool Program improved the lives of its participants without increasing their IQ scores, demonstrating why it is problematic to focus curricula exclusively on improving cognitive test scores" (*12*). There is now ample evidence that—whether by altering the noncognitive aspects of behavior stressed by Gintis and Heckman or by raising cognitive performance—improved education (for example, smaller class size) can raise the adult incomes and other measures of socioeconomic success among the children of poor parents (*13*, *14*).

The book stands out among economic studies in its attention to noncognitive skills, "including strength of motivation, an ability to act on long-term plans, and the socioemotional regulation needed to work with others" or "character." We know that the labor market values these traits (*15*), although calling character a skill is not only odd, it hides a possible difficulty (one raised in two of the commentaries that follow Heckman's essay). By a skill, we typically mean some capacity of which more is uncontroversially better; so few parents or citizens object when children are subjected to compulsory skill enhancement (schooling). But if by noncognitive skill or character Heckman means, as it seems, whatever social behavior the labor market rewards, the case is more complicated. There is some evidence, for example, that American workers and students are penalized by firms and schools (in promotions and grades, respectively) if they are seen to be "independent" and "creative" (*16*). Of course, parents want their child to become the kind of adult that employers seek out rather than shun. But nobody (including Heckman, I'm sure) would want the labor market's litmus test—an individual's expected contribution to an employer's profits—to become the sole adjudicator of the kinds of people our children are to become.

For the United States, Heckman makes a strong case that government should provide substitutes to fill the gaps when poor parents—too preoccupied and stressed out making ends meet or getting adequate medical

care, or for any other reason—do not do all that is needed for their kids. But giving poor kids a fair chance requires more than plugging the parenting gaps. It requires addressing the problem of poverty itself.

By the measure of cognitive scores, the youth of a great many countries outscore their American counterparts. What is distinctive about the consistently high-scoring countries such as Finland, Belgium, and South Korea is not the amount they spend on schooling, but the fact that they are far less economically polarized than the United States. The interventions Heckman advocates, as well as other policies to end the inheritance of poverty, are necessary but hardly sufficient. Addressing the poverty of the parents is no less urgent. As the economic dynamism of the countries just mentioned suggests, it need not come at a heavy cost.

References

1. G. S. Becker, N. Tomes, *J. Law Econ.* **4**, 51 (1986).
2. G. Becker, *Am. Econ. Rev.* **78**, 1 (1988).
3. A. A. Jensen, *Harv. Educ. Rev.* **39**, 1 (1969).
4. B. Mazumder, in *Unequal Chances: Family Background and Economic Success*, S. Bowles, H. Gintis, M. Osborne-Groves, Eds. (Princeton Univ. Press, Princeton, NJ, 2005), pp. 80–99.
5. D. J. Zimmerman, *Am. Econ. Rev.* **82**, 409 (1992).
6. S. Bowles, *J. Polit. Econ.* **80** (S3), S219 (1972).
7. S. Bowles, H. Gintis, *J. Econ. Perspect.* **16**, 3 (2002).
8. M. Corak, in *The Economics of Inequality, Poverty, and Discrimination in the 21st Century*, R. Rycroft, Ed. (Praeger, Westport, CT, 2013), pp. 107–124.
9. W. Dobbie, R. G. Fryer Jr., *Am. Econ. J. Appl. Econ.* **3**, 158 (2011).
10. W. Dobbie, R. G. Fryer Jr., "Getting beneath the veil of effective schools: Evidence from New York City," www.nber.org/papers/w17632.
11. H. Gintis, *Am. Econ. Rev.* **61**, 266 (1971).
12. J. J. Heckman, T. Kautz, *Labour Econ.* **19**, 451 (2012).
13. R. Chetty *et al.*, *Q. J. Econ.* **126**, 1593 (2011).
14. P. Fredriksson *et al.*, *Q. J. Econ.* **128**, 249 (2013).
15. S. Bowles *et al.*, *J. Econ. Lit.* **39**, 1137 (2001).
16. S. Bowles, H. Gintis, *Schooling in Capitalist America: Educational Reform and the Contradictions of Economic Life* (Basic Books, New York, 1976).

10.1126/science.1239638

ANTHROPOLOGY

Evolving Beyond Stone Age Fantasies

Catherine Woods

We all yearn for the good old days, but it is probably safe to say most of us aren't referring to the Paleolithic era. A few hardy souls, however, have adopted a paleo lifestyle in the belief that humans are evolutionarily better suited for a presumed environmental and cultural setting that our ancestors occupied between 2.3 million and 10 thousand years ago. Wearing webbed FiveFinger running shoes, eating only meat, and donating blood regularly (to mimic ancestral iron levels), these paleo devotees drastically change their lives to be more like our prehistoric ancestors. They subscribe to the belief that our physiology and culture are at an imbalance with our current climate. They are, in short, living out paleofantasies.

Paleofantasy
What Evolution Really Tells Us About Sex, Diet, and How We Live
by Marlene Zuk
Norton, New York, 2013
336 pp. $27.95, C$29.50.
ISBN 9780393081374.

In *Paleofantasy: What Evolution Really Tells Us About Sex, Diet, and How We Live*, Marlene Zuk tackles the paleofantasies of exercise, diet, and family dynamics with a clever sense of humor. Using content from scientific journals to informal paleo blogs, Zuk (an evolutionary biologist at the University of Minnesota) works hard to convey a simple idea—longing for the days before tool use is not only unnecessary but silly.

Let's paint a basic picture of this fantastical Paleolithic man. He is a barefoot forager with a wife and kids. His battles come in spurts, requiring strength to throw stones but not endurance to run long distances. His family's mobile existence prevents them from keeping animals and managing crops. And the most essential component of the fantasy: no Paleolithic man deviates from this routine.

Although Zuk dissects these behaviors, her primary arguments resonate against all aspects of the paleo lifestyle. She highlights the growing evidence that the behavior of paleo humans, whether it is diet or matrimony practices, was not uniform. The lives of our paleo ancestors differed, much in the same way that not all humans today live in high-rises or do yoga.

Paleofantasy reinforces the theme that evolution continues, even for humans. Zuk acknowledges that our ability to take down a saber-toothed tiger would require more gadgets (running shoes, contact lenses, a global positioning system) than our prehistoric ancestors might need. But how would a caveman fare in managing our modern-day stock market or finding his way out of an Ikea? Bipedalism and big brains emerged from the Paleolithic era to be used against today's challenges. Humans are most certainly still evolving, just not necessarily in ways we might expect.

Zuk also does well to remind us that evolution has no specific end goals: "[N]o organism gets to a point of perfect adaptation, heaves a sigh of genetic relief, and stops." The biggest problem with paleofantasies is that they assume that at one point humans were in balance with their surroundings. But evolution never stops to rest. Climate, geography, bacteria, and even humans do not exist independent of one another; as changes occur in one part of the world, evolution follows in all other parts.

While evolution may seem like a dry topic to some, Zuk keeps readers entertained by poking fun at her paleo opponents and using clever section titles such as "Cavemen in Condos." Even for those who haven't heard of the paleo lifestyle, Zuk's book is full of entertaining tidbits such as recently evolved genetic variants that predict athleticism or give us the ability to breathe at high altitudes.

Targeting the popularized Paleolithic man is really just a strategy for Zuk's larger goal of celebrating evolution. The degree to which she emphasizes present-day adaptations over paleo counterarguments can leave the reader thirsty for more details on evolution.

At no point does Zuk make dire predictions that practicing the paleo lifestyle will lead to tragedy, illness, or death. Rather, she dispels the idea that living like our ancestors provides some kind of advantage. *Paleofantasy* is not another self-help book offering answers on how to eat, exercise, or love better in our evolving world. Instead, Zuk emphasizes that we can approach these aspects of our lives differently based on our genetic makeup.

All of Zuk's facts and anecdotes remind us that who we are goes far beyond our career or recent recollections. Instead we carry with us a set of genes molded by the lives of our ancestors—cavemen, explorers, colonists, and even hippies. We do not need to live like we are still in the past, because in essence the past has made us capable of all we can do today.

The reviewer is at the Center for Neural Science, New York University, 4 Washington Place, Room 809, New York, NY 10003, USA. E-mail: caw448@nyu.edu

10.1126/science.1239724

WEBINAR

Fluorescent Probes and Digital Imaging

Where We Are and Where We're Going

Wednesday, June 12, 2013

12 noon Eastern, 9 a.m. Pacific, 5 p.m. UK, 6 p.m. Central Europe

Register Now!
webinar.sciencemag.org

The discovery of green fluorescent protein a half century ago heralded a new and explosive era in microscopy, forever changing the landscape for biology imaging. The ability to fuse a genetically encoded fluorescent probe to an almost-unlimited variety of proteins has enabled scientists to investigate signaling pathways and the movement of intracellular proteins in living cells with unprecedented detail, particularly when coupled with powerful widefield fluorescence and confocal microscopy techniques. Today, using the expanded selection of probes now available, researchers can even monitor multiple proteins simultaneously, in real time. This webinar will investigate how fluorescent protein probes are currently being utilized for live cell imaging, with a focus on applications in cancer research and where newly developed probes might take us in the near future.

During this webinar, the speakers will:

- Outline the current advances in fluorescent protein probes
- Discuss how fluorescent probes are currently being used to image intracellular processes in live cells across a range of cancer research applications
- Investigate the potential of new probe technology such as biosensors, photoswitchable probes, and probes emitting in the far-red and infrared portions of the spectrum
- Answer your questions live and in real time!

Speakers

Alan Waggoner, Ph.D.
Carnegie Mellon University
Pittsburgh, PA

W. E. Moerner, Ph.D.
Stanford University
Stanford, CA

Marcel Bruchez, Ph.D.
Carnegie Mellon University
Pittsburgh, PA

Webinar sponsored by

Leica MICROSYSTEMS

Brought to you by the *Science*/AAAS Custom Publishing Office

Science AAAS

POINT-COUNTERPOINT

Ethics and Genomic Incidental Findings

Laboratories have an obligation to report clinically beneficial incidental findings.

Amy L. McGuire,[1*†] Steven Joffe,[2*] Barbara A. Koenig,[3] Barbara B. Biesecker,[4] Laurence B. McCullough,[1] Jennifer S. Blumenthal-Barby,[1] Timothy Caulfield,[5] Sharon F. Terry,[6] Robert C. Green[7†]

The American College of Medical Genetics and Genomics (ACMG) recently issued a statement (*1*) recommending that all laboratories conducting clinical sequencing seek and report pathogenic and expected pathogenic mutations for a short list of carefully chosen genes and conditions. The recommendations establish a baseline for reporting clinically relevant incidental findings and articulate ethical principles relevant to their disclosure. The ACMG acknowledged that the list will evolve over time and is developing a mechanism for community input (*2*). This paper focuses on the ethical framework for the recommendations, rather than on the choice of which genes to include on the list.

Standards Are Needed

An increasing number of laboratories conduct clinical whole-genome and whole-exome sequencing (WGS-WES) (*3*) and have the potential to seek and report incidental findings, but there are no standards to guide their scope of analysis or reporting. The results a clinician receives depend in part on what laboratory is used, and some laboratories may report incidental findings of limited or uncertain clinical utility. The recommendations set a standard for best laboratory practices, by limiting the obligations of laboratories to incidental findings that meet a high threshold of clinical utility. The recommendations thus aim to discourage potentially harmful overreporting and unjustified variation in reporting practices.

The threshold for reporting incidental findings was based on variant frequency, the potential for medical intervention to mitigate disease, the strength of association between specific gene abnormalities and the condition, and penetrance of those genes. The recommendation's authors estimate that only about 1% of patients will receive such an incidental finding (*1*). Criteria were intentionally set high to include only "unequivocally pathogenic mutations in genes where pathogenic variants lead to disease with very high probability and where evidence strongly supports the benefits of early intervention" (*2*). In other words, these are clinically relevant findings, knowledge of which is likely to benefit the patient and promote health.

"The recommendations represent an initial attempt to set a professional standard for best laboratory practices..."

The recommendations essentially argue that laboratory personnel have a professional obligation to conduct a comprehensive evaluation of available test results to identify such clinically significant findings. This is true in all areas of medicine. To treat genomic information differently would constitute unjustified genetic exceptionalism. This ethical standard already governs clinical genetics practice. For example, if a patient is being evaluated for a hereditary cardiac condition, practice standards for the geneticist dictate that he or she should take a three-generation family history and search for patterns that reveal genetic predisposition to disease. If a predisposition to cancer is recognized, it should be communicated and followed up on. The transition from gene and panel testing to WGS-WES creates the same opportunity and obligation to identify and report clinically beneficial incidental findings.

Respect for Patient Autonomy

The recommendations reflect a core principle of professional medical ethics: The decision about appropriate scope of analysis and judgments about which findings are clinically beneficial are matters of expert professional judgment. Patients retain the decisional right to decline clinical sequencing, but, as is true for other diagnostic and screening procedures, the decision about the minimum list of genes to be interrogated requires professional expertise (*4*). Some have characterized this as borderline coercive (*5*) and testing without informed consent (*6*). This incorrectly assumes that analysis of clinically beneficial incidental findings is a discrete test requiring separate consent, whereas in reality it is integral to the primary interrogation. WGS-WES constitute a single comprehensive assessment using complex analytic algorithms for interpretation. The recommendations state that the ordering clinician is responsible for obtaining informed consent for this test and providing both pretest and posttest counseling "so that the patient is aware of not only the implications and limitations of the primary testing, but also the analysis that is being performed for incidental findings" (*1*). In other words, consistent with the ethical standards of informed consent and the principle of respect for patient autonomy (*7*), patients should be informed of the benefits of testing, as well as its risks and alternatives.

The recommendations' ethical standard for informed consent actually exceeds the legal standard in most states. Most diagnostic and risk assessment evaluations, including genetic testing in the majority of states (*8*), are performed under a general, simple consent to treat, because it is justifiably assumed that a reasonable patient would agree to a comprehensive evaluation to identify clinically beneficial information.

[1]Center for Medical Ethics and Health Policy, Baylor College of Medicine, Houston, TX 77030, USA. [2]Department of Pediatric Oncology, Dana-Farber Cancer Institute, Department of Medicine, Boston Children's Hospital, Harvard Medical School, Boston, MA 02215, USA. [3]Department of Social and Behavioral Sciences, Institute for Health and Aging, Department of Anthropology, History, and Social Medicine, University of California, San Francisco, CA 94143, USA [4]Social and Behavioral Research Branch, National Human Genome Research Institute, Bethesda, MD 20892, USA. [5]Health Law Institute, University of Alberta, Edmonton, Alberta T6G 2H5, Canada. [6]Genetic Alliance, Washington, DC 20008, USA. [7]Division of Genetics, Department of Medicine, Brigham and Women's Hospital and Harvard Medical School, Boston, MA 02115, USA.

*Corresponding author. E-mail: amcguire@bcm.edu (A.L.M.), steven_joffe@dfci.harvard.edu (S.J.) †Although some of us (A.L.M., R.C.G.) were members of the ACMG Working Group that wrote the recommendations, this paper does not represent the official views of the Working Group or the ACMG.

Some mistakenly infer from the recommendations that patients have no choice about which results they receive, thus violating a patient's right not to know. The right not to know is ethically controversial, and most of the relevant literature relates to findings for which no clearly beneficial interventions are available (*9*). Nonetheless, the recommendations explicitly state that the clinician-patient interaction is the appropriate place for incidental findings to be managed (*1*). Although the recommendations set a minimum standard for analysis and reporting, the physician and patient may decide together whether additional analyses and disclosures would be beneficial. There may be rare circumstances in which a physician, in consultation with the patient, decides not to follow the recommendations; for example, where WGS-WES will likely be beneficial to the patient for his or her primary clinical concern, no other test alternative is available (e.g., targeted testing is unavailable, has been tried, or is too expensive), and the patient insists that he or she does not want to be informed about incidental findings, even if disclosure could lead to beneficial intervention. When this occurs, the clinician must ensure that the patient's refusal is informed. If refusal persists, and the clinician agrees not to follow the recommendations, then the clinician should document this as a deviation from recommended analysis and disclosure, equivalent to refusing disclosure of any other clinically significant information. The clinician should inform the patient about practical constraints, including the difficulty of keeping the laboratory report out of the electronic medical record.

Treat Children and Adults Equally

Traditional guidance for genetic testing of children, reflected in a joint statement by the ACMG and the American Academy of Pediatrics (AAP), recommends that "predictive genetic testing [of children] for adult-onset conditions generally should be deferred unless an intervention initiated in childhood may reduce morbidity or mortality" (*10*). It follows that, barring unusual psychosocial circumstances or a request by a mature minor, genetic testing for adult-onset conditions should not be performed even when parents request it. The primary rationale is a desire to preserve the child's ability, when he or she reaches adulthood, to make an autonomous informed decision about testing.

The recommendations suggest that seeking and reporting incidental findings should not be contingent on the age of the person being sequenced. This does not contradict the AAP-ACMG position, because the two statements reflect fundamentally different contexts. The AAP-ACMG statement addresses the child who is known to be at risk of an adult-onset genetic condition for which no intervention can be initiated during childhood. For this child, the relevant alternatives are to (i) offer testing now, or (ii) defer testing until the child can make his or her own informed decision. Whereas option (i) may impose a test on a child that he or she might otherwise have chosen not to undergo, there is essentially no harm associated with option (ii), other than restriction of parental choice and authority. The issue of testing the child can safely be addressed when the child is an adult. In addition, because other at-risk adult family members are presumably aware of the proband's condition and of their own risk, they can elect to undergo testing.

The current recommendations address a very different context, in which the balance of interests, both of the child and of the family, must be reconsidered. In the case of incidental findings, where there is no prior information that identifies the family as at risk, the laboratory can either: (i) seek and report incidental findings included on the list to the ordering clinician, or (ii) not seek or report such findings. Option (i) runs the risk of imposing knowledge on the parents, child, and future young adult that they might nonetheless prefer not to have received, but offers potential medical benefit both to the child and to at-risk family members. In contrast, option (ii) withholds information that is potentially lifesaving for the child, one of the parents, and potentially other family members—information that they would otherwise have no reason to suspect (*2*). Furthermore, because the clinician and family are unaware of the child's risk, deferral of testing is not an option and preservation of the child's ability to make a future autonomous choice—the motivation underlying the AAP-ACMG proscription—is logically precluded. Thus, if the laboratory and clinician do not alert the child and family to the newly discovered risk information, they ignore potentially preventable harm to the child and other family members, fail to recognize parents' obligation to protect and promote the best interests of the child, and prevent them from making informed decisions about their child's and their own subsequent clinical management.

Implications and Next Steps

The recommendations represent an initial attempt to set a professional standard for best laboratory practices that will responsibly minimize variation in laboratory analysis and reporting of clinically beneficial incidental findings. They should be seriously considered by laboratory personnel, but they do not have the force of law. In the event of malpractice litigation, the recommendations may be introduced as evidence of the standard of care. Ultimately, they will be considered in light of all other evidence to determine whether the defendant's actions were consistent with what a reasonable professional might have done. The recommendations set a minimum standard for analysis and reporting of clinically beneficial incidental findings. By setting a high threshold for the reporting of findings with likely clinical benefit, they may also protect against liability for failure to report incidental findings that are not included on the list.

Tremendous investment has been made in studying the clinical utility of WGS-WES, including psychosocial benefits and harms of receiving incidental findings (*11*). As new evidence emerges, the list of reportable genes will be refined. Careful consideration should also be given to the application of these and/or other recommendations to preconception, prenatal, and newborn sequencing and sequencing of those without symptoms.

References and Notes

1. R. C. Green *et al.*, *Genet. Med.* (2013); www.acmg.net/docs/ACMG_Releases_Recommendations_on_Incidental_Findings_in_Clinical_Exome_and_Genome_Sequencing.pdf.
2. ACMG, *Genet. Med.* (2013); www.acmg.net/docs/Incidental_Findings_in_Clinical_Genomics_A_Clarification.pdf.
3. R. C. Green, H. L. Rehm, I. Kohane, in *Genomic and Personalized Medicine*, G. Ginsburg, H. Willard, Eds. (Elsevier, San Diego, 2013), vol. 1, pp. 102–122.
4. A. L. McGuire, L. B. McCullough, J. P. Evans, *JAMA* **309**, 1465 (2013).
5. M. Allyse, M. Michie, *Trends Biotechnol.* (2013). 10.1016/j.tibtech.2013.04.006
6. S. M. Wolf, G. J. Annas, S. Elias, *Science* **340**, 1049 (2013); 10.1126/science.1239119.
7. R. R. Faden, T. L. Beauchamp, N. M. P. King, *A History and Theory of Informed Consent* (Oxford Univ. Press, New York, 1986).
8. A. L. McGuire, M. J. Wang, F. J. Probst, *J. Law Med. Ethics* **40**, 1040 (2012).
9. R. Rhodes, *J. Med. Philos.* **23**, 10 (1998).
10. Committee on Bioethics, Committee on Genetics, ACMG Social Ethical and Legal Issues Committee, *Pediatrics* **131**, 620 (2013).
11. National Human Genome Research Institute (NHGRI), Clinical Sequencing Exploratory Research, (2012); www.genome.gov/27546194.

Acknowledgments: Supported by NIH, NHGRI, and National Cancer Institute (NCI) grants: HG006612-02 (A.L.M.); HG006485 (A.L.M. and L.B.M.); HG006500 (A.L.M., J.S.B.-B., and R.C.G.); HG006492 (S.J.); R01-CA154517 (B.A.K.); HG02213, HG005092, CA154517, HG006615, and HG003178 (R.C.G.); and the Intramural Research Program of the NHGRI (B.B.B.). The contents of this article are solely the responsibility of the authors and do not necessarily represent the views of NIH, NCI, or NHGRI. We thank L. Feuerman for research assistance with this manuscript.

10.1126/science.1240156

POINT-COUNTERPOINT

Patient Autonomy and Incidental Findings in Clinical Genomics

Returning genetic incidental findings without patient consent is misguided.

Susan M. Wolf,[1*] George J. Annas,[2] Sherman Elias[3]

Exome and whole-genome sequencing are rapidly moving into clinical application to aid diagnosis and treatment. However, a startling statement by the American College of Medical Genetics and Genomics (ACMG) may prove to be a stumbling block (*1*). Rather than reconfirming well-established principles of patient autonomy and informed consent that have long applied in medical genetics and in medical practice more broadly, ACMG recommends an abrupt change.

When clinical sequencing is undertaken to look for a "primary finding" (i.e., "a pathogenic alteration in a gene or genes that are relevant to the diagnostic indication for which the sequencing was ordered"), the ACMG calls for laboratories to search for "pathogenic and likely pathogenic variants" in an additional 57 specified genes and report results without seeking patient consent. These "incidental findings" are "results that are not related to the indication for ordering the sequencing but that may nonetheless be of medical value or utility to the ordering physician and the patient." However, the ACMG addresses only "the results of a deliberate search" for specific variants, not other genetic findings discovered unexpectedly, the more common use of the term "incidental findings" (*2*–*4*).

The ACMG calls for clinicians to report the results of the deliberate search for incidental findings to the patient, with no opportunity for the patient to decline unwanted information. The patient's only choice is to decline sequencing altogether, even if medically indicated. The ACMG imposes these requirements even when the patient is a child who has no medical need for these results during his or her childhood. The ethical and legal problems raised are profound. A recent ACMG clarification of this practice statement, in response to concerns, makes the problems worse (*5*). The clarification reiterates that patients cannot opt-out of testing on the 57 genes and now says that failing to report these test results would be "unethical."

Patient Decisions and the Right Not to Know

The ACMG rejects the need for the patient's informed consent to a deliberate search for these incidental findings, claiming that the amount of genetic counseling required would be too great. Yet the report marshals no data to support this conclusion and never considers proposals in the literature for streamlining the consent process when large numbers of genes are evaluated, such as "generic consent," which would allow the patient to consider categories of genetic tests together (*6*). The report also rejects the idea that laboratories should mask analysis of certain genes when there was no consent to search for them or could tailor reports, based on unsubstantiated fears of "unrealistic burden upon laboratories."

"Autonomy protects the patient's right to make a decision different from what the clinician might choose."

Rejecting the need for the patient's informed consent to look for mutations in a predetermined list of 57 genes is a profound departure from prevailing law and norms. Informed consent is a well-established legal requirement designed to protect patient autonomy—not a matter susceptible to modification by experts in human genetics, no matter how learned. Circumstances in which clinicians can test without consent are rare exceptions. In a medical emergency that prevents seeking consent—for example, when the life or health of an incompetent or unconscious patient is in imminent danger, and no one is available to consent—society allows physicians to treat without consent (*7*). However, this does not apply when laboratories and clinicians perform clinical sequencing, because they are not responding to a medical emergency threatening imminent harm and preventing them from seeking consent.

ACMG suggests that their recommended search for incidental findings is analogous to a radiologist spotting and reporting an unexpected tumor or other finding of concern on an x-ray. The analogy is misplaced. A deliberate hunt on a predetermined list of genes unrelated to the diagnostic reason for which sequencing was ordered is very different from the unexpected finding of a tumor in or near the area of primary concern in the field imaged by an x-ray. Patients would have no reason to expect a hunt for incidental findings in the 57 disparate genes on the ACMG list, especially when the list includes genes whose analysis and reporting have long required patient consent.

The ACMG is mistaken in basing their search and disclosure recommendations on a "fiduciary duty" to prevent the harms these findings may suggest. In both ethics and law, the clinician has a core fiduciary duty to respect the patient's right to decide what testing to undergo and what information to receive. Patients have an established right to refuse unwanted medical tests and the information they might disclose, even if that information would offer potential medical benefit (*8*, *9*). Indeed, the ACMG has recently affirmed the right to refuse unwanted incidental findings in clinical genomic sequencing (*10*). If the ACMG is now worried about potential liability for failing to return results from their list, they should urge clinicians to document the patient's refusal, not strip patients of the right to decide. Inflicting unwanted information on patients carries its own risk, as unwanted information may lead to anxiety, further clinical workup, and potentially burdensome interventions.

The ACMG's "minimum list" includes mutations in genes that patients have long been able to refuse testing for, including cancer risk mutations (such as *BRCA1*) and cardiovascular risk mutations. There are many circumstances in which a patient may decline such testing and information, even if the results could open avenues for intervention. The patient may already be battling another disease, such as advanced cancer, or be late in life and see more burden than benefit in

[1]University of Minnesota, Minneapolis, MN 55455, USA. [2]Boston University, Boston, MA 02118, USA. [3]Department of Obstetrics and Gynecology, Feinberg School of Medicine, Northwestern University, Chicago, IL 60611, USA.

*Corresponding author. swolf@umn.edu

added genetic information. The patient may also fear that "extra" results in their medical record will invite risk of discrimination (*11*).

The whole idea behind informed consent is that patients are individuals who are entitled to make medical decisions in keeping with their own values. Autonomy protects the patient's right to make a decision different from what the clinician might choose and even to reject information and treatment that might maximize life expectancy. Although ACMG's new clarification refers to "shared decision-making" by provider and patient, there is no recognition of the patient's right to refuse testing and results. Indeed, ACMG's claim that failure to report the findings on their list would be unethical will likely compel laboratories and physicians to report. Yet this claim is incorrect. Patients have the right to refuse testing and findings, even if potentially lifesaving. Just because many patients might want this information does not mean that it can or should be imposed on all.

The Child's Right to Limits on Testing

The report also departs from long-standing consensus recommendations on testing children. The ACMG acknowledges that "standards for predictive testing in clinical genetics recognize a distinction between providing results to adults and providing results to children and adolescents, with consistent recommendations that predictive testing for adult-onset diseases not be offered to children." This consensus has stood since at least 1995, when the ACMG and American Society of Human Genetics published recommendations (*12*). Just this year, the ACMG and American Academy of Pediatrics reiterated that "Decisions about whether to offer genetic testing and screening should be driven by the best interest of the child" (*13*, *14*).

The report emphasizes that searching for incidental findings in the child's 57 genes is an opportunity for other family members to learn of variants that may be important for their own health. Yet this is exactly what past recommendations have rightly rejected, in limiting genetic testing and disclosure of genetic information to what is medically necessary during childhood. Delaying testing and return of genetic information not medically useful in childhood allows the child to reach adulthood and then make a choice based on his or her own values. The child's right to genetic privacy and future choice is preserved. ACMG argues that potential health benefit to a parent may benefit the child, but past guidance has found the clear risk of harms to the child more compelling.

ACMG's clarification now claims that limits on testing children for adult-onset conditions do not apply to the incidental findings on their list. Yet consensus limits on pediatric testing have long applied to variants conferring risk of serious adult-onset disease. When children have undergone clinical sequencing, they can choose at adulthood whether to request their findings. Even for child-onset conditions, past guidelines have required consent to testing (*13*).

Problems with the List

In addition to the problems of unconsented testing and disclosure, even in children, there are problems raised by ACMG's list of 57 genes. These genes and the types of variants that laboratories must search for and report can be broken down into three basic categories covering a wide range of medical conditions: risks for developing cancer and noncancerous tumors (24 genes), cardiovascular risks (31 genes), and adverse reactions to commonly used anesthetics (2 genes). The report indicates that the criteria they used include: "clinical validity and utility," recognized or expected pathogenicity of the sequence variant, "variants with a higher likelihood of causing disease" (although ACMG notes "that there are limited data available in many cases to make that assessment"), availability of "preventive measures and/or treatment," inclusion of mutations that "might be asymptomatic for long periods of time," and availability of "confirmatory approaches for medical diagnosis" (although ACMG recognized "that this standard could not be met for all of the conditions listed").

If the ACMG was trying to justify required search and disclosure of incidental findings without patient consent, the criteria should have been considerably more stringent (such as significant likelihood of substantial harm in the near future if not communicated). The broad criteria used would actually justify a much longer list of genes, including a number associated with risk of other cancers. Singling out this selection of 57 genes appears arbitrary. This problem is exacerbated by the fact that ACMG says a laboratory may look for incidental variants in additional genes "as deemed appropriate by the laboratory." The criteria that laboratories will use remain unclear. The ACMG itself also plans to revisit its list annually. As the list expands, so will the scope of testing without consent and the number of incidental findings potentially reported to the patient.

The report tries to confine the impact of these recommendations by saying the authors chose not to consider preconception, prenatal, or newborn sequencing. However, if testing for incidental findings in the list of 57 genes is so important that they must be looked for whenever sequencing is performed, why shouldn't they be looked for in preconception, prenatal, and newborn sequencing? Starting down the path of unconsented testing and reporting in clinical genomics leads to grave difficulties, and should not be done without more careful analysis.

Next Steps–Restoring Respect for Patients

The ACMG should reconsider this practice statement. Clinical sequencing is a medically important tool, already deployed for certain indications. Access should not be conditioned on patients' surrender of established rights. Especially in the case of children, who will generally not even be able to exercise the option of walking away from sequencing, long-standing protections remain essential. The era of medical genomics requires a trusting partnership with patients, based on respect for their rights.

References and Notes

1. R. C. Green *et al.*, *Genet. Med.* (2013); www.acmg.net/AM/Template.cfm?Section=Home3.
2. I. S. Kohane, D. R. Masys, R. B. Altman, *JAMA* **296**, 212 (2006).
3. S. M. Wolf *et al.*, *J. Law Med. Ethics* **36**, 211 (2008).
4. S. M. Wolf *et al.*, *Genet. Med.* **14**, 361 (2012).
5. ACMG, Incidental findings in clinical genomics: A clarification (2013); www.acmg.net/docs/Incidental_Findings_in_Clinical_Genomics_A_Clarification.pdf.
6. S. Elias, G. J. Annas, *N. Engl. J. Med.* **330**, 1611 (1994).
7. G. J. Annas, *The Rights of Patients* (New York Univ. Press, New York, ed. 3, 2004), p. 128.
8. NIH Task Force on Genetic Testing, *Promoting Safe and Effective Genetic Testing in the United States* (NIH, Bethesda, MD, 1997), chap. 1; www.genome.gov/10001733.
9. UNESCO, Universal Declaration on the Human Genome and Human Rights (1997); http://portal.unesco.org/en/ev.php-URL_ID=13177&URL_DO=DO_TOPIC&URL_SECTION=201.html.
10. ACMG, Points to consider in the clinical application of genomic sequencing (2012); www.acmg.net/StaticContent/PPG/Clinical_Application_of_Genomic_Sequencing.pdf.
11. G. J. Annas, P. Roche, R. C. Green, *Bioethics* **22**, ii (2008).
12. American Society of Human Genetics Board of Directors and ACMG Board of Directors, *Am. J. Hum. Genet.* **57**, 1233 (1995).
13. Committee on Bioethics, Committee on Genetics, the ACMG Social, Ethical, and Legal Issues Committee, *Pediatrics* **131**, 620 (2013).
14. L. F. Ross, H. M. Saal, K. L. David, R. R. Anderson, *Genet. Med.* **15**, 234 (2013).

Acknowledgments: S.M.W. was supported by NIH, National Cancer Institute, and National Human Genome Research Institute grant 1-R01-CA154517 and Robert Wood Johnson Foundation grant 69763. The contents of this article are solely the responsibility of the authors and do not necessarily represent the views of the funders.

10.1126/science.1239119

CELL BIOLOGY

Vitamin Currency in a Lipid Exchange Market

A lipid transfer protein moves vitamin E through the cell to the cell surface by exchanging it for a phosphoinositide in the plasma membrane.

Bruno Mesmin and Bruno Antonny

The most abundant form of vitamin E in mammals, α-tocopherol, is a vital lipid-soluble antioxidant that prevents damage to cellular lipids containing polyunsaturated fatty acids. A deficiency of this antioxidant leads to severe degenerative diseases such as ataxia, infertility, muscle degeneration, and perhaps atherosclerosis. Although vitamin E is present in appreciable amounts in food, regulation of its availability in the body is complex and involves several steps both outside and inside the cell (*1*). On page 1106 of this issue, Kono *et al.* (*2*) reveal how the vitamin becomes localized at the plasma membrane, poised for release into the circulation, through a lipid transport protein that exchanges it for a very different lipid, a phosphoinositide.

α-Tocopherol is the form of dietary vitamin E that is preferentially absorbed by the small intestine. It is transported to the liver by lipoproteins called chylomicrons, and then is released into the plasma as a component of the water-soluble very low density lipoprotein. One major mechanism for controlling the amount of circulating α-tocopherol involves a 30-kD intracellular protein in liver cells called α-tocopherol transfer protein (α-TTP) (*3*). α-TTP transports α-tocopherol from the cytosolic-facing leaflet of endosomal compartments to the cytosolic-facing leaflet of the plasma membrane (see the figure). Structural studies of α-TTP revealed that a mobile lid covering a hydrophobic pocket adopts an open conformation when α-tocopherol is not loaded, which suggests that the lid controls α-tocopherol exchange between α-TTP and membranes (*4*).

Inherited mutations in the gene encoding α-TTP result in a rare autosomal recessive neurodegenerative disease called ataxia with vitamin E deficiency (AVED) (*5*). Intriguingly, none of the nine heritable point mutations in this gene found in AVED patients affect the lipid-binding pocket or the lid. Kono *et al.* noticed that three of the mutations are located in a positively charged cleft on the protein surface and hypothesized that this region could be critical for α-TTP function. The authors demonstrated that when residues in the positively charged cleft were mutated, α-TTP could no longer bind to negatively charged phosphoinositides (*6*). Phosphoinositides are minor lipid components of cell membranes but play a major role in the "geography" within a cell by acting as a signpost for organelles. Each type of phosphoinositide has a defined subcellular localization and its polar head group is recognized by specific protein domains (*7*). Through its positively charged cleft, α-TTP binds specifically to phosphatidylinositol 4,5-bisphosphate (PIP_2), which is localized at the plasma membrane.

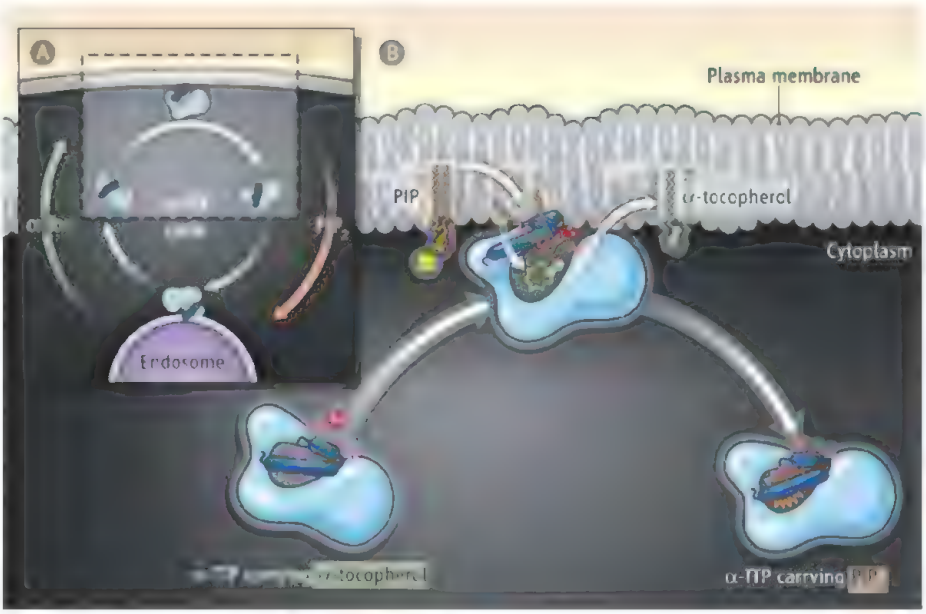

Dealing lipids. (**A**) α-TTP carries vitamin E from endosomes to the plasma membrane. (**B**) Delivery of vitamin E (α-tocopherol) to the plasma membrane is coupled to extraction of a very different lipid, PIP_2, from this membrane.

The surprise is not that α-TTP interacts with the head group of PIP_2; many peripheral proteins do so to target the plasma membrane. Rather, what is unexpected is that α-TTP extracts PIP_2 from the membrane. Kono *et al.* resolved the crystal structure of α-TTP in a ternary complex with α-tocopherol and PIP_2 and observed that α-tocopherol is located in the hydrophobic pocket whereas the head group of PIP_2 is bound to the positively charged cleft. The acyl chains of PIP_2, although poorly resolved, point toward the hydrophobic pocket. The molecular lid of α-TTP displays a position that is intermediate between that of the closed and open conformations (*4*). These observations suggest that the ternary complex is a snapshot of a transition state in a lipid exchange reaction in which PIP_2 in the membrane is swapped for α-tocopherol.

Kono *et al.* reconstituted this lipid exchange reaction using artificial membranes (liposomes). When α-tocopherol and PIP_2 were present in the same liposomes, they bound to α-TTP in a competitive manner, despite their contrasting structure and chemistry. When the two ligands were present in two different liposomes, α-TTP transferred them in opposite directions. Considering the high affinity (dissociation constant K_d ~10 nM) of α-TTP for α-tocopherol (*8*), PIP_2 exchange appears as a very powerful mechanism to release the vitamin from the transporter protein. How does PIP_2 binding trigger the opening of the lid and α-tocopherol displacement? The structure of the ternary complex suggests two possibilities: steric repulsions by the acyl chains of PIP_2 or allosteric rearrangements imposed by the polar head of PIP_2.

Institut de Pharmacologie Moléculaire et Cellulaire, Université de Nice et CNRS, 660 route des Lucioles, 06560 Valbonne, France. E-mail: antonny@ipmc.cnrs.fr

α-TTP belongs to the Sec14 family of evolutionarily conserved lipid transfer proteins. Structural studies on the yeast Sec14 homolog 1 (Sfh1), a phosphatidylinositol (PI)/phosphatidylcholine transfer protein, showed that residues critical for PI binding are conserved among the Sec14 family members (*9*). It appears that positive residues critical for PIP_2 binding in α-TTP are conserved as well, suggesting that phosphoinositide exchange activity might be a general property of Sec14 proteins. It is noteworthy that mutations in the conserved positively charged cleft of the Sec14-like cellular retinaldehyde binding protein, which transports 11-*cis*-retinal (the pigment of photoreceptor cells), lead to hereditary retinopathy (*10*). Moreover, exchanging a specific lipid for a phosphoinositide applies not only to Sec14 family members but also to another family of lipid transporters, the oxysterol-binding homology (Osh)/oxysterol-binding protein-related proteins (ORPs). For example, the yeast protein Osh4p reportedly exchanges sterol for phosphatidylinositol 4-phosphate between membranes in vitro (*11*).

The evolutionary pressure for conserving such a mechanism among different families of lipid transfer proteins probably resides with the chemistry and metabolism of phosphoinositides. Their complex polar head provides possibilities for initial contacts between proteins and membranes before the actual lipid exchange reaction takes place, a likely decisive advantage for fast and efficient reactions. Furthermore, phosphoinositides are constantly transformed through phosphorylation and dephosphorylation reactions and, as such, might be easily removed from the transporter to allow multiple cycles of lipid transfer. The study of Kono *et al.* points to an exchange market in cells, with key lipophilic compounds such as vitamins, sterols, pigments, and phosphoinositides acting as the currency.

References

1. M. G. Traber, *Annu. Rev. Nutr.* **27**, 347 (2007).
2. M. Kono *et al.*, *Science* **340**, 1106 (2013); 10.1126/science.1233508
3. M. Arita, K. Nomura, H. Arai, K. Inoue, *Proc. Natl. Acad. Sci. U.S.A.* **94**, 12437 (1997).
4. R. Meier, T. Tomizaki, C. Schulze-Briese, U. Baumann, A. Stocker, *J. Mol. Biol.* **331**, 725 (2003).
5. I. Di Donato, S. Bianchi, A. Federico, *Neurol. Sci.* **31**, 511 (2010).
6. S. Krugmann *et al.*, *Mol. Cell* **9**, 95 (2002).
7. R. Behnia, S. Munro, *Nature* **438**, 597 (2005).
8. S. Morley *et al.*, *Biochemistry* **45**, 1075 (2006).
9. G. Schaaf *et al.*, *Mol. Cell* **29**, 191 (2008).
10. X. He, J. Lobsiger, A. Stocker, *Proc. Natl. Acad. Sci. U.S.A.* **106**, 18545 (2009).
11. M. de Saint-Jean *et al.*, *J. Cell Biol.* **195**, 965 (2011).

10.1126/science.1239800

CHEMISTRY

A New Twist on Cooperative Catalysis

Two independent catalysts working synergistically allow the controlled synthesis of all four stereoisomers in a reaction that forms carbon-carbon bonds.

Corinna S. Schindler and Eric N. Jacobsen

The stereochemical configuration of an organic compound is often linked directly to its physical and biological properties. Larger molecules can contain multiple stereochemical elements, and chiral catalysts are often used to control each of these defined spatial arrangements in the efficient synthesis of a complex target (*1*). Many powerful enantioselective catalysts, which control the handedness or absolute configuration of a product, have been developed (*2*), but full control of the relative configuration in compounds can be a greater challenge if multiple stereocenters are generated; high diastereoselectivity, where one relative configuration is established, may be achieved, but access to the complementary diastereomeric product usually requires major redesign of the catalyst, substrate, and/or reaction conditions, and in some cases is not possible at all (see the figure, panel A) (*3*). On page 1065 of this issue, Krautwald *et al.* (*4*) demonstrate an elegant solution to this challenge based on the cooperative action of multiple chiral catalysts in a single reaction.

The idea of activating two different reacting partners independently with two distinct catalysts has been termed "dual catalysis" or "synergistic catalysis" (*5*). This strategy has been applied in asymmetric catalysis with some success by using a chiral catalyst and the cooperative effect of a second, achiral catalyst (*6*). In a much smaller number of cases, researchers have successfully engaged two different chiral catalysts in a synergistic man-

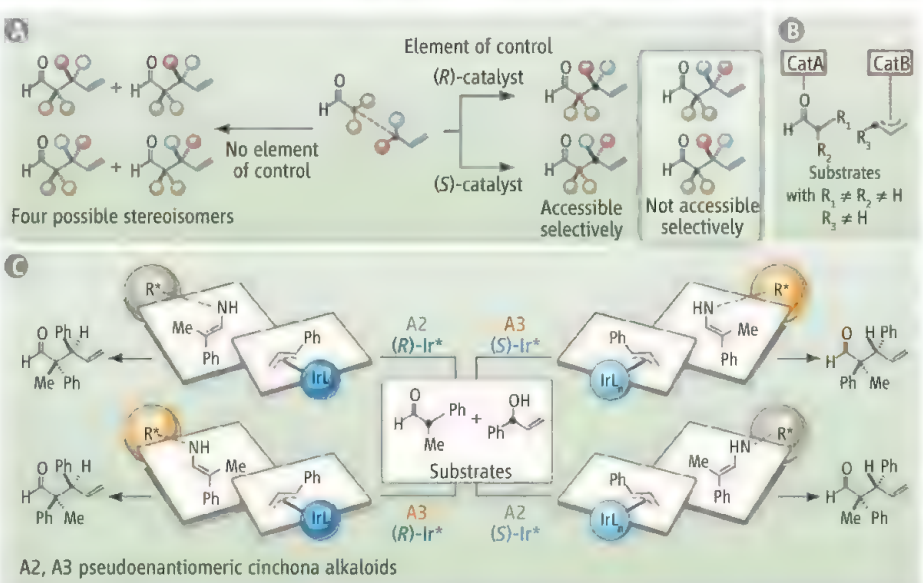

Working hand in hand. The α-allylation of branched aldehydes generates two contiguous stereocenters. (**A**) Bond formation between the two reacting partners can form four stereoisomers as a complex reaction mixture. With an element of control present, e.g., a chiral catalyst, specific stereoisomers can be formed selectively. However, not all four stereoisomers are accessible. (**B**) A dual catalytic system independently activates each substrate by a distinct catalyst. (**C**) Krautwald *et al.* used stereodivergent dual catalysis in the α-allylation of branched aldehydes. Selective access to any stereoisomer is possible in a single transformation from the same set of substrates simply by choice of the appropriate catalyst combination.

Department of Chemistry and Chemical Biology, Harvard University, Cambridge, MA 02138, USA. E-mail: cschindl@fas.harvard.edu; jacobsen@chemistry.harvard.edu

ner. In one example, two chiral catalysts were used to induce conjugate addition reactions of cyanide (*7*). Only one stereocenter is created in that process, but substantial enhancement in enantioselectivity was observed through the "matching" of the two chiral catalysts. In another example, researchers used two different chiral secondary amine catalysts in the same reaction to effect a sequential enantioselective conjugate addition and then trapping of the intermediate enolate (*8*). Through ingenious reaction design, the first catalyst was induced to fall off after the initial step, and the second catalyst entered and controlled the diastereoselectivity of the second stereocenter formation. As such, both stereocenters of the product can be controlled, and thus all four of the possible stereoisomers could be accessed through proper choice of the two chiral catalysts. That work represented an extraordinary illustration of a well-established strategy in asymmetric synthesis: chiral catalyst-controlled diastereoselectivity in a reaction of an enantioenriched substrate.

Krautwald *et al.* also use two different chiral catalysts to control the formation of two stereocenters. However, their approach is fundamentally different from previous efforts in that it relies on the independent activation of two distinct reacting partners in a single reaction (see the figure, panel B). The goal is not for one catalyst to overcome or complement the effect of the other, but rather for the two catalysts to induce stereoselectivity independently yet simultaneously.

The concept is illustrated in the α-allylation of branched aldehydes, a carbon-carbon bond-forming reaction that generates two contiguous stereocenters (see the figure, panel C). Relying on previously established catalytic reactivity principles, the aldehyde is activated by an amine catalyst, and the allylic electrophile is activated by an iridium catalyst. The authors show in an unambiguous set of experiments that each catalyst controls the stereoselectivity of one of the substrates but has essentially no effect on the stereocenter derived from the other reacting partner. Then, in a stunning set of results, they show that two chiral catalysts working together achieve the desired effect of nearly perfect and independent control of each center. Selective access to every possible stereoisomer can thus be achieved in a single transformation from the same set of substrates simply by choice of a distinct catalyst combination.

In principle, this has the potential to emerge as a powerful new strategy for reaction design, applicable to a wide range of important reactions. Many of the most powerful transformations in organic chemistry involve bond formation between two potentially prochiral reaction partners and thus can introduce multiple stereocenters in one operation. Notable examples include the Diels-Alder reaction, the aldol reaction, and cyclopropanation reactions. Effective enantioselective catalytic variants are known for each of these classes of reactions but in all cases rely on the use of a single chiral catalyst. The question now is whether dual chiral catalysis of the type uncovered by Krautwald *et al.* might be applied to these and other broadly useful reactions in organic chemistry, thereby making it possible to access every stereochemical permutation of the products of interest by the same method, varying only the stereochemistry of the catalysts.

References and Notes

1. M. S. Taylor, E. N. Jacobsen, *Proc. Natl. Acad. Sci. U.S.A.* **101**, 5369 (2004).
2. E. N. Jacobsen, A. Pfaltz, H. Yamamoto, Eds., *Comprehensive Asymmetric Catalysis: Vol. I-III, Suppl. I-II* (Springer, New York, 1999).
3. Enantiomers are stereoisomers, i.e., isomers that have the same bond connectivity but different spatial relationships, that differ in being nonsuperimposable mirror-image partners (such as a matched pair of left and right shoes). In organic compounds, this occurs when there is a single stereochemical element, most often a stereogenic carbon center bearing four different substituents. Diastereomers are stereoisomers that are not enantiomers (such as a left foot in a left shoe versus a left foot in a right shoe), and these occur in structures that have multiple stereogenic carbon centers.
4. S. Krautwald *et al.*, *Science* **340**, 1065 (2013).
5. A. E. Allen, D. W. C. MacMillan, *Chem. Sci.* **3**, 633 (2012).
6. C. Zhong, X. Shi, *Eur. J. Org. Chem.* **2010**, 2999 (2010).
7. G. M. Sammis *et al.*, *J. Am. Chem. Soc.* **126**, 9928 (2004).
8. Y. Huang *et al.*, *Am. Chem. Soc.* **127**, 15051 (2005).

10.1126/science.1238769

CLIMATE CHANGE

What Are Climate Models Missing?

A better representation of the coupling between atmospheric water and circulation is necessary to reduce imprecision in climate model projections.

Bjorn Stevens[1] and Sandrine Bony[2]

Fifty years ago, Joseph Smagorinsky published a landmark paper (*1*) describing numerical experiments using the primitive equations (a set of fluid equations that describe global atmospheric flows). In so doing, he introduced what later became known as a General Circulation Model (GCM). GCMs have come to provide a compelling framework for coupling the atmospheric circulation to a great variety of processes. Although early GCMs could only consider a small subset of these processes, it was widely appreciated that a more comprehensive treatment was necessary to adequately represent the drivers of the circulation. But how comprehensive this treatment must be was unclear and, as Smagorinsky realized (*2*), could only be determined through numerical experimentation. These types of experiments have since shown that an adequate description of basic processes like cloud formation, moist convection, and mixing is what climate models miss most.

[1]Max Planck Institute for Meteorology, Bundesstraße 53, 20146 Hamburg Germany. [2]Laboratoire de Météorologie Dynamique–Institut Pierre Simon Laplace, CNRS, Université Pierre et Marie Curie, Paris, France. E-mail: bjorn.stevens@mpimet.mpg.de

From GCMs to Earth System Models

Smagorinsky's GCM was designed around the premise that studies of the general circulation required a model capable of resolving the heat transport from the equator to the poles. Its formulation was the next logical step in a program of hierarchical model development best known for its pioneering contributions to numerical weather prediction (*3*). The work paved the way for fundamental studies of the atmospheric general circulation, and hence Earth's climate.

Over the past half century, many of these studies have focused on the types of numerical experiments anticipated by Smagorinsky. Beginning with basic processes like moist convection and cloud formation, which have long been appreciated as central to the energetics of the troposphere, a long succession of processes and couplings have been added to primitive-equation descriptions of the atmospheric general circulation. In so doing, GCMs have gradually morphed into Global Climate Models, and with the more recent incorporation of models of the biosphere and the associated cycles of important chemical nutrients, Earth System Models (*4*, *5*).

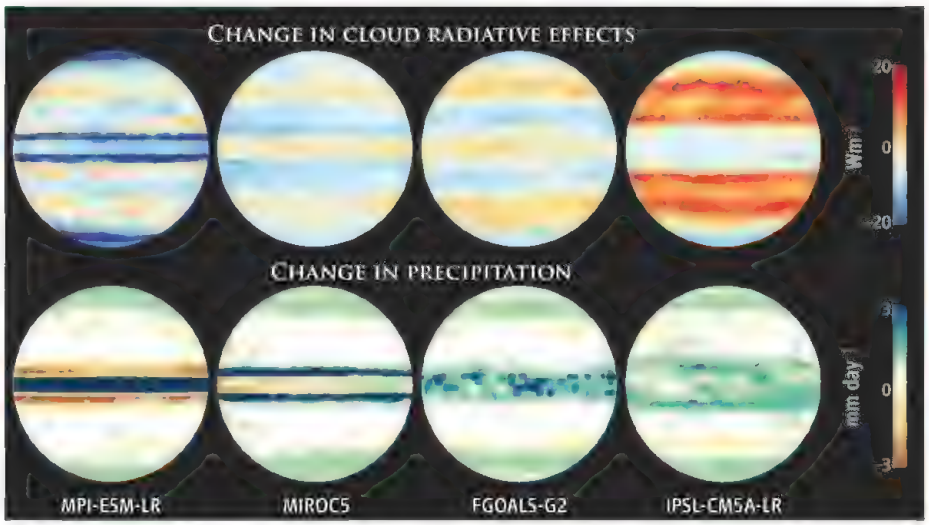

Wide variation. The response patterns of clouds and precipitation to warming vary dramatically depending on the climate model, even in the simplest model configuration. Shown are changes in the radiative effects of clouds and in precipitation accompanying a uniform warming (4°C) predicted by four models from Phase 5 of the Coupled Model Intercomparison Project (CMIP5) for a water planet with prescribed surface temperatures.

Key Uncertainties

The increase in complexity has greatly expanded the scope of questions to which GCMs can be applied (*5*). Yet, it has had relatively little impact on key uncertainties that emerged in early studies with less comprehensive models (*6*). These uncertainties include the equilibrium climate sensitivity (that is, the global warming associated with a doubling of atmospheric carbon dioxide), arctic amplification of temperature changes, and regional precipitation responses. Rather than reducing biases stemming from an inadequate representation of basic processes, additional complexity has multiplied the ways in which these biases introduce uncertainties in climate simulations (*7*, *8*).

For instance, a poor understanding of what controls the distribution of tropical precipitation over land, and hence vegetation dynamics, limits attempts to understand the carbon cycle (*9*). Similarly, uncertainties in arctic amplification of warming hinder predictions of permafrost melting and resultant changes in soil biogeochemistry.

Although the drive to complexity has not reduced key uncertainties, it has addressed Smagorinsky's question (*2*) as to what level of process detail is necessary to understand the general circulation. There is now ample evidence that an inadequate representation of clouds and moist convection, or more generally the coupling between atmospheric water and circulation, is the main limitation in current representations of the climate system.

That this limitation constitutes a major roadblock to progress in climate science can be illustrated by simple numerical experiments. In idealized simulations of a waterworld that neglect complex interactions among land surface, cryosphere, biosphere, and aerosol and chemical processes (see the figure), the key uncertainties associated with the response of clouds and precipitation to global warming are as large as they are in comprehensive Earth System Models (*10*).

Differences among the simulations in the figure are especially evident in the tropics, where the sign of cloud changes and the spatial structure of the precipitation response differ fundamentally between models. This diversity of responses arises because, at low latitudes, the coupling between water and circulation is disproportionately dependent on the representation of unresolved processes, such as moist convection and cloud formation (*11*, *12*). The mid-latitudes show more robust responses because much of the energy transport is carried by baroclinic eddies; these, too, are fundamentally coupled to water, but they are much better described and resolved by modern GCMs, as foreseen by Smagorinsky (*1*).

The uncertain interplay between water and circulation that underlies differences in the response of the climate system to warming (see the figure) can be expressed in terms of more specific questions. For instance, how do marine boundary-layer clouds depend on their environment? Or how do atmospheric circulations couple to moist convection through surface and radiative fluxes? The first question ends up being key to explaining the intermodel spread in climate sensitivity (*13*, *14*), the second to the pattern of the regional response to warming. Differences in regional responses also influence ocean circulations, and hence how oceans take up heat, as well as patterns of precipitation, and hence how the land biosphere takes up carbon.

Back to Basics

A deeper understanding and better representation of the coupling between water and circulation, rather than a more expansive representation of the Earth System, is thus necessary to reduce the uncertainty in estimates of the climate sensitivity and to guide adaptation to climate change at the regional level. This knowledge should help focus efforts and lead to progress in reducing the imprecision of climate models in the next 50 years. Here, Numerical Weather Prediction (NWP) provides a good example. By focusing on key limitations in the model initialization, spatial resolution, and the representation of key parameterized processes, NWP has improved forecast skill substantially over the past 30 years (*15*).

It is time to draw lessons from the era of experimentation that Smagorinsky launched half a century ago, and focus climate modeling efforts on advancing understanding and improving the numerical representations of how clouds, moist convection, and heating couple to the general circulation.

References and Notes

1. J. Smagorinsky, *Mon. Weather Rev.* **91**, 99 (1963).
2. In (*1*), Smagorinsky concluded: "In pursuing the objective to generalize theoretical models we must ask ourselves whether greater detail in formulating the contributing processes is warranted by truncation errors, by sensitivity of the results to detail, by the resulting increase in computational complexity and time, and by ignorance of the way these processes really work. Very often this cannot be determined in advance, but must wait for computational experiments to be performed.
3. J. G. Charney, A. Eliassen, *Tellus* **1**, 38 (1949).
4. W. J. Collins *et al.*, *Geosci. Model Dev.* **4**, 1051 (2011).
5. G. M. Flato, *WIREs Clim. Change* **2**, 783 (2011).
6. S. Bony *et al.*, in *Climate Science for Serving Society: Research, Modelling and Prediction Priorities*, G. R. Asrar, J. W. Hurrell, Eds. (Springer, Berlin, 2013).
7. Q. Min, S. Wang, *Geophys. Res. Lett.* **35**, L02406 (2008).
8. I. B. Ocko, V. Ramaswamy, P. Ginoux, Y. Ming, L. W. Horowitz, *J. Geophys. Res.* **117**, D20203 (2012).
9. P. Good *et al.*, *J. Clim.* **26**, 495 (2013).
10. B. Medeiros *et al.*, *J. Clim.* **21**, 4974 (2008).
11. B. Oueslati, G. Bellon, *J. Clim.* **26**, 2931 (2013).
12. D. Popke *et al.*, *J. Adv. Model. Earth Syst.* **5**, 1 (2013).
13. S. Bony, J.-L. Dufresne, *Geophys. Res. Lett.* **32**, L20806 (2005).
14. J.-L. Dufresne, S. Bony, *J. Clim.* **21**, 5135 (2008).
15. A. J. Simmons, A. Hollingsworth, *Q. J. R. Meteorol. Soc.* **128**, 647–677 (2002).

Acknowledgments: The simulations presented in the figure are taken from Phase 5 of the Coupled Model Intercomparison Project. We acknowledge the World Climate Research Programme's Working Group on Coupled Modelling, which is responsible for CMIP5, and thank the climate modeling groups for making available their model output. Additional support was provided through funding from the European Union Seventh Framework Programme (FP7/2007-2013) under grant agreement number 244067.

10.1126/science.1237554

PLANETARY SCIENCE

Pebbles on Mars

The observation of conglomerates by the Mars rover Curiosity provides the most definitive proof yet of ancient river flow.

Douglas J. Jerolmack

Mars is a cold, dry place. Yet there is abundant evidence that fluvial (river) processes have carved the planet's surface; witness deep canyons, streamlined islands, and drainage networks. Most of these features formed more than 3 billion years ago, and a long line of research has led to the "warm and wet early Mars" hypothesis. The idea is that early Mars had a thicker atmosphere with an enhanced greenhouse effect that allowed stable liquid water and a hydrologic cycle to exist (*1*). The search for life on Mars, or at least conditions suitable for life, is predicated on this idea. Until now, no observations have unambiguously identified and characterized river-lain sediments, although the Mars Exploration Rovers turned up some evidence of a watery past (*2*). As the first major finding from the Mars Science Laboratory mission and its car-sized rover, Curiosity, Williams *et al.* (*3*) report on page 1068 of this issue the discovery of conglomerates on Mars—pebbles mixed with sand and turned to rock—resulting from ancient river deposits. The finding provides the clearest view yet on the nature of early martian rivers and should provide momentum for Curiosity's mission moving forward.

Department of Earth and Environmental Science, University of Pennsylvania, Philadelphia, PA 19104, USA. E-mail: sediment@sas.upenn.edu

The most striking fluvial features on Mars are huge canyons (>1000 km long) eroded into bedrock. They have been associated with catastrophic outburst floods (*1*), but how large these floods were is hard to say; imagine trying to estimate the discharge of the Colorado River from the size of the Grand Canyon. Thus, we must look elsewhere to constrain ancient flows on Mars. All eroded channel material must be deposited somewhere. On Earth, river deltas and alluvial fans (collectively "fans") form at the mouths of rivers debouching into oceans and basins, respectively. Their deposits consist of stacked river channels and floodplains whose history can be read by the trained eye. Until a decade ago, however, no such features had ever been observed on Mars. [One likely culprit for this absence of evidence is aeolian (wind) processes, which have had more than 3 billion years to erode or bury early martian fluvial features.]

The discovery from satellite images of the first putative river delta on Mars in 2003 (*4*) marked a turning point. The beautifully preserved depositional channels made it possible to measure the width, depth, and slope of the ancient river. Discharge estimates were rather pedestrian, comparable to medium-sized rivers on Earth (*5*, *6*). This discovery was hailed as a smoking gun for the warm and wet early Mars hypothesis, and focused searching with better imagery has turned up dozens of fans (*7*). However, it has been pointed out that such deposits could form in decades and may have resulted from impulsive heating (e.g., crater formation or volcanic intrusions) rather than a globally warmer planet (*6*, *8*).

Until now, the sediments composing martian fans were unknown, leaving some room for doubt regarding their formative processes. Curiosity was sent to Gale crater to explore the promising mountain of stacked sedimentary deposits at its center, informally called Mount Sharp and thought to be of lacustrine and fluvial origin (*9*). The conglomerates dis-

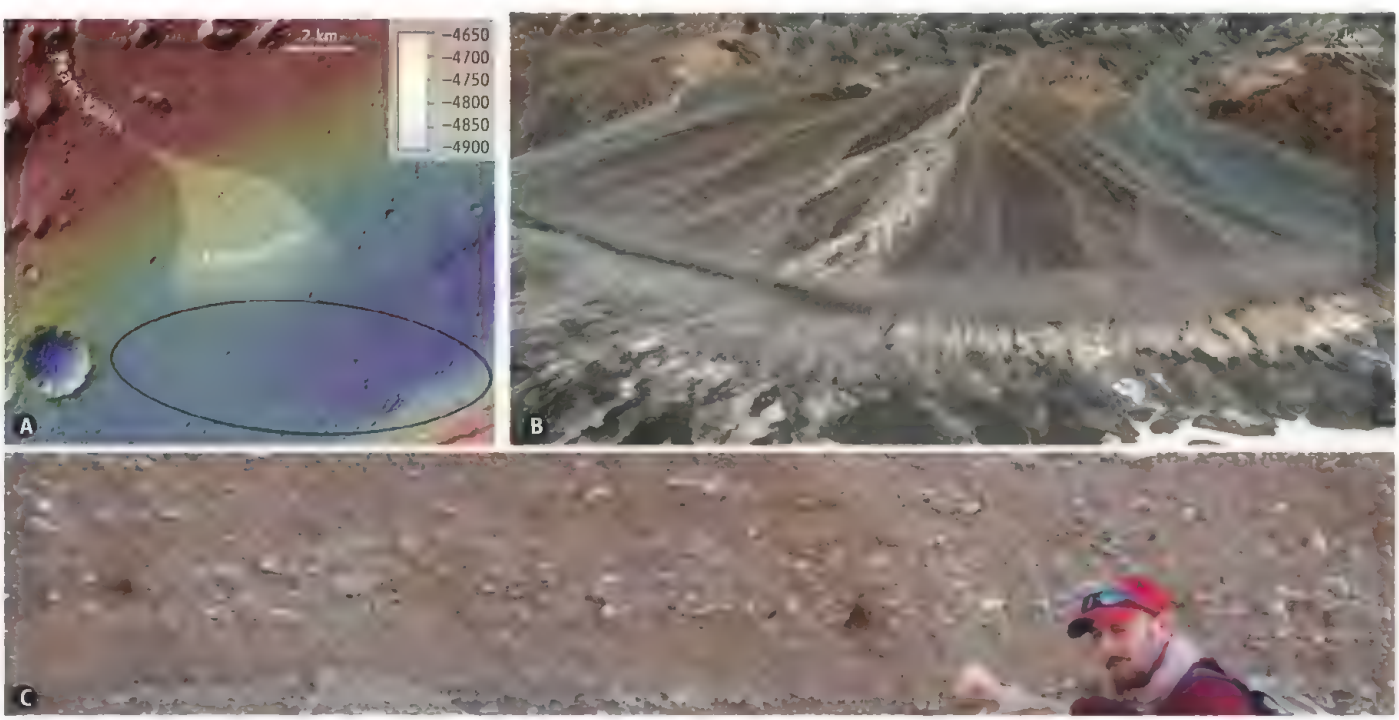

CREDIT: (A) NASA/JPL-CALTECH/ASU; (B) GOOGLE EARTH; (C) DOUGLAS J. JEROLMACK

Alluvial fans and associated deposits. (**A**) Topographic map draped on images showing the landing ellipse (oval) and landing site (cross) of Curiosity in Gale crater, Mars. (**B**) Google Earth perspective view of an alluvial fan in the Mojave Desert, USA. (**C**) Alluvial fan deposits exposed in a river bank in New Mexico. Note the alternating gravel and sand sheets, similar to those described at Gale crater by Williams *et al.*

covered by Williams *et al.* lie on a relatively flat crater floor, several kilometers downslope from the eroded terminus of an alluvial fan (see the figure). The deposits are estimated to be older than 3.5 billion years. The rounded pebbles, mixed in alternating layers with sand-sized particles, are indicative of a free-flowing gravel stream. Additional support comes from the observation of imbricated clasts, pebbles arranged like a train of collapsed dominoes, which are strictly associated with fluvial transport.

On Earth such deposits are a common feature; the finding is a breakthrough for Mars, however, because (i) it is the first definitive in situ identification of river sediments; (ii) the rounding of the pebbles indicates abrasion during transport, suggesting that particles traveled at least several kilometers from their source area; and (iii) it allows quantitative reconstruction of ancient flows. Under reasonable assumptions associated with near-threshold fluvial transport, the formative river flow had depths in the range 0.03 to 0.9 m and velocities in the range 0.2 to 0.75 m/s. The main uncertainty is associated with river slope, which cannot be obtained directly from the deposits.

Williams *et al.* are conservative in their interpretation, but the nature of the sediments and their proximity to the fan terminus are consistent with deposition on an alluvial fan. Noncohesive gravel streams on Earth typically exhibit critical flow, where fluid inertial and gravitational forces approximately balance (*10*), and dimensionless shear stresses are slightly in excess of the threshold of motion (*11*). A friction factor typical of gravel streams (0.01) would result in a slope of 1%, the same value as the adjacent alluvial fan. Corresponding flow depth and velocity would be 0.1 m and 0.6 m/s, respectively.

The finding of Williams *et al.* shows that martian rivers can be similar to terrestrial ones, all the way down to the grain scale; this suggests a depositional environment similar to the distal regions of typical alluvial fans observed in the American Southwest (*12*). As the authors point out, climate conditions must have been appreciably warmer and wetter at the time of sediment transport relative to modern conditions. Whether sediments were laid down over a long time in an arid region with intermittent rain (as in terrestrial deserts) or deposited more rapidly under a sustained outflow cannot be determined. Meanwhile, fresh challenges to the warm and wet early Mars hypothesis are emerging. Some point to new physical and chemical evidence that supports a cold and dry early Mars interrupted by brief bursts of wetness (*13*, *14*); other recent work (*15*) suggests that Mount Sharp itself is composed primarily of aeolian rather than water-lain strata.

Skepticism about the warm and wet early Mars hypothesis will continue. This debate is healthy, however, and has encouraged formation of clear hypotheses and targeted missions. Our understanding of Earth's present and past climate comes from observations of the surface and subsurface across the globe, coupled with sophisticated modeling. It is becoming clear that the landscapes on Mars are almost as varied and complex as those on Earth. Thus, there is unlikely to be a smoking gun for a warm and wet early Mars. Rather, the case will be built from circumstantial evidence accumulated over decades of lander and satellite missions. Onward, Curiosity!

References

1. M. H. Carr, *Philos. Trans. R. Soc. London Ser. A* **370**, 2193 (2012).
2. S. W. Squyres *et al.*, *Science* **306**, 1698 (2004).
3. R. M. E. Williams *et al.*, *Science* **340**, 1068 (2013).
4. M. C. Malin, K. S. Edgett, *Science* **302**, 1931 (2003).
5. J. M. Moore *et al.*, *Geophys. Res. Lett.* **30**, 2292 (2003).
6. D. Jerolmack *et al.*, *Geophys. Res. Lett.* **31**, L21701.
7. J. M. Moore, A. D. Howard, *J. Geophys. Res.* **110**, E04005 (2005).
8. N. Mangold *et al.*, *Icarus* **220**, 530 (2012).
9. J. P. Grotzinger *et al.*, *Space Sci. Rev.* **170**, 5 (2012).
10. G. E. Grant, *Water Resour. Res.* **33**, 349 (1997).
11. C. Paola*et al.*, *Basin Res.* **4**, 73 (1992).
12. J. Stock *et al.*, *Geol. Soc. Am. Bull.* **120**, 619 (2008).
13. E. Hand, *Nature* **484**, 153 (2012).
14. R. Wordsworth *et al.*, *Icarus* **222**, 1 (2013).
15. E. S. Kite *et al.*, *Geology* **41**, 543 (2013).

10.1126/science.1239343

CELL BIOLOGY

GATORs Take a Bite Out of mTOR

A negative regulator of amino acid sensing by the mTOR signaling pathway is identified and discovered to be inactivated in cancers.

Reuben J. Shaw

Coupling nutrient availability to cellular growth is essential for all organisms. Across eukaryotes, the serine-threonine kinase called target of rapamycin (TOR; or mTOR in mammals) is a master regulator of cell growth. It is the catalytic subunit of two molecular complexes, mTORC1 and mTORC2. The mTORC1 complex is acutely sensitive to concentrations of both growth factors and nutrients, including glucose and amino acids (*1*). The mTORC1 signaling pathway in cells is hyperactivated in a broad spectrum of human cancers and in metabolic disease (*2*). On page 1100 in this issue, Bar-Peled *et al.* (*3*) identify a protein complex that negatively regulates mTORC1 and functions as a tumor suppressor, pointing to new possible therapeutic strategies for cancer.

Molecular and Cell Biology Laboratory, Howard Hughes Medical Institute, The Salk Institute for Biological Studies, La Jolla, CA 92037, USA. E-mail: shaw@salk.edu

Genetic studies in the fly *Drosophila melanogaster* and in mammals identified the tuberous sclerosis complex (TSC) tumor suppressors as critical inhibitors of mTORC1 under conditions of low growth factors. The *TSC1* and *TSC2* genes are genetically inactivated in sporadic cancers in addition to the inherited disorder tuberous sclerosis (*1*). The TSC2 protein encodes a guanosine triphosphatase (GTPase)–activating protein (GAP) that inactivates Rheb, a small GTPase that binds to and activates mTOR. In response to amino acid abundance, a different set of small GTPases, the Rag proteins, bind to and activate mTORC1 (*4*). When amino acid availability increases, Rag proteins translocate to the outer surface of the lysosome where they bind to Ragulator, a protein complex that loads RagA (or RagB) with GTP. In this state, Rag proteins can recruit mTORC1 to the lysosomal surface (*5*) where it becomes activated and can signal. Thus, when amino acid availability is low, mTORC1 does not translocate and remains inactive in the cytosol.

Given that the TSC complex serves to suppress mTORC1 by inhibiting Rheb, Bar-Peled *et al.* investigated whether negative regulators of Rag proteins exist as well. The authors identified a protein complex, which they call GAP activity toward Rags (GATOR), that acts upstream of the Rag proteins (see the figure). The eight proteins that comprise GATOR can be divided into two subcomplexes based on the affinity of protein-protein interactions and epistasis experiments that examined their effects on mTORC1. Inhibition of GATOR1 constituents [dishevelled, Egl-10 and pleckstrin (DEP) domain–containing 5 (DEPDC5); nitrogen permease

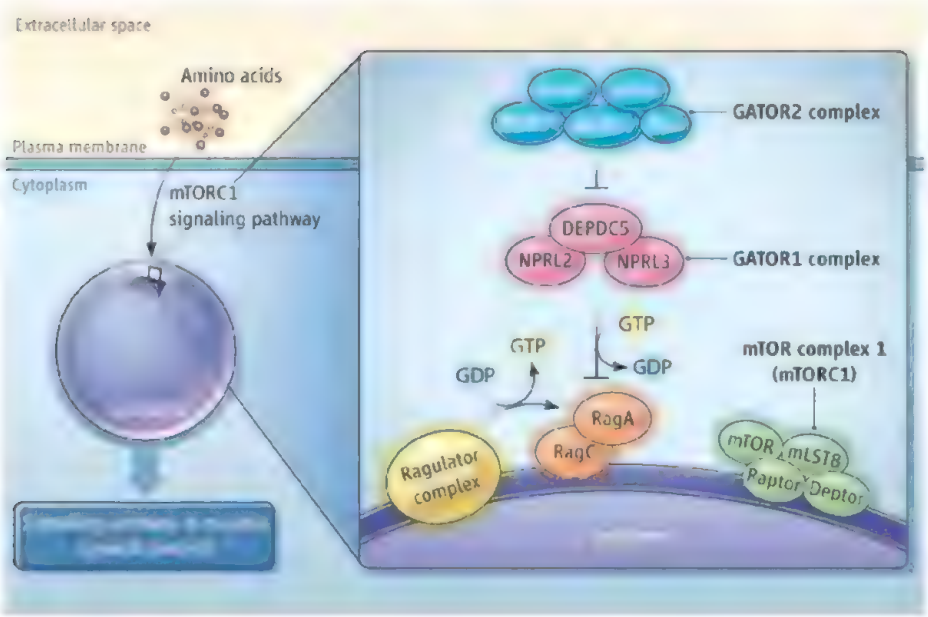

Amino acid–dependent control of cell growth. GATOR1 and GATOR2 complexes regulate RagA, a small GTPase that controls activation of mTORC1 at the surface of the lysosomes in response to amino acid availability. Ragulator serves to stimulate GTP loading of RagA and activate mTORC1 in response to amino acids, whereas GATOR1 acts to turn RagA off by stimulating its intrinsic GTPase activity.

regulator 2-like (NPRL2); and NPRL3] renders mTORC1 insensitive to amino acids and consequently leaves mTORC1 constitutively active. By contrast, inhibition of GATOR2 components [Mios; Sec13; Seh1l, WD repeat containing protein 24 (WDR24); and WDR59] results in loss of mTORC1 activity, which was reversed by loss of GATOR1, further indicating that GATOR1 is a more proximal regulator of the Rags.

The findings of Bar-Peled *et al.* fit well with those of Panchaud *et al.* (*6*), who determined that the yeast homologs of GATOR1 proteins have GAP activity toward a Rag ortholog (Gtr1p) in *Saccharomyces cerevisiae*. Amino acid deprivation caused the DEPDC5 homolog (Iml1p) to interact with the RagA homolog (Gtr1p) at the surface of the lysosome-like vacuole and stimulate the GTPase activity of Gtr1p, thereby turning it off and leaving yeast TORC1 in an inactive state. Indeed, the yeast homologs of NPRL2 (Npr2) and NPRL3 (Npr3) were previously identified in a genome-wide screen for regulators of TORC1 in response to amino acid deprivation (*7*). Npr2 and Npr3 occur together in a complex with Iml1 and with orthologs of mammalian GATOR2 components (*8*). Interestingly, yeast GATOR1 controls autophagy (*9*), the breakdown of cellular components in the vacuole (or in mammalian lysosomes) during starvation to maintain cellular metabolism. This indicates that the functional roles of mammalian GATOR are extremely well conserved.

The discovery of such fundamental conserved regulators of cell biology and human health raise many questions. How are amino acids sensed by the GATOR and/or Ragulator complexes? What other signaling pathways control GATOR activity? It is also not clear how GATOR2 regulate GATOR1. Intriguingly, proteins in the GATOR2 subcomplex are composed almost entirely of WD repeats, as is the protein mLST8, which is a component of mTORC1 and mTORC2. Another common component of both mTORC1 and mTORC2 is the negative regulator Deptor (originally called DEPDC6), so DEP-domain–containing proteins now emerge at multiple locations in the core mTORC1 pathway as negative regulators. It is also not clear where the catalytic "heart" of the GATOR1 GAP activity lies. In yeast (*6*), it lies in Iml1 where a specific conserved arginine is the critical catalytic residue, though the arginine does not reside within a domain containing recognizable homology to GAPs for other small GTPases.

Given how many of the upstream regulators of mTORC1 by growth factors are mutated in human cancer, an open question is whether any of the components that regulate mTORC1 in response to amino acids might also be altered in human tumors. Because the GATOR1 complex acts analogously to the TSC complex to inactivate mTORC1, and TSC components are mutated in both familial and sporadic human tumors, one might expect GATOR1 components to similarly be mutated. Indeed, the genes encoding NPRL2 and DEPDC5 localize to chromosome regions deleted in lung (*10*) and glioblastoma tumors (*11*), and using available data from The Cancer Genome Atlas, Bar-Peled *et al.* identify a subset of ovarian and glioblastoma cancers with nonsense and frameshift mutations or truncating deletions in genes encoding GATOR1 constituents. Further, the authors identify several cancer cell lines bearing homozygous deletions in the genes encoding DEPDC5, NPRL2, or NPRL3. Analysis of these GATOR1-deficient lines revealed that mTOR was localized to the surface of lysosomes even when amino acids were deprived, which is analogous to what occurs when there are mutations in RagA that lock it into the activated state (*12*). GATOR1-deficient cancer cells were exquisitely sensitive to rapamycin, a small-molecule inhibitor of mTORC1, which suggests that GATOR1 genes could be screened in tumors to predict responders to these clinically approved anticancer agents (*1*).

In addition to these roles in human cancer, DEPDC5 was recently identified in studies searching for the gene on chromosome 22q22 that is responsible for most cases of familial focal epilepsy with variable foci, an autosomal dominant inherited form of epilepsy (*13*, *14*). Interestingly, epilepsy is also the most common presenting symptom of tuberous sclerosis (*15*), the disorder caused by mutations in the *TSC1* and *TSC2* genes. That two GAPs (TSC2, DEPDC5) that suppress mTORC1 are both mutated in cancer and familial forms of epilepsy emphasizes the central role that mTORC1 plays in many diseases.

References

1. M. Laplante, D. M. Sabatini, *Cell* **149**, 274 (2012).
2. M. Cornu, V. Albert, M. N. Hall, *Curr. Opin. Genet. Dev.* **23**, 53 (2013).
3. L. Bar-Peled *et al.*, *Science* **340**, 1100 (2013).
4. Y. Sancak *et al.*, *Science* **320**, 1496 (2008).
5. L. Bar-Peled, L. D. Schweitzer, R. Zoncu, D. M. Sabatini, *Cell* **150**, 1196 (2012).
6. N. Panchaud, M.-P. Péli-Gulli, C. De Virgilio, *Sci. Signal.* **6**, ra42 (2013).
7. T. K. Neklesa, R. W. Davis, *PLoS Genet.* **5**, e1000515 (2009).
8. S. Dokudovskaya, M. P. Rout, *Autophagy* **7**, 1392 (2011).
9. X. Wu, B. P. Tu, *Mol. Biol. Cell* **22**, 4124 (2011).
10. J. Li *et al.*, *Cancer Res.* **64**, 6438 (2004).
11. T. J. Seng *et al.*, *Genes Chromosomes Cancer* **43**, 181 (2005).
12. A. Efeyan *et al.*, *Nature* **493**, 679 (2013).
13. L. M. Dibbens *et al.*, *Nat. Genet.* **45**, 546 (2013).
14. S. Ishida *et al.*, *Nat. Genet.* **45**, 552 (2013).
15. A. M. van Eeghen, M. E. Black, M. B. Pulsifer, D. J. Kwiatkowski, E. A. Thiele, *Eur. J. Hum. Genet.* **20**, 510 (2012).

10.1126/science.1240315

NEUROSCIENCE

Neuronal Birth to Cortical Circuitry

Developmental genetics of single neuron populations can reveal how cortical circuits are built and how neuropsychiatric diseases arise.

Stewart Anderson[1] and Douglas Coulter[2]

Neuropsychiatric diseases, such as schizophrenia and autism, likely involve dysfunction in cerebral cortical microcircuits. Although some of this dysfunction probably results from disruptions near the time of symptom onset, some also likely evolves from abnormalities that occurred earlier during cortical neuron development. However, a major challenge has been to link microcircuitry dysfunction to a disruption in the developmental trajectories of constituent neuronal subtypes. A recent paper in *Science* by Taniguchi *et al.* (*1*) lays crucial groundwork for meeting this challenge. They describe a method for reliably labeling a distinct subtype of cortical neuron, the chandelier interneuron, from its genesis through postnatal development. Their work advances understanding of cortical microcircuitry development, and highlights the potential challenges of using the current genetic armamentarium to label increasingly specific subsets of cortical neurons.

The neocortex is composed of diverse neuronal subtypes with distinct patterns of connectivity and activity. This complexity has hindered our ability to understand the development and function of cortical circuitry, and thus how it malfunctions in disease. The neuronal cytoarchitecture of the neocortex involves projection neurons that are mainly excitatory, and local circuit neurons (interneurons) that are mainly inhibitory. Neuronal subgrouping is often defined by single characteristics, such as laminar location, expression of a particular protein, morphology, or electrophysiological properties. Subtypes of neurons are then categorized by clustering these characteristics (*2*), such as layer 5, callosally projecting pyramidal neurons expressing Dkk3 (*3*), or vertically oriented, vasoactive intestinal peptide (VIP)–expressing interneurons with regular and nonaccommodating spiking features (*4*).

Recent advances in the labeling and manipulation of neuronal subgroups are enabling characterization according to their function in cortical microcircuits. For example, in mice, labeling of somatostatin (SST)–expressing interneurons with a fluorescent protein revealed that cortical layer 3 SST interneurons primarily inhibited the activity of pyramidal neuron dendrites, whereas layer 4 SST interneurons selectively targeted fast-spiking inhibitory interneurons (*5*). Thus, within the SST-expressing subgroup, neuronal subtypes residing in distinct cortical layers can have apposing influences on cortical excitation.

Although genetic labeling of cortical neuronal subgroups and elucidation of their functional connectivity in microcircuits are resulting in many insightful studies, the labeling methods are often restricted to later stages of the target cell's development. This is an important limitation, because symptoms of neuropsychiatric disorders can be the manifestations of disruptions that began much earlier. Fortunately, advances in the genetic labeling of cortical subpopulations are allowing a temporally and spatially defined approach to the study of cortical neuron development (*6*). One such approach uses an estrogen receptor–Cre recombinase fusion protein, CreERT2. Administration of tamoxifen induces permanent mutagenesis through Cre-mediated recombination of Loxp-flanked DNA target sequences, with both tissue and temporal selectivity (see the figure).

Taniguchi *et al.* take this approach to a new level—the selective labeling of a subtype of interneuron, the chandelier cell, from its birth within the subcortical telencephalon to its maturation within the postnatal neocortex. Chandelier cells innervate the axon initial segment of cortical pyramidal neurons (*7*). Notably, this interneuron subtype also has dense, sometimes conjoint innervation of most of the pyramidal neurons within its axonal field (*8*), and displays synaptic abnormalities in schizophrenia (*9*). Chandelier cells derive from Nkx2.1-expressing progenitors of the subcortical forebrain (*10*), especially within the most ventral portion of the medial ganglionic eminence (MGE) late in the period of cortical neurogenesis (*1*, *11*).

Using Nkx2.1CreERT2 to label Nkx2.1-expressing cells at the end of gestation, Taniguchi *et al.* found a tremendous enrichment for labeling of chandelier cells. The labeling of chandelier cells as progenitors meant that their development could be studied over the first postnatal weeks, before and during their development of axo-axonic synapses that define the subtype. Remarkably, chandelier cell precursors (postmitotic, fate-committed but immature neurons) formed a previously unknown plexus along the border of layers 1 and 2 by postnatal day 7 (P7), just after the end of pyramidal neuron radial migration, when their apical dendrites are extending through layer 2 and into layer 1. P7 is also a time when the gradient for chloride across the pyramidal neuron plasma membrane favors a depolarizing response to the activation of γ-aminobutyric acid type A ($GABA_A$) receptors, raising the possibility that chandelier cells provide a major excitatory drive to cortical projection neurons just as they are forming their connectivity. Just 3 weeks later, most

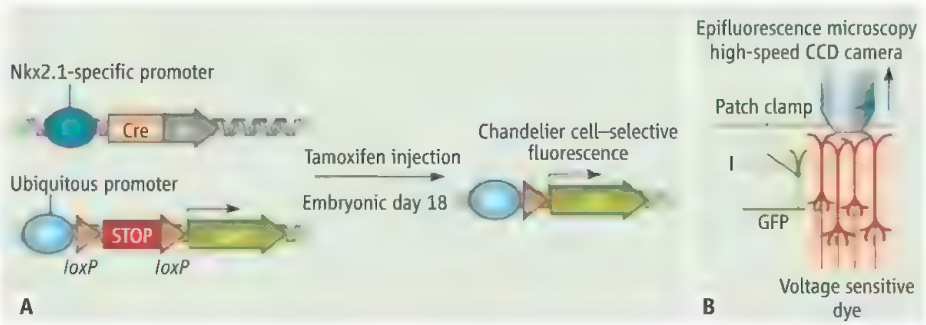

Studying cortical microcircuitry. Schema of one approach for studying the development of cortical microcircuitry extending from the work of Taniguchi *et al.* (**A**) Nkx2.1CreERT2 mice are crossed with mice containing a green fluorescent protein (GFP) reporter, such that injection of tamoxifen late in gestation results in GFP expression that, for the cortex, is highly selective for chandelier interneurons. (**B**) Patch-clamp recording and activation of chandelier interneurons in slices of developing cerebral cortex, while imaging the effects on pyramidal neuron network activity using voltage-sensitive dyes. CCD, charge-coupled device.

[1]Department of Psychiatry, Children's Hospital of Philadelphia–University of Pennsylvania School of Medicine, Philadelphia, PA 19104–5127, USA. [2]Division of Pediatric Neurology, Children's Hospital of Philadelphia–University of Pennsylvania School of Medicine, Philadelphia, PA 19104–5127, USA. E-mail: andersons3@email.chop.edu; coulterd@email.chop.edu

chandelier cells at the layer 1–2 border were no longer detectable.

In conjuction with evidence that an analogous process may be occurring across layers 2 to 6 in primates (*12*), these results suggest that chandelier cells play a previously unrecognized role in the development of cortical circuitry. This could be explored by using Cre-based combinatorial approaches to, for example, genetically encode activity indicators, such as calcium (GCaMPs) or voltage indicators (*13*); express optogenetic activators and silencers, or other proteins that alter membrane potential (*14*); and inducibly express selective cellular silencers or suicide mediators (*6*). In addition, postmortem studies of schizophrenia have identified abnormalities in chandelier cells (*9*), but whether the abnormalities are a cause or an effect of the core etiology is unclear. Thus, the ability to selectively label these cells enables the study of whether chandelier cell–specific mutations of interneuron-expressed schizophrenia risk genes, such as *Disc1* or *Erb4* (*9*), can induce schizophrenia-related phenotypes in mice.

The above techniques require the identification of subclass-selective genes whose regulatory regions can be harnessed as Cre "drivers." In the case of chandelier cells, investigators found specificity of labeling because chandelier cells are the latest-born of the interneurons derived from Nkx2.1-expressing progenitors. Although combining the selectivity of gene expression with the temporally restricted activation of labeling should enable Cre-based study of additional subtypes, for the developmental study of microcircuitry involving most cortical subtypes, it will be necessary to identify relatively selective genetic markers of fate-committed neuronal subtypes when they are immature.

Fortunately, the evidence to date, further bolstered by the Taniguchi *et al.* study, is that fate commitment of both cortical pyramidal neuron and interneuron subtypes generally occurs before or shortly after cell cycle exit (*4*, *15*, *16*). Although the genetic code responsible for maintaining neuronal subtype fate through the migration and maturation processes may be combinatorial, it should be possible to identify genes with adequately selective expression patterns that, together with the temporal restriction of labeling, will enable developmental studies of the microcircuitry involving most cortical neurons. These approaches are likely to revolutionize the discovery of the etiological antecedents of neuropsychiatric disease.

References

1. H. Taniguchi, J. Lu, Z. J. Huang, *Science* **339**, 70 (2013).
2. G. A. Ascoli *et al.*, *Nat. Rev. Neurosci.* **9**, 557 (2008).
3. B. J. Molyneaux *et al.*, *J. Neurosci.* **29**, 12343 (2009).
4. S. J. Butt *et al.*, *Neuron* **48**, 591 (2005).
5. H. Xu *et al.*, *Neuron* **77**, 155 (2013).
6. A. Urban, J. Rossier, *Prog. Brain Res.* **196**, 163 (2012).
7. P. Somogyi, *Brain Res.* **136**, 345 (1977).
8. M. Inan *et al.*, *J. Neurosci.* **33**, 1907 (2013).
9. O. Marín, *Nat. Rev. Neurosci.* **13**, 107 (2012).
10. Q. Xu, M. Tam, S. A. Anderson, *J. Comp. Neurol.* **506**, 16 (2008).
11. M. Inan, J. Welagen, S. A. Anderson, *Cereb. Cortex* **22**, 820 (2012).
12. S. A. Anderson *et al.*, *Neuroscience* **67**, 7 (1995).
13. J. Akerboom *et al.*, *J. Neurosci.* **32**, 13819 (2012).
14. L. Madisen *et al.*, *Nat. Neurosci.* **15**, 793 (2012).
15. S. J. Franco *et al.*, *Science* **337**, 746 (2012).
16. S. K. McConnell, *J. Neurosci.* **8**, 945 (1988).

10.1126/science.1235778

BIOCHEMISTRY

Structural MS Pulls Its Weight

Mass spectrometry provides insights into the structure and dynamics of ever-larger protein assemblies and associated biomolecules.

Michal Sharon

When we step on the scale, we usually respond in one of two ways: disappointment or joy. When we measure the mass of protein assemblies, on the other hand, we get a glimpse into a rich and interesting world. A simple measure of mass can give information on the inherent properties of protein complexes and expose a multiprotein assembly's composition, the number of copies of each subunit, their topological arrangement, and the assembly's overall structure (*1*, *2*) (see the figure). These capabilities, together with the modest sample requirements, speed of analysis, selectivity, tolerance to heterogeneity, and lack of an upper mass limit, have transformed structural mass spectrometry (MS) from an emerging technique to an integral part of the structural biology toolkit.

MS is often associated with protein identification, posttranslational modification, and quantification. These terms reflect the wide capabilities of proteomics—a field based on the analysis of peptides derived from a target sample—but do not capture the essence of structural MS. Unlike proteomics, structural MS is based on the ability to transfer intact protein complexes to the gas phase while maintaining weak interactions between subunits and associated biomolecules such as DNA and ligands (*1*, *2*).

One study that served as a rite of passage for structural MS was the three-dimensional model constructed for the 10-subunit yeast RNA exosome, a protein assembly that had evaded other structural biology techniques. On the basis of MS data, the subunit interaction map of the complex, isolated from cells at its natural expression levels, was constructed and developed into an atomic model via homology modeling (*3*). The subunit interactions and overall architecture of this model were soon corroborated by x-ray crystallography and electron microscopy (EM) studies, setting the stage for tackling more challenging systems.

Advances in obtaining quaternary information on protein complexes were made possible by the development of a hybrid instrument that measures both mass and ion mobility (*4*). The time that it takes for an ion to travel through a tube densely filled with an inert gas depends not only on the mass, but also on the shape of the analyzed protein complex. An assembly with a large volume will experience more collisions with the gas and thus travel more slowly than a complex with the same mass but a more compact structure. The traveling time of the macromolecule can be converted into a numerical value that reflects the area of the analyzed protein complex. This information allows the packing and topology of subunits within an assembly to be deduced.

In the first application of the ion mobility/MS method, Ruotolo *et al.* showed that an 11-member protein complex retains its ring-type topology in the mass spectrometer (*4*). This finding provided experimental evidence that protein quaternary structure can be maintained in the gas phase, and the approach has since been applied to other heterogeneous multisubunit complexes.

Department of Biological Chemistry, Weizmann Institute of Science, Rehovot 76100, Israel. E-mail: michal.sharon@weizmann.ac.il

Structural MS can also be used to study multisubunit complexes embedded in membranes. These assemblies perform crucial biological tasks as transporters, channels, receptors, and recognition and adhesion molecules. Yet their poor solubility, weak interactions between subunits, and tendency to aggregate make it very difficult to elucidate their structures.

Barrera *et al.* (*5*) overcame these problems. In their approach, the surrounding detergent molecules are not removed before MS analysis. Rather, the intact membrane protein complex is projected into the gas phase within a protective detergent micelle that is released within the mass spectrometer. This leaves the protein complex largely devoid of loosely associated detergent molecules, but with protein subunit and specific lipid-binding interactions intact. Thus, subunit composition can be determined and the interacting lipids characterized, paving the way toward understanding how lipid-protein interactions modulate the functionality of membrane protein complexes (*6*).

Yet dissecting the structural architecture of a protein complex is not enough. Protein motion and dynamics are integral aspects of function, and a complete description of a biomolecule's activity must therefore include the dimension of time. The analysis of separation speeds afforded by MS place the method in a good position to capture both intramolecular motion (such as unfolding and conformational changes) and intermolecular transitions (such as subunit exchange and protein assembly pathways). Real-time MS analyses have opened a window onto the kinetics of protein folding, enzymatic reactions, ligand interactions, subunit exchange, and biogenesis pathways (*7*, *8*).

Another powerful property of structural MS is that in a single spectrum, all coexisting subpopulations of a protein complex can be resolved. This ability, together with the high resolving power of the technique, offers a way to address mechanistic questions. For example, structural MS can detect differences in mass due to the binding of single ligand molecules and can determine the relative populations of ligand-bound states of a protein complex, thus making it possible to distinguish between various allosteric mechanisms, as shown recently in the case of the chaperonin GroEL (*9*). MS can thus provide insight not only into the structure but also into the activity of large protein complexes.

Combinations of structural MS and other techniques—particularly EM, x-ray crystallography, and nuclear magnetic resonance (NMR)—not only offer a more comprehensive description of molecular assemblies but also enable examination of systems resistant to characterization by any single technique. In a recent study of polydisperse proteins, which interconvert between different oligomeric states, Baldwin *et al.* integrated information from NMR, MS, ion mobility, and EM to determine the structures of the main states of the molecular chaperone αB-crystallin and to explain why they can easily exchange architectures (*10*).

Advances in MS technology promise even greater insights. The Orbitrap mass spectrometer, for instance, provides high resolution and mass accuracy and has revolutionized proteomics since its introduction in 2005. However, its applications were limited to small molecules and peptides. Recently, Rose *et al.* modified an Orbitrap benchtop instrument to enable analyses of large protein complexes (*11*). This advance may broaden the scope of structural MS to less abundant protein complexes and allow posttranslational modifications to be resolved directly on intact proteins and assemblies (*12*). Other technical advances suggest that it may become possible to analyze macromolecular assemblies directly from individual cells (*13*, *14*) or from tissue surfaces (*15*).

Traditionally, scientists have conceived protein assemblies as largely uniform in both composition and function. However, the time may have come to view protein complexes as dynamic entities that alter their composition depending on where they reside and when they are examined. This emerging perspective of plasticity in protein assemblies can be exposed by MS, peeling away an additional layer from the complexity of life.

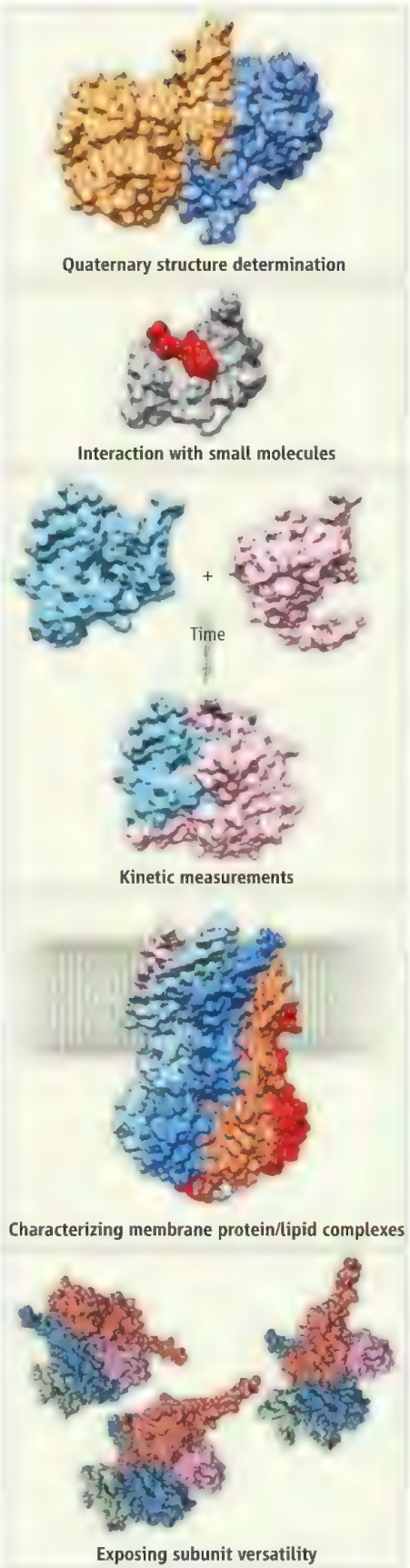

Structural mass spectrometry offers a range of capabilities.

References

1. A. J. Heck, *Nat. Methods* **5**, 927 (2008).
2. J. A. Loo, *Mass Spectrom. Rev.* **16**, 1 (1997).
3. T. Taverner *et al.*, *Acc. Chem. Res.* **41**, 617 (2008).
4. B. T. Ruotolo *et al.*, *Science* **310**, 1658 (2005).
5. N. P. Barrera, N. Di Bartolo, P. J. Booth, C. V. Robinson, *Science* **321**, 243 (2008).
6. M. Zhou *et al.*, *Science* **334**, 380 (2011).
7. G. Ben-Nissan, M. Sharon, *Chem. Soc. Rev.* **40**, 3627 (2011).
8. L. Konermann, J. Pan, Y. H. Liu, *Chem. Soc. Rev.* **40**, 1224 (2011).
9. A. Dyachenko, R. Gruber, L. Shimon, A. Horovitz, M. Sharon, *Proc. Natl. Acad. Sci. U.S.A.* **110**, 7235 (2013).
10. A. J. Baldwin *et al.*, *Structure* **19**, 1855 (2011).
11. R. J. Rose, E. Damoc, E. Denisov, A. Makarov, A. J. Heck, *Nat. Methods* **9**, 1084 (2012).
12. S. Rosati *et al.*, *Angew. Chem. Int. Ed.* **51**, 12992 (2012).
13. J. S. Mellors, K. Jorabchi, L. M. Smith, J. M. Ramsey, *Anal. Chem.* **82**, 967 (2010).
14. P. L. Urban, T. Schmid, A. Amantonico, R. Zenobi, *Anal. Chem.* **83**, 1843 (2011).
15. C. N. Ferguson, S. A. Benchaar, Z. Miao, J. A. Loo, H. Chen, *Anal. Chem.* **83**, 6468 (2011).

10.1126/science.1236303

IBI* SERIES WINNER

Students as Collaborators in Systems Biology Research

Quantitative Trait Mapping, an IBI prize–winning module, immerses students in the role of a systems biology researcher.

Susan McClatchy,[1] Deborah McGann,[2] Robert Gotwals,[3] Amanda Baskett,[4] Gary Churchill[1]†

In his 1854 speech at the University of Lille, Louis Pasteur stated "In the fields of observation, chance favors only the prepared mind." Preparation for scientific inquiry is critical for the future of research, yet opportunities are rare in the early stages of education. This discrepancy can be resolved by immersing students in genuine research activities as early as possible. We have created an experience for high school students to engage in and contribute to ongoing research. We prepare students to formulate and test hypotheses using computational tools and data collected in our laboratory, or available from public repositories.

The Quantitative Trait Mapping (QTM) module (fig. S1) is a core component of Independent Studies in Computational Biology (ISCB), a two-semester systems biology research course offered to talented high school students by The Center for Genome Dynamics at The Jackson Laboratory (*1*). Introductory high-school genetics and statistics are prerequisites. We employ a hybrid strategy of online learning and in-class instruction in which students and teachers from three publicly funded magnet schools participate via Web conference. Students and their teachers become active partners in our group's research and some have published their work in peer-reviewed journals (*2*, *3*).

Students and teachers meet in their classrooms during the week, and all sites attend a weekly Web conference with a Jackson Laboratory researcher, who acts as their scientific mentor. In the first semester, students read and present information from scientific literature. We select review articles, summaries of featured literature, and reports of experimental findings from leading journals. Students present and discuss papers in journal club, honing their critical thinking and communication skills. Each student writes a brief literature review on a topic of their choosing. In parallel, we provide students with instruction and hands-on practice in statistical analysis of quantitative traits. Students analyze published data from quantitative trait loci (QTL) mapping studies (e.g., QTL Archive; qtlarchive.org) by means of R/qtl software (*4*); they learn how to employ Web-based resources to dig deeper, obtaining up-to-date information on genetic variation and functional annotation. The semester culminates with a written NIH-style grant proposal that integrates material from these exercises.

In the second semester, we begin the research phase of the course. Student teams of two to four are given relevant data but must decide on an analytical strategy that will address their hypothesis. This is a challenging step for students and involves Web conferences with their scientific mentor, who is a practicing research scientist in our lab, to arrive at clear hypotheses that are testable with the data in hand. The students' creative expression of their own ideas must be balanced against the scope of available data resources. This hypothesis-driven approach prepares the student with a conceptual framework for finding biological meaning amid the network of statistical relations that can emerge from large-scale data analysis (see the figure).

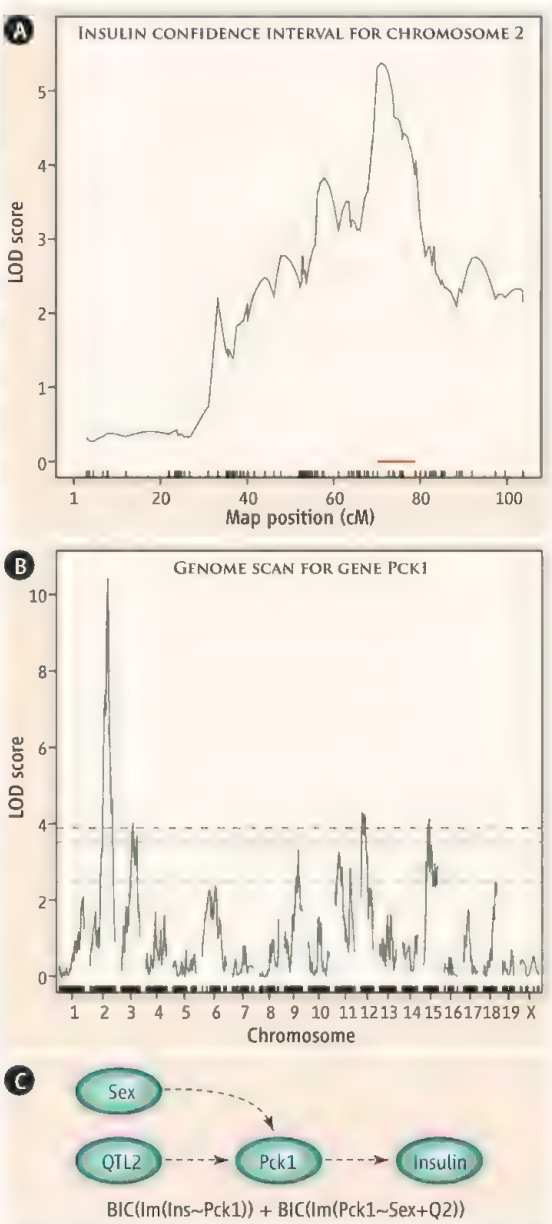

A student-initiated project begins with a hypothesis. In this example, the student identified a quantitative trait locus (QTL) for plasma insulin on chromosome 2. **(A)** The support interval for the QTL contains dozens of genes. Using database resources including Mouse Genome Informatics (www.informatics.jax.org), she generated a gene list along with functional annotation and allelic variants. She then carried out a systematic evaluation of each gene. On the basis of her hypothesis, she mapped gene expression traits in adipose tissue. **(B)** She evaluated genes using structural equation models to identify causal intermediates of the effect on plasma insulin. **(C)** She identified Pck1, an enzyme in the pathway that converts triglycerides to glucose, as a candidate with a potential role in diabetes and proposed a follow-up study that could provide validation for her finding.

[1]The Center for Genome Dynamics, The Jackson Laboratory, Bar Harbor, ME 04609, USA. [2]Maine School of Science and Mathematics, Limestone, ME 04750, USA. [3]North Carolina School of Science and Mathematics, Durham, NC 27705, USA. [4]Rockdale Magnet School for Science and Technology, Conyers, GA 30012, USA.

*IBI, *Science* Prize for Inquiry-Based Instruction; www.sciencemag.org/site/feature/data/prizes/inquiry/.

† Corresponding author: gary.churchill@jax.org

Examples of student-initiated investigations include the following:

- Activation of brown adipose tissue reduces obesity. Gene expression data were examined from mice fed either standard or high-fat diets. Causal inference methods were used to explore relations between adiposity and the expression of specific brown fat–associated genes.
- Adipocytes communicate to pancreatic beta cells. The relation of adipokines to pancreatic gene expression and plasma insulin levels was investigated by using data from a mouse intercross population.

Students communicate findings in weekly oral progress updates with the scientific mentor. Web conferences provide a venue for addressing students' questions and evaluating student progress and continued development of communication skills. We assess student understanding of background information and review critical concepts on an as-needed basis. E-mail exchanges among students, teachers, and mentors clarify interpretation of results and strategic approach. Classroom teachers, develop their own assessment tools for course assignments (see sample assessment in supplementary materials).

Student projects frequently require refinement or redirection, which can be a frustrating and difficult experience for high-performing students accustomed to having all of the correct answers. They learn that, in scientific inquiry, success is not a foregone conclusion and that there are neither predictable outcomes nor answers at the back of the book. And yet, we have witnessed acceptance of failure leading to perseverance. Often, seemingly false starts lead to unexpected results and novel insights as students experience the process of discovery firsthand (see the photo). The semester concludes with a final oral research presentation and a written report of student findings and conclusions.

We have considered how the QTM module might be expanded to reach a wider audience, including college undergraduates. Toward that end, we provide background reading material, recorded lectures, links to data and software resources, and examples illustrating data-analysis techniques (www.sysgenonline.org). Instructors can supplement this material by guiding students to selections from the scientific literature, selecting data for analysis, and assisting students in the use of Web resources. The didactic content of the module can save class time for discussion and interaction.

Although online learning modules can be widely disseminated, they cannot replace the personal elements of one-on-one interactions with a scientific mentor, a critical component of success. The scientist provides overall direction for the students' projects, as well as data and the expertise to interpret it. Educated and prepared teachers are also essential to the process. They evaluate students' progress, help students find information and resources, debug R code, and review students' practice presentations. The levels of personal attention and dedication required from the scientist and teachers are limiting factors in course expansion. We invite educators and scientists to contact us and join our weekly Web conferences to learn how to implement the module.

Students display a two-dimensio scan to detect interaction between loci.

Although the footprint of our course has been small (~70 students have completed or are currently enrolled in the course), its impact on these students has been enormous. Testimonials from course alumni, while anecdotal, indicate the power of this research experience in shaping education and career paths. One former student reported that "I'm graduating in Quantitative Biology … because of this class!" and another stated that "The course taught me how to pursue scientific problems from a computational mindset." Students are not the only beneficiaries of the course. As an indication of the effect of this experience on educators, one of our instructors commented, "I anticipated the course would have a great impact on our students, but could not have known how much the experience would influence me as a teacher, re-igniting a drive and desire to ask questions and explore."

Immersing students in scientific research as early as possible bridges the divide between practices in education and research. Early exposure to authentic systems biology–research experiences produces students with "prepared minds" who understand and value scientific research as a career choice, and who are comfortable speaking the languages of biology, mathematics, and computing.

About the authors

Susan McClatchy is the outreach coordinator for the Center for Genome Dynamics at The Jackson Laboratory. **Deborah McGann** teaches chemistry and biology at the Maine School of Science and Mathematics. **Robert Gotwals** is a chemistry and research instructor at the North Carolina School of Science and Mathematics. **Amanda Baskett** teaches research and microbiology at the Rockdale Magnet School for Science and Technology. **Gary Churchill** is a statistical geneticist at The Jackson Laboratory and director of the Center for Genome Dynamics, a National Center for Excellence in Systems Biology.

References and Notes

1. R. Von Smith *et al.*, *NCSSSMST J.* **15**, 10 (2009).
2. K. R. Shockley, D. Witmer, S. L. Burgess-Herbert, B. Paigen, G. A. Churchill, *Physiol. Genomics* **39**, 172 (2009).
3. M. Feng *et al.*, *Hypertension* **54**, 802 (2009).
4. K. W. Broman, S. Sen, *A Guide to QTL Mapping with R/qtl* (Springer Science+Business Media, New York, 2009).

Acknowledgments: Research reported in this publication was supported by the National Institute of General Medical Sciences, NIH, under award no. P50GM076468. We gratefully acknowledge feedback and suggestions from M. A. Handel, I. Hurley, and S. Munger. We thank K. Broman for his excellent R/qtl tutorials. A special thank you goes to R. Von Smith for originating the independent studies in computational biology course.

Supplementary Materials
www.sciencemag.org/cgi/content/full/340/6136/1061/DC1

10.1126/science.1229906

AAAS S&T POLICY FORUM

In a Tough Fiscal Climate, Coping Strategies Emerge

Amid continuing economic and political threats to fundamental research, seven foundations have launched an initiative to "renew and reinvigorate America's support of basic science." Robert Conn, president of The Kavli Foundation, introduced this Coalition of Foundations for Science at the AAAS Forum on Science and Technology Policy, where several leaders struck bright notes amidst otherwise bleak trends for federally funded research.

The foundations' initiative could open new channels of support for U.S. basic research, which has increasingly come under attack as policy-makers struggle to narrow a projected $744 billion U.S. budget gap.

The new coalition plans to help focus nongovernment resources on "high risk/high reward" research, in complement with government programs. In contrast, federal agencies tend to be somewhat risk averse and favor projects with clear and tangible outcomes, despite downsides to such conservative funding. "If you're succeeding all the time, you're clearly not aiming high enough," said co-panelist Chris Mentzel, program officer for the Gordon and Betty Moore Foundation's Data-Driven Discovery/Science Program.

Initiatives like this are not big enough to compensate for declines in government funding for science, the speakers cautioned. Collectively, foundations in the United States contribute about $2 billion per year to basic science, 75% of which goes to medical and biological research, Conn noted. The federal government, in contrast, spent around $30 billion on basic research in 2011.

The current pressures on federal research stood out in sharp relief on 2 to 3 May, at the 38th annual AAAS Forum on Science and Technology Policy in Washington, D.C. More than 400 people attended the forum, the premier venue for discussing issues at the intersection of science and technology with public policy. Throughout the meeting S&T leaders revealed they are thinking seriously about how to cope with the new conditions.

Creative approaches have become necessary since spending cuts forced by the Budget Control Act, also known as sequestration, drove federal R&D spending for fiscal year 2013 down to 0.8% of the gross domestic product (GDP)—the lowest level seen in 40 years. If sequestration continues, federal R&D as a share of GDP would likely drop below that 0.8% mark, according to Matt Hourihan, director of the AAAS R&D Budget and Policy Program.

Basic science, including research in the social and behavioral sciences, is particularly vulnerable as Congress seeks ways to maximize the impact of limited federal resources. Lawmakers have introduced proposals that would constrain the peer-review process by which the National Science Foundation (NSF) evaluates certain funding proposals. In March, a Senate amendment was passed as part of the bill to fund the government for the remainder of fiscal year 2013, prohibiting NSF from awarding grants to political science studies unless the director can "certify" that they "promote national security or the economic interests of the United States." Since then, there has been a hearing and additional discussion over a draft bill in the House Science, Space and Technology Committee to extend that same policy to all NSF grants.

Because basic research seeks solely to expand knowledge without special considerations for practical applications, these restrictions "would throw the basic research baby out with the bathwater," said presidential science adviser John Holdren, who criticized these developments in his keynote address.

Leaders at agencies that fund both basic and "use-inspired" research are also finding ways to make their dollars stretch farther.

It's elementary. John Holdren affirmed the White House's support for basic research.

Representatives from the U.S. Department of Agriculture, the Department of Energy's Office of Science, and the National Institutes of Health (NIH) each described new funding strategies aimed at solving problems efficiently by bringing researchers together across institutions or lowering barriers between academic research and commercial applications.

Kathy Hudson, deputy director for science, outreach, and policy at NIH, described with enthusiasm two new efforts: the recently announced BRAIN initiative for neuroscience, which NIH is a major partner in, and the National Center for Advancing Translational Sciences (NCATS), established in 2011.

A notable success at NCATS has been an effort to shorten the drug-development pipeline, by coordinating with eight pharmaceutical companies to select 58 drug candidates that had passed safety tests in humans but were then abandoned. Via crowdsourcing, NIH scientists identified promising new uses for these compounds more quickly than conventional drug testing would have.

The Defense Advanced Research Projects Agency (DARPA) is also increasingly recognizing the bottom line, according to the agency's director, Arati Prabhakar. "We in the leading-edge technology community have tended to treat cost for military systems as something that's someone else's problem. … And now I think we are going to be critically dependent on innovation that doesn't tweak at cost but starts flipping the cost equation," she said.

While creative new funding opportunities represent bright spots, it was clear the budget cuts will be deeply felt. Hudson summed up NIH's efforts by quoting Winston Churchill, who said "If you're going through hell, keep going." *–Kathy Wren and Sarah Zielinski*

COMMUNICATION

Screeners Needed for Journalism Awards

Volunteer scientists in the Washington, D.C., area are needed to review the scientific accuracy of entries in the prestigious AAAS Kavli Science Journalism Awards competition in print, online, radio, television, and children's science categories. If interested, please contact Katharine Zambon (kzambon@aaas.org).

CREDIT: AAAS/ROBERT BEETS

Accelerating Next-Generation Vaccine Development for Global Disease Prevention

Wayne C. Koff,* Dennis R. Burton, Philip R. Johnson, Bruce D. Walker, Charles R. King, Gary J. Nabel, Rafi Ahmed, Maharaj K. Bhan, Stanley A. Plotkin

Background: Vaccines have provided some of the greatest successes in the history of medicine, including the eradication of smallpox, the near eradication of polio, and the prevention of considerable morbidity and mortality from numerous infectious diseases each year. However, past strategies for vaccine development are unlikely to succeed in the future against major global diseases such as AIDS, tuberculosis, and malaria. For such diseases, the correlates of protection are poorly defined, and the pathogens evade immune detection and/or exhibit extensive genetic variability. Limitations of animal models to predict human immune responses to vaccines, coupled with low success rates for vaccine development compared with biopharmaceuticals, suggest that new paradigms must be implemented for accelerating vaccine development.

Advances: Recent technological advances in molecular genetics, molecular and cellular immunology, structural biology, bioinformatics, computational biology, nanotechnology, formulation methods, and systems biology are ushering in a new era of vaccine discovery. For example, genomic-based antigen discovery is being exploited for the design of vaccines against multiple bacterial pathogens. Similarly, interrogation of the memory B cell and antibody repertoires from virus-infected subjects has led to the identification of broadly neutralizing antibodies against HIV, influenza, and other viruses, which are now being exploited as tools to design highly conserved epitope-based vaccines. Advances in adjuvant and vector delivery technologies are providing novel approaches for immune potentiation of vaccines, offering new strategies for improving vaccine response rates in neonates and the elderly. However, translation of these advances into vaccines remains impeded by major gaps in our knowledge of human immune responses, including methods to focus immune responses on subdominant protective epitopes, to elicit long-term memory responses, and to drive antibody maturation processes. These gaps can now be addressed given the technological advances described, including the development of approaches to analyze immune responses at the single-cell and systems levels.

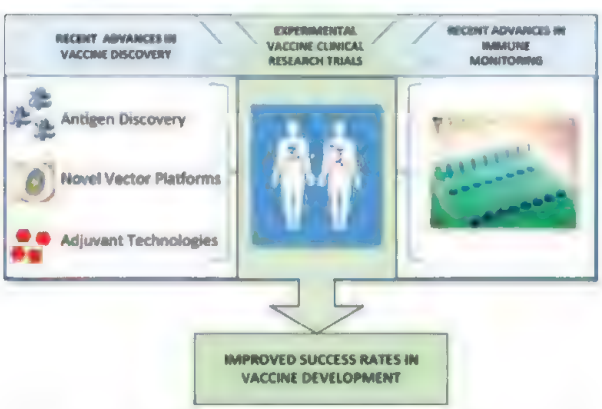

Accelerating next-generation vaccine development. Recent advances in vaccine discovery and immune monitoring will enable new human immunology–based clinical research studies to address major gaps in knowledge of vaccine-induced human immune responses and thereby accelerate development of next-generation vaccines. [Photo credit: IAVI]

Outlook: Successful development of vaccines against the major global diseases for which vaccines do not currently exist would be transformational for public health, with huge benefits across society. To accelerate next-generation vaccine development, we propose that new human immunology–based clinical research initiatives be established, with the goal of elucidating and more effectively generating vaccine-induced protective immune responses. Collectively, such a "Human Vaccines Project" holds the potential to greatly accelerate the development of next-generation vaccines against major global killers such as AIDS, tuberculosis, malaria, and other infectious diseases; enable more successful vaccine development against allergies, autoimmune diseases, and cancers; and provide a foundation for vaccine development against new and emerging diseases.

The list of author affiliations is available in the full article online.
*Corresponding author. E-mail: wkoff@iavi.org

READ THE FULL ARTICLE ONLINE
http://dx.doi.org/10.1126/science.1232910

Cite this article as W. C. Koff *et al.*, *Science* **340**, 1232910 (2013). DOI: 10.1126/science.1232910

ARTICLE OUTLINE

BACKGROUND READING

Recent advances in human immunology and vaccine discovery have led to a unique opportunity to advance the development of vaccines for globally important diseases. The references below highlight some of these advances.

S. Plotkin, W. Orenstein, P. Offit, Eds., *Vaccines, 6th Edition* (W. B. Saunders, London, 2013).

D. R. Burton *et al.*, A blueprint for HIV vaccine discovery. *Cell Host Microbe* **12**, 396 (2012). doi:10.1016/j.chom.2012.09.008

A. Sette, R. Rappuoli, Reverse vaccinology: Developing vaccines in the era of genomics. *Immunity* **33**, 530 (2010). doi:10.1016/j.immuni.2010.09.017

L. M. Walker *et al.*, Broad and potent neutralizing antibodies from an African donor reveal a new 486 HIV-1 vaccine target. *Science* **326**, 285 (2009). doi:10.1126/science.1178746

R. L. Coffman, A. Sher, R. A. Seder, Vaccine adjuvants: Putting innate immunity to work. *Immunity* **33**, 492 (2010). doi:10.1016/j.immuni.2010.10.002

B. Pulendran, S. Li, H. I. Nakaya, Systems vaccinology. *Immunity* **33**, 516 (2010). doi:10.1016/j.immuni.2010.10.006

Accelerating Next-Generation Vaccine Development for Global Disease Prevention

Wayne C. Koff,[1]* Dennis R. Burton,[2,4,11] Philip R. Johnson,[3] Bruce D. Walker,[4,5,11] Charles R. King,[1] Gary J. Nabel,[6] Rafi Ahmed,[7,11] Maharaj K. Bhan,[8] Stanley A. Plotkin[9,10]

Vaccines are among the greatest successes in the history of public health. However, past strategies for vaccine development are unlikely to succeed in the future against major global diseases such as AIDS, tuberculosis, and malaria. For such diseases, the correlates of protection are poorly defined and the pathogens evade immune detection and/or exhibit extensive genetic variability. Recent advances have heralded in a new era of vaccine discovery. However, translation of these advances into vaccines remains impeded by lack of understanding of key vaccinology principles in humans. We review these advances toward vaccine discovery and suggest that for accelerating successful vaccine development, new human immunology–based clinical research initiatives be implemented with the goal of elucidating and more effectively generating vaccine-induced protective immune responses.

At the end of the 18th century, Edward Jenner used cowpox-infected materials to immunize against smallpox and introduced the term " vaccine" (*1*). A century later, Louis Pasteur developed methods for attenuation of bacteria (*2*), and Salmon and Smith developed methods for inactivation of microorganisms (*3*). Together, these advances ushered in a new scientific era of vaccinology. Virus propagation in cell culture enabled the development of methods for attenuating viral vaccines (*4*), leading to a golden age of vaccine development in the second half of the 20th century with the development of several vaccines, including polio, measles, mumps, and rubella (*5*–*9*). By the latter part of the 20th century, most of the vaccines that could be developed by direct mimicry of natural infection with live attenuated or killed/inactivated vaccines had been developed. New technologies, including protein conjugation to capsular polysaccharides and the advent of methods to engineer recombinant DNA, led to the development of vaccines for prevention of bacterial pneumonia and meningitis, hepatitis B, and the recent development of the human papillomavirus (HPV) vaccine (*10*–*12*). Vaccines have now led to the eradication of smallpox, near eradication of polio, and prevention of untold millions of deaths from infectious diseases each year, and are one of the most effective public health measures available (*13*). For example, before the introduction of the measles vaccine in the United States, the incidence of measles peaked at nearly 900,000 cases per year, compared with an average of less than 100 cases of measles per year in recent years in the United States (*14*). Similarly, using metrics to measure cost-effectiveness of vaccines such as disability-adjusted life year (DALY), global vaccination for measles results in US$17 per DALY, one of the most cost-effective health interventions in developing countries (*15*). Table 1 provides an overview of vaccine-preventable diseases by currently licensed vaccines.

There are several diseases, however, that cause considerable global morbidity and mortality for which vaccines do not currently exist (Table 2). In general, the viruses, bacteria, and parasites for which new vaccines are needed are either much more complex in their pathogenesis, exhibit extensive variability, or have evolved immune evasion mechanisms to thwart the human immune system. For example, there are many cases, such as influenza and dengue viruses, for which immunologic memory induced by natural infection protects against reinfection by homologous serotypes but not by heterologous serotypes (*16*). Thus, minor changes in the outer glycoproteins from circulating strains of the influenza virus result in the need for annual immunizations against influenza. For viruses such as respiratory syncytial virus (RSV), reinfection with the same virus can occur, although disease is generally less severe with these sequential reinfections (*17*). For HIV, the hypervariability of the virus coupled with its capacity to integrate in the host genome results in the inability of the host to clear the infection (*18*). Finally, for pathogens such as cytomegalovirus (CMV), herpes simplex, and *Mycobacterium tuberculosis*, a carrier state is established with reactivation occurring in situations of immunosuppression (*19*). Clearly, new vaccine discovery and novel immunization paradigms will likely be required for successful vaccine development against HIV, *Mycobacterium tuberculosis*, *Plasmodium falciparum*, hepatitis C (HCV), and other challenging pathogens for which there currently are no licensed vaccines.

Recent technological advances in molecular genetics, molecular and cellular immunology, structural biology, bioinformatics, computational biology, nanotechnology, formulation technologies, and systems biology have heralded in a new era in immunogen design, adjuvant discovery (i.e., agents that enhance immune responses) and immune monitoring. However, translation of these advances into successful vaccines remains substantially impeded by a lack of understanding of key vaccinology principles in humans. This includes the need for greater understanding of disease-specific mechanisms of protective immunity, immune evasion mechanisms, and strategies to drive the immune system toward preferred responses by immunization.

Although based on sound scientific principles, currently licensed vaccines have largely been developed empirically, and protection by these vaccines is generally conferred by antigen-specific antibodies, which prevent or reduce infection (*20*). Viral neutralizing antibodies prevent virus replication by blocking virus binding and entry into cells. For hypervariable viral pathogens such as HIV and hepatitis C, it is likely that broadly neutralizing antibodies (bnAbs) (i.e., those targeting highly conserved regions of these viruses) will be necessary for globally effective vaccines. Many bnAbs against HIV have now been identified from HIV-positive subjects (*21*), but most of these bnAbs exhibit a high level of somatic hypermutation (*22*). Moreover, there is currently limited understanding of the optimal immunization strategies in humans necessary to drive the antibody maturation process from germ line to a mature broadly neutralizing antibody (*23*). Strategies for focusing immune responses on protective epitopes and away from immunodominant decoy epitopes are also undefined, as are the strategies for induction of long-term memory responses. Moreover, most of what we know of human immunology has come from the study of blood, whereas the battle between pathogen and the immune system largely takes place in lymph nodes and other tissues. Finally, little is known of ways to overcome neonatal immaturity and immune senescence in the elderly, important for the development and optimal coverage of next-generation vaccines. Although small-animal and nonhuman primate models serve a critical role in basic science and preclinical vaccine discovery, they are considerably limited when it comes to extrapolation in

[1]International AIDS Vaccine Initiative (IAVI), New York, NY 10004, USA. [2]Department of Immunology and Microbial Science and IAVI Neutralizing Antibody Center and The Scripps Research Institute, La Jolla, CA 92037, USA. [3]The Children's Hospital of Philadelphia, Philadelphia, PA 19104, USA. [4]Ragon Institute of Massachusetts General Hospital, Massachusetts Institute of Technology, and Harvard, Cambridge, MA 02129, USA. [5]Howard Hughes Medical Institute, Chevy Chase, MD 20815, USA. [6]Sanofi-Aventis, 270 Albany Street, Cambridge, MA 02139, USA. [7]Emory Vaccine Center, Emory University of School of Medicine, Atlanta, GA 30329, USA. [8]Department of Biotechnology, Government of India, New Delhi, India. [9]University of Pennsylvania, Philadelphia, PA 19104, USA. [10]Vaxconsult, Doylestown, PA 18902, USA. [11]Center for HIV/AIDS Vaccine Immunology and Immunogen Discovery, The Scripps Research Institute, La Jolla, CA 92037, USA.

*Corresponding author. E-mail: wkoff@iavi.org

humans, in large part due to differences in immunogenetics, species specificity of pathogens, and the resident microbiota that influences species-specific responses.

Here, we discuss the technological advances that are fueling a new era in vaccine discovery, highlight advances in immune-monitoring technologies and systems biology that offer substantial potential for discovering new biomarkers of protective immunity, and identify the limitations of animal models for screening and prioritizing human vaccines. Based on this analysis, we conclude that new human immunology–based clinical research initiatives with the goal of elucidating and more effectively generating vaccine-induced protective immune responses would greatly accelerate the development of next-generation vaccines against major global killers such as AIDS, tuberculosis, and malaria and provide a foundation for vaccine development against new and emerging diseases.

The 21st Century Technological Revolution Fueling a New Era in Vaccine Discovery

Effective vaccines work by eliciting effector and memory immune responses that confer protection against infection and disease. New technologies have recently been developed that are now fueling a revolution in vaccine discovery, which should help to address vaccine development challenges such as pathogen diversity and immune evasion. These technologies can be divided into three major categories related to antigen discovery, adjuvants and vaccine delivery, and deciphering human immune responses.

Antigen Discovery Technologies

The capacity to sequence whole genomes of microorganisms and use bioinformatics for the design of vaccines is a relatively recent approach to antigen discovery and has been termed "reverse vaccinology" (*24*). The first pathogen for which reverse vaccinology was attempted was meningococcus B, the cause of 50% of global meningococcal meningitis. With the genome of the bacterium sequenced, more than 600 potential antigens were assessed for antigenicity, resulting in the identification of more than 90 newly detected surface proteins, 30% of which could induce bactericidal antibodies. A subset of these antigens, when formulated as immunogens induced protective immunity in mice, provides proof of concept for ongoing clinical development (*25*). Reverse vaccinology has now been applied to many other bacterial pathogens as full genome sequencing has advanced, including group B streptococcus, group A streptococcus, *Streptococcus pneumoniae*, *Staphylococcus aureus*, and *Chlamydia* (*26*). Besides reverse vaccinology, genomic-based antigen discovery has been enhanced by new technologies enabling interrogation of the comprehensive antigenic repertoire using libraries of genetically expressed antigens and screening for immunogenicity of the proteins during infection, termed "antigenome analysis" (*27*). In addition, advances in mass spectrometry have enabled direct testing of the presence and quantity of antigens on the surface of bacteria (*28*).

Although these reverse vaccinology and antigenome technologies hold considerable promise, particularly for identifying potential antigens for inclusion in vaccines, they remain limited in their capacity to predict which antigens are protective, as recently demonstrated by a phase III trial of an experimental *Staphylococcus aureus* vaccine (*29*). Thus, greater efforts on understanding correlates of protection from human natural history studies, coupled with small, iterative clinical trials aimed at driving immune responses toward less immunedominant but protective epitopes, offers potential for greater use of these antigen discovery technologies.

Antigen discovery technologies have also advanced for identification of antigens to be used in vaccine candidates to induce neutralizing antibody responses and for the generation of T cell–based vaccines. For pathogens that are hypervariable, such as HIV reverse engineering of vaccines, the concept that protective antigens could be identified through interrogation of the antibody repertoire from subjects infected with the pathogen (*30*) and formulated into effective vaccines is now being more fully exploited as a result of recent technological advances in isolating monoclonal antibodies from memory B cells and plasma cells from infected patients, deep sequencing, and bioinformatics. These efforts include (i) identification of subjects with broadly neutralizing antibody serum responses (*21*); (ii) identification of bnAbs from such subjects by single-cell memory B cell techniques with or without antigen selection and cloning the heavy and light chains into immunoglobulin G vectors (*31*–*35*); (iii) determination of the structure of the binding sites of such bnAbs at the structural level using crystallographic methods (*31*–*35*); and (iv) Mimicking the epitopic binding sites of such bnAbs on carrier protein scaffolds or vectors to serve as the basis for immunogens to elicit such bnAbs (*32*, *33*) (Fig. 1). In addition to HIV, bnAbs against HCV (*36*) and influenza (*37*) are serving as templates for antigen designs for HCV and universal flu vaccines. The first proof of concept for reverse engineering of vaccines has now been achieved for RSV, where computationally designed immunogens mimicking the binding site for an RSV-neutralizing monoclonal antibody have successfully elicited RSV-specific neutralizing antibodies in monkeys (*38*).

The technologies above highlight advances in vaccine discovery for which antibodies to the pathogen are the principal biomarker of vaccine efficacy. Similarly, there have been major technological advances in the past decade with respect to antigen discovery and evaluation of cell-mediated immune (CMI) responses. CMI responses play an integral role in controlling many acute and chronic diseases, provide critical helper signals for elicitation of antibody responses, and thus are important components of vaccine development strategies against some parasites, intracellular bacteria, and some viral infections. Recent technological advances in CMI assays including enzyme-linked immunosorbent spot (ELISPOT) and intracellular cytokine staining (ICS), mass spectrometry coupled with epitope-identification algorithms (*39*), tetrameric staining reagents (*40*), genomics and proteomics of more complex pathogens such as mycobacterium and plasmodium (*41*, *42*), and advances in immune monitoring (see below) have

Table 1. Major global infections prevented by vaccines. The level of efficacy for the vaccines noted here varies in different populations and regions of the world.

Bacterial	Viral
Cholera	Adenovirus-based Diseases
Diphtheria	Hepatitis A
Haemophilus influenza	Hepatitis B
Meningococcal meningitis	Human papillomavirus
Plague	Influenza
Pneumococcal pneumonia	Japanese encephalitis
Tetanus	Measles
Tuberculosis	Mumps
Typhoid fever	Polio
	Rabies
	Rotavirus diarrhea
	Rubella
	Smallpox
	Tick-borne encephalitis
	Varicella zoster
	Yellow fever

Table 2. Major global diseases for which vaccines do not currently exist.

Disease
Campylobacter
Chlamydia
Cytomegalovirus
Dengue
Epstein-Barr (mononucleosis)
Helicobacter pylori: Gastrointestinal ulcers
Hepatitis C
Herpes Simplex
HIV
Influenza (universal flu vaccine to replace need for annual flu vaccine)
Leishmaniasis
Malaria
Respiratory syncytial virus
Rhinovirus
Schistosomiasis
Shigella
Streptococcus groups A and B
Tuberculosis
Urinary tract infections
Other: Allergies, Autoimmune diseases, Cancers*

*HBV and HPV vaccines are effective in preventing liver and cervical cancers, respectively.

combined to enable advances for T cell–based vaccine antigen discovery. For example, long peptides encompassing conserved regions of HIV have been identified that induce polyfunctional T cells in macaques with breadth superior to single-gene vaccines (*43*). In addition, computational optimization methods have been applied to the design of "mosaic" proteins, assembled from fragments of natural viral genetic sequences, that provide diversity coverage comparable to that of thousands of separate peptides but are tractable for vaccines (*44*).

These technologies are beginning to be applied both for antigen identification and for assessment of vaccine efficacy. With respect to antigen identification, epitope-specific algorithms aimed at identifying key cellular immunity epitopes have been assessed for vaccinia virus to better understand the protective components of the efficacious smallpox vaccine. Antigens recognized by CD4+ responses differed from those recognized by CD8+ responses, with such data now being applied to reverse vaccinology strategies for development of epitope-specific vaccines (*45*, *46*).

Simian immunodeficiency virus (SIV) vaccine efficacy studies with heterologous adenovirus vectors compared in nonhuman primates the level of Gag-specific CMI responses with viral load. Greater control of infection correlated with numbers of Gag-specific epitope responses (*47*). More recently, using major histocompatibility complex (MHC)–typed monkeys to probe the efficacy of an SIV epitope-based vaccine, it was demonstrated that CMI responses to epitope-specific targets could control SIV infection in nonhuman primates (*48*). In contrast, studies with malaria immunogens demonstrated that heterologous vectors [chimp Adeno 63 + modified vaccinia Ankara (MVA)] induced robust cellular immunity to specific blood-stage antigens as measured by the magnitude of interferon-gamma ELISPOT responses but had no effect on parasite growth rates in the blood (*49*). Similarly, a recently completed efficacy trial of MVA85A, a new tuberculosis vaccine in infants previously vaccinated with Bacille Calmette-Guérin, elicited modest CD4+ cellular immune responses as measured by ELISPOT and ICS assays but failed to demonstrate efficacy against tuberculosis (*50*).

Adjuvants and Vaccine Vector Delivery Technologies

In the past decade, there have been considerable advances in identification of signaling pathways and receptors of the innate immune system and a greater appreciation of the importance of innate immunity in influencing adaptive immune responses (*51*). Detection of microbes by the innate immune system is largely driven by pattern recognition receptors, such as toll-like receptors (TLRs), that recognize common molecular structures found on microbes. In recent years, there has been a revolution in understanding of the receptors and molecules that drive innate immune responses (*52*–*54*), and this is now leading to the development and testing of novel vaccine adjuvants.

Adjuvants are an important component of vaccine formulations that potentiate immune responses through interaction with one or more TLRs, particularly important for those vaccines composed of proteins that are not highly immunogenic. For example, codelivery of vaccine antigens with pattern recognition receptor agonists may lead to enhanced immune responses to vaccines (*55*–*57*). This enables more mechanistic-based design of adjuvants for potentiation of humoral and cellular immune responses. By extension, this should help to facilitate the development of next-generation adjuvants to help address vaccine challenges where immune responses may be compromised or less than optimal, such as with immune senescence in the elderly. For example, adjuvant trials in individuals hyporesponive to hepatitis B vaccines (HBV) showed that the addition of CpG to HBV enhanced the kinetics, magnitude, and longevity of the seroprotective response (*58*). However, there is still a very limited database on improved efficacy in the elderly with adjuvanted vaccines, highlighting the need for additional studies in these populations. Adjuvants currently used in licensed vaccines include aluminum salts, oil in water emulsions, and virosomes and TLR4 agonists such as bacterially derived monophosphoryl lipid A (MPL). In addition, there are a large number of adjuvants currently in development, aimed at boosting CD4+ helper T cell, CD8+ cytotoxic T cell, and humoral immune responses (*51*).

Many emerging and reemerging pathogens, including those responsible for respiratory, gastrointestinal, and sexually transmitted diseases for which vaccines do not currently exist, initiate infection at a mucosal surface, suggesting that induction of mucosal immunity may be necessary or beneficial for prevention and control (*59*). Vector delivery systems designed to stimulate mucosal and systemic immunity have advanced in recent years, with some already in clinical trials, including adenovirus, paramyxovirus, and some bacterial vectors (*60*). Viral vectors enable heterologous antigens to be delivered to antigen-processing pathways needed to stimulate human leukocyte antigen (HLA) class I restricted cytotoxic T cell responses, in addition to priming for effective humoral immune responses. Further, replicating viral vectors more closely mimic the attributes of efficacious live attenuated vaccines (*61*). However, one of the major challenges for vector delivery systems is the need to overcome preexisting immunity specific to the vector. For example, adenovirus type 5 (Ad5) is a potent vector for induction of cell-mediated immune responses, yet the majority of the world's population has been previously exposed to Ad5 or closely related

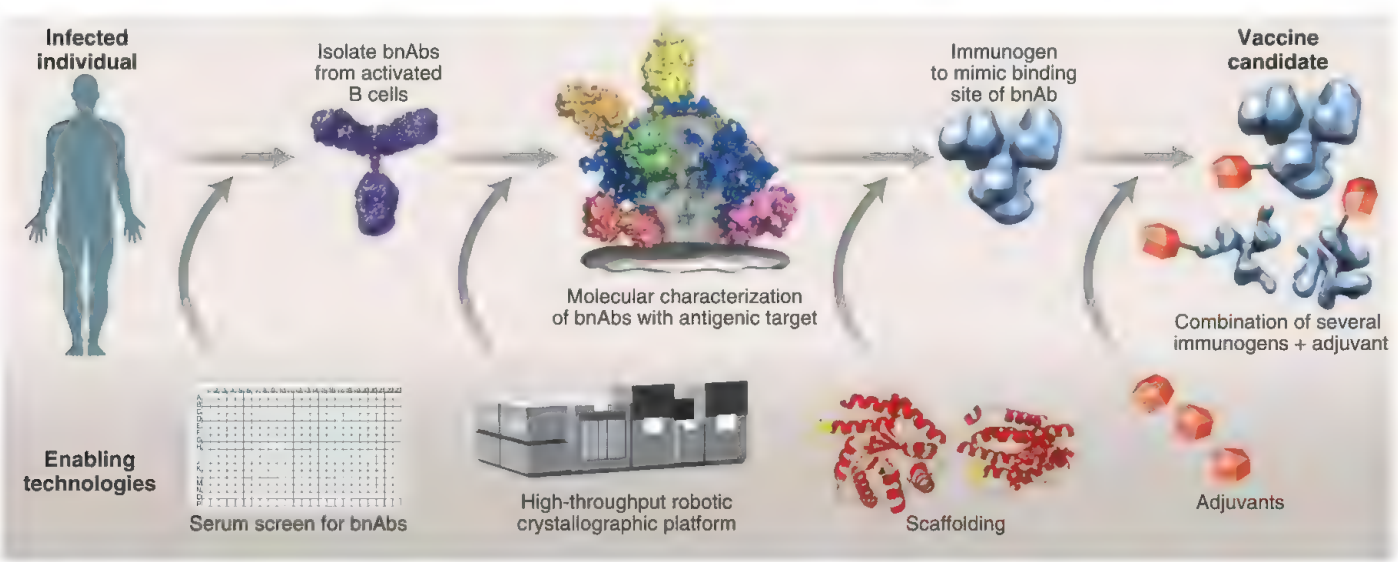

Fig. 1. Reverse engineering of vaccines. The figure schematically depicts the identification of bnAbs; technological advances in high-throughput robotic crystallization platforms to enable greater precision in identifying the epitope targets for bnAbs; computational methods to design scaffolds mimicking the binding site of the bnAbs; and, finally, greater understanding at the mechanistic level for selection of adjuvants to include in vaccine formulations for potentiating immune responses.

adenoviruses, thus limiting the potential of this vector for vaccine development, particularly for use in the developing world. Strategies to overcome preexisting or nascent antivector immunity are now being assessed, including use of vectors against which humans have low seroprevalence, simian and canine vectors for which preexisting immunity in human populations is negligible, prime-boost regimens, and administration of vector-based vaccines by a mucosal route. Low seroprevalence adenoviruses, such as Ad26, Ad35, and chimpAd63, are currently in clinical trials, and preclinical studies with cytomegalovirus vectors have demonstrated the capacity for overcoming antivector immunity (*62*).

Dendritic cells (DC) are antigen-presenting cells that provide initial surveillance mechanisms for exposure to pathogens, whereupon they undergo rapid maturation and migrate to lymph nodes where induction of immune responses occurs. DCs play a central role in the induction of vaccine-mediated immune responses by providing antigen-specific and costimulatory signals required for T cell activation. Increased understanding of the mechanisms of antigen presentation, guided by elucidation of dendritic cell subsets and their functional plasticity, offer additional opportunities for targeting and potentiation of immune responses by vaccines (*63*). Targeting dendritic cells in vivo with antibodies to specific DC cell surface receptors is now being explored for vaccines (*64*). Some viral vectors, such as vesicular stomatitis virus (VSV), target dendritic cells, which may account for the potent immune responses when VSV is used as a vector (*65*).

Deciphering Human Immune Responses

Along with advances in antigen discovery, adjuvant, and vaccine vector delivery technologies, the past decade has seen a technological revolution in the capacity to analyze immune responses at both the single cell and the systems level, which offers tremendous potential for deciphering human immune responses to vaccines and identification of immune correlates of protection. Advances in systems biology, coupled with recent gains in understanding the pivotal role of innate immunity in augmenting adaptive immune responses, are now being applied to vaccine discovery in what is termed "systems vaccinology" (*66*). Technological advances with DNA microarrays and high-throughput DNA sequencing, mass spectrometry–powered proteomics, bioinformatics, and computational methods enable data integration that serves as the basis of systems vaccinology (*67*). Initial studies on yellow fever vaccination in humans have identified early innate signatures that correlate with immunogenicity of the vaccines (*68*), and similar approaches are now being undertaken for influenza and malaria vaccine development. Interrogation of the antibody repertoire by deep sequencing and bioinformatics has led to the identification of intermediates on the path to broadly neutralizing antibodies that is now helping to guide HIV vaccine development (*69*) (Fig. 2). Concomitant with advances in systems biology approaches, immune-monitoring technologies have advanced to enable new approaches to characterize and interrogate human immune responses (*70*). Multiplexed flow cytometric and intracellular cytokine staining assays now allow analyses of cell phenotype, subset identity, activation, and intracellular signaling status and effector activities (*71*–*73*), and single-cell gene expression analyses allow greater specificity in immune monitoring. Such monitoring should enable greater precision in assessments of correlates of protection for currently licensed vaccines, which will help guide next-generation vaccine development. For example, induction of effector memory responses as determined by flow cytometric analysis is thought now to play an important role in the considerable control of SIV infection conferred by CMV vector-based vaccine candidates (*62*). Combining these tools with other new methods for analysis of antigen-specific cells using multiplexed tetramer technologies and highly sensitive microarray and sequencing technologies will allow not only for assessment of responses in blood but, because of the sensitivity of these methods, may also provide insights into selected tissue-level responses. This will enable future analyses to be made in the tissues, where the battle between pathogen and host largely takes place, rather than simply relying on measurements from peripheral blood.

Taken together, recent progress in technological development for antigen discovery, adjuvant and vector discovery, and technologies aimed at deciphering human immune responses provide the foundation for major advances in vaccine discovery and their application toward accelerating vaccine development against the major global diseases for which vaccines do not currently exist.

The Importance of Studying Vaccines in Humans: Limitations of Current Animal Models

Despite best efforts, in vitro and small-animal models do not effectively recapitulate the dynamics of human immune responses to vaccines. Mouse models, in particular the use of inbred mice, have been extremely effective as a tool for basic immunologists, yet have been largely unsuccessful as models for clinical application (*74*, *75*). For example, inbred mice often have a number of homozygous recessive defects that alter the regulation of immune responses (*76*). Differences in pattern recognition receptors (e.g.,

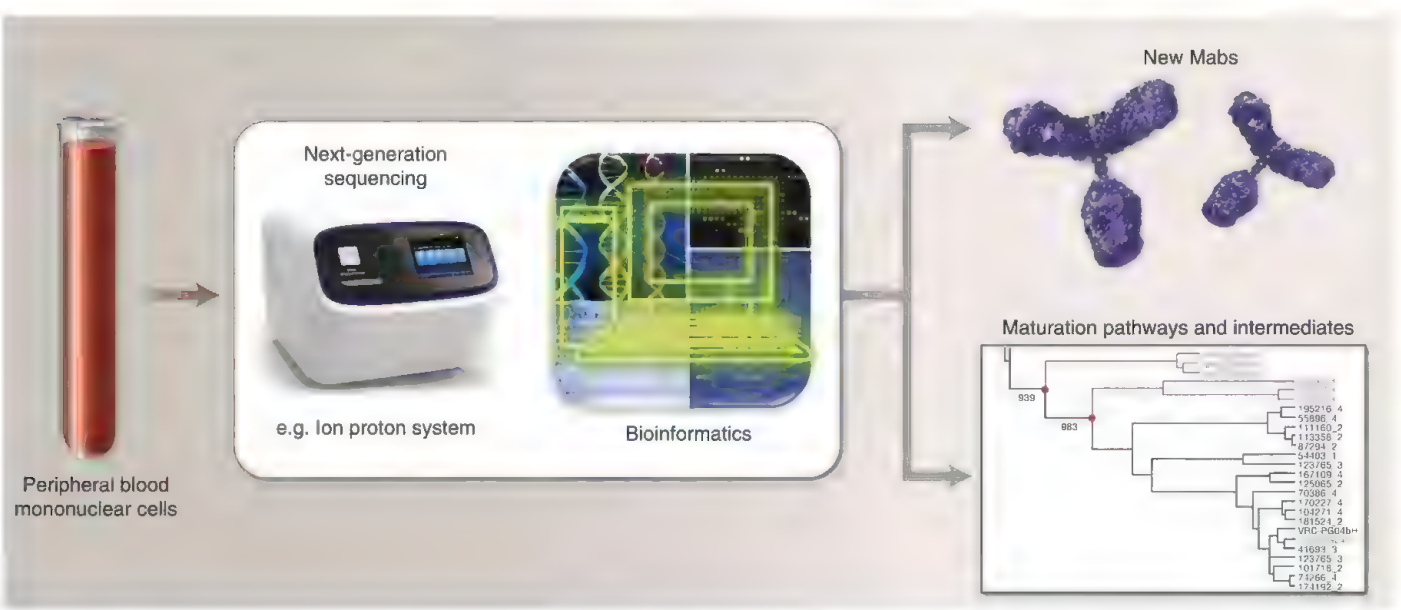

Fig. 2. Technological advances toward deciphering human immune responses. This figure depicts technological advances in deep sequencing and bioinformatics that now allow identification of the antibodyome and tracing antibody development from germ line through somatically hypermutated intermediates to the designated fully mature antibody. Such tracing can help guide B cell lineage–based vaccine design (*23*).

TLR9 expression) may account for considerable differences between humans and rodents in response to microbial stimuli (*77*, *78*). In addition, protocols in small animal models do not adequately reflect human vaccination studies. Many murine studies use intravenous or intraperitoneal injections, whereas human vaccines are generally administered intramuscularly or subcutaneously (*79*). Different routes of immunization—for example, mucosal versus intramuscular—can change patterns of recognition by dendritic cell subsets, leading to modifications in immune responses (*80*). In addition, dose and regimen of immunizations are often different between small-animal studies and human clinical trials, which can affect the quality and quantity of priming, effector, and memory responses.

As a result of these deficiencies, there is renewed interest in the use of "humanized" mice, which are usually immunodeficient mice that are reconstituted with human hematopoietic stem cells, peripheral blood mononuclear cells, or tissue transplants. Although these models are potentially very promising, they have yet to be validated for predicting human immune responses to licensed vaccines, and human hematopoietic cells developed from stem cell transplantation in immunodeficient mice are not always phenotypically and functionally identical to those that develop in humans (*81*). Thus, such mice may not fully recapitulate human immune responses, particularly where T cell helper and other effector cell mechanisms are integral for optimization of vaccine-induced immune responses.

Although nonhuman primates have played an important role in the development of vaccines for hepatitis B and other diseases, there are additional limitations of nonhuman primate models with respect to human vaccine development, including differences in immunogenetics between macaques and humans, species specificity of some viral vectors being developed as vaccine candidates, and the impact of the microbiome of humans on vaccine evaluation. For example, HIV vaccine developers primarily rely on SIV replication in rhesus macaques as a challenge model for assessing vaccine concepts due to the limited replication of HIV in macaques (*82*). However, the hypervariability of HIV cannot readily be modeled by SIV because of the limited numbers of referenced strains of SIV. Moreover, differences between MHC restrictions in monkeys and HLA restrictions in humans limits the assessment of epitopes for inclusion in vaccine candidates. In addition, vectors carrying HIV genes such as cytomegalovirus and replication-competent adenovirus type 4 are species-specific for humans.

The microbiome of humans consists of the plethora of viruses, bacteria, and parasites that infect and reside in our tissues, contributing a substantial proportion of genetic information to our metagenome and thus affecting susceptibility and resistance to disease, particularly inflammatory diseases such as type 1 diabetes, ulcerative colitis, and Crohn's disease (*83*). The concept of the microbiome is being applied to personalized medicine but also should be viewed as a limitation when contemplating animal models for human vaccine development (*84*) .

In summary, although murine models have provided important insights into basic immunology, and small-animal models plus nonhuman primates have been important in the development of some currently licensed vaccines, there are considerable limitations of these models in predicting human responses to vaccines. This was demonstrated yet again when simian-human immunodeficiency virus (SHIV) protection studies in monkeys suggested that an Ad5-based HIV vaccine could suppress viral load and control disease, yet human efficacy trials failed to confirm these observations (*85*, *86*). Thus, greater attention needs to be focused on immunogenicity studies in humans aimed at answering specific questions that impede vaccine development and translating this information toward the development of next-generation and more efficacious vaccines against globally important diseases.

Future Directions: Optimizing Protective Immune Responses in Humans

Although licensed vaccines continue to provide tremendous public health benefits, success rates in vaccine development are not optimal and are even worse for the subset of complex pathogens for which variability and immune-evasion mechanisms present additional challenges. For example, in one survey of more than 200 vaccine development projects, success rates for vaccines was only 22%, compared with 40% for biopharmaceuticals (*87*). In our view, this high rate of failure for vaccines is directly related to (i) lack of information about mechanisms for protective immunity directly applicable to pathogen-specific vaccine development and (ii) lack of understanding of optimal strategies to elicit vaccine-induced protective immune responses in humans and thus inability to effectively predict which immunogens would have a greater chance for success in vaccine efficacy trials.

For the major global diseases for which vaccines do not currently exist (Table 2), identification of vaccine-induced protective immune responses will require greater understanding of pathogen-specific mechanism(s) of protective immunity, particularly from human natural history studies and, in some cases, from human challenge models when available, such as malaria. This is important in cases where natural infection by specific pathogens provides protection against subsequent exposure but also in cases where natural infection does not confer such protection. Thus, greater linkages of human disease–specific pathogenesis studies with applied vaccinology studies will be central to accelerating next-generation vaccine development.

Moreover, when one factors in the current lack of understanding in humans of (i) how to fine-control the antibody affinity maturation that is likely required to elicit broadly protective responses to highly antigenically variable pathogens, (ii) how to focus immune responses on subdominant yet critical protective epitopes, and (iii) how to elicit long-term central and effector memory responses, it's no surprise that vaccine success rates against complex pathogens such as HIV, mycobacteria, and plasmodium are worse than those against nonvariable, acute infections. However, the confluence of recent technological advances for vaccine discovery, systems biology, and immune monitoring yields a tremendous opportunity for accelerating vaccine development. If harnessed effectively, they can lead to a greater understanding of disease-specific mechanisms of protective immunity, elucidate key principles of vaccinology, and be used to optimize humoral and cellular protective immune responses. Application of this information across the spectrum of disease-specific vaccine development programs will likely shorten the time required for successful development of new and improved vaccines.

Clinical trials of vaccines are currently driven by product-specific issues, because sponsors or vaccine developers have preferred to quickly advance candidates from phase I/II safety immunogenicity trials to phase IIb/III efficacy trials rather than prioritize vaccine discovery related issues. Unfortunately, for diseases such as HIV, tuberculosis, malaria, and others, the gap in understanding how best to elicit the requisite humoral and cellular effector and memory responses in humans has slowed the pace of vaccine development. In the absence of a greater understanding of these key vaccinology principles in humans, the vaccine field is left to rely on large and expensive field trials to provide any guidance. Such trials can cost US$50 million to $100 million or more, can take several years to complete, and often are undertaken with low probabilities of success. This is not to suggest that field trials should be abandoned. It is rather to suggest that, in parallel, considerable resources be directed toward conducting small, iterative, human clinical studies to address key questions currently impeding the development of next-generation candidate vaccines.

In summary, successful development of vaccines against the major global diseases for which vaccines do not currently exist would be transformational for public health, with huge benefits across society. Historical paradigms of empirical product development efforts alone are unlikely to be successful against major global killers that cause substantial morbidity and mortality today. This is due in large part to the current lack of understanding of mechanisms for protective immunity, immune-evasion mechanisms, and immunization strategies on how best to elicit protective immune responses against such pathogens in humans to mimic the best attributes of successful licensed vaccines. To accelerate next-generation vaccine development, we suggest that new human immunology–based clinical research initiatives be established, focused on addressing key questions impeding vaccine development, with

the goal of elucidating and more effectively generating vaccine-induced protective immune responses. Collectively, such a "Human Vaccines Project" holds the potential to greatly accelerate the development of next-generation vaccines against major global killers such as AIDS, tuberculosis, malaria, and other infectious diseases; enable more successful vaccine development against allergies, autoimmune diseases, and cancers; and provide a foundation for vaccine development against new and emerging diseases.

References and Notes

1. E. Jenner, *The Origin of the Vaccine Inoculation* (Shury, London, UK, 1801).
2. L. Pasteur, De l'attenuation du virus du choléra des poules. *CR Acad. Sci. Paris.* **91**, 673 (1880).
3. D. Salmon, T. Smith, On a new method of producing immunity from contagious diseases. *American Vet. Review.* **10**, 63 (1886).
4. J. F. Enders, T. H. Weller, F. C. Robbins, Cultivation of the Lansing strain of poliomyelitis virus in cultures of various human embryonic tissues. *Science* **109**, 85 (1949). doi: 10.1126/science.109.2822.85; pmid: 17794160
5. M. R. Hilleman, E. B. Buynak, R. E. Weibel, J. Stokes Jr., Live, attenuated mumps-virus vaccine. *N. Engl. J. Med.* **278**, 227 (1968). doi: 10.1056/NEJM196802012780501; pmid: 4169706
6. S. A. Plotkin, J. D. Farquhar, M. Katz, F. Buser, Attenuation of RA 27-3 rubella virus in WI-38 human diploid cells. *Am. J. Dis. Child.* **118**, 178 (1969). pmid: 5794813
7. A. B. Sabin, W. A. Hennessen, J. Winsser, Studies on variants of poliomyelitis virus. I. Experimental segregation and properties of avirulent variants of three immunologic types. *J. Exp. Med.* **99**, 551 (1954). doi: 10.1084/jem.99.6.551; pmid: 13163327
8. J. E. Salk *et al.*, Formaldehyde treatment and safety testing of experimental poliomyelitis vaccines. *Am. J. Public Health Nations Health* **44**, 563 (1954). doi: 10.2105/AJPH.44.5.563; pmid: 13148396
9. M. R. Hilleman *et al.*, Development and evaluation of the Moraten measles virus vaccine. *JAMA* **206**, 587 (1968). doi: 10.1001/jama.1968.03150030043009; pmid: 5695578
10. S. Black *et al.*; Northern California Kaiser Permanente Vaccine Study Center Group, Efficacy, safety and immunogenicity of heptavalent pneumococcal conjugate vaccine in children. *Pediatr. Infect. Dis. J.* **19**, 187 (2000). doi: 10.1097/00006454-200003000-00003; pmid: 10749457
11. C. McNeil, Who invented the VLP cervical cancer vaccines? *J. Natl. Cancer Inst.* **98**, 433 (2006). doi: 10.1093/jnci/djj144; pmid: 16595773
12. R. Schneerson, O. Barrera, A. Sutton, J. B. Robbins, Preparation, characterization, and immunogenicity of *Haemophilus influenzae* type b polysaccharide-protein conjugates. *J. Exp. Med.* **152**, 361 (1980). doi: 10.1084/jem.152.2.361; pmid: 6967514
13. D. A. D'Argenio, C. B. Wilson, A decade of vaccines: Integrating immunology and vaccinology for rational vaccine design. *Immunity* **33**, 437 (2010). doi: 10.1016/j.immuni.2010.10.011; pmid: 21029955
14. J. Ehreth, The value of vaccination: A global perspective. *Vaccine* **21**, 4105 (2003). doi: 10.1016/S0264-410X(03)00377-3; pmid: 14505886
15. M. A. Miller, A. R. Hinman, in *Vaccines,* S. A. Plotkin, W. A. Orenstein, P. A. Offit, Eds. (Saunders, Philadelphia, 2008), pp. 1594–1610.
16. S. Green, A. Rothman, Immunopathological mechanisms in dengue and dengue hemorrhagic fever. *Curr. Opin. Infect. Dis.* **19**, 429 (2006). doi: 10.1097/01.qco.0000244047.31135.fa; pmid: 16940865
17. F. Sallusto, A. Lanzavecchia, K. Araki, R. Ahmed, From vaccines to memory and back. *Immunity* **33**, 451 (2010). doi: 10.1016/j.immuni.2010.10.008; pmid: 21029957
18. M. J. McElrath, B. F. Haynes, Induction of immunity to human immunodeficiency virus type-1 by vaccination. *Immunity* **33**, 542 (2010). doi: 10.1016/j.immuni.2010.09.011; pmid: 21029964
19. J. C. Sacchettini, E. J. Rubin, J. S. Freundlich, Drugs versus bugs: In pursuit of the persistent predator *Mycobacterium tuberculosis*. *Nat. Rev. Microbiol.* **6**, 41 (2008). doi: 10.1038/nrmicro1816; pmid: 18079742
20. C.-A. Siegrist, in *Vaccines: Sixth Edition*, S. A. Plotkin, W. Orenstein, P. A. Offit, Eds. (W.B. Saunders, London, 2013), pp. 14–32.
21. M. D. Simek *et al.*, Human immunodeficiency virus type 1 elite neutralizers: individuals with broad and potent neutralizing activity identified by using a high-throughput neutralization assay together with an analytical selection algorithm. *J. Virol.* **83**, 7337 (2009). doi: 10.1128/JVI.00110-09; pmid: 19439467
22. D. R. Burton *et al.*, A blueprint for HIV vaccine discovery. *Cell Host Microbe* **12**, 396 (2012). doi: 10.1016/j.chom.2012.09.008; pmid: 23084910
23. B. F. Haynes, G. Kelsoe, S. C. Harrison, T. B. Kepler, B-cell-lineage immunogen design in vaccine development with HIV-1 as a case study. *Nat. Biotechnol.* **30**, 423 (2012). doi: 10.1038/nbt.2197; pmid: 22565972
24. R. Rappuoli, Reverse vaccinology. *Curr. Opin. Microbiol.* **3**, 445 (2000). doi: 10.1016/S1369-5274(00)00119-3; pmid: 11050440
25. M. M. Giuliani *et al.*, A universal vaccine for serogroup B meningococcus. *Proc. Natl. Acad. Sci. U.S.A.* **103**, 10834 (2006). doi: 10.1073/pnas.0603940103; pmid: 16825336
26. A. Sette, R. Rappuoli, Reverse vaccinology: Developing vaccines in the era of genomics. *Immunity* **33**, 530 (2010). doi: 10.1016/j.immuni.2010.09.017; pmid: 21029963
27. C. Giefing *et al.*, Discovery of a novel class of highly conserved vaccine antigens using genomic scale antigenic fingerprinting of pneumococcus with human antibodies. *J. Exp. Med.* **205**, 117 (2008). doi: 10.1084/jem.20071168; pmid: 18166586
28. M. J. Rodríguez-Ortega *et al.*, Characterization and identification of vaccine candidate proteins through analysis of the group A streptococcus surface proteome. *Nat. Biotechnol.* **24**, 191 (2006). doi: 10.1038/nbt1179; pmid: 16415855
29. R. S. Daum, in *Vaccines: Sixth Edition*, S. A. Plotkin, W. Orenstein, P. A. Offit, Eds. (W.B. Saunders, London, 2013), pp. 1161–1168.
30. D. R. Burton, Antibodies, viruses and vaccines. *Nat. Rev. Immunol.* **2**, 706 (2002). doi: 10.1038/nri891; pmid: 12209139
31. L. M. Walker *et al.*; Protocol G Principal Investigators, Broad and potent neutralizing antibodies from an African donor reveal a new HIV-1 vaccine target. *Science* **326**, 285 (2009). doi: 10.1126/science.1178746; pmid: 19729618
32. P. D. Kwong, J. R. Mascola, Human antibodies that neutralize HIV-1: Identification, structures, and B cell ontogenies. *Immunity* **37**, 412 (2012). doi: 10.1016/j.immuni.2012.08.012; pmid: 22999947
33. D. R. Burton, P. Poignard, R. L. Stanfield, I. A. Wilson, Broadly neutralizing antibodies present new prospects to counter highly antigenically diverse viruses. *Science* **337**, 183 (2012). doi: 10.1126/science.1225416; pmid: 22798606
34. T. Zhou *et al.*, Structural basis for broad and potent neutralization of HIV-1 by antibody VRC01. *Science* **329**, 811 (2010). doi: 10.1126/science.1192819; pmid: 20616231
35. J. F. Scheid *et al.*, Sequence and structural convergence of broad and potent HIV antibodies that mimic CD4 binding. *Science* **333**, 1633 (2011). doi: 10.1126/science.1207227; pmid: 21764753
36. M. Law *et al.*, Broadly neutralizing antibodies protect against hepatitis C virus quasispecies challenge. *Nat. Med.* **14**, 25 (2008). doi: 10.1038/nm1698; pmid: 18064037
37. D. C. Ekiert *et al.*, A highly conserved neutralizing epitope on group 2 influenza A viruses. *Science* **333**, 843 (2011). doi: 10.1126/science.1204839; pmid: 21737702
38. W. Schief, Epitope-focused vaccines. *Retrovirology* **9 Suppl. 2**, S03.04 (2012).
39. Q. Zhang *et al.*, Immune epitope database analysis resource (IEDB-AR). *Nucleic Acids Res.* **36**, (Web Server), W513 (2008). doi: 10.1093/nar/gkn254; pmid: 18515843
40. A. H. Bakker, T. N. Schumacher, MHC multimer technology: Current status and future prospects. *Curr. Opin. Immunol.* **17**, 428 (2005). doi: 10.1016/j.coi.2005.06.008; pmid: 15967654
41. D. L. Doolan *et al.*, Identification of *Plasmodium falciparum* antigens by antigenic analysis of genomic and proteomic data. *Proc. Natl. Acad. Sci. U.S.A.* **100**, 9952 (2003). doi: 10.1073/pnas.1633254100; pmid: 12886016
42. J. McMurry *et al.*, Analyzing *Mycobacterium tuberculosis* proteomes for candidate vaccine epitopes. *Tuberculosis (Edinb.)* **85**, 95 (2005). doi: 10.1016/j.tube.2004.09.005; pmid: 15687033
43. M. Rosario *et al.*, Long peptides induce polyfunctional T cells against conserved regions of HIV-1 with superior breadth to single-gene vaccines in macaques. *Eur. J. Immunol.* **40**, 1973 (2010). doi: 10.1002/eji.201040344; pmid: 20468055
44. W. Fischer *et al.*, Polyvalent vaccines for optimal coverage of potential T-cell epitopes in global HIV-1 variants. *Nat. Med.* **13**, 100 (2007). doi: 10.1038/nm1461; pmid: 17187074
45. M. Moutaftsi *et al.*, A consensus epitope prediction approach identifies the breadth of murine T(CD8+)-cell responses to vaccinia virus. *Nat. Biotechnol.* **24**, 817 (2006). doi: 10.1038/nbt1215; pmid: 16767078
46. M. Moutaftsi *et al.*, Vaccinia virus-specific CD4+ T cell responses target a set of antigens largely distinct from those targeted by CD8+ T cell responses. *J. Immunol.* **178**, 6814 (2007). pmid: 17513729
47. J. Liu *et al.*, Immune control of an SIV challenge by a T-cell-based vaccine in rhesus monkeys. *Nature* **457**, 87 (2009). doi: 10.1038/nature07469; pmid: 18997770
48. P. A. Mudd *et al.*, Vaccine-induced CD8+ T cells control AIDS virus replication. *Nature* **491**, 129 (2012). doi: 10.1038/nature11443; pmid: 23023123
49. S. H. Sheehy *et al.*, ChAd63-MVA-vectored blood-stage malaria vaccines targeting MSP1 and AMA1: Assessment of efficacy against mosquito bite challenge in humans. *Mol. Ther.* **20**, 2355 (2012). doi: 10.1038/mt.2012.223; pmid: 23089736
50. M. D. Tameris *et al.*; the MVA85A 020 Trial Study Team, Safety and efficacy of MVA85A, a new tuberculosis vaccine, in infants previously vaccinated with BCG: A randomised, placebo-controlled phase 2b trial. *Lancet* **381**, 1021 (2013). doi: 10.1016/S0140-6736(13)60177-4; pmid: 23391465
51. R. L. Coffman, A. Sher, R. A. Seder, Vaccine adjuvants: Putting innate immunity to work. *Immunity* **33**, 492 (2010). doi: 10.1016/j.immuni.2010.10.002; pmid: 21029960
52. B. A. Beutler, TLRs and innate immunity. *Blood* **113**, 1399 (2009). doi: 10.1182/blood-2008-07-019307; pmid: 18757776
53. A. Iwasaki, R. Medzhitov, Toll-like receptor control of the adaptive immune responses. *Nat. Immunol.* **5**, 987 (2004). doi: 10.1038/ni1112; pmid: 15454922
54. O. Takeuchi, S. Akira, Pattern recognition receptors and inflammation. *Cell* **140**, 805 (2010). doi: 10.1016/j.cell.2010.01.022; pmid: 20303872
55. J. W. Huleatt *et al.*, Vaccination with recombinant fusion proteins incorporating Toll-like receptor ligands induces rapid cellular and humoral immunity. *Vaccine* **25**, 763 (2007). doi: 10.1016/j.vaccine.2006.08.013; pmid: 16968658
56. H. Tighe *et al.*, Conjugation of immunostimulatory DNA to the short ragweed allergen amb a 1 enhances its immunogenicity and reduces its allergenicity. *J. Allergy Clin. Immunol.* **106**, 124 (2000). doi: 10.1067/mai.2000.107927; pmid: 10887315
57. U. Wille-Reece *et al.*, HIV Gag protein conjugated to a Toll-like receptor 7/8 agonist improves the magnitude and quality of Th1 and CD8+ T cell responses in nonhuman primates. *Proc. Natl. Acad. Sci. U.S.A.* **102**, 15190 (2005). doi: 10.1073/pnas.0507484102; pmid: 16219698

58. C. L. Cooper, J. B. Angel, I. Seguin, H. L. Davis, D. W. Cameron, CPG 7909 adjuvant plus hepatitis B virus vaccination in HIV-infected adults achieves long-term seroprotection for up to 5 years. *Clin. Infect. Dis.* **46**, 1310 (2008). doi: 10.1086/533467; pmid: 18444872
59. K. Chen, A. Cerutti, Vaccination strategies to promote mucosal antibody responses. *Immunity* **33**, 479 (2010). doi: 10.1016/j.immuni.2010.09.013; pmid: 21029959
60. M. A. Liu, Immunologic basis of vaccine vectors. *Immunity* **33**, 504 (2010). doi: 10.1016/j.immuni.2010.10.004; pmid: 21029961
61. W. C. Koff *et al.*, Replicating viral vectors as HIV vaccines: Summary report from IAVI sponsored satellite symposium, International AIDS Society Conference, July 22, 2007. *Biologicals* **36**, 277 (2008). doi: 10.1016/j.biologicals.2008.04.004; pmid: 18555698
62. S. G. Hansen *et al.*, Effector memory T cell responses are associated with protection of rhesus monkeys from mucosal simian immunodeficiency virus challenge. *Nat. Med.* **15**, 293 (2009). doi: 10.1038/nm.1935; pmid: 19219024
63. K. Palucka, J. Banchereau, I. Mellman, Designing vaccines based on biology of human dendritic cell subsets. *Immunity* **33**, 464 (2010). doi: 10.1016/j.immuni.2010.10.007; pmid: 21029958
64. L. Lai *et al.*, Prevention of infection by a granulocyte-macrophage colony-stimulating factor co-expressing DNA/modified vaccinia Ankara simian immunodeficiency virus vaccine. *J. Infect. Dis.* **204**, 164 (2011). doi: 10.1093/infdis/jir199; pmid: 21628671
65. J. E. Boudreau *et al.*, Recombinant vesicular stomatitis virus transduction of dendritic cells enhances their ability to prime innate and adaptive antitumor immunity. *Mol. Ther.* **17**, 1465 (2009). doi: 10.1038/mt.2009.95; pmid: 19401673
66. B. Pulendran, S. Li, H. I. Nakaya, Systems vaccinology. *Immunity* **33**, 516 (2010). doi: 10.1016/j.immuni.2010.10.006; pmid: 21029962
67. D. R. Hyduke, B. O. Palsson, Towards genome-scale signalling network reconstructions. *Nat. Rev. Genet.* **11**, 297 (2010). doi: 10.1038/nrg2750; pmid: 20177425
68. T. D. Querec *et al.*, Systems biology approach predicts immunogenicity of the yellow fever vaccine in humans. *Nat. Immunol.* **10**, 116 (2009). doi: 10.1038/ni.1688; pmid: 19029902
69. X. Wu *et al*; NISC Comparative Sequencing Program, Focused evolution of HIV-1 neutralizing antibodies revealed by structures and deep sequencing. *Science* **333**, 1593 (2011). doi: 10.1126/science.1207532; pmid: 21835983
70. R. N. Germain, Vaccines and the future of human immunology. *Immunity* **33**, 441 (2010). doi: 10.1016/j.immuni.2010.09.014; pmid: 21029956
71. D. R. Bandura *et al.*, Mass cytometry: Technique for real time single cell multitarget immunoassay based on inductively coupled plasma time-of-flight mass spectrometry. *Anal. Chem.* **81**, 6813 (2009). doi: 10.1021/ac901049w; pmid: 19601617
72. P. K. Chattopadhyay, C. M. Hogerkorp, M. Roederer, A chromatic explosion: The development and future of multiparameter flow cytometry. *Immunology* **125**, 441 (2008). doi: 10.1111/j.1365-2567.2008.02989.x; pmid: 19137647
73. K. R. Schulz, E. A. Danna, P. O. Krutzik, G. P. Nolan, Single-cell phospho-protein analysis by flow cytometry. *Curr. Protoc. Immunol.* **Chapter 8**, Unit 8 17 (2007).
74. M. M. Davis, A prescription for human immunology. *Immunity* **29**, 835 (2008). doi: 10.1016/j.immuni.2008.12.003; pmid: 19100694
75. J. Seok *et al.*; Inflammation and Host Response to Injury, Large Scale Collaborative Research Program, Genomic responses in mouse models poorly mimic human inflammatory diseases. *Proc. Natl. Acad. Sci. U.S.A.* **110**, 3507 (2013). doi: 10.1073/pnas.1222878110; pmid: 23401516
76. M. G. von Herrath, G. T. Nepom, Lost in translation: Barriers to implementing clinical immunotherapeutics for autoimmunity. *J. Exp. Med.* **202**, 1159 (2005). doi: 10.1084/jem.20051224; pmid: 16275758
77. J. D. Campbell *et al.*, CpG-containing immunostimulatory DNA sequences elicit TNF-alpha-dependent toxicity in rodents but not in humans. *J. Clin. Invest.* **119**, 2564 (2009). doi: 10.1172/JCI38294; pmid: 19726873
78. J. Mestas, C. C. Hughes, Of mice and not men: Differences between mouse and human immunology. *J. Immunol.* **172**, 2731 (2004). pmid: 14978070
79. L. Quintana-Murci, A. Alcaïs, L. Abel, J. L. Casanova, Immunology *in natura*: Clinical, epidemiological and evolutionary genetics of infectious diseases. *Nat. Immunol.* **8**, 1165 (2007). doi: 10.1038/ni1535; pmid: 17952041
80. E. Klechevsky *et al.*, Functional specializations of human epidermal Langerhans cells and CD14+ dermal dendritic cells. *Immunity* **29**, 497 (2008). doi: 10.1016/j.immuni.2008.07.013; pmid: 18789730
81. R. Ito, T. Takahashi, I. Katano, M. Ito, Current advances in humanized mouse models. *Cell. Mol. Immunol.* **9**, 208 (2012). doi: 10.1038/cmi.2012.2; pmid: 22327211
82. B. Song *et al.*, Retrovirus restriction by TRIM5alpha variants from Old World and New World primates. *J. Virol.* **79**, 3930 (2005). doi: 10.1128/JVI.79.7.3930-3937.2005; pmid: 15767395
83. H. W. Virgin, J. A. Todd, Metagenomics and personalized medicine. *Cell* **147**, 44 (2011). doi: 10.1016/j.cell.2011.09.009; pmid: 21962506
84. H. W. Virgin, E. J. Wherry, R. Ahmed, Redefining chronic viral infection. *Cell* **138**, 30 (2009). doi: 10.1016/j.cell.2009.06.036; pmid: 19596234
85. D. I. Watkins, D. R. Burton, E. G. Kallas, J. P. Moore, W. C. Koff, Nonhuman primate models and the failure of the Merck HIV-1 vaccine in humans. *Nat. Med.* **14**, 617 (2008). doi: 10.1038/nm.f.1759; pmid: 18535579
86. S. P. Buchbinder *et al.*; Step Study Protocol Team, Efficacy assessment of a cell-mediated immunity HIV-1 vaccine (the Step Study): A double-blind, randomised, placebo-controlled, test-of-concept trial. *Lancet* **372**, 1881 (2008). doi: 10.1016/S0140-6736(08)61591-3; pmid: 19012954
87. M. M. Struck, Vaccine R&D success rates and development times. *Nat. Biotechnol.* **14**, 591 (1996). doi: 10.1038/nbt0596-591; pmid: 9630948

Acknowledgments: This work was supported by the network of IAVI donors, including, the U.S. Agency for International Development (USAID) and the Bill & Melinda Gates Foundation (BMGF) (W.C.K and C.R.K); the International AIDS Vaccine Initiative (IAVI) and the National Institutes of Health (NIH) (P.R.J.); the Centers for HIV/AIDS Vaccine Immunology and Immunogen Discovery (CHAVI-ID), with funding from the National Institute of Allergy and Infectious Diseases (NIAID), part of NIH (D.R.B., R.A, and B.D.W). Additionally, S.A.P is a paid scientific advisor and consultant for Sanofi, GlaxoSmithKline, Novartis, Merck, Pfizer, Medimmune, Inovio Pharmaceuticals, Dynavax, and Glycovaxyn, and B.D.W. is a paid scientific advisor and consultant for Merck, Bristol-Myers Squibb, and Globe Immune. The authors also wish to thank S. Glass, L. Gieber, O. Shmaïdenko, M. Dees, and B. Hayes for their administrative support.

10.1126/science.1232910

AAAS is here – bringing scientific expertise to policy making.

Good science policy is the result of politicians understanding science and scientists understanding policy. Toward this end, AAAS manages the Science & Technology Policy Fellowships program, which embeds scientists and engineers in the federal government for up to two years. From Congress to the State Department, each class of Fellows contributes to the policy-making process while getting hands-on experience at the intersection of science and policy. As a AAAS member your dues support these efforts. If you're not yet a AAAS member, join us. Together we can make a difference.

To learn more, visit **aaas.org/plusyou/fellows**

AAAS + U = Δ

Enantio- and Diastereodivergent Dual Catalysis: α-Allylation of Branched Aldehydes

Simon Krautwald, David Sarlah, Michael A. Schafroth, Erick M. Carreira*

An important challenge in asymmetric synthesis is the development of fully stereodivergent strategies to access the full complement of stereoisomers of products bearing multiple stereocenters. In the ideal case, where four products are possible, applying distinct catalysts to the same set of starting materials under identical conditions would in a single step afford any given stereoisomer. Herein, we describe the realization of this concept in a fully stereodivergent dual-catalytic synthesis of γ,δ-unsaturated aldehydes bearing vicinal quaternary/tertiary stereogenic centers. The reaction is enabled by chiral iridium and amine catalysts, which activate the allylic alcohol and aldehyde substrates, respectively. Each catalyst exerts high local stereocontrol irrespective of the other's inherent preference.

The field of asymmetric synthesis has experienced considerable progress over the past three decades, and a wide range of enantiopure compounds can now be readily prepared using enantioselective methods based on bio-, transition metal-, and organocatalysis (*1*). In addition, chemists can rely on a number of structural elements, such as stereoelectronic, steric, or directing effects, to exert diastereocontrol in the reactions of chiral substrates (*2*). Although enantiomers can be prepared by simply selecting between a pair of enantiomeric catalysts, a notable challenge associated with the synthesis of molecules bearing multiple stereogenic centers is access to any stereoisomer at will from the same set of starting materials with full absolute and relative stereocontrol.

Access to the complete set of stereoisomers of a compound from the same substrates has been realized through a number of strategies. These include change of solvent, the use of additives, and selection of distinct catalysts (*3*–*9*). In a different approach termed cycle-specific aminocatalysis, a pair of chiral amine catalysts may be employed in a two-step sequence of reactions with enamine after iminium activation (*10*). A characteristic feature of this approach is that the two stereogenic centers are formed sequentially: After enantioselective formation of the first stereocenter, the second catalyst needs to overcome the stereochemical bias present in the chiral product of the first step. Thus, the overall strategy combines an enantioselective reaction with a catalyst-controlled diastereoselective step.

In a conceptually different construct aimed at the synthesis of compounds with a pair of stereogenic centers, two chiral catalysts employed concurrently could dictate the configuration of the stereocenters in the product. Ideally, these would operate independently and set both configurations in a single transition state with minimal matched/mismatched interactions. Herein, we report the realization of this concept in the development of a method for the stereodivergent dual-catalytic α-allylation of aldehydes.

Dual catalysis involves the concurrent activation of both nucleophile and electrophile using distinct catalysts (Fig. 1A) and has recently emerged as an attractive strategy for enantioselective synthesis (*11*–*13*). Its implementation relies on the combination of chiral and achiral catalysts to furnish products enantioselectively (*14*–*18*). We reasoned that a dual-catalytic system in which both catalysts are chiral (***Cat^1** and ***Cat^2**) and each is capable of exercising full control over the configuration of its corresponding stereocenter would provide stereodivergent access to the full matrix of stereoisomeric products simply by using the four available permutations (**Cat^1_R + Cat^2_R**, **Cat^1_R + Cat^2_S**, **Cat^1_S + Cat^2_R**, and **Cat^1_S + Cat^2_S**) (Fig. 1B).

Dual Catalysis by Chiral Ir and Chiral Amine

Ir-catalyzed allylic substitution has become a useful method for the synthesis of chiral building blocks (*19*–*22*). A salient feature of these processes is the formation of the branched product resulting from addition of the nucleophile to the more substituted carbon of the allyl moiety. In this context, our own studies have demonstrated direct substitution of allylic alcohols using an Ir/(P,olefin) complex in combination with Brønsted acid promoters (*23*, *24*). We anticipated that intercepting a reactive allyliridium intermediate such as **I** with a nucleophile (**II**) activated by a second chiral catalyst could result in an allylation process that permits control of the configuration of both stereocenters (Fig. 1B). Amines are known to readily and reversibly form nucleophilic enamines from the corresponding aldehydes (*25*, *26*). Specifically, cinchona-alkaloid–derived primary amines such as **A2** and **A3** have been shown to be useful activators in the stereoselective functionalization of carbonyls (*27*–*29*). A particularly attractive feature of the reaction involving **I** and **II** is that the two reactive species are planar in the region where C–C bond formation ensues, potentially minimizing matched-mismatched effects at the transition state. Consequently, we began our study by examining the reaction of hydratropaldehyde (**1a**) and phenyl vinyl carbinol (**2a**) mediated by the various combinations of amine catalysts **A1** and **A2** and Ir/(P,olefin) complexes **L1** and **(*R*)-L** (Fig. 2). The first set of experiments examined the effect of using a pair of catalysts in which only one is chiral (#1 and #2). The results demonstrate the ability of the amine **A2** and the Ir/**(*R*)-L** catalyst to control the α or β configuration, respectively (*30*). The observed

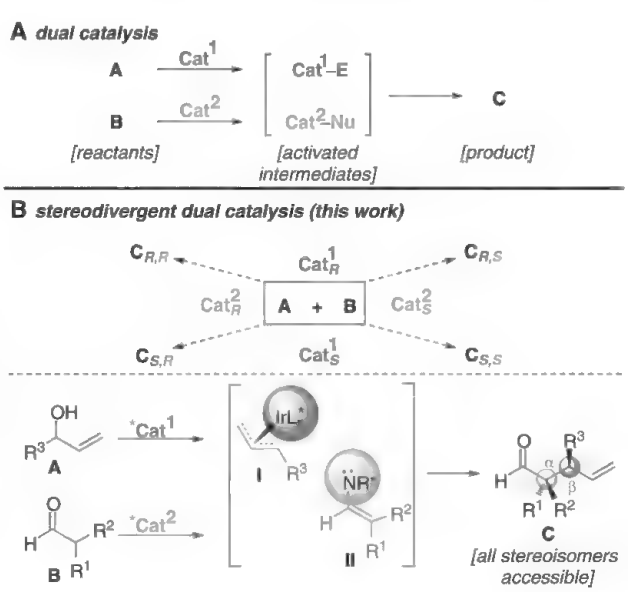

Fig. 1. Dual and stereodivergent dual catalysis. (A) Dual catalysis. Simultaneous activation of two reactants, A and B, by two distinct catalysts leading to reaction. **(B)** Stereodivergent dual catalysis. The use of two distinct chiral catalysts enables access to the full complement of stereoisomeric products by simple catalyst permutation. The specific example illustrates the proposed coupling of amine and iridium catalysis.

Eidgenössische Technische Hochschule Zürich, 8093 Zürich, Switzerland.

*Corresponding author. E-mail: carreira@org.chem.ethz.ch

relative stereocontrol in each case indicates that neither catalyst is able to control the configuration of both stereocenters. This is consistent with the observations of the experiment involving achiral catalysts (#3). The observation of poor relative stereocontrol in both cases suggested to us that the combined use of amine **A2** and Ir/(***R***)-**L** could result in highly diastereoselective formation of the product. In the experiment (#4), product **3a** was indeed isolated with excellent relative [>20:1 diastereomeric ratio (d.r.)] and absolute [>99% enantiomeric excess (ee)] stereocontrol. Although these experiments established the feasibility of a diastereoselective process, they left unanswered the question of whether a stereodivergent dual-catalytic method could be realized.

We then set out to examine whether the full array of stereoisomers of **3a** might be accessible (*31*). The experiments involving the complete set of catalyst permutations **A2** and its pseudoenantiomer **A3** along with (***R***)-**L** and (***S***)-**L** establish the operation of a stereodivergent process (Fig. 3). Thus, from the same set of starting materials **1a** and **2a**, all four stereoisomers of **3a** are obtained in good yields (71 to 80%) and superb enantio- (>99% ee) and diastereoselectivity (d.r. 15:1 to >20:1).

Substrate Scope

The scope of allylic alcohols in the α-allylation was explored using hydratropaldehyde **1a** (Fig. 4). A range of allylic alcohols substituted with arenes bearing halogens, electron-withdrawing, electron-donating, and alkyl substituents furnish products (**3b** to **3m**) in excellent selectivities (14:1 to >20:1 d.r., >99% ee). In addition, allylic alcohols incorporating other arenes such as naphthyl (**3n**) and thiophene (**3o**) proved to be good substrates for the reaction. An electrophilic aldehyde in the arene did not interfere with the process, and **3f** was obtained in 72% yield. Under the reaction conditions described, no potentially competitive aldol process was observed.

We then turned our attention to investigating the scope of the reaction with regard to the aldehyde component (Fig. 5). A range of aldehydes bearing common functional groups affords products (**3p** to **3t**) in good yield and 4:1 to >20:1 diastereoselectivity. Finally, symmetrical aldehydes (**3u** to **3w**) can also be allylated in good yield and excellent enantioselectivity.

After exploring the substrate scope, we sought to further demonstrate the stereodivergence of the reaction with hydratropaldehyde (**1a**) under the conditions described above. Substrates **2f**, **2k**, and **2o** were chosen as representative examples based on their diverse electronic properties (Fig. 6), including electron-poor, electron-rich, and hetarenes. In each case, the corresponding stereoisomeric products were isolated in good yields, with >99% ee and 10:1 to >20:1 d.r.

We subsequently subjected the substitution reaction to a highly challenging substrate by examining the use of diallyl alcohol **2x** (Fig. 7). In

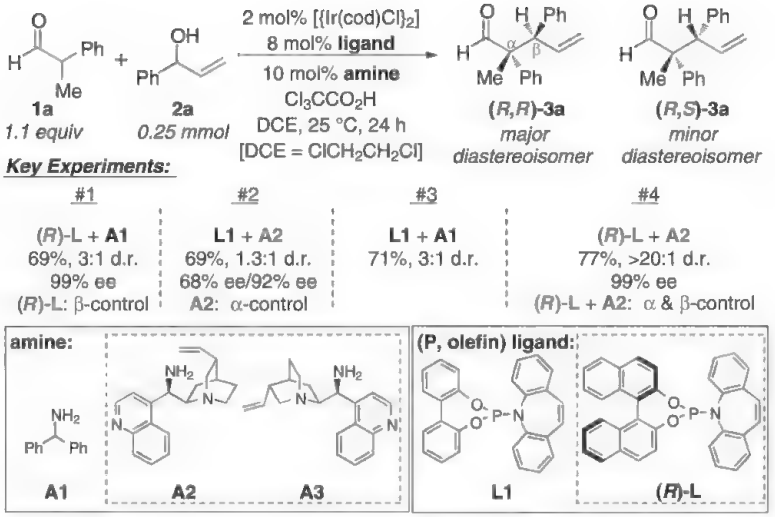

Fig. 2. Key experiments in the evaluation of diastereocontrol.

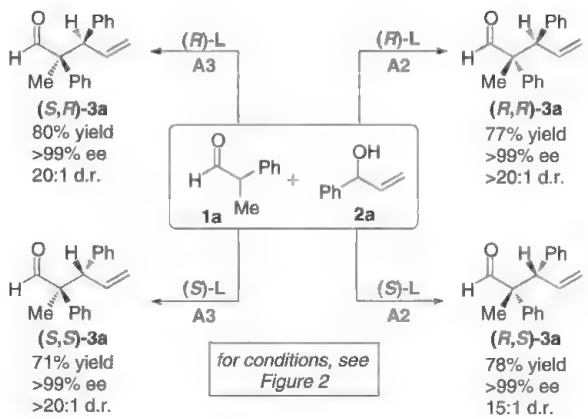

Fig. 3. Stereodivergent dual catalytic synthesis of all stereoisomers of 3a.

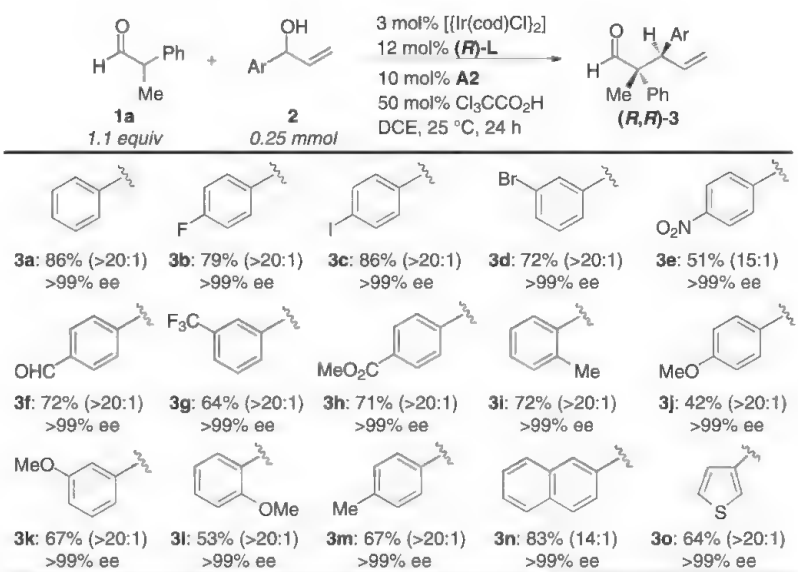

Fig. 4. Allylic alcohol scope of the allylation.

the experiment, **2x** afforded diene **3x** in 57% yield (98% ee, 5:1 d.r.). This example underscores that the process we have described displays both enantio- and diastereoselectivity in the generation of vicinal quaternary/tertiary stereocenters (*32*, *33*) as well as regiocontrol, resulting from substitution at the more hindered end of the of the pentadienyl system. This observation in combination with those described above lead us to suggest a conceptual model to account for the high degree of stereodivergence in this dual-catalytic process. In this respect, the operation of an outer sphere mechanism in which the stereocontrol elements are positioned opposite the reactive diastereofaces for each reactant allows two independent catalysts with a high degree of local diastereofacial differentiation to participate in a single transition state with minimization of matched and mismatched effects.

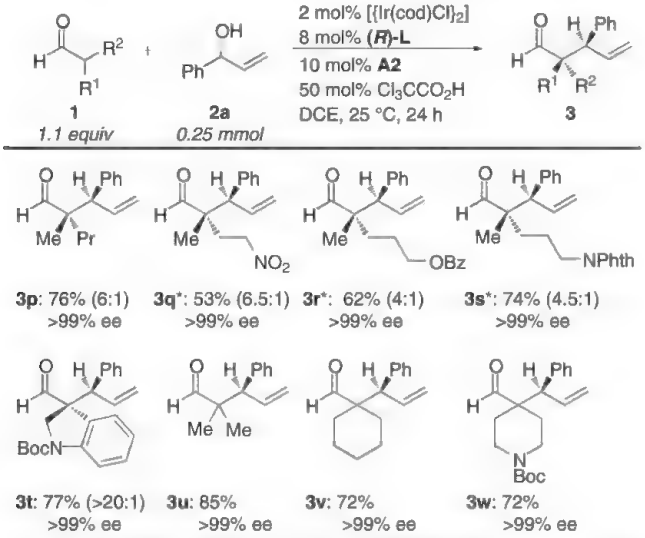

* 20 mol% **A2** and 100 mol% Cl_3CCO_2H were used.

Fig. 5. Aldehyde scope of the allylation.

stereoisomeric products obtained by catalyst permutation*

(*R*)-L+A2	(*R*)-L+A3	(*S*)-L+A2	(*S*)-L+A3
(*R*,*R*)-**3f** 72% (>20:1) >99% ee	(*S*,*R*)-**3f** 67% (20:1) >99% ee	(*R*,*S*)-**3f** 63% (20:1) >99% ee	(*S*,*S*)-**3f** 75% (>20:1) >99% ee
(*R*,*R*)-**3k** 67% (>20:1) >99% ee	(*S*,*R*)-**3k** 73% (15:1) >99% ee	(*R*,*S*)-**3k** 67% (>20:1) >99% ee	(*S*,*S*)-**3k** 73% (14:1) >99% ee
(*R*,*R*)-**3o** 64% (>20:1) >99% ee	(*S*,*R*)-**3o** 70% (11:1) >99% ee	(*R*,*S*)-**3o** 64% (10:1) >99% ee	(*S*,*S*)-**3o** 70% (>20:1) >99% ee

*for conditions, see Fig. 4

Fig. 6. Representative examples of stereodivergence.

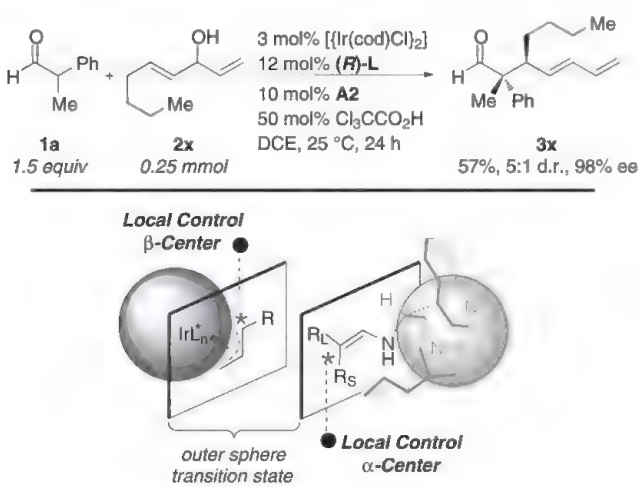

Fig. 7. Synthesis of diene 3x and analysis.

Outlook

We have disclosed an enantioselective α-allylation of branched aldehydes that proceeds through iridium-catalyzed allylic substitution of allylic alcohols with in situ–generated enamines. The method delivers products bearing quaternary stereocenters in a vicinal relationship to tertiary stereocenters in good yields and excellent selectivities. The successful coupling of amine and Ir-catalysis via chiral enamine and allyl metal intermediates serves as proof of concept for stereodivergent dual catalysis in which two distinct and highly face-selective catalytic cycles are merged and provide access to all possible stereoisomers of a target compound in enantiomerically pure form. We expect the broader consequences of this concept to be applicable to the development of other stereodivergent dual-catalytic asymmetric reactions.

References and Notes

1. E. N. Jacobsen, A. Pfaltz, H. Yamamoto, Eds., *Comprehensive Asymmetric Catalysis: Vol. I-III, Suppl. I-II* (Springer, New York, 1999).
2. A. H. Hoveyda, D. A. Evans, G. C. Fu, *Chem. Rev.* **93**, 1307 (1993).
3. X.-X. Yan *et al.*, *J. Am. Chem. Soc.* **130**, 14362 (2008).
4. B. Wang, F. Wu, Y. Wang, X. Liu, L. Deng, *J. Am. Chem. Soc.* **129**, 768 (2007).
5. X. Tian *et al.*, *J. Am. Chem. Soc.* **133**, 17934 (2011).
6. M. Luparia *et al.*, *Angew. Chem. Int. Ed.* **50**, 12631 (2011).
7. A. Nojiri, N. Kumagai, M. Shibasaki, *J. Am. Chem. Soc.* **131**, 3779 (2009).
8. E. L. McInturff, E. Yamaguchi, M. J. Krische, *J. Am. Chem. Soc.* **134**, 20628 (2012).
9. M. Morgen, S. Bretzke, P. Li, D. Menche, *Org. Lett.* **12**, 4494 (2010).
10. Y. Huang, A. M. Walji, C. H. Larsen, D. W. C. MacMillan, *J. Am. Chem. Soc.* **127**, 15051 (2005).
11. G. M. Sammis, H. Danjo, E. N. Jacobsen, *J. Am. Chem. Soc.* **126**, 9928 (2004).
12. C. Zhong, X. Shi, *Eur. J. Org. Chem.* **2010**, 2999 (2010).
13. A. E. Allen, D. W. C. MacMillan, *Chem. Sci.* **3**, 633 (2012).
14. G. Jiang, B. List, *Angew. Chem. Int. Ed.* **50**, 9471 (2011).
15. D. A. Nicewicz, D. W. C. MacMillan, *Science* **322**, 77 (2008).
16. N. Z. Burns, M. R. Witten, E. N. Jacobsen, *J. Am. Chem. Soc.* **133**, 14578 (2011).
17. D. A. DiRocco, T. Rovis, *J. Am. Chem. Soc.* **134**, 8094 (2012).
18. S. Afewerki, I. Ibrahem, J. Rydfjord, P. Breistein, A. Córdova, *Chem. Eur. J.* **18**, 2972 (2012).
19. R. Takeuchi, M. Kashio, *Angew. Chem. Int. Ed. Engl.* **36**, 263 (1997).
20. J. P. Janssen, G. Helmchen, *Tetrahedron Lett.* **38**, 8025 (1997).
21. J. F. Hartwig, M. J. Pouy, *Top. Organomet. Chem.* **34**, 169 (2011).
22. D. J. Weix, J. F. Hartwig, *J. Am. Chem. Soc.* **129**, 7720 (2007).
23. C. Defieber, M. A. Ariger, P. Moriel, E. M. Carreira, *Angew. Chem. Int. Ed.* **46**, 3139 (2007).
24. M. Roggen, E. M. Carreira, *Angew. Chem. Int. Ed.* **50**, 5568 (2011).

25. P. I. Dalko, Ed., *Enantioselective Organocatalysis* (Wiley, Weinheim, Germany, 2006).
26. B. List, Ed., *Asymmetric Organocatalysis: Topics in Current Chemistry Vol. 291* (Springer, New York, 2009).
27. J.-W. Xie *et al.*, *Angew. Chem. Int. Ed.* **46**, 389 (2007).
28. S. H. McCooey, S. J. Connon, *Org. Lett.* **9**, 599 (2007).
29. P. Melchiorre, *Angew. Chem. Int. Ed.* **51**, 9748 (2012).
30. W. Chen, J. F. Hartwig, *J. Am. Chem. Soc.* **135**, 2068 (2013).
31. Materials and methods are available as supplementary materials on *Science* Online.
32. C. Uyeda, E. N. Jacobsen, *J. Am. Chem. Soc.* **130**, 9228 (2008).
33. J. Tan, C.-H. Cheon, H. Yamamoto, *Angew. Chem. Int. Ed.* **51**, 8264 (2012).

Acknowledgments: We are grateful to the Swiss National Science Foundation for a grant supporting this work (200020 135224). S.K. thanks the Fonds der Chemischen Industrie for support (Chemiefonds-Stipendium). We thank S. Müller for insightful discussions. Structural parameters for a carbamate derived from **(*R*,*R*)-3a** are available free of charge from the Cambridge Crystallographic Data Centre under reference number CCDC 933469.

Supplementary Materials

www.sciencemag.org/cgi/content/full/340/6136/1065/DC1
Materials and Methods
Supplementary Text
Tables S1 to S8
References (*34*–*41*)

26 February 2013; accepted 15 April 2013
10.1126/science.1237068

Martian Fluvial Conglomerates at Gale Crater

R. M. E. Williams,[1]* J. P. Grotzinger,[2] W. E. Dietrich,[3] S. Gupta,[4] D. Y. Sumner,[5] R. C. Wiens,[6] N. Mangold,[7] M. C. Malin,[8] K. S. Edgett,[8] S. Maurice,[9] O. Forni,[9] O. Gasnault,[9] A. Ollila,[10] H. E. Newsom,[10] G. Dromart,[11] M. C. Palucis,[3] R. A. Yingst,[1] R. B. Anderson,[12] K. E. Herkenhoff,[12] S. Le Mouélic,[7] W. Goetz,[13] M. B. Madsen,[14] A. Koefoed,[14] J. K. Jensen,[14] J. C. Bridges,[15] S. P. Schwenzer,[16] K. W. Lewis,[17] K. M. Stack,[2] D. Rubin,[18]† L. C. Kah,[19] J. F. Bell III,[20] J. D. Farmer,[20] R. Sullivan,[21] T. Van Beek,[8] D. L. Blaney,[22] O. Pariser,[22] R. G. Deen,[22] MSL Science Team‡

Observations by the Mars Science Laboratory Mast Camera (Mastcam) in Gale crater reveal isolated outcrops of cemented pebbles (2 to 40 millimeters in diameter) and sand grains with textures typical of fluvial sedimentary conglomerates. Rounded pebbles in the conglomerates indicate substantial fluvial abrasion. ChemCam emission spectra at one outcrop show a predominantly feldspathic composition, consistent with minimal aqueous alteration of sediments. Sediment was mobilized in ancient water flows that likely exceeded the threshold conditions (depth 0.03 to 0.9 meter, average velocity 0.20 to 0.75 meter per second) required to transport the pebbles. Climate conditions at the time sediment was transported must have differed substantially from the cold, hyper-arid modern environment to permit aqueous flows across several kilometers.

Decades of spacecraft observations of Mars have revealed abundant evidence for past water flows on the basis of a variety of landforms, including deltas, alluvial fans, valley network comparable to terrestrial river valleys, and giant outflow channels carved by catastrophic floods [e.g., (*1*–*3*)]. Although martian landforms commonly possess morphology and scaling relationships similar to their counterparts on Earth, the resolution of satellite images is insufficient to reveal sediment particle size, shape, and sorting patterns. Such detailed sedimentary observations are required to confirm that certain martian landforms derived from fluvial processes and provide critical data to perform paleohydrologic modeling. Before the NASA Mars Science Laboratory (MSL) mission, surface observations on Mars occurred at six locations associated with the Viking, Pathfinder, Mars Exploration Rovers, and Phoenix missions. Collectively, observations from surface instruments showed limited evidence for water transport processes at only two sites. At the Pathfinder landing site, observations of aligned and touching boulders were inferred to reflect clast imbrication by high-velocity catastrophic floods (*4*–*6*). In Meridiani Planum, centimeter-scale cross-lamination at Eagle and Erebus craters was interpreted to have resulted from shallow surface flows (with velocities of a few tenths of a meter per second) within an interaeolian dune paleoenvironment (*7*–*9*). However, no definitive in situ evidence of a sustained fluvial overland transport system has been encountered by previous landers.

The MSL Curiosity rover arrived at equatorial Gale crater on 6 August 2012 UTC (Fig. 1). The final landing ellipse was chosen in part because of its proximity to Aeolis Mons (known informally as Mt. Sharp), the central, 5-km-high layered mound within Gale crater, but also because it was close to a prominent alluvial fan, the Peace Vallis fan (*10*, *11*). During the first 100 sols of the mission, Curiosity traveled ~400 m from its landing site across the Bradbury Rise toward bedrock exposed at Glenelg (*12*, *13*). Here, we analyze a suite of rocks encountered along this traverse based on data acquired by the Mast Camera (Mastcam) and ChemCam instruments (*14*–*16*).

Outcrop Characteristics

The surface of Bradbury Rise is characterized by two distinct elements: a rock pavement of loose clasts (*17*) (fig. S1) and occasional horizontal to subhorizontal blocks with embedded pebbles. Here we focus on the latter component, which is present within a narrow (~5 m) elevation range, displays generally similar characteristics, and is interpreted as exposures of a distinct geologic unit or facies. This facies consists of thin (<0.1 m thick), coherent blocks that appear to have a well-defined base and limited areal outcrop extent (<1 m^2). Although the contact with subjacent rocks is not directly observed, the slabs typically form protruding ledges that imply that the substrate is finer in grain size or less indurated, and easily erodes.

Multiple outcrops of these pebble-rich rock slabs were observed along the first 275 m traversed by the rover, with high-resolution Mastcam images acquired at three locations: Goulburn, Link, and Hottah (Fig. 1C). Goulburn was exposed at the landing site by thrust impingement scouring driven by one of the four pairs of descent engines, which removed unconsolidated regolith and revealed the underlying lithified rock (fig. S2). At this location, a horizontal rock layer composed of pebbles and an unresolved finer component was observed. The other two locations, Link and Hottah, were observed within ~100 m of Goulburn, and displayed tilted, fractured pebble-rich rock slabs with sufficient competency to maintain near-vertical faces (Fig. 2A and Fig.

[1]Planetary Science Institute, Tucson, AZ 85719, USA. [2]Division of Geological and Planetary Sciences, California Institute of Technology, Pasadena, CA 91125, USA. [3]Earth and Planetary Science Department, University of California, Berkeley, CA 94720, USA. [4]Department of Earth Science and Engineering, Imperial College London, London SW7 2AZ, UK. [5]Geology Department, University of California, Davis, CA 95616, USA. [6]Los Alamos National Laboratory, Los Alamos, NM 87545, USA. [7]Laboratoire Planétologie et Géodynamique de Nantes, LPGN/CNRS UMR6112 and Université de Nantes, 44322 Nantes, France. [8]Malin Space Science Systems, San Diego, CA 92121, USA. [9]Institut de Recherche en Astrophysique et Planétologie (IRAP), Université de Toulouse/CNRS, 31400 Toulouse, France. [10]Department of Earth and Planetary Sciences, University of New Mexico, Albuquerque, NM 87131, USA. [11]Laboratoire de Géologie de Lyon, Université de Lyon, 69364 Lyon, France. [12]U.S. Geological Survey, Flagstaff, AZ 86001, USA. [13]Max-Planck-Institut für Sonnensystemforschung, 37191 Katlenburg-Lindau, Germany. [14]Niels Bohr Institute, University of Copenhagen, 2100 Copenhagen, Denmark. [15]Space Research Centre, Department of Physics and Astronomy, University of Leicester, Leicester LE1 7RH, UK. [16]Department of Physical Sciences, The Open University, Milton Keynes MK7 6AA, UK. [17]Department of Geosciences, Princeton University, Princeton, NJ 08544, USA. [18]U.S. Geological Survey, Santa Cruz, CA 95060, USA. [19]Department of Earth and Planetary Sciences, University of Tennessee, Knoxville, TN 37996, USA. [20]School of Earth and Space Exploration, Arizona State University, Tempe, AZ 85287, USA. [21]Center for Radiophysics and Space Research, Cornell University, Ithaca, NY 14853, USA. [22]Jet Propulsion Laboratory, California Institute of Technology, Pasadena, CA 91109, USA.

*Corresponding author. E-mail: williams@psi.edu
†Present address: Department of Earth and Planetary Sciences, University of California, Santa Cruz, CA 95064, USA.
‡MSL Science Team authors and affiliations are listed in the supplementary materials.

3A). At both locations, multiple decimeter-scale slabs outcrop, separated by linear fractures that display vertical offsets of 2 to 10 cm. The exposed block surfaces dip at approximately constant but gentle angles relative to the ground.

In all three outcrops, the resolvable grains range from very coarse sand (diameter 1 mm) to pebbles (diameter 2 to 40 mm; table S1). The grain size distribution (transformed to a phi scale) approximates a normal (Gaussian) distribution and indicates moderately sorted sediment (Fig. 4) (*17*). The clast size distributions determined from these rocks are truncated because smaller particles are not sufficiently distinct in the Mastcam images; hence, the measured size distribution is somewhat coarser than the actual grain size distribution within the rocks. In the first 100 sols, the highest-resolution view of this type of rock is from the ChemCam Remote Micro-Imager (RMI, ~50 μm per pixel in this case). The RMI images of Link (Fig. 5) do not allow us to determine whether the matrix consists of fine sand or clay-size grains. The matrix between resolvable grains is generally darker-toned and may include interstitial cement as well as fine grains.

On surfaces that appear less dust-covered, both bright (white or translucent) and dark pebbles are present in color Mastcam images (e.g., Figs. 2 and 3 and fig. S2), with up to half visually appearing as black or gray. In grayscale RMI images on Link, about two-thirds of clasts larger than 2 mm are light-toned and the remainder are dark-toned (Fig. 5). The variability in size, shape, and color of the pebbles in outcrops reflects different clast compositions and likely multiple provenance lithologies.

Within the outcrops, observable clasts are arranged in grain-to-grain contact. Locally grains form tightly packed clusters (Fig. 3C), including in the highest-resolution images of Link where pebbles are in contact with very coarse sand grains (Fig. 5). In Hottah, parallel stratification is evident in a few relatively dust-free cross-sectional surfaces oriented approximately perpendicular to the rover (Fig. 3B). Elongate clasts are commonly aligned parallel to stratification, and in several examples these clasts show imbrication (Fig. 3D). In places, layers of pebbles are separated by finer-grained, recessed layers that form repeating couplets up to 5 cm thick (Fig. 3C).

Most pebbles observed within these outcrops are distinguished by smooth, rounded perimeters and an equant to tabular shape (fig. S3). The roundness of the pebbles is documented in two ways (*17*) (table S2). Qualitative roundness indices for the majority of pebbles are classified as subrounded or rounded, and the mean quantitative relative roundness is moderate (~0.42 in Hottah and ~0.44 near Link).

Rounded pebbles observed by MSL differ from the dominantly angular clasts (>1 cm) documented at prior martian lander and rover locations (Viking, Pathfinder, and Mars Exploration Rovers). The quantitative roundness of clasts measured here by Curiosity are an order of magnitude higher than reported at Pathfinder (0.083) (*18*). Clasts at other martian landing sites have been interpreted as a single lithology of volcanic origin with minimal modification by impact cratering and aeolian processes (*18*–*20*). The intermediate roundness values for a portion of the particles at the Viking 1 and Pathfinder landing sites, located in circum-Chryse outflow channels, are consistent with high-energy, short-duration abrasion associated with catastrophic flooding (*18*–*20*).

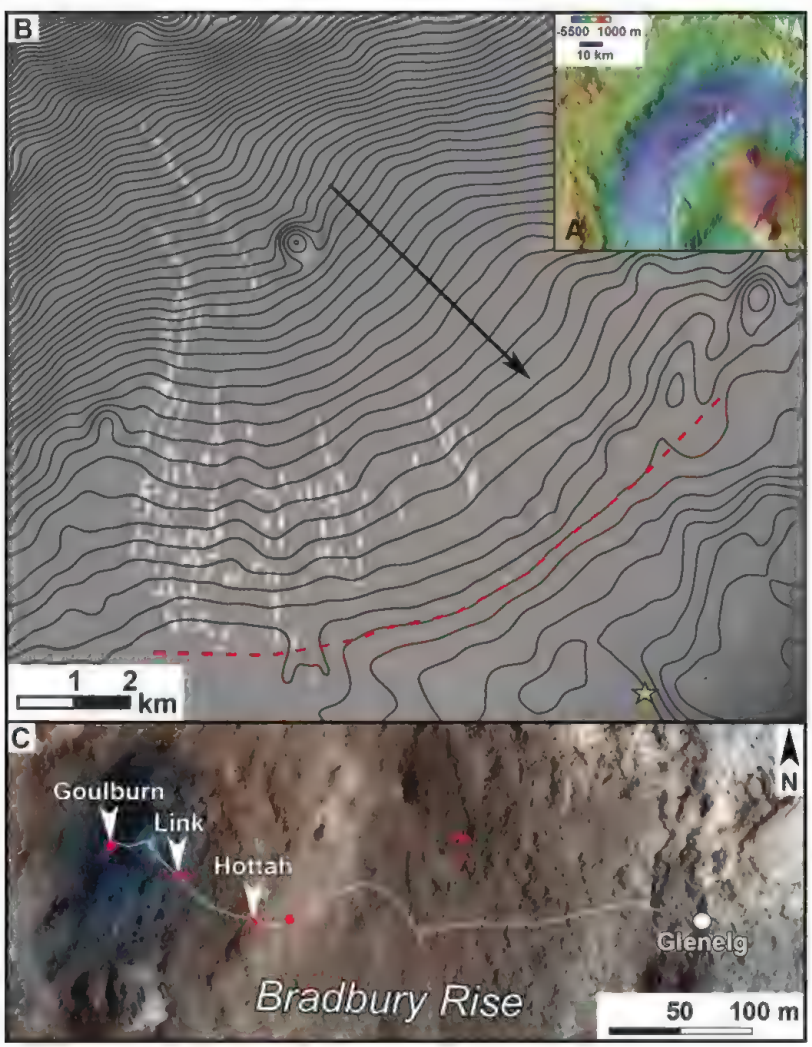

Fig. 1. Location of study site. (**A**) (inset) The Curiosity rover landed on the Aeolis Palus lowlands in northwestern Gale crater [white box corresponds to (B)]. Color topographic map displays elevation values from the Mars Orbiter Laser Altimeter (MOLA) instrument (*39*). (**B**) The Peace Vallis fan is characterized by convex topographic contours (black lines; contour interval is 5 m, arrow marks downslope direction) from smoothed High Resolution Imaging Science Experiment [HiRISE (*40*)] stereo data. The broad topographic expression of the alluvial fan becomes less distinct downslope of the dashed red line. Sinuous ridges interpreted to record former flow paths (i.e., inverted channels) are mapped in white. Bradbury Landing is marked by yellow star. (**C**) Curiosity's route in the first 100 sols across Bradbury Rise from the darkened "blast zone" at the landing site toward Glenelg is marked on a HiRISE image (ESP_028335_1755) acquired on 11 August 2012. The locations of pebble conglomerates are marked with red dots.

Sediment Transport Processes

The sedimentologic characteristics of these outcrops at Gale crater provide insights into sediment transport processes. Bedload collisional processes in flows produce rounding for heterogeneous clasts, and this is a particularly relevant mechanism for rounding the largest size fraction observed (pebbles with long axis of 10 to 40 mm). Sediment transported by traction (bedload) will slide or roll along the bed. Particles transported in a fluid are subjected to mechanical erosion, or abrasion, of the irregular edges of a particle through numerous impacts and grinding, ultimately producing a smooth surface (*21*, *22*).

The particle size, roundness, sorting, and fabric exposed in these rocks lead us to interpret them as water-transported sediment. The clast size and rounded perimeter of pebbles within these rocks are consistent with their classification as fine-pebble fluvial conglomerates (e.g., a coarse-grained sedimentary rock that is commonly

cemented and made up of rounded to subangular rock fragments larger than 2 mm in diameter in a finer-grained matrix of sand or silt).

Additional evidence for a fluvial interpretation is the stratification at Hottah. Alternating pebble-rich and sand layers (Fig. 3C) indicate fluctuations within sediment transport that result in size sorting of the deposits. In bedload transport, the presence of sand mixed with fine pebbles leads to a sorting instability within flows that produces shallow migrating bedforms (bedload sheets), resulting in fine-scale vertical variations in grain sorting (*23*), as observed at Hottah.

Alternative sediment transport mechanisms to water flows are inconsistent with the observed rock characteristics. For example, the well-developed rounding of the pebbles together with clast fabric, specifically the grain-to-grain contact and local imbrication, make mass transport as a debris flow unlikely. Likewise, pebble clusters and the relatively wide size range of pebbles within the deposit are inconsistent with transport and deposition by wind. The largest grains mobilized by wind will move via creep driven by impacts from abundant saltating finer grains. On Mars, 1- to 2-mm grains are driven by creep, leading to formation of megaripples observed at both Mars Exploration Rover landing sites [e.g., (*24*)]. The result of this process is a relatively thin surface layer of uniformly sized clasts due to size-dependent downwind (creep) migration rates, which differs in both geometry and the coarse grain size range (2 to 40 mm) within the martian conglomerates described here. The higher density of liquid fluids relative to air results in higher bed shear stress (and a buoyancy force on the particle), which can mobilize coarse sediment.

A number of factors influence the development of rounded clast perimeters in fluvial transport, including the original clast size, shape, and lithology, as well as the grain size of the bed material (*21*, *25*). Sand commonly acts as an abrasive agent when transported with pebbles in fluvial systems, causing the coarser particles to round more rapidly (*21*, *22*). The presence of coarse sand and rounded pebbles in the martian rocks is consistent with a highly abrasive flow. For clasts of the same size, lithology is the major factor affecting the rate of downstream rounding [e.g., (*25*–*27*)]. On the basis of published data for pebbles in natural streams and fluvial abrasion experiments for a range of compositions [e.g., (*25*–*27*)], and assuming an initial angular pebble, we estimate a minimum transport distance of a few kilometers to produce a rounded pebble surface. On Mars, the elastic collisions within the flow may have had lower energy due to the reduced gravity, resulting in lower abrasion rates and longer transport distances to achieve similarly rounded pebbles. Overall, the rounded pebbles of apparently diverse lithology within the martian conglomerates are strong evidence for sustained fluvial transport.

The grain size distribution can be used to estimate the critical shear stress for sediment mobility, and in turn the flow depth and mean velocity assuming a water surface slope between 0.1 and 1% (*17*, *28*–*30*) (tables S3 to S5). This range of slope values corresponds to the nearby alluvial fan slope (1%) and an approximate lower value (0.1%) for gravel-bedded streams [e.g., (*31*, *32*)]. For the clast size distributions observed in the three conglomerates, the minimal flow depth (sufficient to initiate motion) is 0.03 to 0.9 m and the corresponding average flow velocity is estimated to be 0.20 to 0.75 m/s. In all cases, the estimated

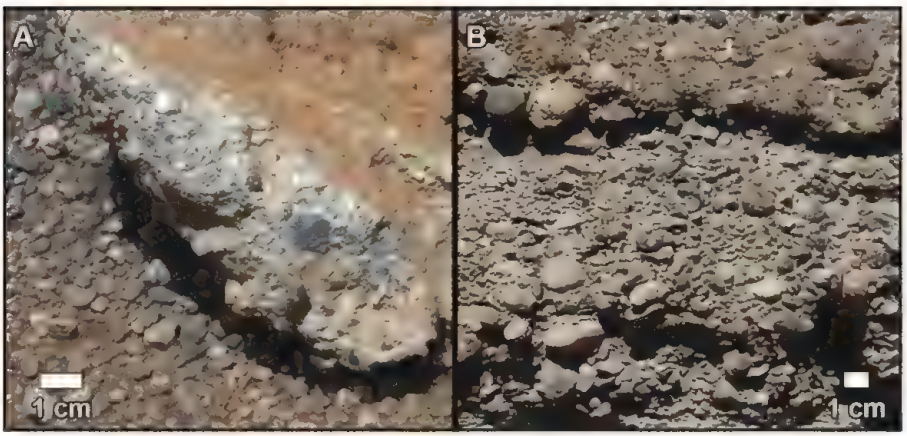

Fig. 2. Comparison of pebbles at Link and a terrestrial analog site. (**A**) Link was imaged with the 100-mm Mastcam on sol 27 (*17*). (**B**) Rounded clasts of similar size and shape are observed in comparably sized distal alluvial fan deposits on Earth, such as this example from the Atacama Desert, Chile.

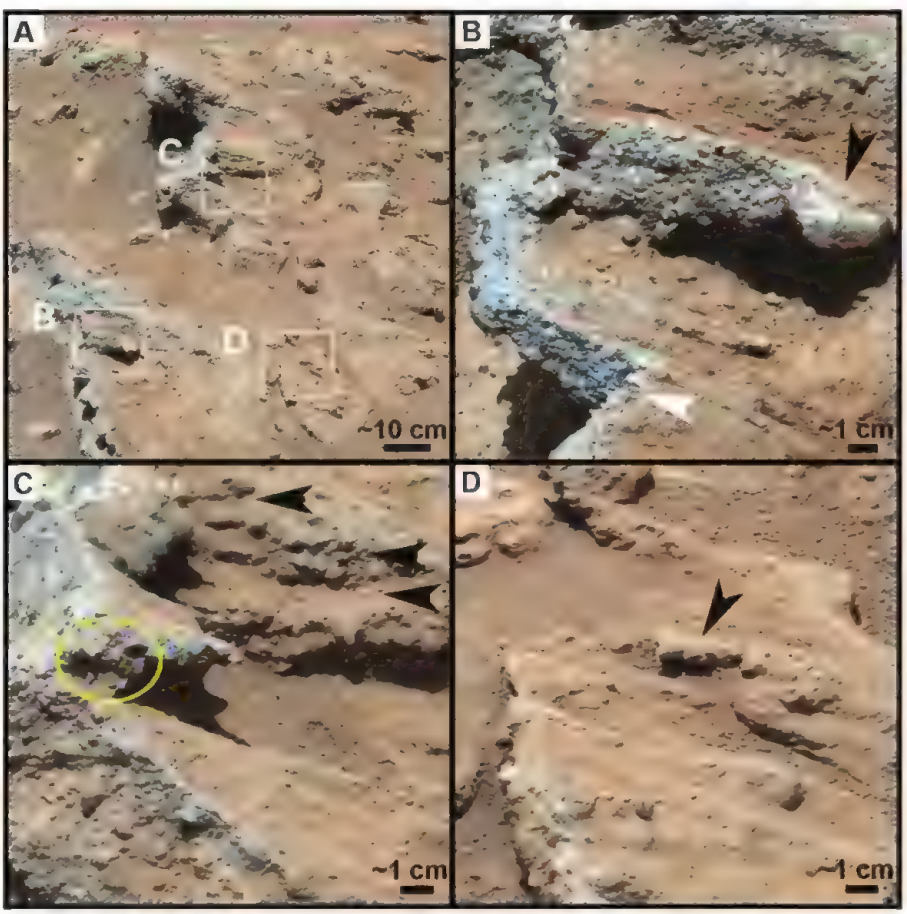

Fig. 3. Examples of sedimentary texture and fabric in the Hottah outcrop. (**A**) The Hottah outcrop has fractured and gently tilted (~30°) blocks, as seen in this mosaic of Mastcam images taken on sol 39 (*17*). (**B**) The perimeter of a well-rounded pebble protruding from the outcrop (upper black arrow, long axis ~3 cm) is smooth. White arrow points to parallel stratification. (**C**) In places, there are alternating protruding, pebble-rich layers (black arrows) and recessive layers. An example of a clast-supported pebble cluster is marked by the yellow circle. (**D**) Example of imbricated clasts.

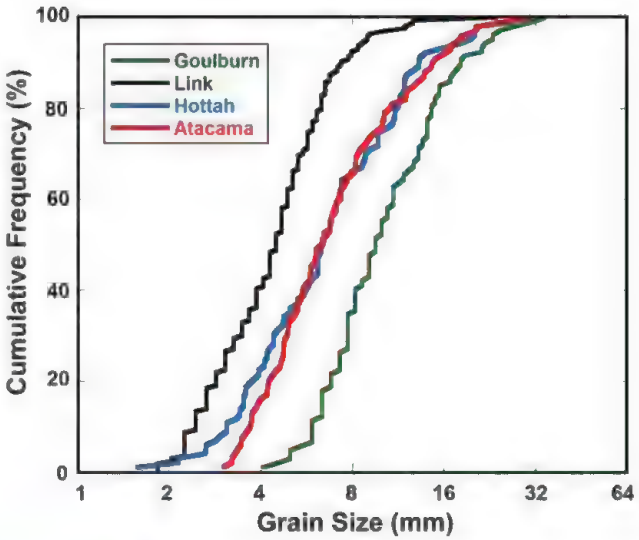

Fig. 4. Cumulative grain size frequency plot. The *x* axis is the phi scale, which we have converted to millimeters (*17*). The grain size distributions for martian conglomerates and a terrestrial analog are normal in all cases, with most of the particles sizes clustered around the median value, consistent with fluvially transported sediment (*41*).

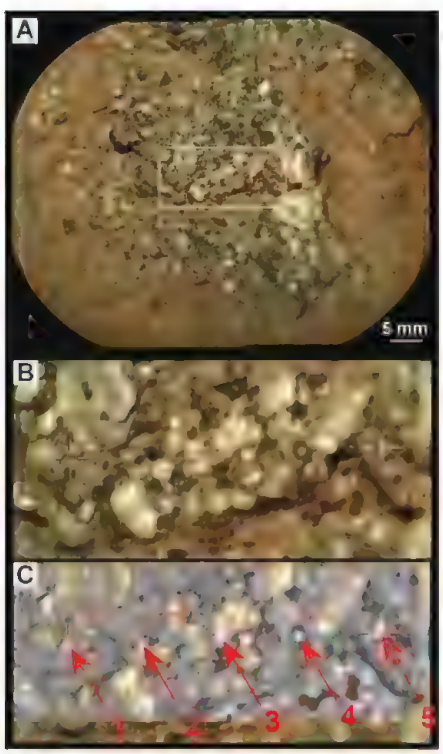

Fig. 5. Highest-resolution view of Link. (A) Mosaic of two RMI images (*17*) from a distance of 2.66 m to the Link outcrop, with color merged from Mastcam images. This composite image has a resolution of ~50 μm per pixel. White box outlines the field of view in (B) and (C). **(B)** This enlarged view shows coarse sand grains in contact with light-toned pebbles, and rounded to sub-rounded grain shape. The interstitial component between resolvable grains appears dark-toned, suggests a mafic composition. The ends of a five-point LIBS line are marked by crosshairs. LIBS sampled mainly lighter grains with the exception of point 5, which sampled a darker area. In contrast to LIBS holes observed in some other rocks, LIBS shot points did not leave obvious marks on Link. **(C)** Difference map (from images acquired before and after laser activity) superimposed on the same view, showing the locations of the five ablated points.

threshold conditions correspond to subcritical flows where the gravitational force is greater than the inertial driving force [Froude number < 1 (*17*)]. Flows likely exceeded these threshold conditions.

Composition

The composition of the conglomerates is indicative of the sediment source and depositional environments. The Laser-Induced Breakdown Spectrometer (LIBS) of the ChemCam instrument (*14*–*16*) was used to determine elemental composition at the Link outcrop. Five points ~400 μm in diameter spanning a distance of ~15 mm provided a compositional sampling of minerals in the coarse-grained rocks (Figs. 5 and 6). Laser shot points appear to have sampled predominantly the light-toned fraction of Link. The target is especially high in Si, K, and Na relative to typical martian basaltic rocks, and Rb is detected in concert with K at the 100- to 200-ppm level (*17*). The partial least squares (PLS) processed results show a composition corresponding to high silica and high alkaline content (table S6). The high Si content and normative plagioclase and orthoclase suggest a substantial feldspar component, consistent with the presence of light-toned grains [see (*33*) for additional detail]. The presence of alkaline elements (i.e., mobile cations such as Ca, Na, and K) in Link indicates that prolonged aqueous alteration has not occurred (table S6).

A Fe-, Ti-, and Cr-rich component identified in point 5 (Fig. 6B) is similar in composition to typical martian regolith [approximately basalt composition (*17*)]. However, the RMI images of Link (Fig. 5) confirm that the rock is largely free of a loose surface coating. In addition, a thicker dust mantling here is discarded as a possibility because of the compositional difference between point 5 and average dust (table S6). The phase with high Fe and Ti abundance may correspond to fine basaltic grains that were transported with larger clasts, reflecting different provenance, or to an iron-rich cement.

In addition, all Link spectra display a hydrogen peak visible at 656 nm, consistent with the presence of a low proportion of hydrated mineral(s). This peak is present in all points but seems to be higher for the first 25 shots at point 5 (Fig. 6B), corresponding to the Fe-, Ti-, and Cr-bearing component. The depletion of mobile elements (e.g., Na) relative to aluminum in this phase may be consistent with limited alteration. We cannot determine whether the observed hydration is related to in situ aqueous alteration of fine grains, or to minor alteration phases that were already present in the martian crust and transported as fines with the larger clasts. The isolated rock exposures and consistent thickness of beds suggests localized induration after flows ceased.

Overall, the chemical data are consistent with a rock comprising first-cycle clastic sediments with preservation of coarse feldspar grains and minimal alteration products. We conclude that clast size and shape developed predominantly from mechanical rock breakdown by fluvial abrasion, in contrast to terrestrial rivers where the development of weathering rinds is a secondary mechanism contributing to clast diminution and form [e.g., (*34*)].

Stratigraphic Interpretation

The conglomerates have a complex geologic setting: The ancient impact basin they lie within formed approximately 3.6 to 3.8 billion years ago, around the Noachian-Hesperian transition (*35*, *36*), and may have filled completely with sediment before being eroded to the current morphology through aeolian erosion (*36*). The Bradbury conglomerates are within the crater-fill stratigraphy and document the role of fluvial processes in sedimentation within Gale crater.

Multiple fluvial pathways have been identified at Gale crater from orbital images [e.g., (*10*)], but none can be connected with confidence to the conglomerates. Both Aeolis Mons and the crater rim show geomorphic evidence for fluvial incision (*10*, *37*) (Fig. 1) and could have been sediment sources for the conglomerates. For example, the conglomerates are located downslope of a large, crater rim–sourced alluvial fan (~80 km^2). The transport distances across the alluvial fan (~14 km) and from its drainage basin (>40 km) are consistent with the rounded clast observations. The distal Peace Vallis alluvial fan slope (~1% gradient) can be projected across a topographic depression ~5 km to the conglomerate outcrops. However, there is no evidence to date, except topography, indicating that the Peace Vallis fan extended to this area. In the absence of contact relationships between the Bradbury Rise conglomerates and mapped geomorphic features interpreted as water-formed, the overall stratigraphic context and relative age of the conglomerates are uncertain. Thus, the most parsimonious interpretation is that the conglomerates are distal alluvial fan deposits of unknown age.

Despite the uncertainty in their stratigraphic context, the Bradbury conglomerates constitute a record of past conditions at Gale crater that contrast

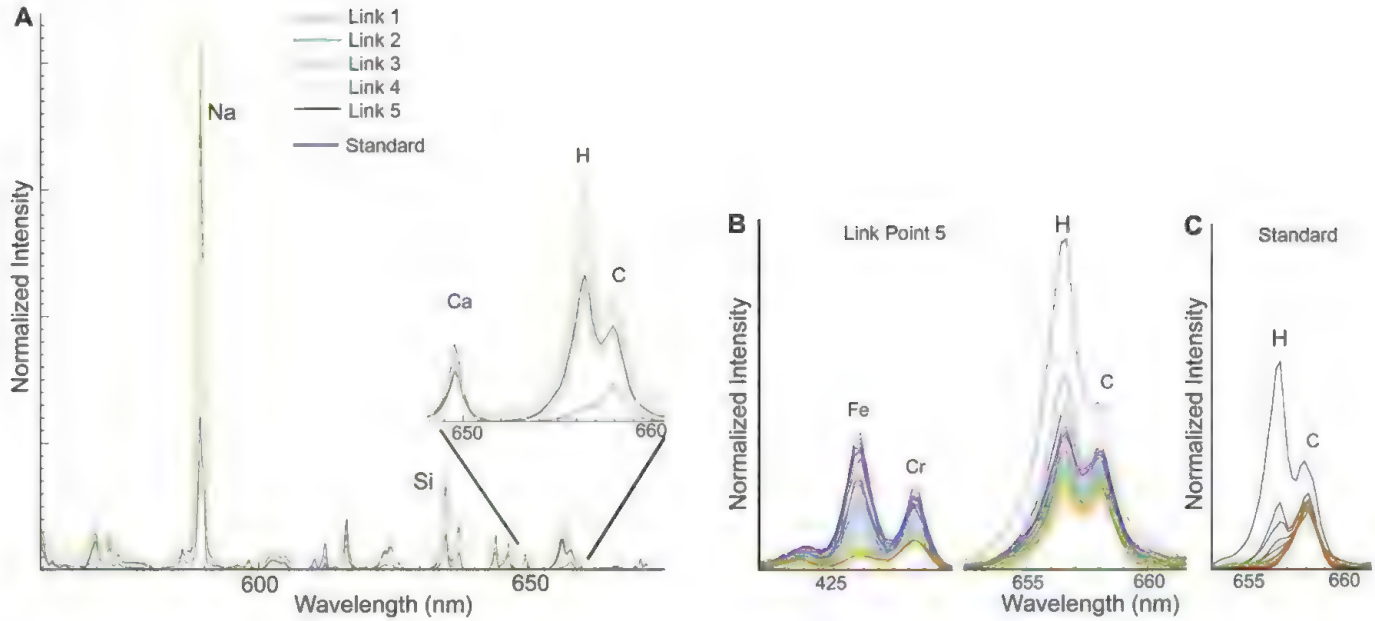

Fig. 6. Emission spectra from Link. **(A)** ChemCam averaged spectra (*17*) in selected wavelengths for five points (Fig. 5C) on the Link outcrop and an anhydrous rover-mounted calibration standard [norite composition (*42*) in navy blue]. All Link spectra have higher Si and Na than the norite standard (in contrast, Ca is slightly higher in the norite), in agreement with quantitative analyses (table S6). Enlargement of the hydrogen line region at 656 nm shows detection of hydrogen in the average spectra of all points at Link. The emission line at 658 nm corresponds to atmospheric carbon and varies only because of the correlated variations in hydrogen. **(B)** Shot-by-shot data over the 50 shots at point 5 (black, shot 0; red, shot 50). The first half of these shots have higher Fe, Cr, and H emission lines than the second half, corresponding to a progressive change in composition with depth (table S6). **(C)** By comparison, the onboard norite standard shows H only in the first five shots (surficial dust contribution), whereas most of the target is dry, as expected.

with the modern martian environment, where liquid water is unstable under current atmospheric conditions (*38*). These ancient fluvial deposits indicate sustained liquid water flows across the landscape—a finding that raises prospects for the former presence of habitable environments on Mars.

References and Notes

1. M. C. Malin, K. S. Edgett, *Science* **302**, 1931 (2003).
2. J. M. Moore, A. D. Howard, *J. Geophys. Res.* **110**, E04005 (2005).
3. Mars Channel Working Group, *Geol. Soc. Am. Bull.* **94**, 1035 (1983).
4. P. H. Smith *et al.*, *Science* **278**, 1758 (1997).
5. Rover Team, *Science* **278**, 1765 (1997).
6. Rocks at the Pathfinder site with possible sockets and knobs were proposed as candidate conglomerates, but low image quality made this interpretation equivocal.
7. S. W. Squyres *et al.*, *Science* **306**, 1709 (2004).
8. J. P. Grotzinger *et al.*, *Earth Planet. Sci. Lett.* **240**, 11 (2005).
9. J. P. Grotzinger *et al.*, *Geology* **34**, 1085 (2006).
10. R. B. Anderson, J. F. Bell, *Mars* **5**, 76 (2010).
11. J. P. Grotzinger *et al.*, *Space Sci. Rev.* **170**, 5 (2012).
12. A sol is a martian day.
13. Names have been assigned to areographic features and rocks by the MSL team for planning and operations purposes. These names are not formally recognized by the International Astronomical Union.
14. Cameras on Curiosity's remote sensing mast include four monochrome navigation cameras, each with a 45° field of view (FOV), and two color cameras (Bayer pattern color filter array) that constitute the stereo Mastcam instrument. The left camera has a 34-mm focal length with 15° FOV; the right camera has a 100-mm focal length and 5° FOV. At a distance of 2 m, the Mastcam pixel scales are 440 and 148 μm, respectively. The ChemCam instrument is a package of a Laser-Induced Breakdown Spectrometer (LIBS) coupled to a Remote Micro-Imager (RMI). The full FOV for each RMI is 20 milliradians. The Mars Hand Lens Imager (MAHLI) and Alpha-Proton X-ray Spectrometer (APXS) instruments were not commissioned for tactical operations when the conglomerates were encountered.
15. R. C. Wiens *et al.*, *Space Sci. Rev.* **170**, 167 (2012).
16. S. Maurice *et al.*, *Space Sci. Rev.* **170**, 95 (2012).
17. See supplementary materials on *Science* Online.
18. R. A. Yingst, A. F. C. Haldemann, K. L. Biedermann, A. M. Monhead, *J. Geophys. Res.* **112**, E06002 (2007).
19. J. B. Garvin, P. J. Mouginis-Mark, J. W. Head, *Moon Planets* **24**, 355 (1981).
20. R. A. Yingst *et al.*, *J. Geophys. Res.* **113**, E12S41 (2008).
21. R. L. Folk, *The Petrology of Sedimentary Rocks* (Hemphills, Austin, TX, 1980).
22. W. C. Krumbein, L. L. Sloss, *Stratigraphy and Sedimentation* (Freeman, New York, 1963).
23. P. J. Whiting, W. E. Dietrich, L. B. Leopold, T. G. Drake, R. L. Shreve, *Geology* **16**, 105 (1988).
24. D. J. Jerolmack, D. Mohrig, J. P. Grotzinger, D. A. Fike, W. A. Watters, *J. Geophys. Res.* **111**, E12S02 (2006).
25. H. H. Mills, *J. Sediment. Petrol.* **49**, 295 (1979).
26. N. S. Davies, R. K. Vessell, R. C. Miles, M. G. Foley, S. B. Bonis, in *Fluvial Sedimentology*, A. D. Miall, Ed. (Canadian Society of Petroleum Geologists, Calgary, 1977), Memoir 5, pp. 61–84.
27. J. Lewin, P. A. Brewer, *Earth Planet. Sci. Lett.* **27**, 145 (2002).
28. Scaling analysis suggests that Mars' lower gravity has only a minor effect on fluvial gradients at the threshold of motion and bedform configuration. Therefore, it is appropriate to compare terrestrial fluvial bedforms and gradients to their martian counterparts.
29. V. T. Chow, *Open-Channel Hydraulics* (Blackburn, Caldwell, NJ, 1959).
30. P. D. Komar, *Icarus* **42**, 317 (1980).
31. G. Parker, P. R. Wilcock, C. Paola, W. E. Dietrich, J. Pitlick, *J. Geophys. Res.* **112**, F04005 (2007).
32. R. S. Anderson, S. P. Anderson, *Geomorphology: The Mechanics and Chemistry of Landscapes* (Cambridge University Press, Cambridge, 2010).
33. R. C. Wiens *et al.*, *44th Lunar and Planetary Science Conference*, Abstract 1363 (2013); www.lpi.usra.edu/meetings/lpsc2013/pdf/1363.pdf.
34. P. L. Heller *et al.*, *Geology* **29**, 971 (2001).
35. The Noachian is a geologic system on Mars representing the oldest period of the planet's geologic history, characterized by high impact rates.
36. B. J. Thomson *et al.*, *Icarus* **214**, 413 (2011).
37. M. C. Malin, K. S. Edgett, *Science* **290**, 1927 (2000).
38. R. M. Haberle *et al.*, *J. Geophys. Res.* **106**, 23317 (2001).
39. D. E. Smith *et al.*, *J. Geophys. Res.* **106**, 23689 (2001).
40. A. S. McEwen *et al.*, *J. Geophys. Res.* **112**, E05S02 (2007).
41. K. Bunte, S. R. Abt, *U.S. Department of Agriculture General Technical Report RMRS-GTR-74* (2001).
42. S. M. Fabre *et al.*, *Spectrochim. Acta B* **66**, 280 (2011).

Acknowledgments: We thank K. Tanaka and L. Kestay (USGS-Flagstaff) and four anonymous referees for constructive reviews of this manuscript. This research was carried out for the Jet Propulsion Laboratory, California Institute of Technology, under a contract with NASA under the Mars Program Office, including JPL contracts 1449884 (R.M.E.W.) and 1273887 (Malin Space Science Systems). Work in France was carried out with funding from the Centre National d'Etudes Spatiales. Work in the UK was funded by the UK Space Agency. Work in Denmark was funded by the Danish Council for Independent Research/Natural Sciences (FNU grants 12-127126 and 11-107019) and the TICRA Foundation. Work in Germany was partly funded by Deutsche Forschungsgemeinschaft grant GO 2288/1-1. Data in this manuscript are available from the NASA Planetary Data System. This is PSI contribution 603.

Supplementary Materials

www.sciencemag.org/cgi/content/full/340/6136/1068/DC1
Methods
Supplementary Text
Figs. S1 to S3
Tables S1 to S6
References (*43–56*)

4 March 2013; accepted 7 May 2013
10.1126/science.1237317

High-Strength Chemical-Vapor–Deposited Graphene and Grain Boundaries

Gwan-Hyoung Lee,[1,2]* Ryan C. Cooper,[1]* Sung Joo An,[1] Sunwoo Lee,[3] Arend van der Zande,[1,4] Nicholas Petrone,[1] Alexandra G. Hammerberg,[1] Changgu Lee,[5,6] Bryan Crawford,[7] Warren Oliver,[7] Jeffrey W. Kysar,[1]† James Hone[1]†

Pristine graphene is the strongest material ever measured. However, large-area graphene films produced by means of chemical vapor deposition (CVD) are polycrystalline and thus contain grain boundaries that can potentially weaken the material. We combined structural characterization by means of transmission electron microscopy with nanoindentation in order to study the mechanical properties of CVD-graphene films with different grain sizes. We show that the elastic stiffness of CVD-graphene is identical to that of pristine graphene if postprocessing steps avoid damage or rippling. Its strength is only slightly reduced despite the existence of grain boundaries. Indentation tests directly on grain boundaries confirm that they are almost as strong as pristine. Graphene films consisting entirely of well-stitched grain boundaries can retain ultrahigh strength, which is critical for a large variety of applications, such as flexible electronics and strengthening components.

In bulk three-dimensional (3D) materials, the inevitable presence of bulk and surface defects limits the tensile strength to a value that typically falls well short of the intrinsic strength predicted for homogeneous tensile cleavage (*1*). Low-dimensional materials such as 2D graphene or quasi-1D carbon nanotubes can achieve record strength in part because of the lack of surface defects that often initiate fracture in 3D materials. However, using the ultrahigh strength of low-dimensional materials on the macroscale remains an open challenge, both from a technological perspective and as a matter of fundamental interest. At sufficiently large scales, all materials will contain lattice defects, and the effects of such defects should be magnified in low-dimensional materials because of a reduction in the number of dimensions in which a material can receive structural support: In the limit of a 1D atomic chain, even a single vacancy will reduce the tensile strength to zero. Moreover, the same lack of surface-bulk distinction that eliminates surface defects in low-dimensional materials also renders them extremely sensitive to damage during processing.

We have previously used nanoindentation of freely suspended films in an atomic force microscope (AFM) to show that graphene isolated through mechanical exfoliation is the strongest known material and, in its defect-free pristine state, can achieve its intrinsic strength before succumbing to rupture (*2*). However, graphene produced

[1]Department of Mechanical Engineering, Columbia University, New York, NY 10027, USA. [2]Samsung–Sungkyunkwan University (SKKU) Graphene Center (SSGC), Suwon 440-746, Korea. [3]Department of Electrical Engineering, Columbia University, New York, NY 10027, USA. [4]Energy Frontier Research Center, Columbia University, New York, NY 10027, USA. [5]School of Mechanical Engineering, SKKU, 2066, Seobu-ro, Jangan-gu, Suwon, Gyeonggi 440-746, Korea. [6]SKKU Advanced Institute of Nanotechnology (SAINT), SKKU, 2066, Seobu-ro, Jangan-gu, Suwon, Gyeonggi 440-746, Korea. [7]Nanomechanics, Oak Ridge, TN 37830, USA.

*These authors contributed equally to this work.
†Corresponding author. E-mail: jh2228@columbia.edu (J.H.); jk2079@columbia.edu (J.W.K.)

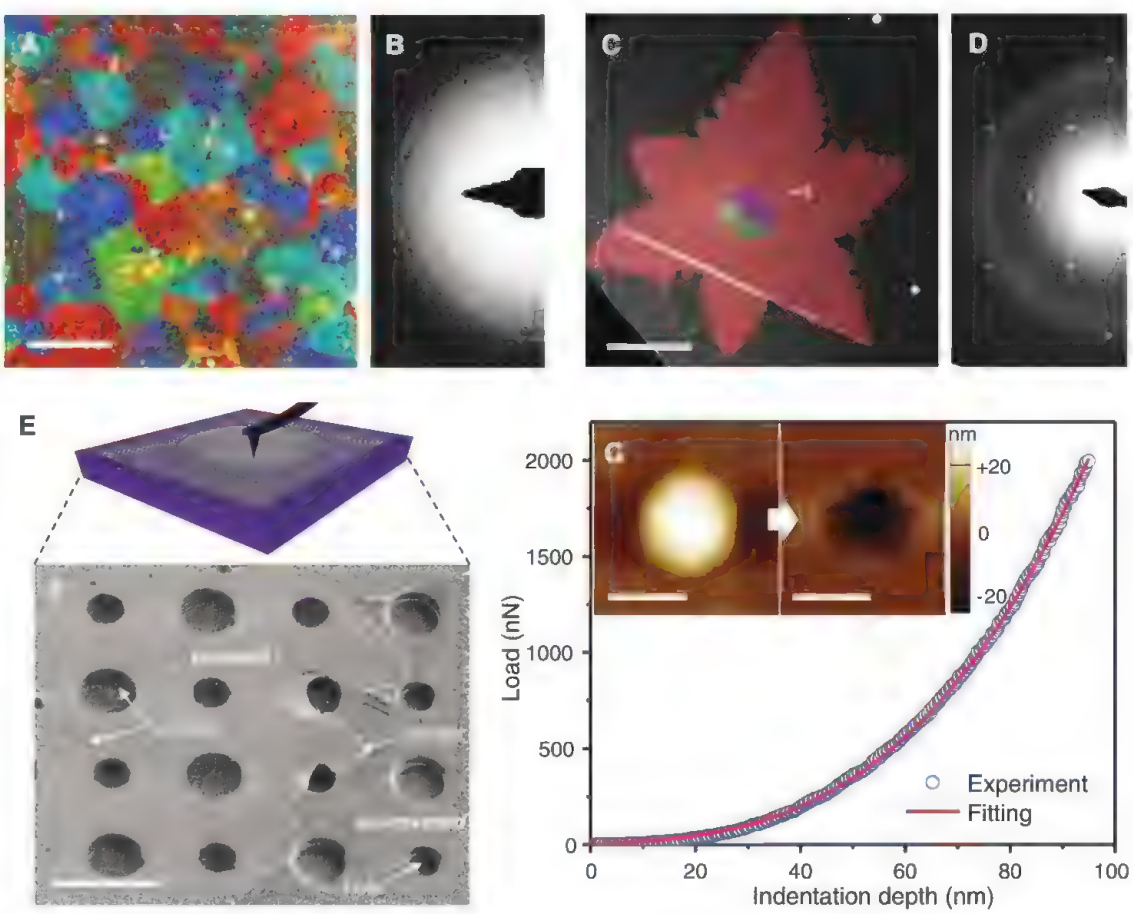

Fig. 1. Materials and testing methods. (**A** and **C**) False-color DF-TEM images and (**B** and **D**) SAED patterns of SG graphene and LG graphene films. (**E**) Schematic of the suspended graphene film over hole for AFM nanoindentation tests. (**F**) SEM images of the suspended LG graphene film over holes. The border of the graphene-covered area is indicated by a dashed line for visualization. Wrinkles often present in the transferred graphene can be seen. (**G**) Force-displacement curve of the SG graphene film in AFM nanoindentation. The red line is a fitting curve to equation 2 of (*1*). (Inset) The AFM topology images of the suspended SG graphene film before and after fracture. Scale bars, (A) and (F) 3 μm; (C) 20 μm; (G) 1 μm.

through scalable methods—such as chemical vapor deposition (CVD)—produces graphene with various defects, especially grain boundaries (*3*–*7*). It is of fundamental importance to understand how the nature and presence of such defects will degrade the mechanical properties. Recent theoretical studies have argued that graphene grain boundaries can be as strong as the pristine lattice, depending on their exact configuration, such as tilt angle (*8*) and arrangement of defects (*9*). On the other hand, nanoindentation tests have shown that both the elastic stiffness and fracture strength of CVD-graphene with micrometer-scale grain size are much smaller than those of defect-free pristine graphene and that fracture occurs at grain boundaries (*3*, *5*). However, continued progress in development of techniques for processing graphene motivates reexamination of this question from an experimental standpoint. Indeed, we find here that techniques used in earlier studies, which were standard practice at the time and remain widely used, significantly degrade the strength of graphene (supplementary materials). In this work, we used new processing techniques that leave graphene's strength intact. We used a commercial nanoindenter to test a large number of samples for statistical analysis and combined nanoindentation and transmission electron microscopy (TEM) characterization to test individual grain boundaries. The data were analyzed by using a multiscale model that is based on density functional theory and has been experimentally validated for pristine graphene.

Two types of graphene were grown on copper foil: continuous graphene films with small grains (SG) and isolated single-crystals with large grains (LG) (supplementary materials, materials and methods). Dark-field TEM (DF-TEM) imaging (*3*) was used to map the grain structure of the graphene films (Fig. 1, A and C); each false-color area indicates a distinct crystal orientation from the selected area electron diffraction (SAED) patterns of Fig. 1, B and D. These patterns confirm that the SG graphene is similar to the films studied previously (*3*–*5*): It is polycrystalline, with 1- to ~5-μm grains that are stitched at well-defined grain boundaries, that have been observed to consist of pentagon and heptagon carbon rings without any other defects, such as holes (*3*, *4*). Small bilayer patches are occasionally present in the middle of grains. The star-shaped LG graphene grains are 50- to ~200-μm single crystals (Fig. 1D) (*10*, *11*) of single-layer graphene with small multilayer patches at the center. All of the nanoindentation experiments reported below were performed on the single-layer areas of the SG and LG graphene films.

To create suspended membranes, graphene films grown on copper foil were transferred onto a silicon dioxide substrate with an array of holes with 1- and 1.5-μm diameters (Fig. 1E; figs. S1 and S2; and supplementary materials, materials and methods). We found that two of the processing techniques used in previous studies (*3*, *5*) severely weakened the grain boundaries in CVD-graphene: etching the copper with ferric chloride ($FeCl_3$) and removal of a polymer support by baking in air (figs. S3 and S4). Both steps were avoided herein; the copper was etched with ammonium persulfate instead of $FeCl_3$, and polydimethylsiloxane (PDMS) was used to support the graphene during copper etching and to dry-stamp it onto the substrate without baking. The transferred LG graphene film is shown in the scanning electron microscopy (SEM) image of Fig. 1F (SG graphene is shown in fig. S3A). The graphene films form membranes tautly suspended above the holes, with little contamination. Raman spectroscopy confirms that the membranes are highly crystalline graphene with few defects (fig. S5).

We used nanoindentation to measure mechanical properties of the suspended membranes, as described in (*2*, *12*). A representative force-displacement curve obtained by using an AFM with a diamond tip of 26-nm radius is shown in Fig. 1G. The curve was well fitted by use of a quasi-empirical polynomial form (*2*). The cubic fitting parameter yielded 99% confidence intervals for the mean of elastic stiffness of 328 ± 15 N/m near that of pristine graphene (340 N/m) and an order of magnitude higher than the value previously reported for CVD-graphene (55 N/m) (*5*). Moreover, the force required to break the membrane is 2000 ± 420 nN, which is much greater than that previously observed (50 to 120 nN) (*3*, *5*). A SG membrane before and after fracture are shown in the AFM images in the inset. The samples showed no sign of slippage at the periphery, and the fracture pattern was similar to that observed for pristine graphene (fig. S6).

For statistical analysis of stiffness and strength, we tested a large number of specimens using a nanoindenter, with a 38-nm-radius diamond tip (fig. S7A). Each membrane was cyclically tested to increasing depth to fracture; the nonhysteretic force-displacement curves were analyzed as above. Histograms of the derived elastic stiffness are shown in Fig. 2, A and B, for LG and SG graphene (that of pristine graphene is available in fig. S7B). We obtained elastic moduli of 324 ± 13, 339 ± 17, and 328 ± 17 N/m (which correspond to a 3D Young's modulus of ~1 TPa) for pristine, LG, and SG graphene, respectively. According to one-way analysis of variance (ANOVA) analyses, there are no statistical differences among these three values or between these and the value previously obtained for pristine graphene (fig. S8A and table S1) (*2*); all are in agreement with theoretical predictions in the absence of grain boundaries (*13*). The wider distributions observed for SG and LG graphene may be due to the presence of wrinkles and small bilayer patches in the CVD-grown membranes.

The measured fracture loads for LG and SG membranes are shown in Fig. 2, C and D (pristine is available in fig. S7C). The measurements yield fracture loads of 3410 ± 260, 3370 ± 340, and 2590 ± 380 nN for the pristine, LG, and SG films, respectively. The fracture load of the SG films is statistically different from that of the pristine and

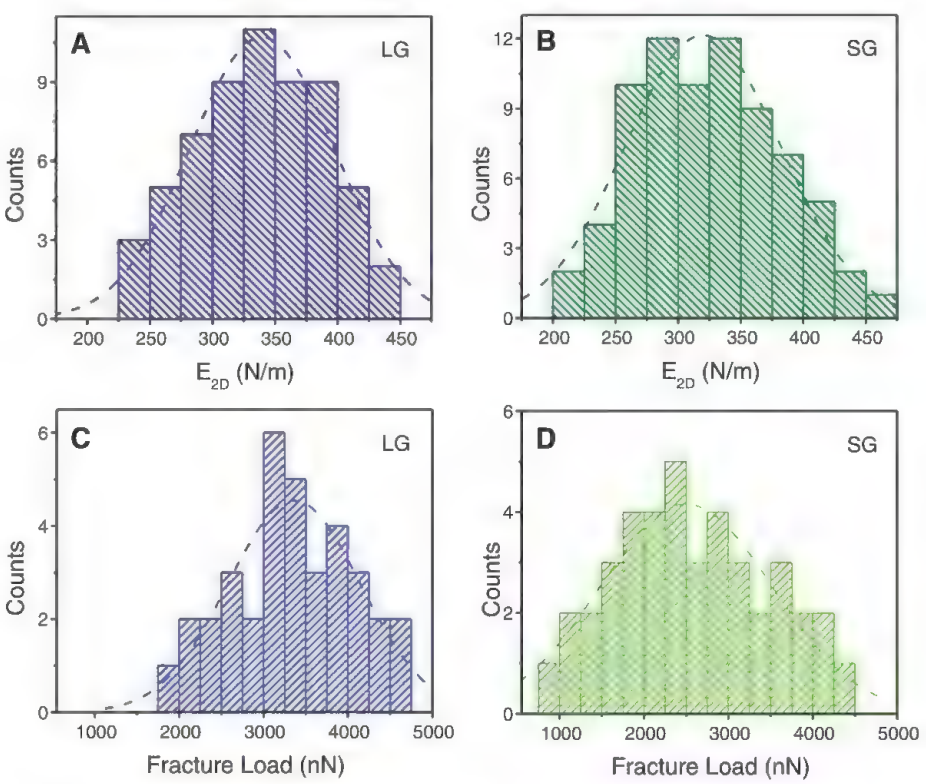

Fig. 2. Statistical analyses of nanoindenter results. (**A** and **B**) The histograms of the elastic stiffness of (A) LG and (B) SG graphene films. (**C** and **D**) The histograms of fracture load for (C) LG and (D) SG graphene films. A tip with a 38-nm radius was used in all tests. The dashed lines indicate fitted Gaussian distributions.

LG films, whereas there is no statistical difference between the fracture loads of the pristine and LG graphene according to one-way ANOVA (fig. S8B and table S2). The smaller mean fracture load and wider distribution observed for SG graphene indicates that the strength is influenced by the randomly occurring defects and grain boundaries in the membranes. Nevertheless, the measured fracture load of the SG graphene is much larger than seen in previous measurements (*3*, *5*).

We calculated the breaking strength of the graphene films as a function of the measured fracture load and tip diameter with an experimentally validated multiscale model based on atomic-scale ab initio density functional theory (*14*). This constitutive model informs a continuum description of anisotropic and nonlinear elastic behavior for in-plane deformation (*14*, *15*) that permits numerical modeling of the stress in the graphene up to the point of rupture. Shown in fig. S9 is the equibiaxial true stress versus load under the center of a 38-nm indenter tip for pristine graphene, which yields an equibiaxial breaking strength of 34.5 N/m (103 GPa, when expressed as a 3D value). The mechanical strength or peak stress that can be supported by graphene is a function of the loading configuration. For uniaxial stress in the armchair direction, the same model predicts a strength of 39.5 N/m (118 GPa), which is consistent with our previously reported value of 42 ± 4 N/m for the same loading configuration (supplementary materials). With an identical fracture load, LG graphene has an equivalent breaking strength to pristine graphene. The average equibiaxial strength of SG graphene is only slightly smaller, 33 N/m (98.5 GPa). A similar value was obtained for SG membranes tested with AFM. These results demonstrate that polycrystalline graphene with well-stitched grains can act as a large-area ultrastrong material.

Because the stress decreases inversely with distance from the indenter tip, the stress under the tip at rupture does not necessarily correspond to the grain boundary strength. Therefore, we performed indentation tests directly on a few grain boundaries identified through TEM. SG films were transferred onto TEM grids with 2.5-μm holes by using a poly(methyl methacrylate) (PMMA) transfer technique (*3*, *7*), followed by annealing in hydrogen and argon so as to remove the PMMA without reducing the strength of the films. The bright-field TEM (BF-TEM) image of Fig. 3A shows a suspended SG film, with adsorbates (likely PMMA residue) that decorate grain boundaries, as confirmed with higher-resolution imaging (Fig. 3B) (*3*, *13*); these adsorbates are not observed in LG films (fig. S10). The corresponding grain structure is illustrated in the DF-TEM map of Fig. 3C. The adsorbates render the grain boundaries visible in AFM (Fig. 3E and fig. S11) but are also present at wrinkles, so that AFM imaging alone is not sufficient to identify grain boundaries. Adsorbates are not expected to affect the grain

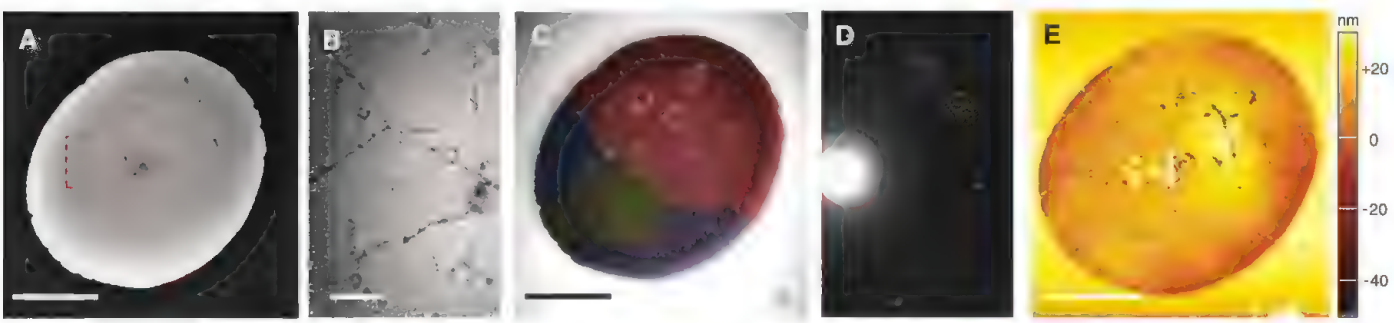

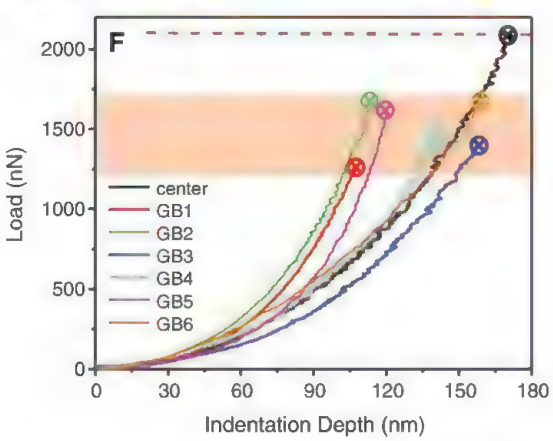

Fig. 3. TEM observation of grain boundaries and AFM nanoindentation on grain boundaries. (**A** and **B**) BF-TEM images of (A) suspended SG graphene film over a hole and (B) enlarged BF-TEM image of red-dashed area in (A). (**C**) False-color DF-TEM image. (**D**) SAED of the same region. The diffraction spots corresponding to each color of (C) are indicated in (D) with circles of different colors. (**E**) AFM topology image shows that arrays of PMMA residue adhere to grain boundaries. The grain boundaries and indentation point are indicated by dashed lines and the white arrow. (**F**) AFM indentation results show that fracture occurs at a slightly lower load when AFM tip indents on the grain boundary. Scale bars, 1 μm; (B) 200 nm.

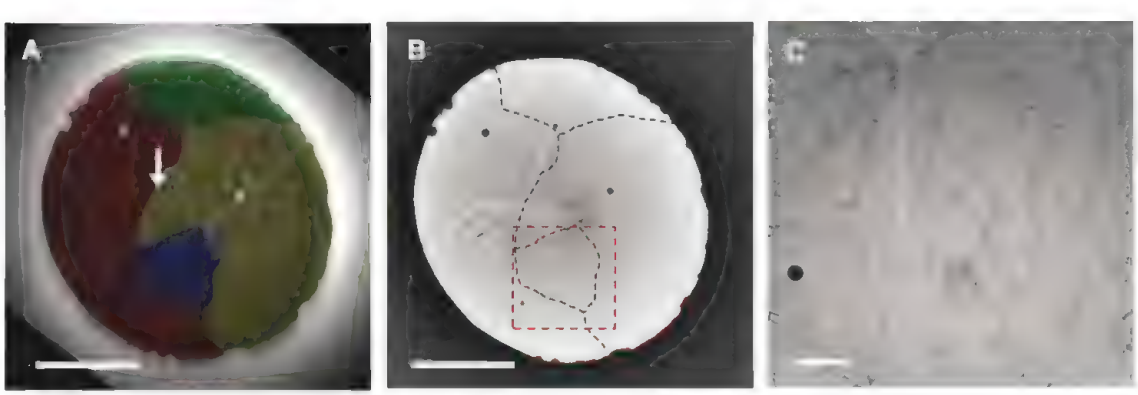

Fig. 4. Crack propagation during nanoindentation. (**A**) False-color DF-TEM image of the suspended SG graphene film over a hole before indentation. The white arrow indicates the indentation point. (**B**) BF-TEM image after indentation. The black-dashed lines indicate grain boundaries. (**C**) Enlarged BF-TEM image of the red-dashed area of (B). Scale bars, 1 μm; (C) 200 nm.

boundary properties because of the very low stiffness and strength of PMMA.

The results of six indentation tests are shown in Fig. 3F, with the tip placed directly on asymmetric tilt grain boundaries near the center of the membrane. An additional test performed at the center of a grain away from grain boundaries (fig. S11I) yielded fracture load similar to that of pristine graphene. The fracture loads at the grain boundaries are 20 to 40% smaller but still an order of magnitude larger than previously measured (*3*, *5*). The same multiscale analysis described above gives a range of equibiaxial stress of 30 to 33 N/m (90 to 99 GPa) for the strength of the grain boundaries, representing at most a 15% reduction from the intrinsic strength. These results confirm that grain boundaries in graphene can achieve ultrahigh strength.

Atomistic scale simulations of symmetric tilt grain boundaries predict that grain boundaries with large tilt angles can achieve near-intrinsic strength (above 30 N/m), but those with low tilt angles possess a lower strength of 13 to 26 N/m, depending on the precise arrangement of defects (*8*, *9*). The simulated grain boundaries consist of periodically spaced pentagon-heptagon ring defects along straight grain boundaries. The simulations predict rupture initiation at the bond joining the pentagonal and heptagonal (5-7) rings, and that decreasing its initial equilibrium length (smaller misfit "prestrain") increases grain boundary strength (*8*, *9*).

The asymmetric tilt grain boundaries in the experiments, which cover a wide range of tilt angles (fig. S12 and table S3), consistently exhibited strength above 30 N/m, suggesting that the predicted variation in strength with tilt angle does not occur in these samples. The tortuous atomic structure of random (*3*) asymmetric grain boundaries is substantially more complex than that assumed for the simulations of symmetric grain boundaries (*8*, *9*). The more complex energy-minimizing structure (*16*) likely leads to a smaller misfit "prestrain" of the critical atomic bonds at in the 5-7 defects, thus explaining the ultrahigh strength (details are available in the supplementary materials) (fig. S12 and table S3).

In addition to well-stitched grain boundaries, we also occasionally observed boundaries in which the adjacent graphene grains overlap (50 nm in width) but do not covalently join (*3*, *4*) (fig. S13). These boundaries were observed to be extremely weak, with no measurable force upon AFM indentation. Overlapped grain boundaries have been observed to possess higher conductance (*4*) than that of stitched boundaries but will result in much weaker films.

To further elucidate the fracture behavior of graphene, AFM nanoindentation on SG membranes was performed to failure, and the ruptured films were observed with TEM. Indentation on a grain boundary (Fig. 4A, white arrow) initiates an intergranular crack (Fig. 4B and fig. S14) under the approximately equibiaxial stress state beneath the indenter tip, thus demonstrating the grain boundary to be somewhat weaker than graphene. The crack later kinks into the adjoining grains because of the more complex stress state. Contrary to the prediction or experimental observation during electron irradiation (*13*), the torn edges of the transgranular cracks have irregular saw-tooth shapes, as shown in the enlarged BF-TEM image of Fig. 4C and fig. S15.

Our measurements reveal that the elastic stiffness and strength of CVD-graphene are comparable with those of pristine graphene, despite the existence of grain boundaries. Moreover, the strength of grain boundaries is much stronger than previously measured, which is in agreement with the maximum values predicted in simulations. This study establishes CVD-graphene as a large-area, high-strength material for flexible electronics and strengthening components.

References and Notes

1. M. Meyers, K. Chawla, *Mechanical Behavior of Materials* (Cambridge, London, ed. 2, 2009).
2. C. Lee, X. D. Wei, J. W. Kysar, J. Hone, *Science* **321**, 385 (2008).
3. P. Y. Huang *et al.*, *Nature* **469**, 389 (2011).
4. A. W. Tsen *et al.*, *Science* **336**, 1143 (2012).
5. C. S. Ruiz-Vargas *et al.*, *Nano Lett.* **11**, 2259 (2011).
6. Q. K. Yu *et al.*, *Nat. Mater.* **10**, 443 (2011).
7. K. Kim *et al.*, *ACS Nano* **5**, 2142 (2011).
8. R. Grantab, V. B. Shenoy, R. S. Ruoff, *Science* **330**, 946 (2010).
9. Y. Wei *et al.*, *Nat. Mater.* **11**, 759 (2012).
10. X. S. Li *et al.*, *J. Am. Chem. Soc.* **133**, 2816 (2011).
11. N. Petrone *et al.*, *Nano Lett.* **12**, 2751 (2012).
12. M. Poot, H. S. J. van der Zant, *Appl. Phys. Lett.* **92**, 063111 (2008).
13. K. Kim *et al.*, *Nano Lett.* **12**, 293 (2012).
14. X. D. Wei, J. W. Kysar, *Int. J. Solids Struct.* **49**, 3201 (2012).
15. X. D. Wei, B. Fragneaud, C. A. Marianetti, J. W. Kysar, *Phys. Rev. B* **80**, 205407 (2009).
16. F. Ernst *et al.*, *Z. Metallk.* **87**, 911 (1996).

Acknowledgments: We acknowledge support from Air Force Office of Scientific Research grants FA9550-09-1-0048 and FA9550-09-1-0705 and NSF grant CMMI-0927891. C.L. was supported by Basic Science Research Program (2011-0014209) and the Global Frontier Research Center for Advanced Soft Electronics (2011-0031629) through the National Research Foundation funded by the Korean government Ministry of Education, Science, and Technology. We thank P. Y. Huang and D. Muller (Cornell University) for help in TEM imaging.

Supplementary Materials

www.sciencemag.org/cgi/content/full/340/6136/1073/DC1
Materials and Methods
Supplementary Text
Figs. S1 to S15
Tables S1 to S3
References (*17*–*31*)

14 January 2013; accepted 16 April 2013
10.1126/science.1235126

Unwinding of a Skyrmion Lattice by Magnetic Monopoles

P. Milde,[1]* D. Köhler,[1] J. Seidel,[2] L. M. Eng,[1] A. Bauer,[3] A. Chacon,[3] J. Kindervater,[3] S. Mühlbauer,[4] C. Pfleiderer,[3] S. Buhrandt,[5] C. Schütte,[5] A. Rosch[5]

Skyrmion crystals are regular arrangements of magnetic whirls that exist in a wide range of chiral magnets. Because of their topology, they cannot be created or destroyed by smooth rearrangements of the direction of the local magnetization. Using magnetic force microscopy, we tracked the destruction of the skyrmion lattice on the surface of a bulk crystal of $Fe_{1-x}Co_xSi$ ($x = 0.5$). Our study revealed that skyrmions vanish by a coalescence, forming elongated structures. Numerical simulations showed that changes of topology are controlled by singular magnetic point defects. They can be viewed as quantized magnetic monopoles and antimonopoles, which provide sources and sinks of one flux quantum of emergent magnetic flux, respectively.

The notion of topological stability refers to those properties of a system that remain unchanged under continuous (elastic) deformations such as bending or stretching (*1*, *2*). Because topologically stable structures cannot easily be created and destroyed, they play an important role in both fundamental and applied physics. An area in which topological stability is important are spin configurations in magnetic materials. Magnetic domain walls are examples of planar, two-dimensional topological defects. Various types of magnetic whirls form one-dimensional topological structures, and hedgehogs, where the magnetization points in all directions, are examples of pointlike (zero-dimensional) defects. A major challenge in systems exhibiting topological stability is to experimentally observe the unwinding of topologically stable configurations and to identify its mechanism.

The recent discovery of skyrmion lattices in chiral magnets with B20 crystal structure (Fig. 1A) has attracted great interest, as it provides an example of lattice order composed of topologically

[1]Institut für Angewandte Photophysik, TU Dresden, D-01069 Dresden, Germany. [2]School of Materials Science and Engineering, University of New South Wales, Sydney NSW 2052, Australia. [3]Physik-Department E21, Technische Universität München, D-85748 Garching, Germany. [4]Forschungsneutronenquelle Heinz Maier-Leibnitz, Technische Universität München D-85747 Garching, Germany. [5]Institut für Theoretische Physik, Universität zu Köln, D-50937 Cologne, Germany.

*Corresponding author. E-mail: peter.milde@iapp.de

quantized magnetic whirls (*3*–*8*). A single skyrmion is a linelike structure oriented parallel to a small external magnetic field, where the magnetization winds once around the unit sphere in the plane perpendicular to the field. Skyrmion lattices are regular arrangements of skyrmion lines. They are ideally suited to explore the question of topological phase conversion experimentally. They occur in all B20 compounds with helimagnetic order comprising metallic, semiconducting, and insulating systems such as MnSi, $Fe_{1-x}Co_xSi$, and Cu_2OSeO_3, respectively. As the distance of skyrmions varies strongly among these systems, one may select compounds amenable to the experimental question of interest. In addition, skyrmion lattices in chiral magnets have been studied microscopically in great detail by means of neutron scattering (*3*, *4*, *8*) and transmission electron microscopy (TEM) (*5*, *6*, *9*, *10*). All properties, including the magnetic phase diagram, are in excellent agreement with theory, providing a sound basis for studies of the topological unwinding. Beyond these fundamental aspects, there is also great interest in skyrmions in chiral magnets as a new route toward spintronics applications (*9*, *11*, *12*).

The complex magnetic texture of skyrmions causes the electron spin to pick up a Berry phase, which allows for an efficient coupling of currents to the magnetic structure (*11*, *12*). This coupling may be elegantly described by associating to each skyrmion an artificial "emergent" magnetic field (*12*–*14*), which is, because of the topology of the skyrmion, quantized to one flux quantum per skyrmion. The corresponding forces on electrons can be observed directly in the Hall effect (*12*, *15*, *16*). As skyrmion lines have a one-to-one association with a quantized magnetic flux, their creation or destruction is naturally associated with quantized sources or sinks of emergent magnetic flux. These can be identified with "emergent magnetic monopoles." Quantized magnetic monopoles were originally introduced as a hypothetical particle by Dirac (*17*) to explain the quantization of electric charge. Whereas magnetic monopoles have so far not been found experimentally as elementary particles, the concept has been used to describe spin-flip excitations in so-called spin-ice (*18*, *19*).

Combining magnetic force microscopy (MFM), numerical calculations, and topological arguments, we study the transition of a skyrmion lattice in $Fe_{1-x}Co_xSi$ ($x = 0.5$) to conventional magnetic order. Our central result is that the skyrmions unwind by means of hedgehog point defects, which can directly be interpreted as emergent magnetic monopoles and antimonopoles. Figure 1B shows schematically how such a singular point defect merges two skyrmion lines like the slider of a zipper.

For our study, we selected $Fe_{1-x}Co_xSi$ ($x = 0.5$) because the periodicity of the magnetic modulations of ~90 nm for this composition is large as compared with the resolution of ~20 nm of the MFM (*20*). Figure 1, C and D, displays the phase diagram of $Fe_{1-x}Co_xSi$, inferred from magnetization, ac susceptibility, and small-angle neutron scattering in bulk samples (*4*, *20*). Under zero-field cooling (zfc) (Fig. 1C) helimagnetic order (h) appears below the critical temperature, $T_c \approx 45$ K, with a modulation vector parallel to ⟨100⟩. Well below T_c, the helimagnetic order undergoes a spin-flop transition to conical order (c) at $B_{c1} \sim 30$ mT with the modulation vector parallel to the magnetic field, followed by a transition to a spin-polarized state (fm) at $B_{c2} \sim 60$ mT. For temperatures T just below T_c, an additional phase (s) stabilizes, the skyrmion lattice.

Under field cooling (fc) (i.e., cooling while keeping the applied field constant), the phase diagram (Fig. 1D) exhibits several important differences with respect to zfc. First, for field values outside the range of the skyrmion lattice, there is only a paramagnetic to conical transition. Second, for field values in the range of the skyrmion lattice, the skyrmion lattice survives as a metastable state down to the lowest T with the same reversible phase boundaries near T_c as for zfc but irreversible phase boundaries well below T_c.

This metastable skyrmion lattice state made it possible to take measurements at $T << T_c$, which was helpful in two ways. First, as the magnetic moment increases considerably toward low T, the contrast of the MFM data increases substantially, providing unambiguous information. Second, the topological stability of skyrmions relies on the fact that the modulus of the local magnetization is finite everywhere. Close to T_c, strong thermal fluctuations may in principle weaken the topological stability, which is not the case for $T << T_c$, thereby exposing the generic mechanism of the topological unwinding.

Typical MFM data for decreasing applied fields after initial field cooling in +20 mT to 10 K are summarized in Fig. 2 [see (*20*) for details]. Each row is composed of the real-space image, an enlarged section of the same image, and a fast Fourier transform (FFT) (see bottom of Fig. 2 for scales). The MFM measurements reveal a hexagonally ordered pattern (Fig. 2, A1 and B1) with one of the reciprocal lattice vectors approximate-

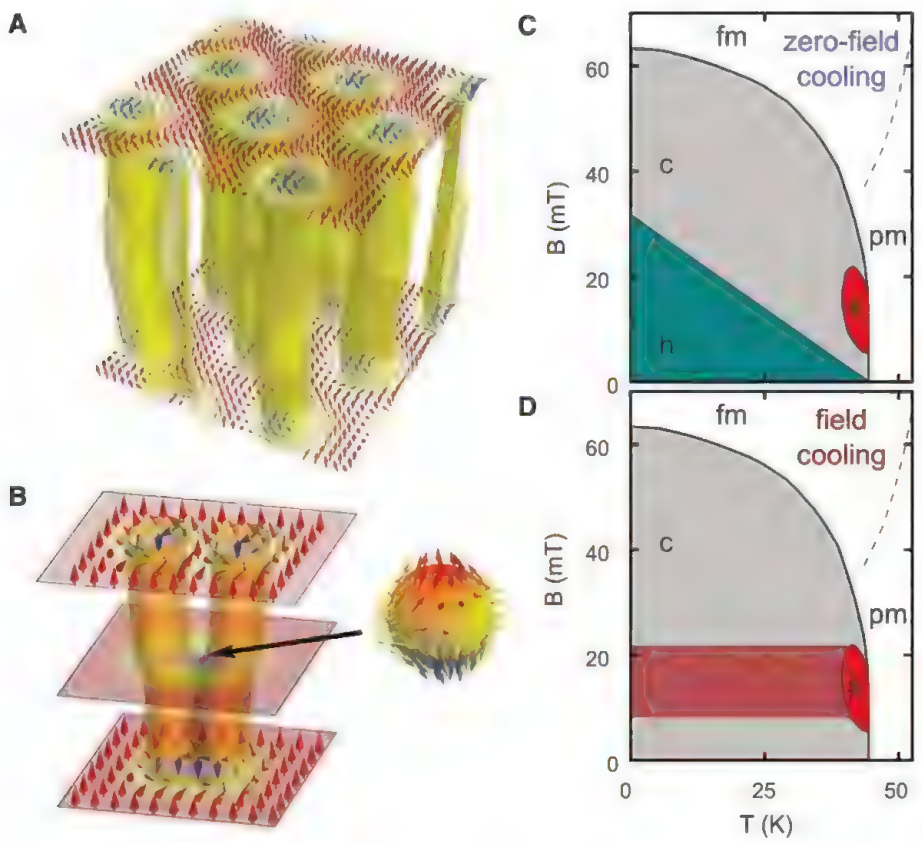

Fig. 1. Phase diagram of $Fe_{1-x}Co_xSi$ for $x = 0.5$ inferred from magnetization, susceptibility, and neutron scattering. The diagram comprises skyrmion-lattice (s), helimagnetic (h), conical (c), ferromagnetic (fm), and paramagnetic (pm) phases. (**A**) Typical spin configuration of a skyrmion lattice (from MC data). (**B**) Sketch of a magnetic configuration describing the merging of two skyrmions. At the merging point the magnetization vanishes at a singular point (arrow). This defect can be interpreted as an emergent magnetic antimonopole, which acts like the slider of a zipper connecting two skyrmion lines. (**C**) Phase diagram observed under zero-field cooling (zfc). The skyrmion lattice is confined to a small phase pocket (red) just below T_c. The field scale corresponds to the externally applied field for the geometry of the sample studied by MFM. (**D**) Phase diagram observed under field cooling (fc). For field values in the range of the skyrmion lattice as observed under zfc, the skyrmion lattice phase persists under field cooling as a metastable state down to the lowest T (red shading).

ly aligned along ⟨100⟩. Upon decreasing magnetic field, first at some places on the surface, two neighboring skyrmions, visible as blue dots, coalesce into one elongated pattern (Fig. 2, A2 and B2). Reducing the magnetic field causes the elongated structures to grow in length, reducing the number of skyrmions (Fig. 2, A3/B3 through A5/B5). Eventually a striped pattern forms with numerous defects, which is characteristic of a one-dimensional modulated state parallel to ⟨100⟩.

To confirm our observations, we performed the following tests (*20*). First, the time constant of the metastable state is long as compared with the time needed to record each image (17 min); e.g., Fig. 2, A3 changed little after a wait of 15 hours. Second, using small-angle neutron scattering, we confirmed that the intensity pattern of the magnetic order in the sample volume corresponds to the FFTs of the MFM data recorded at the sample surface [see (*20*) for details].

Our MFM data suggest a mechanism for the reduction in the number of skyrmions and therefore the topological winding number at the surface: Skyrmions coalesce and form linelike structures. Two immediate (and closely connected) questions arise: (i) How and to what extent does the change in the magnetic structure on the surface reflect similar processes in the bulk? (ii) How can the merging of skyrmions be understood from a microscopic and topological point of view? To answer these questions, we performed a classical Monte Carlo (MC) simulation of 42 × 42 × 30 spins coupled to their nearest neighbors by ferromagnetic exchange and Dzyaloshinksy-Moriya interactions. To track metastable behavior, we used a Metropolis algorithm based on local updates and also used micromagnetic simulations, including the effects of thermal fluctuations (*20*). The MC calculation reproduces the equilibrium phase diagram and captures the metastable behavior, consistent with the micromagnetic simulations and our experiments.

In our simulations, we followed a temperature and field protocol similar to that used in the experiments. First, we cooled the system at a fixed field crossing the skyrmion phase. Similar to experiment, the skyrmion phase survives down to the lowest temperatures. Second, at low temperature the field is reduced, permitting transverse thermal fluctuations of the skyrmion lines to grow until the skyrmions touch and merge. Snapshots of typical field configurations in the bulk are shown in Fig. 3A, where the pattern at the front of the simulated box shows marked similarities with the MFM data.

Figure 3B shows how, on average, the density of skyrmions, measured by the winding number W, is reduced. For $T = 0.6\ J \approx 0.65\ T_c$ [see (*20*) for other temperatures], a small density of skyrmions survives even at $B = 0$. During these sweeps, we did not obtain any field configurations typical for the conical phase (i.e., a phase with ordering vector parallel to the **B** field). Instead, we always obtained a strongly hysteretic transition to a helical phase driven by the merging of skyrmions, reminiscent of our experiments (other types of transition are, e.g., observed when increasing the field). Taken together, our numerical results therefore suggest that the structures seen in our MFM data reflect a similar transition in the bulk of the sample. However, a quantitative comparison of theory with experiment is beyond the scope of the work reported here, because the effects of disorder in $Fe_{1-x}Co_xSi$ cannot be recovered from our numerical simulation of a clean system.

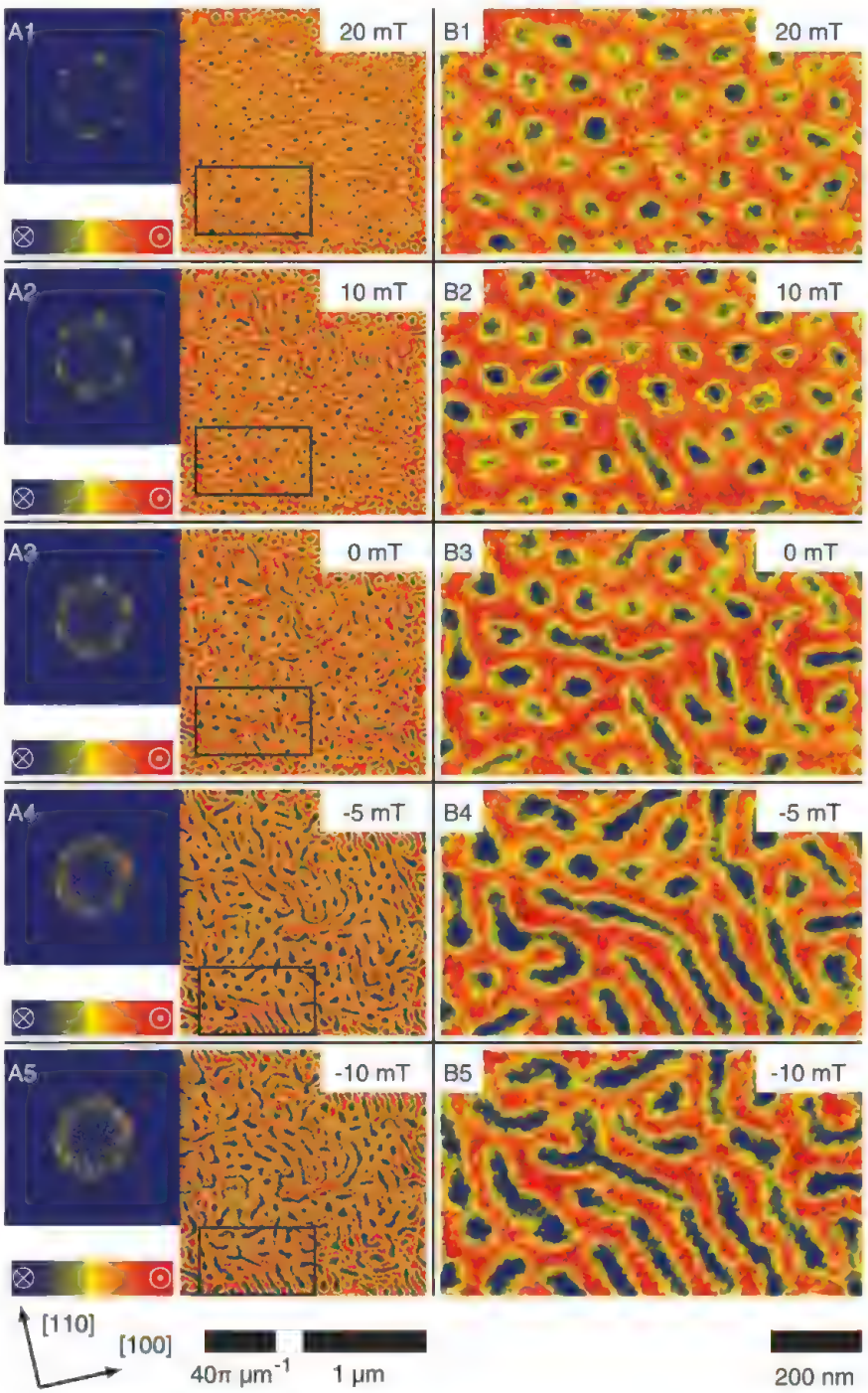

Fig. 2. Typical magnetic force microscopy data at the surface of $Fe_{1-x}Co_xSi$ (x = 0.5). Blue (red) colors correspond to a magnetization pointing parallel (antiparallel) to the line of sight into (out of) the surface, respectively. Panels (A1) through (A5): Data recorded as a function of magnetic field after fc at +20 mT down to T = 10 K. Panel (A1) displays data immediately after fc. After the initial cool-down, the field was reduced at a fixed temperature of 10 K (A2 to A5). During this process, the skyrmions, visible as blue spots, merge and form elongated, linelike structures. The left inset shows a Fourier transformation of the real-space signal. Panels (B1) to (B5) enlarge the region marked by the black rectangle in panels (A1) to (A5).

To appreciate the physics of the merging of the skyrmions observed experimentally and numerically, we note that both the topological nature of the skyrmions and their interaction with electrons are best described (*12*) in terms of the (fictitious) emergent electromagnetic fields (*13*, *14*, *21*)

$$\mathbf{B}_i^e = \frac{\hbar}{2}\varepsilon_{ijk}\hat{n}\cdot(\partial_j\hat{n}\times\partial_k\hat{n}),$$
$$\mathbf{E}_i^e = \hbar\hat{n}\cdot(\partial_i\hat{n}\times\partial_t\hat{n}) \quad (1)$$

where $\hat{n}(\mathbf{r},t) = \mathbf{M}/|\mathbf{M}|$ is the local orientation of the magnetization, $\partial_i = \partial/\partial r_i$ and ε_{ijk} is the totally antisymmetric tensor. Taken together $\mathbf{B}_i^e$ and $\mathbf{E}_i^e$ account for the Berry phase that the spin of a conduction electron accumulates when following the magnetic texture adiabatically. The experimental consequences have been detected directly in terms of an additional (topological) contribution to the Hall signal and an emergent electric field, providing evidence of the motion of the skyrmions (*12*, *15*, *16*).

As the integral of $\mathbf{B}^e/\hbar$ over a surface describes the solid angle covered by $\hat{n}$, the emergent magnetic flux of each skyrmion is exactly given by one (negative) flux quantum $\int\mathbf{B}^e d\sigma = -\frac{2\pi\hbar}{|q^e|} = -\Phi_0$ [we use a convention, where the conduction electrons of the majority (minority) bands carry the charge 1/2 (1/2), respectively (*12*)]. Therefore, the topologically quantized winding number or, equivalently, the quantized magnetic flux has to change when two skyrmions merge. Because of the topological nature of the winding number, this is in fact only possible by a singular field configuration for which the local magnetization vanishes at a point in space. The implications for the topological properties may thereby be seen by integrating $\mathbf{B}^e$ over a closed surface $\partial\Omega$ of the volume Ω

$$\oint_{\partial\Omega}\mathbf{B}^e d\sigma = \int_\Omega \nabla\mathbf{B}^e d\mathbf{r} = -\frac{2\pi}{|q^e|}(N^s_{\text{out}} - N^s_{\text{in}}) = \mp\Phi_0 \quad (2)$$

Here N^s_{out} (N^s_{in}) is the number of ingoing (outgoing) skyrmion lines, respectively. Hence, when two ingoing skyrmions merge, there must be a singular field configuration, a hedgehog defect with winding number +1, which creates one quantum of emergent magnetic flux. The point of coalescence therefore carries a quantized emergent magnetic charge; i.e., it is an "emergent magnetic monopole." Similarly, when an ingoing single skyrmion line splits into two, an antimonopole with winding number −1 is located at the point of separation. Figure 1B shows schematically such an antimonopole; the location of a monopole (MP) is marked by an arrow in Fig. 3A. Monopoles and antimonopoles are related by a time-reversal symmetry transformation, $\mathbf{M} \to -\mathbf{M}$, followed by a rotation by π around an axis perpendicular to the magnetic field.

The merging of skyrmions at the surface of the crystal observed in our MFM experiment implies that one of two processes has taken place. Either the merging of the skyrmion lines has started in the bulk and the antimonopole, which zipped two skyrmion lines together, has moved through the surface. Or, when the merging of two skyrmion lines started at the surface, a monopole has entered the surface. As the line segments can be interpreted as elongated skyrmions, also the merging of the segments implies that an antimonopole (monopole) has moved out of (into) the surface, respectively.

Both our experiments and our numerical calculations suggest that the merging of skyrmions underlies the conversion of the skyrmion phase into the helical phase. The change of topology is thereby governed by the creation and motion of topological point defects, which we identify as emergent magnetic monopoles and antimonopoles. Figure 3C shows the density of separate (*20*) monopoles and antimonopoles during the field sweep. A comparison of Fig. 3, B and C, shows that the destruction of skyrmions at the surface is directly associated with the proliferation of monopoles and antimonopoles [see also fig. S8]. We expect that the energy and dynamics of the monopoles govern the metastability (*4*, *22*) of the skyrmion phase. Because of their singular core, monopoles are expected to pin much stronger to impurities in the sample, an effect not taken into account in our simulations.

It is instructive to compare the emergent magnetic monopoles discussed here with the magnetic monopoles considered in spin ice (*18*, *19*). Monopoles in spin ice are sources of the "real" magnetic *H*-field, but their magnetic charge is not quantized and depends on microscopic details.

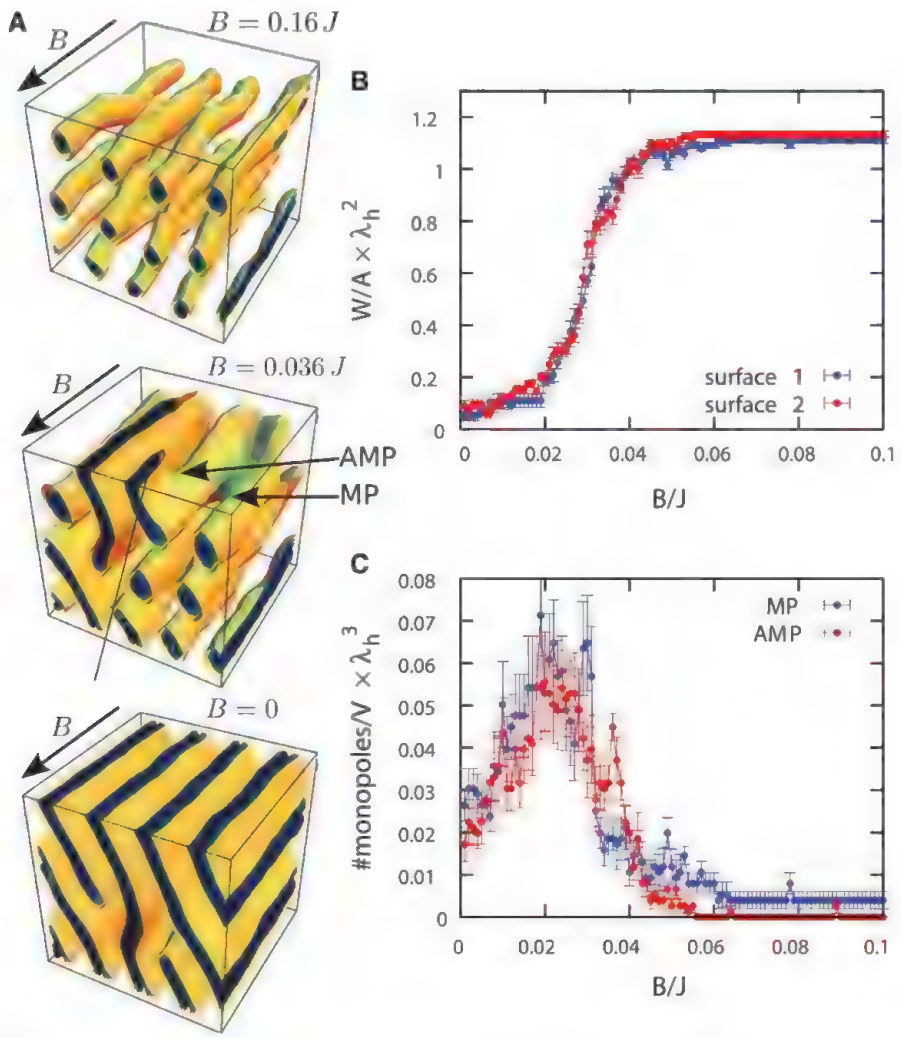

Fig. 3. Monte Carlo simulation for a system first field cooled at $B = 0.16\,J$ (B||[110]) down to $T = 0.6\,J$. [See (*20*) for other temperatures.] After the cool-down, the field is reduced at constant temperature. Below a critical field, skyrmions start to touch and merge. (**A**) Typical magnetic configurations shown by contour surfaces of equal magnetization in [110] direction for $B = 0.16\,J$, $B = 0.036\,J$, and $B = 0$. The arrows labeled MP and AMP point to a monopole and antimonopole, respectively. (**B**) Winding number W (or, equivalently, number of skyrmions) per area in units of the helical wavelength λ_h^2 on the front and back surface of the simulated box computed while B is reduced. (**C**) Number of monopoles (MP) and antimonopoles (AMP) per volume in units of λ_h^3. The plots show averages over 15 cooling cycles; error bars denote standard deviations of the mean.

By contrast, the emergent monopoles that we identify here are sources of the emergent magnetic field that follows Dirac's quantization condition for monopoles (*17*); i.e., they carry one quantum of emergent flux. Furthermore, in spin-ice at zero magnetic field, the monopoles are "deconfined"; i.e., it requires only a finite amount of energy to separate monopole and antimonopole. In the skyrmion phase, the situation is different (similar arguments apply to the helical phase): Deep in the skyrmion phase, it requires a finite amount of energy per length to zip two skyrmions together. Consequently, there is a linear potential (i.e., a finite string tension) holding monopole and antimonopole together. Only during the conversion from one phase to the other, the string tension vanishes or becomes negative. In disordered materials, the string tension may be a random function that competes with potentials pinning the monopoles.

An interesting open question is whether phases of deconfined emergent monopoles in chiral magnets exist, where monopoles and antimonopoles proliferate as independent entities. A candidate for such a phase is the metallic state of MnSi at high pressure. Its properties differ markedly from those of conventional metals [the resistivity is proportional to $T^{3/2}$ over almost three decades in T (*23*)], with highly unconventional "partial" magnetic order on intermediate time and length scales (*24*) and an unconventional Hall signature (*15*). Further experiments and theoretical studies are needed to study the connection of the partial order in MnSi with the emergent monopoles and the electronic properties in the non–Fermi liquid phase of MnSi.

References and Notes

1. P. Chaikin, T. Lubensky, *Principles of Condensed Matter Physics* (Cambridge Univ. Press, Cambridge, 1995).
2. N. Manton, P. Suttcliff, *Topological Solitons* (Cambridge Univ. Press, Cambridge, 2004).
3. S. Mühlbauer *et al.*, *Science* **323**, 915 (2009).
4. W. Münzer *et al.*, *Phys. Rev. B* **81**, 041203(R) (2010).
5. X. Z. Yu *et al.*, *Nature* **465**, 901 (2010).
6. X. Z. Yu *et al.*, *Nat. Mater.* **10**, 106 (2011).
7. S. Seki, X. Z. Yu, S. Ishiwata, Y. Tokura, *Science* **336**, 198 (2012).
8. T. Adams *et al.*, *Phys. Rev. Lett.* **108**, 237204 (2012).
9. X. Yu *et al.*, *Proc. Natl. Acad. Sci. U.S.A.* **109**, 8856 (2012).
10. A. Tonomura *et al.*, *Nano Lett.* **12**, 1673 (2012).
11. F. Jonietz *et al.*, *Science* **330**, 1648 (2010).
12. T. Schulz *et al.*, *Nat. Phys.* **8**, 301 (2012).
13. G. Volovik, *J. Phys. C Solid State Phys.* **20**, L83 (1987).
14. J. Zang, M. Mostovoy, J. H. Han, N. Nagaosa, *Phys. Rev. Lett.* **107**, 136804 (2011).
15. R. Ritz *et al.*, *Nature* **497**, 231 (2013).
16. A. Neubauer *et al.*, *Phys. Rev. Lett.* **102**, 186602 (2009).
17. P. A. M. Dirac, *Proc. R. Soc. Lond., A Contain. Pap. Math. Phys. Character* **133**, 60 (1931).
18. C. Castelnovo, R. Moessner, S. L. Sondhi, *Nature* **451**, 42 (2008).
19. D. J. P. Morris *et al.*, *Science* **326**, 411 (2009).
20. See supplementary materials on *Science* Online.
21. S. Zhang, S. S.-L. Zhang, *Phys. Rev. Lett.* **102**, 086601 (2009).
22. C. Pfleiderer *et al.*, *J. Phys. Condens. Matter* **22**, 164207 (2010).
23. C. Pfleiderer, S. R. Julian, G. G. Lonzarich, *Nature* **414**, 427 (2001).
24. C. Pfleiderer *et al.*, *Nature* **427**, 227 (2004).

Acknowledgments: We thank R. Bamler, P. Böni, K. Everschor, L. Fritz, M. Garst, R. Georgii, S. Mayr, and the team of FRM II, and, especially, D. Meier. We are grateful to B. Pedersen for checking the orientation of our sample on the diffractometer HEIDI at FRM II. Financial support through European Research Council AdG 291079 (TOPFIT) and through SFB 608, SFB TR 12, and SFB TR 80 of the Deutsche Forschungsgemeinschaft (DFG) is gratefully acknowledged. A.B. A.C., and J.K. acknowledge support through the TUM Graduate School, S.B. and C.S. through the Bonn-Cologne Graduate School of Physics and Astronomy (BCGS), D.K. through RTG 1401/2 (DFG), J.S. by the Australian Research Council through a Future Fellowship (FT110100523), and S.B. through the Emmy-Noether group (DFG) of L. Fritz.

Supplementary Materials

www.sciencemag.org/cgi/content/full/340/6136/1076/DC1
Materials and Methods
Supplementary Text
Figs. S1 to S8
References (*25*–*35*)

31 December 2012; accepted 19 April 2013
10.1126/science.1234657

Measurements of Energetic Particle Radiation in Transit to Mars on the Mars Science Laboratory

C. Zeitlin,[1]* D. M. Hassler,[1] F. A. Cucinotta,[2] B. Ehresmann,[1] R. F. Wimmer-Schweingruber,[3] D. E. Brinza,[4] S. Kang,[4] G. Weigle,[5] S. Böttcher,[3] E. Böhm,[3] S. Burmeister,[3] J. Guo,[2] J. Köhler,[3] C. Martin,[3] A. Posner,[6] S. Rafkin,[1] G. Reitz[7]

The Mars Science Laboratory spacecraft, containing the Curiosity rover, was launched to Mars on 26 November 2011, and for most of the 253-day, 560-million-kilometer cruise to Mars, the Radiation Assessment Detector made detailed measurements of the energetic particle radiation environment inside the spacecraft. These data provide insights into the radiation hazards that would be associated with a human mission to Mars. We report measurements of the radiation dose, dose equivalent, and linear energy transfer spectra. The dose equivalent for even the shortest round-trip with current propulsion systems and comparable shielding is found to be 0.66 ± 0.12 sievert.

Understanding the radiation environment inside a spacecraft carrying humans to Mars or other deep space destinations is critical for planning future crewed missions. Without major advances in propulsion systems, a large share of the radiation exposure on such missions will be incurred during outbound and return travel, when the spacecraft and its inhabitants will be exposed to the radiation environment in interplanetary space, shielded only by the spacecraft itself. Here we report measurements of the energetic particle radiation environment inside the Mars Science Laboratory (MSL) during its cruise to Mars between 6 December 2011 and 14 July 2012, with implications for future human Mars missions.

Two forms of radiation pose potential health risks to astronauts in deep space. There is a chronic low-dose exposure to galactic cosmic rays (GCRs), and there is also the possibility of short-term exposures to the solar energetic particles (SEPs) that are sporadically accelerated close to the Sun by solar flares and coronal mass ejections. GCRs tend to be highly energetic, highly penetrating particles that are not stopped by the modest depths of shielding on a typical spacecraft. The distributions of the kinetic energy of GCRs are broad and vary according to the ion species and the phase of the solar cycle, with peaks near 1000 MeV for protons and 500 to 600 MeV per nucleon for heavier ions, with tails extending to much higher energies. The flux of GCRs consists of about 85% protons, which are sparsely ionizing (except at the very end of their ranges), and about 14% helium ions. The remainder of the flux consists of heavier ions referred to as "HZE particles" [high (H) atomic number (Z) and high energy (E)]. HZE particles are densely ionizing, producing biological effects that differ from those produced by sparsely ionizing radiation; there is considerable uncertainty about the effects of HZE particles on biological systems (*1*, *2*).

The SEPs of concern for astronaut safety are typically protons with kinetic energies up to a few hundred mega–electron volts. SEP events can produce very large fluxes of these particles, as well as helium and heavier ions. With the exceptions of extreme and rare SEP events, there is little enhanced flux at the higher energies (above 100 MeV per nucleon) typical of GCRs. The comparatively low energy of typical SEPs means that shielding is much more effective against SEPs than GCRs.

Conventional risk assessment methods (*1*, *3*–*5*) rely on measured distributions of kinetic energy

[1]Southwest Research Institute, Boulder, CO, USA. [2]NASA Johnson Space Center, Houston, TX, USA. [3]Christian Albrechts University, Kiel, Germany. [4]Jet Propulsion Laboratory, California Institute of Technology, Pasadena, CA, USA. [5]Southwest Research Institute, San Antonio, TX, USA. [6]NASA Headquarters, Washington, DC, USA. [7]German Aerospace Center (DLR), Cologne, Germany.
*Corresponding author. E-mail: zeitlin@boulder.swri.edu

or linear energy transfer (LET) in water (in units of kilo–electron volts per micrometer). These spectra are integrated against the quality factors (Q's) to obtain the dose equivalent (H) as defined by the International Commission on Radiological Protection (*6*). The dose equivalent is measured in sieverts (Sv) and has been related to lifetime cancer risk via long-term population studies (*7*). Additional details can be found in the supplementary materials.

The Curiosity rover, with the Radiation Assessment Detector (RAD) mounted to its top deck, was inside the MSL spacecraft on its trip to Mars, sitting immediately beneath the Descent Stage and above the heat shield. Because the spacecraft and internal structures provided shielding against the deep space radiation environment, the RAD measured a mix of primary and secondary particles. (Secondary particles are those produced by nuclear or electromagnetic interactions of primary ions as they traverse the spacecraft mass.) A simplified model of the mass around the RAD was created at the Jet Propulsion Laboratory, working from a highly detailed model of the spacecraft (*8*). Shielding around the instrument was complex, with most of the solid angle lightly shielded (areal density <10 g/cm^2) and the remainder broadly distributed over a range of depths up to about 80 g/ cm^2. The greatest depths correspond to trajectories through a fuel tank filled with hydrazine. Shielding distributions on the International Space Station are similarly complex (*9*). In contrast, the Apollo spacecraft were lightly shielded, averaging 4.5 g/cm^2 of aluminum (*10*). A human crew on a Mars mission would, like the RAD, be exposed to a mixture of primary and secondary radiation, but details of the shielding distribution would probably be quite different. In particular, a spacecraft carrying humans would probably be designed to have a more homogeneous mass distribution, with few if any light-shielded paths into the inhabited areas.

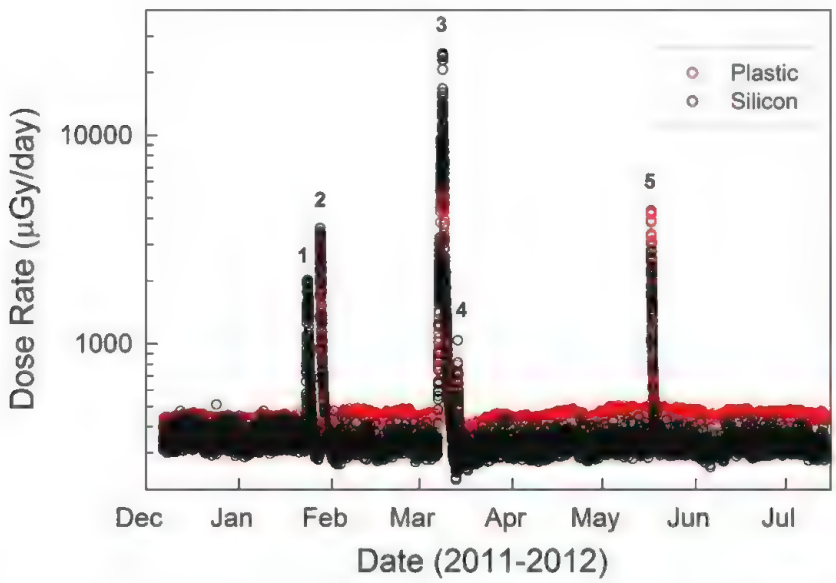

Fig. 1. Dose rates recorded in a silicon detector (black circles) and in a plastic scintillator (red circles) during the MSL's cruise to Mars. The observed SEP events are indicated by numerals. The data have been averaged over 15.5-min intervals. Occasional brief gaps can be seen, usually caused by the RAD having been powered off so that other activities could take place on the spacecraft without interference. For a given incident flux, the dose rate in silicon is generally less than the dose rate in plastic because of the comparatively large ionization potential of silicon.

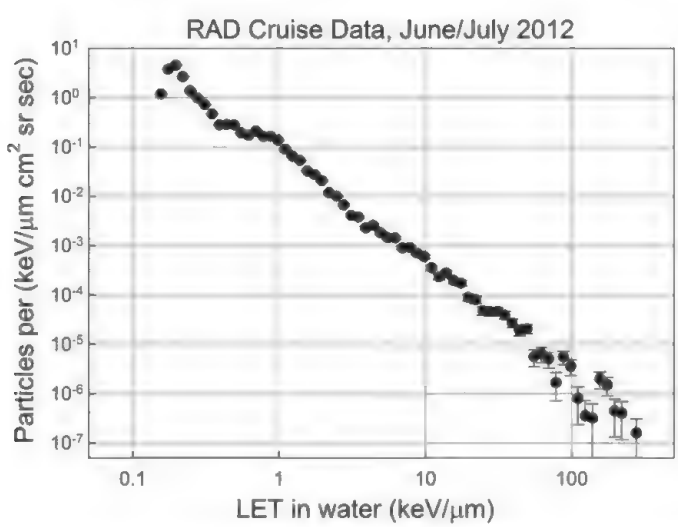

Fig. 2. The LET spectrum in water measured using charged particle coincidence events. Energy deposited in silicon has been converted to LET_∞ in water. Below about 50 keV/μm, the plotting symbols are larger than the error bars.

The RAD instrument has been described in detail in the literature (*11*, *12*). A brief overview is given in the supplementary materials. Two concurrent measurements of dose are made, one using a silicon detector and the other using a plastic scintillator. The latter has a composition similar to that of human tissue, and it is also more sensitive to neutrons than are the silicon detectors. The two dose-rate measurements obtained during the cruise are shown in Fig. 1 (*13*). These measurements differ from previously reported data in that they were obtained in deep space under complex shielding, whereas particle detectors in other deep space missions have measured the unshielded radiation environment.

Measurements were taken from 6 December 2011 to 14 July 2012 (*14*). For solar quiet times, the GCR dose rate in silicon averaged 332 ± 23 μGy/day after subtraction of the background from Curiosity's radioisotope thermoelectric generator (*13*). The error on this result is dominated by uncertainty in the calibration of the silicon detector. To compare with the measured dose rate in plastic and with model predictions, the dose rate in silicon can be converted, approximately, to dose rate in water. A constant factor was applied to relate energy lost per unit of path length (dE/dx) in silicon to LET in water (*15*). After conversion, the dose rate in water as measured in the silicon detector was found to be 481 ± 80 μGy/day, which is identical within uncertainties to the 461 ± 92 μGy/day measured in the plastic scintillator.

We used data from the final month of the cruise (a time period during which no SEP events were observed) to obtain the charged-particle LET distribution for GCR primary particles and GCR-induced secondary particles. We used the resulting spectrum, after conversion of the deposited energy in silicon to LET in water (Fig. 2), to obtain the average quality factor $\langle Q \rangle$, which was found to be 3.82 ± 0.25. The uncertainty on $\langle Q \rangle$ is approximately equal parts statistical (low count rate at high LET) and systematic (calibration, conversion from silicon to tissue, and subtraction of the radioisotope thermoelectric generator background radiation). Combining the tissue dose rate measurement with $\langle Q \rangle$ yields a GCR dose equivalent rate of 1.84 ± 0.33 mSv/day. It is important to

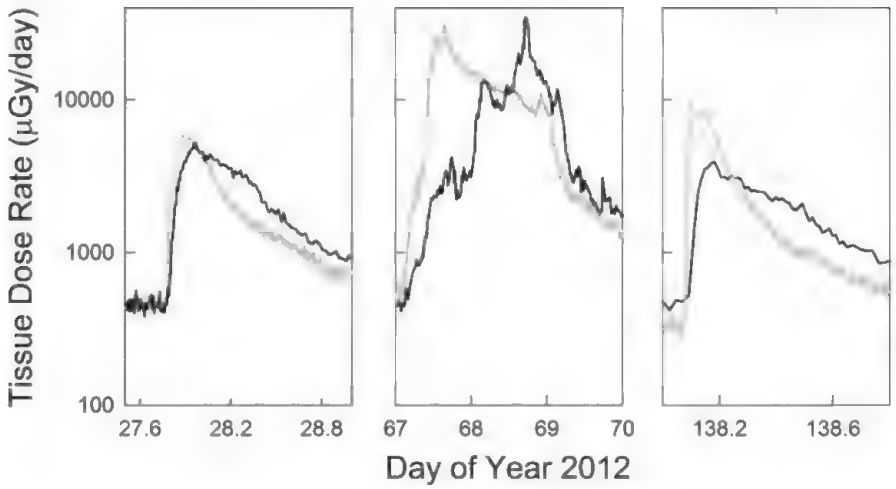

Fig. 3. RAD dose rates as measured by the B detector (black lines) and GOES-11 proton data (gray lines) for three solar events observed during the cruise. The GOES-11 P7 channel measures protons in the energy range from 165 to 500 MeV; those data have been arbitrarily scaled so that they have approximately the same quiet-time level as the RAD data.

note that the measurements depended strongly on heliospheric conditions during the cruise (i.e., near solar maximum), and on the shielding that surrounded the RAD.

Five SEP events were observed during the cruise to Mars: two from 23 to 29 January, two from 7 to 15 March, and one on 17 May (Fig. 2). The events during 7 to 11 March were the largest in terms of dose, but the May event is of interest as well because it was a ground-level event at Earth, and the RAD data indicate that the spectrum was relatively hard. For this event, unlike the other four SEP events, the dose rate recorded in the plastic scintillator exceeded that recorded in the silicon detectors, even though the plastic scintillator is more shielded than the silicon detectors (*16*).

We compare RAD SEP event data to data from the Geostationary Operational Environmental Satellite (*17*–*20*) GOES-11 in Fig. 3. These comparisons may provide useful tests of models of SEP propagation through the inner heliosphere. In all cases, the dose rate peaks in the RAD data occur at later times than the flux peaks in the GOES data. The 7 to 9 March SEP event had three distinct peaks seen by the RAD on 8 and 9 March. The MSL and Earth were nominally connected on the same Parker spiral line (*21*) at this time, and the MSL was only about 1.2 astronomical units from the Sun, but particles arrived at the MSL nearly a full day later than they were seen near Earth. A possible reason for this delay is that GOES-P7 and the RAD are sensitive to different parts of the initial SEP spectrum, which may behave quite differently over time during an event. In addition, there were at least two events [flares and fast coronal mass ejections (CMEs)] seen in the 7 to 9 March time frame. The first one, on 7 March 0036 UT, was directed at −60° longitude (east of the central meridian as viewed from Earth) and the second on 9 March 0425 UT at 0° longitude (directly at Earth). The differences in arrival times may have been caused by a disturbed Parker spiral from the first CME, so it is possible that the MSL and Earth (GOES) were not actually on or near the same field line during the event.

The SEP fluxes observed by the RAD are dominantly protons, for which $Q(L)$ (L, linear energy transfer) is approximately 1. Dose and dose equivalent rates are therefore approximately equal. Table 1 shows the dose equivalent totals recorded during the three periods of measurable solar activity. SEP doses were obtained by subtracting average GCR dose rates from the total for the days shown. The SEP total from these five events is roughly equal to 15 days of GCR dose equivalent during low solar activity.

The MSL's cruise to Mars took 253 days. Treating the measured GCR dose equivalent rate of 1.84 mSv/day as constant during the entire cruise, the estimated total dose equivalent from both GCR and SEP events is 466 ± 84 mSv, with about 5.4% attributable to SEPs. This result is a strong function both of the time in the solar cycle during which the cruise occurred and of the shielding surrounding the RAD during the cruise. The crew exposures during a human mission to (and returning from) Mars would no doubt differ from our findings because of these effects. Actual exposures will of course depend on the details of the habitat shielding and the unpredictable nature of large SEP events. Even so, our results are representative of a trip to Mars under conditions of low to moderate solar activity.

Comparisons between the measured and calculated dose and dose equivalent rates are not sufficient to fully validate or benchmark transport models, but they are highly relevant here because astronaut exposure calculations are made with transport models. It is therefore essential that such models be as accurate as possible, and accuracy is obtained through an iterative process of model development and comparisons with data. Agreement with measured dose or dose equivalent rates is a necessary part of model validation. Although there has been considerable previous work in this area, including recent articles by Schwadron *et al.* (*22*) and McKenna-Lawlor *et al.* (*23*), for present purposes we restrict the discussion to the models used most recently by the NASA Johnson Space Center (JSC), which is responsible for assessing crew exposures (*24*, *25*). The tools used by JSC include the Badhwar-O'Neill GCR model (*26*, *27*), the HZETRN transport model (*28*–*30*), and pion transport codes (*31*–*33*). See the supplementary materials for details.

Table 1. Dose equivalents measured during SEP events.

Time period (2012)	Integrated dose equivalent (mSv)
23 to 29 January	4.0
7 to 15 March	19.5
17 to 18 May	1.2
Cruise SEP Total	24.7

Four transport calculations are shown in Table 2, corresponding to permutations of the JSC model (two versions of the GCR flux model, with pion production simulated or not). These are point values at the RAD position. In all cases, dose and dose equivalent were calculated at several depths of shielding, and polynomials were fit piecewise. The polynomials were integrated against the shielding distribution to obtain the results shown here. It is clear that pions and their decay products make an important difference in the calculated dose under shielding, whereas their contribution to dose equivalent is relatively small, owing to the low LET of the particles. The RAD cruise measurements are shown in the last row of Table 2. For dose rate, the Badhwar-O'Neill 1996 (BO-96) results with and without pions bracket the central value of the measurement, both falling within the range of experimental uncertainty. The dose rate predicted by BO-11 with pions included is close to the central value of the data, whereas BO-11 without pions gives a result outside the 1σ error bar. Predicted dose equivalent rates are comparatively insensitive to these model variations, and all are slightly smaller than the measurement but within the 1σ error on the data. The calculated $\langle Q \rangle$ values are more sensitive to variations in the model than are the dose equivalent rates, and only the BO-96 model without pions and the BO-11 model with pions give values that are within the 1σ experimental uncertainty.

Some of the dose and dose equivalent from GCRs during the cruise is attributable to neutral particles (neutrons and γ rays). A full analysis of these contributions requires the application of an inversion technique (*34*), but a simplified first-order estimate shows that the measured neutral particle contribution was less than 10% of the total.

Table 2. Measured and calculated GCR dose and dose equivalent rates.

GCR flux model	Pions/included in transport	Dose rate (μGy/day)	Dose equivalent rate (mSv/day)	<*Q*>
Badhwar-O'Neill 1996	No	0.429	1.69	3.95
	Yes	0.507	1.70	3.53
Badhwar-O'Neill 2011	No	0.366	1.72	4.69
	Yes	0.445	1.80	4.05
RAD measurement		0.481 ± 0.080	1.84 ± 0.33	3.82 ± 0.25

Several space agencies (the Russian Space Agency, European Space Agency, and Canadian Space Agency) have adopted the conventional risk assessment approach outlined above, using 1 Sv as the astronaut career exposure limit. Because of the large biological uncertainties for HZE particles, NASA has proposed a different approach, defining *Q*'s in terms of Z and E, and estimates an uncertainty distribution for the *Q* for different particle types (*24*). This approach defines astronaut career limits that correspond to a 3% risk of exposure-induced death for cancer and protects against uncertainties in models using the upper 95% confidence interval. Central estimates of dose limits for 30- to 60-year-old never-smokers range from 600 to 1000 mSv and 800 to 1200 mSv for females and males, respectively (*35*). Dose limits at the 95% confidence levels are about one-third the central values.

NASA's "Design Reference" Mars mission (*36*) posits various cruise durations, with a typical figure of about 180 days. The MSL's cruise was longer than this, but with a human crew aboard, it is likely that faster transits would be selected. Assuming a 180-day one-way duration, similar shielding, and a similar time in the solar cycle, we would expect a crew to receive 331 ± 54 mSv from GCRs, with additional (variable) contributions from SEP events. The return trip would double this, to 662 ± 108 mSv in total. It is clear that the exposure from the cruise phases alone is a large fraction of (and in some cases greater than) currently accepted astronaut career limits. Time spent on the surface of Mars might add considerably to the total dose equivalent, depending on shielding conditions and the duration of the stay. This is problematic for both central estimates of cancer risks and NASA's uncertainty analysis, which imposes a safety factor until confidence intervals are significantly narrowed. In this context, the data provided by the RAD experiment contribute to the reduction of uncertainties by facilitating the improvement of transport models.

The models used by NASA predict that the GCR dose rate is a very weak function of shielding depth (up to 100 g/cm^2 of aluminum) because of the high energies of the ions and the copious production of secondary particles. The dose equivalent shows more sensitivity to shielding depth, due to the increasing fraction of heavy ions that fragment as depth increases. Given that the shielding provided by the MSL spacecraft is probably not drastically different from that of the Crew Exploration Vehicle (CEV) or other future vehicles, at least in an average sense, and the modest attenuation of GCR dose with increasing shielding depths, the GCR dose and dose equivalent rates reported here are probably realistic for the expected exposures during future human deep space missions of similar duration. Although only 5% of the contribution to the measured dose equivalent during the MSL's cruise to Mars was from SEP events, it should be remembered that the frequency and intensity of such events are highly variable and that the current cycle appears to be producing a very weak solar maximum (*37*). The SEP contribution could conceivably be many times larger in a different time frame.

References and Notes

1. *Radiation Hazards to Crews on Interplanetary Missions* (National Academy Press, Washington, DC, 1996).
2. F. A. Cucinotta, M. Durante, *Lancet Oncol.* **7**, 431 (2006).
3. *Quantities and Units in Radiation Protection Dosimetry* (ICRU Report 51, International Commission on Radiation Units and Measurements, Bethesda, MD, 1993).
4. *Recommendations of Dose Limits for Low Earth Orbit* (NCRP Report No. 132, National Council on Radiation Protection and Measurements, Bethesda, MD, 2000).
5. *Information Needed to Make Radiation Protection Recommendations for Space Missions Beyond Low-Earth Orbit* (NCRP Report No. 153, National Council on Radiation Protection and Measurements, Bethesda, MD, 2006).
6. International Commission on Radiological Protection, *Ann. ICRP* **21**, 1 (1991).
7. *Health Risks From Exposure to Low Levels of Ionizing Radiation, BEIR VII Phase 2* (National Academies Press, Washington, DC, 2006).
8. The full spacecraft model contains thousands of components, hence the need for simplification. At present, only a subset of materials within the charged particle telescope's field of view is included in the shielding model, the current state of which is described in the supplementary materials.
9. S. L. Koontz, P. A. Boeder, C. Pankop, B. Reddell, "The ionizing radiation environment on the International Space Station: Performance vs. expectations for avionics and materials," in *Radiation Effects Data Workshop, 2005* (IEEE, 2005), pp. 110–116.
10. J. W. Wilson *et al.*, *Galactic and Solar Cosmic Ray Shielding in Deep Space* (NASA Technical Paper No. 3682, NASA, Hampton, VA, 1997).
11. D. M. Hassler *et al.*, *Space Sci. Rev.* **170**, 503 (2012).
12. A. Posner *et al.*, *Adv. Space Res.* **36**, 1426 (2005).
13. Dose rates as measured by the RAD include particles originating from the MSL's power supply, a radioisotope thermoelectric generator that emits a steady background of neutrons and γ rays. These contributions were measured during ground tests and were subtracted from the results presented here. More details about the background subtraction are given in the supplementary materials.
14. Before 27 January 2012, the RAD observed with a 465-s cadence and nearly 100% duty cycle. Subsequently, RAD observations were 929 s in duration, with a 50% duty cycle, reducing the data volume by a factor of 4 to accommodate steadily decreasing telemetry bandwidth. At the same time as the observing cadence was changed, the sensitivity of the plastic scintillator was increased, resulting in a slightly higher value of the GCR dose rate measured by that detector (~10%, visible in Fig. 1).
15. Simulations indicate that the average value of the ratio *dE/dx* in silicon and LET in water is 1.6 for GCRs, with an associated uncertainty of ±15%. Proper calculation of the range of this ratio must account for the effects of straggling, which is a significant factor in thin silicon detectors such as those in the RAD. The LET conversion factor in turn yields a dose conversion factor of 1.45.
16. The spacecraft shielding was equal for both detectors, but the plastic scintillator is additionally shielded by 1.2 cm of plastic scintillator below and on the sides and 2.8 cm of cesium iodide on top. Proton energies required to penetrate these materials are about 35 and 95 MeV, respectively, as compared to about 10 MeV required for a particle in the telescope field of view to reach the silicon detector used for dosimetry.
17. T. Onsager *et al.*, "Operational uses of the GOES energetic particle detectors," in *Proceedings of SPIE 2812, GOES-8 and Beyond* (SPIE, Bellingham, WA 1996), p. 281.
18. The P7 channel measures the proton flux between 165 and 500 MeV. It was chosen for comparison because the reported ratio of peak flux to quiet-time flux was similar to the ratio of peak dose rate to quiet-time dose rate seen in the RAD in the 27 January event. This comparison is not intended to suggest that the P7 channel and the RAD (under shielding) had similar sensitivities in terms of their energy thresholds or ranges.
19. The use of the quiet-time flux of GOES differential proton flux channels is problematic, especially for the higher-energy channels. The differential fluxes are obtained by subtracting fluxes measured in the various integral channels. As there are by definition no negative fluxes, the algorithm used to obtain differential fluxes assumes a background level that cannot be crossed, as discussed in (*20*). Despite this caveat, the dearth of higher-energy proton data from other spacecraft sources led us to arbitrarily scale the GOES data for comparison to the RAD data.
20. A. Posner, *Space Weather* **5**, S05001 (2007).
21. E. N. Parker, *Astrophys. J.* **128**, 664 (1958).
22. N. Schwadron *et al.*, *Space Weather* **8**, S00E04 (2010).
23. S. McKenna-Lawlor, P. Gonçalves, A. Keating, G. Reitz, D. Matthiä, *Planet. Space Sci.* **63-64**, 123 (2012).
24. F. A. Cucinotta, L. Chappell, M. Y. Kim, *Space Radiation Cancer Risk Projections and Uncertainties–2010* [NASA Technical Paper 2011-216155, NASA Scientific and Technical Information (STI) Program, Hampton, VA, 2011].
25. F. A. Cucinotta, L. Chappell, M. Y. Kim, *Space Radiation Cancer Risk Projections and Uncertainties–2012* (NASA Technical Paper 2013-217375, NASA STI Program, Hampton, VA, 2013).
26. G. D. Badhwar, P. M. O'Neill, *Nucl. Tracks Radiat. Meas.* **20**, 403 (1992).
27. P. M. O'Neill, *IEEE Trans. Nucl. Sci.* **57**, 3148 (2010).
28. J. W. Wilson *et al.*, *HZETRN: Description of a Free-Space Ion and Nucleon Transport and Shielding Computer Program* (NASA Technical Paper 3495, NASA STI Program, Hampton, VA, 1995).
29. F. A. Cucinotta *et al.*, *Radiat. Meas.* **41**, 1235 (2006).
30. T. Slaba, S. R. Blattnig, F. F. Badavi, *J. Comput. Phys.* **229**, 9397 (2010).
31. T. Sato, A. Endo, L. Sihver, K. Niita, *Radiat. Environ. Biophys.* **50**, 115 (2011).
32. S. K. Aghara, S. R. Blattnig, J. W. Norbury, R. C. Singleterry, *Nucl. Instrum. Methods* **B264**, 1115 (2009).
33. R. B. Norman, S. R. Blattnig, G. De Angelis, F. F. Badavi, J. W. Norbury, *Adv. Space Res.* **50**, 146 (2012).
34. J. Köhler *et al.*, *Nucl. Instrum. Methods* **B269**, 2641 (2011).
35. F. A. Cucinotta, L. J. Chappell, *Radiat. Res.* **176**, 102 (2011).
36. B. G. Drake, S. J. Hoffman, D. W. Beatty, "Human exploration of Mars, Design Reference Architecture 5.0," in *Aerospace Conference, 2010 IEEE* (IEEE, 2010), pp. 1–24.

37. For 2012, the average modulation potential derived from the Earth-based Oulu neutron monitor (*38*) was less than 700 MV, as compared to values of 1000 MV or greater seen in previous solar maximum periods. The full range of the modulation potential (Φ) during the cruise as measured by the Oulu neutron monitor is available at http://cosmicrays.oulu.fi/phi/Phi_mon.txt.
38. I. G. Usoskin, K. Alanko-Huotari, G. A. Kovaltsov, K. Mursula, *J. Geophys. Res.* **110**, A12108 (2005).
39. A. I. Mrigakshi, D. Matthiä, T. Berger, G. Reitz, R. F. Wimmer-Schweingruber, *J. Geophys. Res.* **117**, A08109 (2012).

Acknowledgments: The RAD is supported by NASA (Human Exploration and Operations Mission Directorate) under Jet Propulsion Laboratory (JPL) subcontract 1273039 to the Southwest Research Institute and in Germany by the German Aerospace Center (DLR) and DLR's Space Administration, grant numbers 50QM0501 and 50 QM1201, to the Christian Albrechts University, Kiel. Part of this research was carried out at JPL, California Institute of Technology, under a contact with NASA. We appreciate discussions with P. O'Neill and M. Kim at NASA's JSC and with S. Blattnig, F. Badavi, T. Slaba, and C. Mertens of NASA's Langley Research Center. We extend thanks to J. Simmonds, J. Grotzinger, J. Crisp, A. Vasvada, H. Mortensen, and the Operations Product Generation Subsystem team at NASA-JPL. We also thank M. Meyer, E. Stolper, G. Allen, C. Moore, and V. Friedensen at NASA headquarters and H. Witte at DLR in Germany for their support of the RAD over the years. The data used in this paper are archived in the NASA Planetary Data System's Planetary Plasma Interactions Node at the University of California, Los Angeles. The archival volume includes the full binary raw data files, detailed descriptions of the structures therein, and higher-level data products in human-readable form. The PPI node is hosted at http://ppi.pds.nasa.gov/.

Supplementary Materials

www.sciencemag.org/cgi/content/full/340/6136/1080/DC1
Materials and Methods
Supplementary Text
Figs. S1 to S3
References (*40, 41*)

1 February 2013; accepted 12 April 2013
10.1126/science.1235989

An Adaptive Response to Uncertainty Generates Positive and Negative Contrast Effects

John M. McNamara,[1] Tim W. Fawcett,[2]* Alasdair I. Houston[2]

Successive contrast effects, in which behavior is dependent on whether conditions are currently better or worse than they were before, are a striking illustration of the fact that animals evaluate the world in relative terms. Existing explanations for these effects are based on descriptive models of psychological and physiological processes, but little attention has been paid to the factors promoting their evolution. Using a simple and general optimality model, we show that contrast effects can result from an adaptive response to uncertainty in a changing, unpredictable world. A wide range of patterns of environmental change will select for sensitivity to past conditions, generating positive and negative contrast effects. Our analysis reveals the importance of incorporating uncertainty and environmental stochasticity into models of adaptive behavior.

Humans, like many other animals, make relative judgments about the world. When making decisions, we compare options to other available options (*1–3*) or to situations that we have experienced in the past (*4*). We care about whether we are better or worse off than before, or than we might otherwise be, had things turned out differently (*5*, *6*).

A striking illustration of this is successive contrast effects, in which the conditions an individual has experienced in the recent past alter its response to current conditions (*4*). Crespi (*7*) demonstrated successive contrast effects in laboratory rats trained to approach a food reward at the end of a runway apparatus. The rats ran faster toward the reward if they had previously been trained with smaller reward amounts, as compared to control rats that had experienced the current, larger amount throughout the experiment—a positive contrast effect (*8*). Conversely, rats previously trained with an even larger reward showed a slower approach speed than controls when shifted to the same reward amount (*7*)—a negative contrast effect (*8*). Similar effects have been found in bees (*9*), starlings (*10*), and a variety of mammals (*11–14*), including humans.

Successive contrast effects pose a serious challenge to accounts of rational choice in which past states or alternative current states are irrelevant (*6*). So far, all theories to explain the existence of contrast effects have been based on descriptive models of psychological or physiological processes (*4*, *7*, *15–18*), largely ignoring their evolutionary basis [though see (*10*)]. Here we address this gap, by developing a simple and general optimality model to show that both positive and negative successive contrast effects can arise from an adaptive response to uncertainty about how conditions change over time.

We consider the behavior of an animal that has to perform work to gain rewards. If the animal expends effort u it gains rewards at rate γu, where γ represents the profitability of the reward source. To reflect the physiological costs of work (*19*) or risks of exposure to predators (*20*), we assume that the animal's mortality rate, $M(u)$, is an increasing, accelerating function of effort. This imposes a trade-off, for which there is some unique level of effort that maximizes the animal's expected lifetime reward (*21*).

In the scenario we consider, the profitability of the reward source fluctuates stochastically over time. The animal can perceive its current profitability γ but does not know when this will change. While still alive, we assume that it pays some small maintenance costs (b energy units per unit of time) and invests all remaining gains directly into reproduction, so its rate of reproductive success is $\gamma u - b$. Under these conditions, to maximize its fitness (expected lifetime reproductive output), the animal must maximize $\gamma u - M(u)V$, where u is its current effort and V its expected future reproductive success (*22*). Broadly, we can interpret γ as the value of work and V as the value of the animal's life (*21*). Differentiating this expression with respect to u, we see that the optimal effort, u^*, that maximizes fitness will satisfy $M'(u^*) = \gamma/V$. Because M is an increasing,

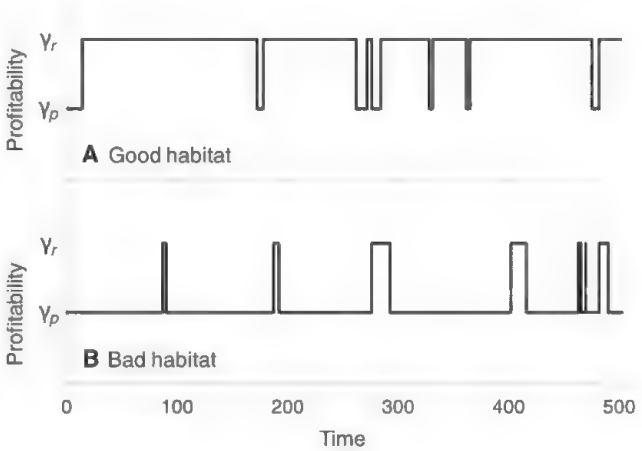

Fig. 1. Examples of the stochastic fluctuations in the profitability of a reward source over time in a (A) good or (B) bad habitat. The animal can perceive whether the source is currently rich (profitability γ_r) or poor (γ_p) but does not know when the next switch will occur, nor which habitat it is in. Parameters: $t_{Gr} = 100$, $t_{Gp} = 10$, $t_{Br} = 10$, $t_{Bp} = 100$.

[1]School of Mathematics, University of Bristol, University Walk, Bristol BS8 1TW, UK. [2]School of Biological Sciences, University of Bristol, Woodland Road, Bristol BS8 1UG, UK.
*Corresponding author. E-mail: tim.fawcett@cantab.net

accelerating function of u, this implies that u^* increases with γ and decreases with V.

The dependence of optimal current behavior (u^*) on future expectations (V) is well established (*23*), but the importance of past conditions has been largely overlooked. In most natural environments, conditions are in some way correlated over time, so the animal's future expectations are influenced by its previous experiences. If it has experienced a sustained period of rich rewards in the recent past, future conditions will tend to be favorable, and therefore its future expectations are high relative to the current value of work. Conversely, if its past experiences have been poor, future conditions are more likely to be unfavorable, and its future expectations are low. So for two animals currently experiencing the same profitability γ, the one that has previously experienced a poor situation has a lower V and therefore should work harder. This represents a successive contrast effect and arises from an optimal response to uncertainty about the pattern of environmental change.

To investigate the factors affecting the magnitude of contrast effects, we consider a specific example in which the animal is living in one of two possible habitats, good (G) or bad (B), but does not know which. The probability that the habitat is good is ρ. This is equivalent to assuming that the animal has evolved in a spatially heterogeneous world in which a fraction ρ of habitats are good and the remainder are bad, and offspring disperse randomly across habitats (*24*). In both habitat types, the environment fluctuates stochastically between rich (r) and poor (p) conditions, yielding gain rates $\gamma_r u$ and $\gamma_p u$ respectively (where $\gamma_r > \gamma_p$). Changes from rich to poor conditions and vice versa occur at constant rates, which differ between the two habitats (Fig. 1). In good habitats, periods of rich conditions last for a mean time t_{Gr}, whereas poor periods last for a mean time t_{Gp}; the corresponding mean times in bad habitats are t_{Br} and t_{Bp}. Conditions are rich more often and poor less often in good habitats (Fig. 1A) than in bad habitats (Fig. 1B); i.e., $t_{Gr}/(t_{Gr} + t_{Gp}) > t_{Br}/(t_{Br} + t_{Bp})$. The animal starts exploiting the source at birth and continues until it dies. As in the general model, mortality is an increasing, accelerating function of effort. Here we assume that the instantaneous rate of mortality is given by $M(u) = m_0 + m_1 u^2$ (with $m_0 = 0.002$ and $m_1 = 0.05$ in the results below). Using a Bayesian approach (*25*) we identify how the animal's effort should depend on current conditions (rich or poor) and the conditions experienced in the past (*22*).

We examine how this optimal strategy, adapted to the stochastically changing world shown in Fig. 1, would perform in the standard laboratory experiments used to demonstrate contrast effects. This represents taking the animal out of the environment to which it is adapted and placing it in an unfamiliar habitat (the experimental setting) where it does not know the conditions. In this novel situation, the optimal strategy generates clear positive and negative contrast effects (Fig. 2). If the animal was initially exposed to poor conditions but then conditions become rich, it should work harder than if conditions have been rich all along (Fig. 2A). Conversely, if it was used to rich conditions but then conditions worsen, it should work less hard than if conditions have always been poor (Fig. 2B). This is because the animal's history of experiences determines its belief that the new habitat is good, and hence its expectations of the future. If it is used to poor conditions then it should capitalize by working harder when conditions improve, because it expects poor conditions to return soon; in comparison, a control animal exposed to rich conditions all along has less urgency. If it is used to rich conditions but then conditions worsen, it should hunker down, because it expects rich conditions to return soon; a control animal continuously exposed to poor conditions cannot afford to do so. In agreement with empirical data (*4*), the predicted effects are transient, with optimal effort converging to that of the controls as conditions after the shift continue (Fig. 2), because this reverses the animal's belief about the habitat type.

These contrast effects are driven by uncertainty about the pattern of environmental change. When the animal knows for certain either that the new habitat is good ($\rho = 1$) or that it is bad ($\rho = 0$), we predict no contrast effects (Fig. 3); optimal effort then depends only on whether the reward source is currently rich or poor and the (known) rate of change. This is also true when good and bad habitats are identical (see fig. S1, for $t_{Gp} = t_{Br} = 100$), which again implies that the animal knows the environmental conditions with complete certainty. In these situations, past experiences provide no new information and hence do not modify future expectations. Contrast effects should emerge whenever there is some uncertainty (i.e., when $0 < \rho < 1$), in which case the animal's past experiences provide information about which habitat it

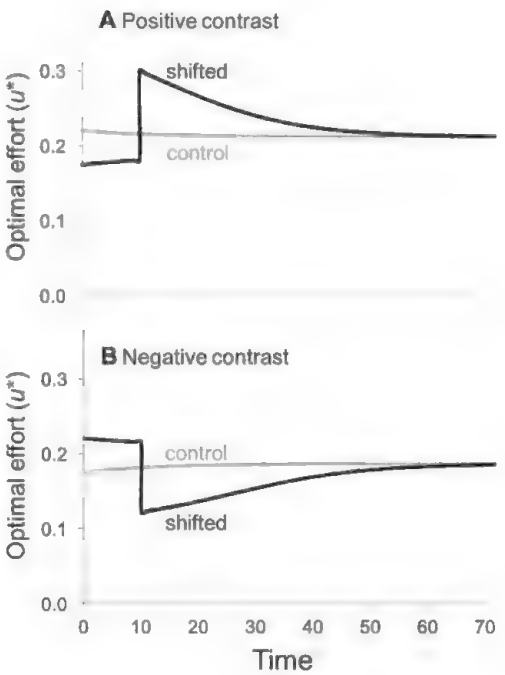

Fig. 2. The optimal, experience-dependent strategy for effort (u^*) in a stochastically changing world (Fig. 1) can generate contrast effects under laboratory conditions. The plots show predicted behavior in the standard paradigm used to demonstrate successive contrast effects: An experimental group of animals ("shifted") is switched at time 10 to the same foraging conditions as control animals who have experienced those conditions since time 0. Before time 10, the experimental animals experienced either (**A**) poorer or (**B**) richer conditions than the controls. Parameters: $t_{Gr} = 100$, $t_{Gp} = 10$, $t_{Br} = 10$, $t_{Bp} = 100$, $\rho = 0.5$, $\gamma_r = 2$, $\gamma_p = 1$.

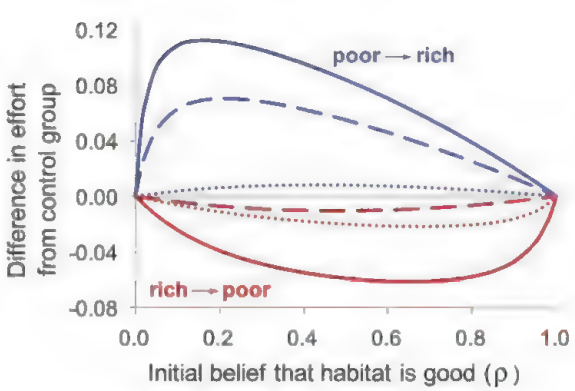

Fig. 3. Uncertainty selects for behavior that generates both positive (blue) and negative (red) contrast effects under laboratory conditions. The difference in effort between control and shifted animals when foraging conditions change at time 10 (Fig. 2) is plotted in relation to ρ, the animal's initial belief (at time 0) that the habitat is good. In all cases, $t_{Gr} = t_{Bp} = 100$, $\gamma_r = 2$, and $\gamma_p = 1$, but we consider three different patterns of temporal change characterized by the mean duration of poor periods in good habitats (t_{Gp}) and rich periods in bad habitats (t_{Br}): $t_{Gp} = t_{Br} = 10$ (solid lines); $t_{Gp} = 10$, $t_{Br} = 100$ (dotted lines); and $t_{Gp} = 100$, $t_{Br} = 10$ (dashed lines).

is in. Adjusting effort levels in response to this information confers a selective advantage over a strategy that never updates its belief about the world (fig. S2). This evolutionary explanation complements an earlier suggestion that, in an uncertain environment, individuals should invest more in exploring alternative options when the current food source unexpectedly deteriorates, as compared to individuals used to experiencing poor foraging returns (*10*). Both of these explanations highlight the significance of uncertainty for successive contrast effects.

The magnitude of the contrast effects predicted by our model depends strongly on the pattern of temporal fluctuations to which the animal is adapted (Fig. 3 and fig. S1). The effects should be strongest in animals adapted to rapidly changing conditions (fig. S1), because this enhances the differential allocation of effort between favorable and unfavorable periods (*26*). Positive contrast effects should be strongest when bad habitats are likely (low ρ) and rich periods in such habitats are very brief (low t_{Br}; Fig. 3, solid and dashed lines), because then it is particularly important to take advantage of a higher gain rate while it lasts. Negative contrast effects should be strongest when good habitats are likely (high ρ) and poor periods in such habitats are very brief (low t_{Gp}; Fig. 3, solid and dotted lines), because the animal can easily afford to reduce its effort until rich conditions return. Consequently, positive contrast should dominate negative contrast when bad habitats have very brief rich periods and good habitats have long poor periods (low t_{Br}, high t_{Gp}; Fig. 3, dashed lines), whereas negative contrast should dominate positive contrast when good habitats have very brief poor periods and bad habitats have long rich periods (low t_{Gp}, high t_{Br}; Fig. 3, dotted lines).

Empirical evidence suggests that negative contrast effects are stronger or more prevalent than positive contrast effects (*4*). According to our model, this bias is expected in animals adapted to relatively benign environments that are favorable most of the time, with only brief exposures to unfavorable conditions (e.g., high t_{Br} combined with low t_{Gp}; Fig. 3 and fig. S1). Arguably, such a pattern characterizes the typical laboratory conditions experienced by domesticated strains of rats and other animals commonly used in studies of instrumental learning.

Models of adaptive behavior have traditionally considered complex rules for responding in highly simplified, static environments, but it is becoming clear that to understand many features of behavior, we need to consider how phenotypes evolve in more complex, dynamic environments that better reflect the natural world (*27*). Stochastic fluctuations in conditions are a potentially important component of selection in real environments (*24*, *26*). For fluctuations over a much longer time scale than the animal's lifetime, optimal behavior could be fully programmed (epi-)genetically. Here we have focused on more rapid changes, which select for individual plasticity. If it is uncertain about the pattern of fluctuations, an animal's experience of past conditions may alter its future expectations and hence its optimal behavior.

Our evolutionary approach has potential applications to cognitive psychology, by offering a novel perspective on people's hedonic responses to a change in their circumstances (*28*). The model could be extended in several interesting directions. One would be to allow habitat type, which we assumed is stable over the animal's lifetime, to change with some small probability. Another would be to let decisions depend on energy reserves, which we ignored here to isolate the effect of past experiences on optimal behavior. Individuals with critically low reserves may not have the option to rest when conditions are poor (*26*).

References and Notes

1. J. Huber, J. W. Payne, C. Puto, *J. Consum. Res.* **9**, 90 (1982).
2. A. Tversky, I. Simonson, *Manage. Sci.* **39**, 1179 (1993).
3. K. V. Morgan, T. A. Hurly, M. Bateson, L. Asher, S. D. Healy, *Behav. Processes* **89**, 115 (2012).
4. C. F. Flaherty, *Incentive Relativity* (Cambridge Univ. Press, Cambridge, 1996).
5. D. Kahneman, A. Tversky, *Econometrica* **47**, 263 (1979).
6. D. Kahneman, *Am. Psychol.* **58**, 697 (2003).
7. L. P. Crespi, *Am. J. Psychol.* **55**, 467 (1942).
8. D. Zeaman, *J. Exp. Psychol.* **39**, 466 (1949).
9. P. A. Couvillon, M. E. Bitterman, *J. Comp. Psychol.* **98**, 100 (1984).
10. E. Freidin, M. I. Cuello, A. Kacelnik, *Anim. Behav.* **77**, 857 (2009).
11. K. R. Kobre, L. P. Lipsitt, *J. Exp. Child Psychol.* **14**, 81 (1972).
12. M. R. Papini, A. E. Mustaca, M. E. Bitterman, *Anim. Learn. Behav.* **16**, 53 (1988).
13. A. E. Mustaca, M. Bentosela, M. R. Papini, *Learn. Motiv.* **31**, 272 (2000).
14. M. Bentosela, A. Jakovcevic, A. M. Elgier, A. E. Mustaca, M. R. Papini, *J. Comp. Psychol.* **123**, 125 (2009).
15. E. J. Capaldi, D. Lynch, *J. Exp. Psychol.* **75**, 226 (1967).
16. J. H. McHose, D. P. Peters, *Anim. Learn. Behav.* **3**, 239 (1975).
17. J. A. Gray, *The Psychology of Fear and Stress* (Cambridge Univ. Press, Cambridge, 1987).
18. A. Amsel, *Frustration Theory: An Analysis of Dispositional Learning and Memory* (Cambridge Univ. Press, Cambridge, 1992).
19. J.-Å. Nilsson, *Proc. R. Soc. London Ser. B* **269**, 1735 (2002).
20. A. I. Houston, J. M. McNamara, J. M. C. Hutchinson, *Philos. Trans. R. Soc. London Ser. B* **341**, 375 (1993).
21. A. I. Houston, J. M. McNamara, *Models of Adaptive Behaviour: An Approach Based on State* (Cambridge Univ. Press, Cambridge, 1999).
22. Materials and methods are available as supplementary materials on *Science* Online.
23. J. M. McNamara, A. I. Houston, *Am. Nat.* **127**, 358 (1986).
24. J. M. McNamara, P. C. Trimmer, A. Eriksson, J. A. R. Marshall, A. I. Houston, *Ecol. Lett.* **14**, 58 (2011).
25. J. M. McNamara, A. I. Houston, *J. Theor. Biol.* **85**, 673 (1980).
26. A. D. Higginson, T. W. Fawcett, P. C. Trimmer, J. M. McNamara, A. I. Houston, *Am. Nat.* **180**, 589 (2012).
27. J. M. McNamara, A. I. Houston, *Trends Ecol. Evol.* **24**, 670 (2009).
28. A. Tversky, D. Griffin, in *Subjective Well-being: An Interdisciplinary Perspective*, F. Strack, M. Argyle, N. Schwarz, Eds. (Pergamon Press, Oxford, 1991), pp. 101–118.

Acknowledgments: We thank A. Higginson, A. Radford, D. Mallpress, and P. Trimmer for discussion and the European Research Council for funding (Advanced Grant 250209 to A.I.H.). J.M.M. and A.I.H. conceived the project, J.M.M. built the model, and T.W.F. analyzed the model and wrote the paper with input from the other authors.

Supplementary Materials

www.sciencemag.org/cgi/content/full/340/6136/1084/DC1
Materials and Methods
Figs. S1 and S2
References (*29*–*31*)

24 September 2012; accepted 21 March 2013
10.1126/science.1230599

Functional Extinction of Birds Drives Rapid Evolutionary Changes in Seed Size

Mauro Galetti,[1]* Roger Guevara,[2] Marina C. Côrtes,[1] Rodrigo Fadini,[3] Sandro Von Matter,[4] Abraão B. Leite,[1] Fábio Labecca,[1] Thiago Ribeiro,[1] Carolina S. Carvalho,[5] Rosane G. Collevatti,[5] Mathias M. Pires,[6] Paulo R. Guimarães Jr.,[6] Pedro H. Brancalion,[7] Milton C. Ribeiro,[1] Pedro Jordano[8]

Local extinctions have cascading effects on ecosystem functions, yet little is known about the potential for the rapid evolutionary change of species in human-modified scenarios. We show that the functional extinction of large-gape seed dispersers in the Brazilian Atlantic forest is associated with the consistent reduction of the seed size of a keystone palm species. Among 22 palm populations, areas deprived of large avian frugivores for several decades present smaller seeds than nondefaunated forests, with negative consequences for palm regeneration. Coalescence and phenotypic selection models indicate that seed size reduction most likely occurred within the past 100 years, associated with human-driven fragmentation. The fast-paced defaunation of large vertebrates is most likely causing unprecedented changes in the evolutionary trajectories and community composition of tropical forests.

High rates of human-driven extinctions, estimated to be 100-fold greater than those of natural extinctions (*1*), have pervasive impacts on the functions and services of ecosystems (*2*, *3*). Despite efforts to understand the immediate and cascading effects of the loss of species on the persistence of other species and biotic interactions (*4*, *5*), little is known about

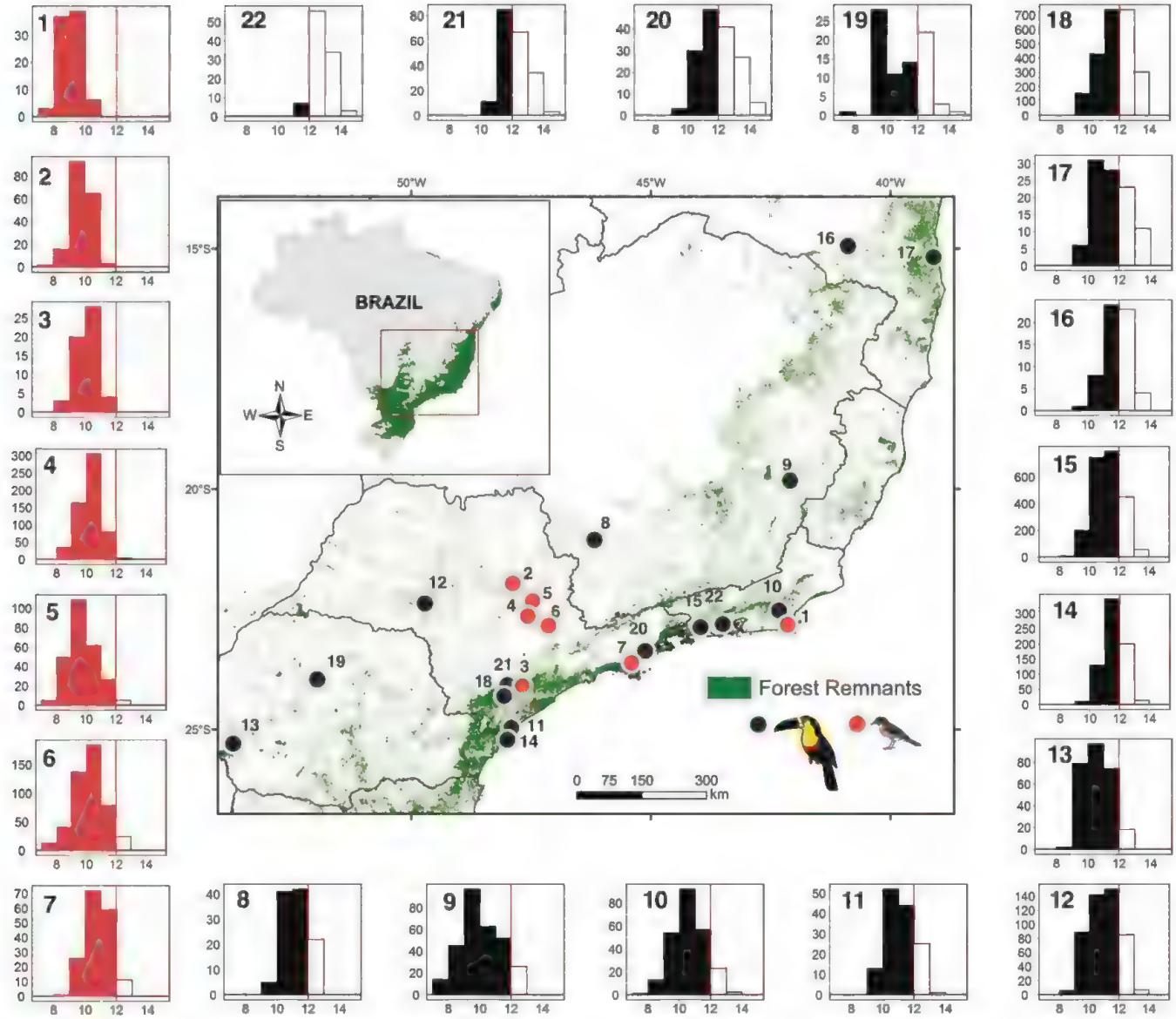

Fig. 1. Geographic variation in seed size in palm populations. Seed size (seed diameter in millimeters, *x* axis) frequency distributions (number of seeds, *y* axis) of 22 palm (*E. edulis*) populations in the remnants of the Brazilian Atlantic forest (green areas). The numbers refer to the population codes given in table S1. The red dots (codes 1 to 7) are defaunated sites, where large-gape frugivores are locally extinct or rare; the black dots are nondefaunated sites (codes 8 to 22). The vertical red line marks the upper size limit for successful dispersal by small birds (gape size 12 mm) in the absence of large-gape frugivores. The solid bars in the histograms indicate seed sizes below this threshold.

[1]Departamento de Ecologia, Universidade Estadual Paulista, Rio Claro, São Paulo, 13506-900, Brazil. [2]Instituto de Ecología, A. C. Red de Biología Evolutiva, Carretera Antigua a Coatepec 351, Xalapa, Veracruz, 91070, Mexico. [3]Instituto de Biodiversidade e Florestas, Universidade Federal do Oeste do Pará, Santarém, Pará, 68035-110, Brazil. [4]Departamento de Biologia Animal, Universidade Federal Rural do Estado do Rio de Janeiro, Seropédica, Rio de Janeiro, 23.897-000, Brazil. [5]Laboratório de Genética & Biodiversidade, Universidade Federal de Goiás, Goiânia, Goiás, 74001-970, Brazil. [6]Departamento de Ecologia, Universidade de São Paulo, São Paulo, São Paulo, 05508-90, Brazil. [7]Departamento de Ciências Florestais, Escola Superior de Agricultura "Luiz de Queiroz," Universidade de São Paulo, Piracicaba, São Paulo, 13418-900, Brazil. [8]Integrative Ecology Group, Estación Biológica de Doñana, EBD-CSIC, Sevilla, E-41092, Spain.

*Corresponding author. E-mail: mgaletti@rc.unesp.br

the potential for rapid evolutionary changes in human-modified ecosystems. Rapid evolutionary changes have been shown in short-lived organisms, such as commercially exploited species, microorganisms, and perennial plants (*6*–*8*).

Here we document the rapid evolutionary reduction of seed size in a keystone palm, *Euterpe edulis*, across the Atlantic rainforest, subsequent to human-driven extensive deforestation (*9*). Seed size is an important trait, positively correlated with seed reserve amount, germination success, seedling size, and reproductive output (*10*). At the same time, seed size constrains the range of effective seed dispersers, because only large-bodied frugivores have gapes wide enough to consume large seeds (*11*).

Populations of large-gape frugivorous birds are directly threatened by hunting. They require extensive tracts of forest and hence are prone to local extinction in smaller forest fragments (*12*). These frugivores disperse several plant species over distances of several kilometers and eat large-seeded species that cannot be swallowed and successfully dispersed by smaller birds, which often are the only species resilient to large-scale disturbances (*13*). The functional loss of large frugivores, either by local extinction or by the severe reduction of population abundance (functional extinction), can affect natural regeneration by impairing the main components of the dispersal process: escape, colonization, and recruitment (*14*). With the functional extinction of large-gape

birds, the fruit and seed traits of large-seeded plants might experience evolutionary changes within ecological time scales. We can expect shifts of the phenotypic selection regime and changes in the outcomes of selection after a substantial fraction of the selective agents (i.e., the large-gape frugivores) has been extirpated from their natural habitats.

We compared the seed size distributions of 22 palm populations in nondefaunated and defaunated areas of the two main physiognomic types (semideciduous and rainforest) in the Brazilian Atlantic forest (*15*) (Fig. 1). We found a consistent trend toward smaller seeds in defaunated forests (Fig. 1 and table S1). We classified an area as "defaunated" when large-gape frugivorous birds (those with a mean gape width >12 mm), such as toucans (*Ramphastos dicolorus* and *R. vitelinus*), toucanets (*Pteroglossus aracari*, *P. bailloni*, and *Selenidera maculirostris*), and large cotingas (*Procnias nudicollis*, *Carpornis* spp., and *Pyroderus scutatus*), are locally or functionally extinct (i.e., present with a very low abundance) (*15*) (fig. S1 and table S3).

Toucans and large cotingas are the major large seed dispersers in nondefaunated forests (the average local richness of large frugivorous birds that disperse palm fruits is 11.9 species; tables S2 and S3). Small-gape thrushes are the most common seed dispersers remaining in defaunated forests, and the species richness of large frugivorous birds is reduced to 5.1 species (tables S2 and S3). A few mammal species very infrequently act as legitimate seed dispersers (table S2). Small-gape frugivores (<12 mm) represent 38% of the species in nondefaunated areas but 49% in defaunated forests (table S2). This distribution, in turn, results in 33% of the fruits being consumed by small-gape frugivores in nondefaunated areas and up to 98% of the fruits in the defaunated areas (table S4). Thus, there is ample potential for small-gape frugivores to have significant selective pressures on fruit traits in defaunated areas.

A nested analysis of variance revealed that variation in seed size is minimally accounted for by the forest physiognomic type (3.7%). In contrast, the defaunation status within each forest type accounted for more than 33.9% of the variance in seed size, with 0.1% accounted for by differences among sites. Most of the total variance in seed size (44.9%) was associated with individual palms within each site, with intra-individual variation (among-year variations and/or positional variation within the infructescence) representing 17.4% (overall nested analysis, $F_{[1,\ 9195]} = 909.8$, $P < 0.0001$). These results demonstrate the marked geographic patterns in seed size potentially related to the local selective regime (the fruit selection process) driven by frugivores according to the defaunation status, with ample among-individual trait variance for natural selection to operate. Many environmental factors can influence seed size. Thus, we modeled seed size as a function of defaunation status and 13 other environmental variables, including climate, soil fertility, relief complexity, and forest cover (table S5). Although biotic variables failed to explain the variation in seed size, the model including defaunation status nested within forest type yielded the best fit to the observed data (table S5) (*15*). These results show that local variation in seed size is unrelated to any of the abiotic predictors or landscape variables but consistently relates to the defaunation status of each site.

The seeds of *E. edulis* are not successfully dispersed either when the fruits fall beneath the plant or when birds drop the fruits with the seeds still within the pulp. Seeds that remain with pulp are less likely to germinate (*16*), and fruits deposited beneath their parent palm usually experience high density-dependent mortality (*17*) (fig. S2E). The seeds dispersed by birds (defecated or regurgitated) collected in the field and from experiments with captive birds revealed that different bird species disperse seeds of different sizes [generalized linear model (GLM) $\chi^2_{[6]} = 94.1$, $P < 0.001$; Fig. 2A]. The seeds dispersed by thrushes were consistently ≤12 mm in diameter, whereas large-gape birds, mainly toucans, dispersed a broader range of seed sizes (Fig. 2A). To corroborate these findings of fruit size selection with bird fruit choice, we estimated the probability of seed dispersal by birds as a function of seed size by recording the diameter of successfully dispersed seeds (regurgitated) and nondispersed seeds (fruits with beak marks) at four pristine and three defaunated sites. The dispersal probability was near zero for seeds >12 mm at all defaunated sites, which is significantly lower than the estimated probability for nondefaunated sites [binomial generalized additive model (GAM) $\chi^2_{[1,20]} = 40.3$, $P < 0.001$; Fig. 2B]. Seeds wider than 12 mm represent approximately 32% of the overall seeds produced by *E. edulis* populations in nondefaunated forests. Our data show that defaunated areas have lost this large size range of the phenotypic seed size variation (Fig. 1), suggesting directional selection for reduced seed size of *E. edulis* at

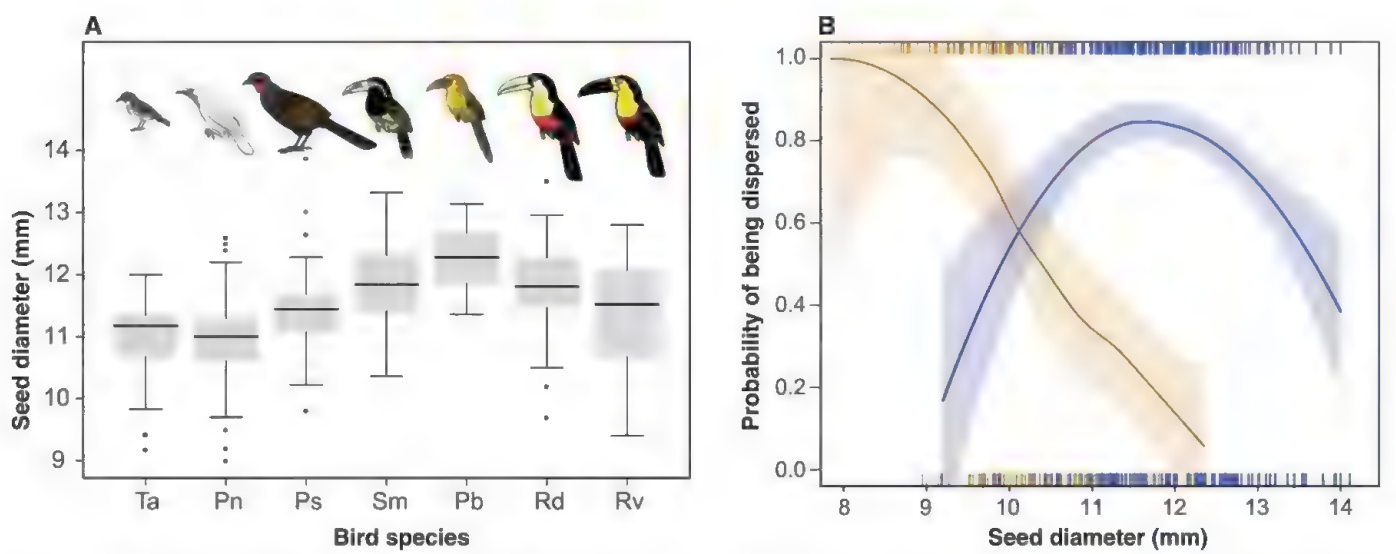

Fig. 2. Patterns of fruit preferences by frugivorous birds and consequences for phenotypic selection on seed size. (**A**) Seed size variation of the palm (*E. edulis*) fruits consumed by birds (from left to right): white-necked thrush (Ta, *Turdus albicollis*), bare-throated bellbird (Pn, *Procnias nudicollis*), rusty-margined guan (Ps, *Penelope superciliaris*), spot-billed toucanet and saffron toucanet (Sm, *Selenidera maculirostris*; Pb, *Pteroglossus bailloni*), and red-breasted and channel toucan (Rd, *Ramphastos dicolorus*; Rv, *R. vitellinus*). The boxes include the mean (horizontal black line), ± 1 SE (gray box), the 95% confidence interval (vertical lines), and outlier values (circles). (**B**) The probability of the dispersal of palm seeds as a function of seed diameter in defaunated forest sites (orange), where large-gape frugivorous birds are functionally extinct, and in nondefaunated forests (blue) [see (*15*) for the trends in local areas; fig. S3]. The vertical lines in the rugged plot indicate the individual seed sizes of undispersed and dispersed seeds.

defaunated sites that contrasts with the stabilizing selection observed in nondefaunated sites (Fig. 2B and fig. S3).

Given that resilient small-gape frugivores (thrushes) only successfully disperse small seeds (≤12 mm), we tested the potential of such differential selection to generate the observed striking reductions in the seed size of *E. edulis* over time in defaunated areas (Fig. 1, panels 1 to 7). We used a simple evolutionary model based on the breeder's equation (*18*) to estimate the number of generations of selection on seed size needed to result in such a size difference between nondefaunated and defaunated forests (*19*, *20*). Our simulations indicate that such an evolutionary change in the seed size of *E. edulis* populations would be possible in less than 100 years after a disturbance event (such as defaunation due to hunting or fragmentation) causing the functional loss of large frugivores (Fig. 3). Our estimates highlight the fact that a period of <75 years after a severe defaunation would be sufficient to cause the observed seed size reduction in palm populations in defaunated areas (Fig. 1). The documented extensive forest conversion to agriculture (mainly coffee) in semideciduous defaunated forests dates back to the 1800s (*21*, *22*), which agrees with the results of our phenotypic selection model and indicates that the observed changes in seed size of *E. edulis* could have evolved very recently in relation to the remnant frugivore fauna (fig. S4). Thus, we argue that defaunation could have triggered the rapid evolutionary change of a phenotypic plant trait, resulting in a consistent size reduction of seeds in defaunated Atlantic forests.

From an ecological perspective, the reduction of seed size may have several negative consequences for plant recruitment and population dynamics (*23*). In *E. edulis*, it results in reductions in the total, shoot, and root biomasses of 1-year-old seedlings (*24*, *25*). Our experiments indicate that the seed size reduction most likely resulted in the significantly increased vulnerability of *E. edulis* recalcitrant seeds to desiccation and decreased seedling size in both semideciduous forest and rainforest defaunated areas (*15*). Thus, seed size reduction may increase seed mortality in drier conditions and result in smaller seedlings, thereby tending to reduce the average fitness of the population. If regeneration becomes critically dependent on small seeds in defaunated areas, extended and intensified periods of drought induced by ongoing climate change, as predicted by climate models for South America (*26*), may be particularly harmful to the seedling establishment of this threatened palm species.

The seed size reduction documented here may be a generalized phenomenon in human-modified ecosystems where large frugivores that act as seed dispersers have been extinct for a long time. We thus foresee pervasive ecological and evolutionary effects of widespread vertebrate defaunation in tropical ecosystems. In particular, the rapid current defaunation in tropical forests will most likely result in unprecedented shifts of selection regimes on key life-history traits and in their evolutionary trajectories.

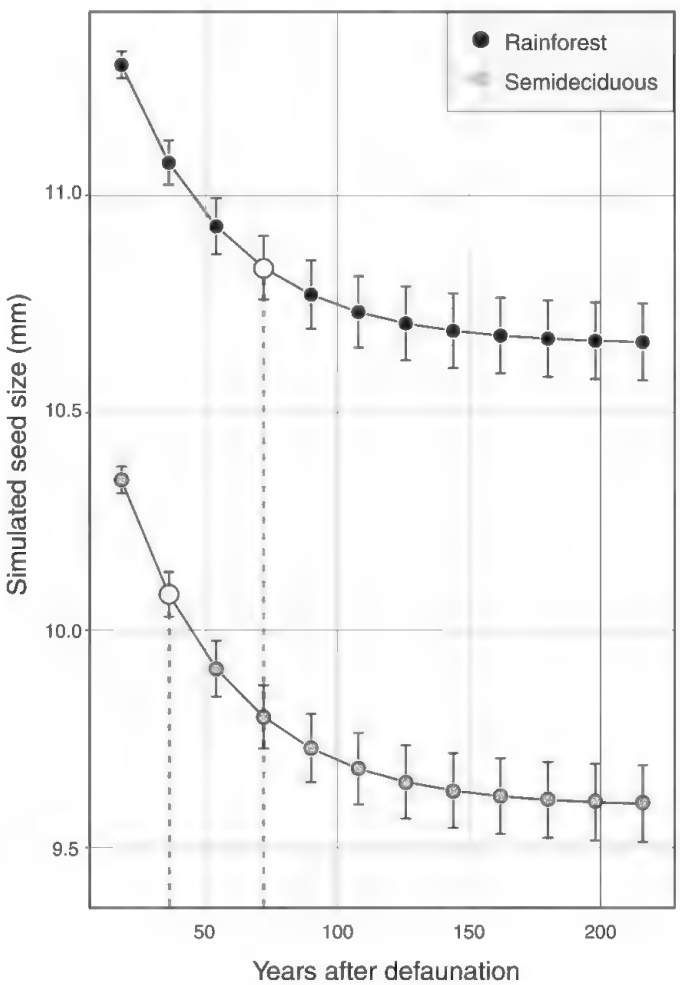

Fig. 3. Simulated phenotypic trends in seed size after loss of major frugivores. Expected trajectories over time, estimated from the phenotypic selection model, of the seed size reduction after defaunation in two Atlantic forest types (rainforest and semideciduous forest) (*15*). The vertical dashed lines with larger open dots denote the position along the mean trajectory when the predicted seed diameter is the closest to the present observed mean seed diameter in defaunated forests. The position where the dashed lines intercept the *x* axis represents the minimum time for the seeds to reach the present-day seed diameter mean value according to the model. Solid dots show the mean values (±1 SD) of the simulated seed size for consecutive years after defaunation.

References and Notes

1. A. D. Barnosky *et al.*, *Nature* **471**, 51 (2011).
2. F. Isbell *et al.*, *Nature* **477**, 199 (2011).
3. A. D. Barnosky *et al.*, *Nature* **486**, 52 (2012).
4. S. H. Anderson, D. Kelly, J. J. Ladley, S. Molloy, J. Terry, *Science* **331**, 1068 (2011).
5. N. J. Cordeiro, H. F. Howe, *Proc. Natl. Acad. Sci. U.S.A.* **100**, 14052 (2003).
6. S. R. Palumbi, *Science* **293**, 1786 (2001).
7. C. T. Darimont *et al.*, *Proc. Natl. Acad. Sci. U.S.A.* **106**, 952 (2009).
8. S. A. B. Roels, J. K. Kelly, *Evolution* **65**, 2541 (2011).
9. The palmito or palm heart (*E. edulis*, Arecaceae) is a dominant palm species endemic to the Atlantic forest and dependent on birds for successful seed dispersal. It also occupies fragmented forest stands originated within the past 200 years since the establishment of extensive coffee plantations in São Paulo state (*21*, *22*).
10. M. R. Leishman *et al.*, in *Seeds: The Ecology of Regeneration in Plant Communities*, M. Fenner, Ed. (CAB International, Wallingford, UK, 2000), pp. 31– 57.
11. D. J. Levey, *Am. Nat.* **129**, 471 (1987).
12. N. S. Sodhi, L. H. Liow, F. A. Bazzaz, *Annu. Rev. Ecol. Evol. Syst.* **35**, 323 (2004).
13. K. M. Holbrook, B. A. Loiselle, *Ecology* **90**, 1449 (2009).
14. J. S. Markl *et al.*, *Conserv. Biol.* **26**, 1072 (2012).
15. Materials and methods are available as supplementary materials on *Science* Online.
16. A. de Barros Leite, P. H. S. Brancalion, R. Guevara, M. Galetti, *J. Trop. Ecol.* **28**, 615 (2012).
17. D. M. S. Matos, R. P. Freckleton, A. R. Watkinson, *Ecology* **80**, 2635 (1999).
18. D. S. Falconer, T. F. C. Mackay, *Introduction to Quantitative Genetics* (Addison Wesley Longman, Essex, UK, 1996).
19. We estimated the heritability (h^2) of seed size in *E. edulis* based on the variance of genetic relatedness between palms with available fruit phenotypic data (*15*). We used seed size data from genotyped individual palms in three populations, yielding $h^2 = 0.35$ (*15*), and the previously reported value of 18.7 years for the generation time of the palm (*20*).
20. M. Franco, J. Silvertown, *Ecology* **85**, 531 (2004).
21. W. Dean, *Rio Claro: A Brazilian Plantation System 1820-1920* (Stanford Univ. Press, Stanford, CA, 1976).
22. The defaunated semideciduous forests are located in the heart of traditional coffee plantations in Brazil. For example, Rio Claro, a typical city in our defaunated region, had 65 coffee farms by 1855.
23. A. T. Moles *et al.*, *Science* **307**, 576 (2005).
24. M. A. Pizo, C. von Allmen, L. P. C. Morellato, *Acta Oecol.* **29**, 311 (2006).
25. M. A. Pizo, I. Simão, *Acta Oecol.* **22**, 229 (2001).
26. J. A. Marengo, M. Rusticucci, O. Penalba, M. Renom, *Clim. Change* **98**, 509 (2010).

Acknowledgments: We thank the Fundação de Amparo do Estado de São Paulo (BIOTA - FAPESP); Conselho Nacional de Desenvolvimento Científico (CNPq), (Excellence Grant-Junta Andalucía (to P.J.); and Programa Iberoamericano de Ciencia y Tecnología para el Desarollo (CYTED) for funding support. We thank J. Bascompte, R. Dirzo, D. Hansen, D. Levey, E. Bruna, D. Lapola, D. McCauley, M. A. Pizo, and three reviewers for useful comments and suggestions; T. A. Ferreira, E. Cazetta,

M. J. Campos, D. Rother, G. Ambar, C. Dracxler, E. R. Castro, R. Laps, P. Develey, M. R. Francisco, and staff from PN Iguaçu for sending us palm seeds and data on frugivores; Fundação Florestal for allowing our study in the Protected Areas; and S. Nazareth and R. Brandolim for field and laboratory assistance. M.G. and P.R.G. receive a research fellowship from Conselho Nacional de Desenvolvimento Científico e Tecnológico.

Data supporting this study are available in the DRYAD repository (http://dx.doi.org/10.5061/dryad.2pm42). Bird plates were done by Carl Buell.

Supplementary Materials
www.sciencemag.org/cgi/content/full/340/6136/1086/DC1
Materials and Methods
Figs. S1 to S4
Tables S1 to S6
References (*27–61*)

7 December 2012; accepted 5 April 2013
10.1126/science.1233774

Tracking Individuals Shows Spatial Fidelity Is a Key Regulator of Ant Social Organization

Danielle P. Mersch,[1]* Alessandro Crespi,[2] Laurent Keller[1]*

Ants live in organized societies with a marked division of labor among workers, but little is known about how this division of labor is generated. We used a tracking system to continuously monitor individually tagged workers in six colonies of the ant *Camponotus fellah* over 41 days. Network analyses of more than 9 million interactions revealed three distinct groups that differ in behavioral repertoires. Each group represents a functional behavioral unit with workers moving from one group to the next as they age. The rate of interactions was much higher within groups than between groups. The precise information on spatial and temporal distribution of all individuals allowed us to calculate the expected rates of within- and between-group interactions. These values suggest that the network of interaction within colonies is primarily mediated by age-induced changes in the spatial location of workers.

Ant colonies, with their complex and efficient social organization, have long fascinated humans (*1*). Essential to their ecological success are high levels of cooperation and sophisticated division of labor. Although workers must perform a multitude of tasks such as foraging, nest construction, and brood rearing, it has become clear that there is no central control of how work is allocated among individuals. Therefore, workers must allocate themselves to tasks in a self-organized manner following simple behavioral rules that incorporate local stimuli received directly from the environment and from interactions with other workers (*2–4*). Despite extensive work on division of labor in social insects (*1*, *3*, *5–7*), the connection between individual task specialization and the social network remains unknown. Another important, yet little studied aspect of social organization is spatial organization. In honeybees, workers change tasks over the course of their lifetime, starting as nurses in the nest and generally ending as foragers outside (*2*, *8*, *9*). This suggests that the rate of interactions between group members may be affected by the task performed and its associated localization in the colony. In our experiment, we used an automated video tracking system based on fiducial identification labels to track all individuals in six colonies of the ant *Camponotus fellah* and to identify individual interactions and patterns of social organization (movie S1).

All colonies were established from a single queen collected after a mating flight. The experiment started when queens were 4 years old, out of a maximum life span of 26 years (*10*). We determined the age of all workers (122 to 192 per colony) by weekly color-coding all newly eclosed workers more than 60 weeks before the experiment began. A month before the start of the experiment, we individually marked all ants with a distinct barcode-like matrix (*11*), enabling individual identification (*12*). Colonies were kept in a constantly dark nest chamber that was connected by a tunnel to a foraging chamber exposed to daily light-dark cycles (fig. S1). The temperature, humidity, light, and food supply were computer-controlled, and both chambers were filmed from above with high-resolution monochrome cameras operating under infrared light (fig. S1) (*12*). We recorded the position and orientation of all individuals twice per second to reconstruct spatial movement and infer all social interactions occurring over the 41 days of the experiment. A pair of ants was considered to interact when the front end of one ant was located within the trapezoidal shape representing the other ant (fig. S4) (*12*). The data set we obtained consisted of a total of 2,433,250,580 ant positions and 9,363,100 social interactions (movies S2 and S3).

We used this data set to first investigate whether workers organize themselves into cohesive social groups by using the Infomap community detection algorithm (*13*). To facilitate data analysis, we split the 41 experimental days into four periods of 11, 10, 10, and 10 days. In each of these periods, we identified pairs of interacting ants. Analyses on the daily interaction networks of the first 11 days (see supplementary text) revealed two robust groups to which the same set of workers was affiliated on almost all days. The first group always comprised the queen and 41 ± 12% of the workers (percentage ± SD across the six colonies) (Fig. 1A), whereas the second group represented 31 ± 11% of the colony's workforce. Depending on days and colonies, we also identified zero to five other groups of workers. A visual analysis of the daily networks of interactions suggested that workers affiliated with the two robust groups on only a few days may form a third group with less marked within-group preferential interactions. These workers represented 28 ± 4% of the colony's workforce and were consistently located between the two other groups in the network (Fig. 1A and figs. S6 to S10). An additional analysis of the interaction frequencies (supplementary text) confirmed that workers of the third group interacted significantly more with members of their group than with workers of the other two groups. Together, these results indicate that colonies of *C. fellah* are structured in three interconnected social groups and that these groups differ in their interaction patterns.

Workers from the three social groups exhibited distinct behavioral signatures (Fig. 2). Workers of the first group performed most of the interactions with the queen [Kruskal-Wallis (KW): $\chi^2 = 514.05$, $P < 10^{-101}$] and visits to the brood. By contrast, workers from the second group performed most (87.3 ± 18.6%) of the foraging trips, whereas workers from the third group exhibited a significantly higher propensity to visit the rubbish pile. For simplicity, we hereafter refer to these three groups as nurses, foragers, and cleaners. Comparison of the normalized age of workers revealed an age-based division of labor. Nurses were younger than cleaners who, in turn, were younger than foragers (KW: $\chi^2 = 108.7$, $P < 10^{-23}$) (fig. S11). However, in all colonies, there was great overlap among the three groups, with some nurses being older and some foragers being younger than the workers' average age. Despite a wide distribution in worker body size (6 to 16 mm), no consistent size difference exists between workers of the three groups (fig. S12).

Our data also allowed us to track temporal changes among the three behavioral groups by performing community detection analyses on the three subsequent 10-day periods of the experimental data (Fig. 3). Workers exhibited a preferred behavioral trajectory, moving from nursing to cleaning to foraging as they age. The most common transition was from cleaner to forager (supplementary text). Such age-related behavioral transitions have been documented in honeybees, in which young bees nurse the brood, then move on to perform various other in-hive tasks and

[1]Department of Ecology and Evolution, University of Lausanne, Switzerland. [2]Biorobotics Laboratory, Ecole Polytechnique Fédérale de Lausanne, Switzerland.

*Corresponding author. E-mail: danielle.mersch@unil.ch (D.P.M.); laurent.keller@unil.ch (L.K.)

finally become foraging bees (*8*, *9*). In ants, age polyethism is also believed to exist, but this is generally based on indirect evidence [reviewed in (*1*), but see (*14*) and supplementary text], with the notable exception of one study of *Lasius niger*, where individual marking of 40 workers revealed a progressive increase of the proportion of foragers over time, but where only 50% of the workers exhibited a behavioral age-related transition (*15*). Our data further emphasize that age-related behavioral maturation is a slow and noisy process in ants with important individual variation.

There were differences among the three groups in the frequency of within-group interactions. In particular, the relative within-group interaction frequency of cleaners was 2.1 times lower than that of nurses and foragers (KW: $\chi^2 = 270.6$, $P < 10^{-53}$), indicating that cleaners' group cohesion is less pronounced. This pattern was confirmed by an analysis considering the time required for a worker to interact with 80% of its nestmates (supplementary text). The observed social group structure and increased within-group interactions could stem from either a propensity of individuals to preferentially interact with members of their group or from differences in the spatial distribution of the different groups. We therefore used spatial grid representations (heat maps) to determine the spatial distribution of workers of each of the three groups over the first 11 days of observation. The heat maps revealed marked differences between nurses, cleaners, and foragers, which occupied distinct spatial locations in the nest area (Fig. 4A and figs. S13A to S17A). Nurses stayed near the brood and foragers near the nest entrance, whereas cleaners occupied the remaining nest areas, which suggests that, in addition to cleaning, they might also patrol the nest.

Similar heat maps for the location of social interactions within and between each of the three groups revealed that most of the within-group interactions occurred in the spatial area most used by individuals of a given group, whereas between-group interactions preferentially occurred at the intersection of the spatial distribution of the pairs of groups considered (Fig. 4B and figs. S13B to S17B). To test whether the social structure and network of interaction might arise solely as a consequence of task-related spatial segregation of workers, we estimated for each worker the expected frequency of interactions within and

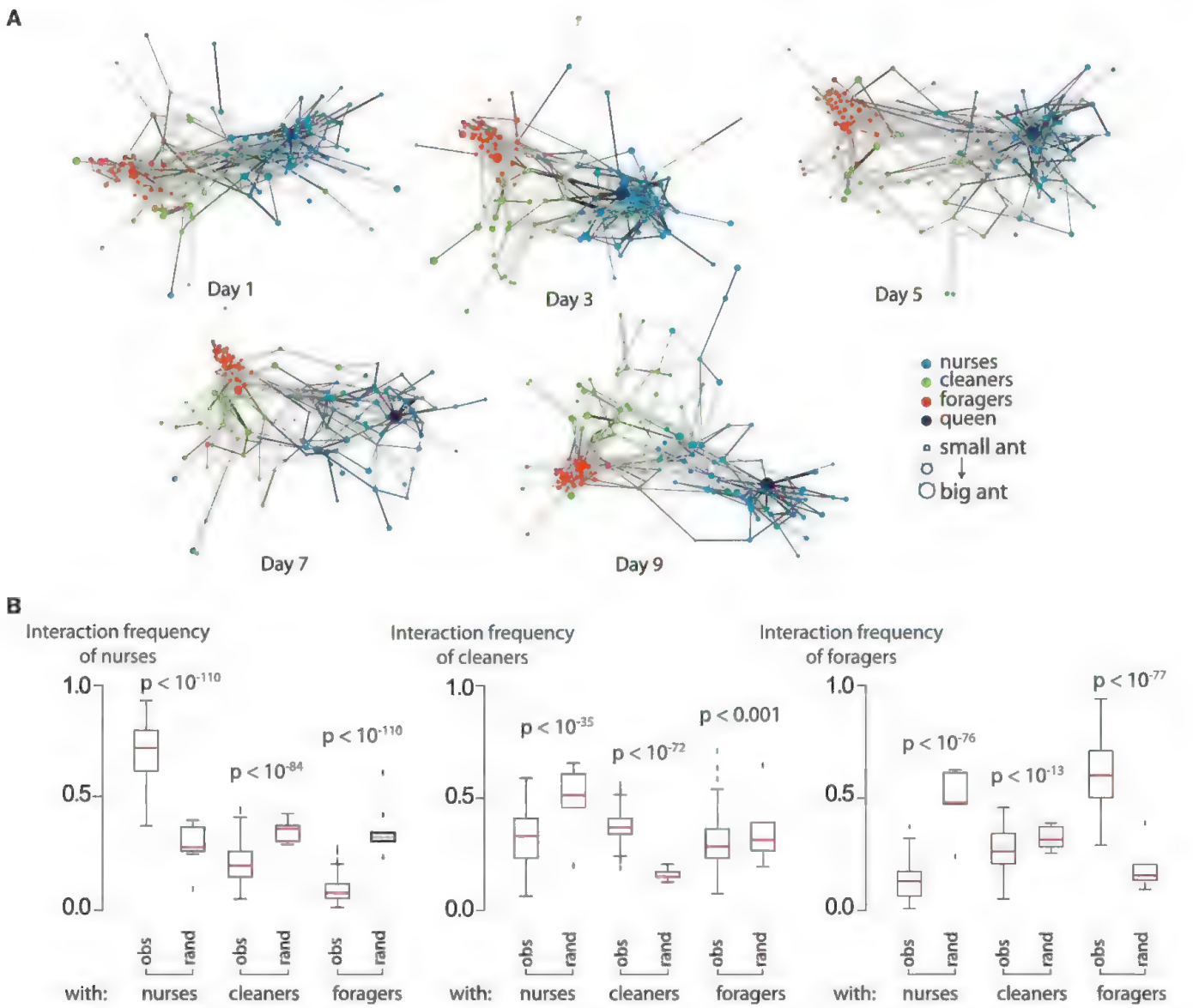

Fig. 1. Colonies are organized in several interconnected social groups within which workers interact frequently. (**A**) Social networks of colony five on days 1, 3, 5, 7, and 9. Edge width is proportional to the number of interactions between pairs of nodes. The darkness of edges is proportional to the average duration of interactions. The network is laid out with the spring embedded layout from Cytoscape (*19*). (**B**) Observed (obs) and theoretically predicted interaction frequencies within- and between-groups of nurses, cleaners, and foragers. Theoretical predictions are based on random (rand) interactions among all ants. *P* values were from Kruskal-Wallis tests with post-hoc comparisons and Bonferroni corrections for multiple testing.

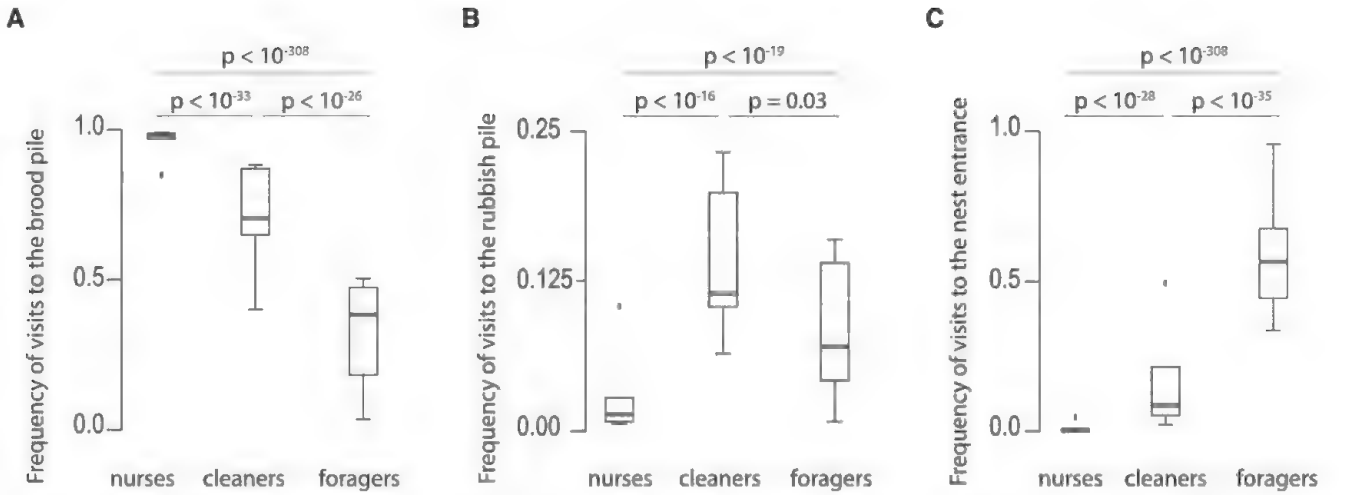

Fig. 2. Behavioral specialization of the three social groups (nurses, cleaners, and foragers). Specialization in (**A**) nursing, (**B**) cleaning, and (**C**) foraging is shown (estimated by the number of visits to the nest entrance, which were strongly correlated with the number of foraging trips). *P* values represent comparisons between adjacent groups and were from Kruskal-Wallis tests with post-hoc comparisons and Bonferroni corrections for multiple testing.

between groups by taking into account the observed between-group spatial segregation (*12*). Accounting for the spatial distribution led to a greatly improved match between the expected and observed rates of interaction compared with when spatial distribution was not considered (KW: $\chi^2 = 1188.7, P < 10^{-259}$). Importantly, there were no significant differences between the expected and observed rates of within- and between-group interactions for each of the three groups (KW: $\chi^2 = 1.4, P = 0.23$) (Fig. 4C), indicating that spatial fidelity and strong spatial assortment of individuals of each of the three groups are the primary mechanisms underlying strong preference for within-group interactions.

The strong link between spatial and social structure further indicates that groups with a more diffuse spatial structure should also have a weaker social group structure. This is exactly what we observed for the cleaners, who have both a more diffuse spatial structure than the two other groups and a lower within-group interaction rate. Similar spatial-social correlations have been observed in reef sharks and bottlenose dolphins, which both form communities that are spatially segregated. However, in contrast to ants, sharks and dolphins actively reinforce their communities by engaging in more interactions with group members than are expected from the spatial structure (*16*, *17*).

The presence of spatial and social structure can limit the speed of information flow (*18*). To quantify the rate of information flow within and between groups, we selected 162 random ants (9 per group and colony) as information carriers and calculated a maximum rate of information flow, assuming that all interactions lead to information transfer (*12*). The analysis shows that as many as 89 ± 14% of the ants in the colony can receive the information within 1 hour, independently of who is the information carrier, thereby indicating that information might circulate rapidly. The role of social structure was reflected by a faster spread within than between groups when the information was emitted by nurses

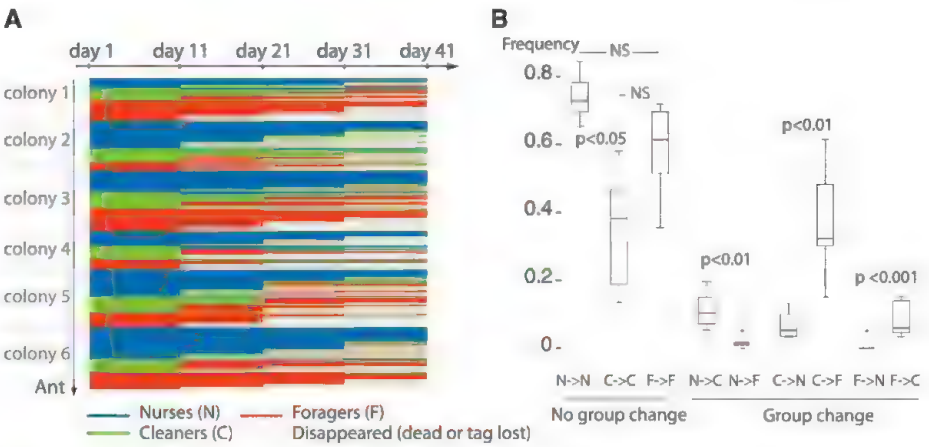

Fig. 3. Behavioral trajectories of workers over the 41 days of the experiments. Workers tend to move from nursing to nest cleaning to foraging. (**A**) Social group affiliations of each worker for each 11- or 10-day interval. Blue, affiliation to the nurse group; green, cleaning group; orange, foraging group. Workers that disappeared because they died or lost their tag are indicated in white. (**B**) Frequencies of group changes for workers of each group (N, nurses; C, cleaners; F, foragers). *P* values were from Kruskal-Wallis tests with post-hoc comparisons and Bonferroni corrections for multiple testing. NS indicates nonsignificant differences.

and foragers (nurses: Wald test = 32.7, $P < 10^{-7}$; foragers: Wald test = 18.7, $P < 10^{-4}$) (fig. S18, A and C). However, this was not the case when cleaners were the information carriers (Wald test = 0.84, $P = 0.36$) (fig. S18B), most likely because they are spatially and topologically in the middle between nurses and foragers (by contrast, nurses and foragers have only cleaners as their neighbors). Thus, although social and spatial structure limit information flow, the extent to which the limits are experienced by the colony depends on who carries the information. These results suggest that spatial structure might function as a regulating mechanism for information flow, division of labor, and colony homeostasis.

Our tracking system allowed us to precisely assess a network of interaction within colonies and uncover the existence of three groups of workers that preferentially interact with individuals of their group and exhibit different behavioral repertoires. The higher-than-expected interaction rate within groups was due to strong differences in the spatial location among individuals of the three groups, highlighting spatial fidelity as a key regulator of network interactions and the spread of information within ant colonies.

References and Notes

1. B. Hölldobler, E. O. Wilson, *The Ants* (Springer, Berlin, 1990).
2. G. E. Robinson, *Annu. Rev. Entomol.* **37**, 637 (1992).
3. A. F. G. Bourke, N. R. Franks, *Social Evolution in Ants* (Princeton Univ. Press, Princeton, NJ, 1995).
4. S. Camazine *et al.*, *Self-Organization in Biological Systems* (Princeton Univ. Press, Princeton, NJ, 2003).
5. E. J. H. Robinson, O. Feinerman, N. R. Franks, *Proc. Biol. Sci.* **276**, 4373 (2009).
6. J. M. Jandt, A. Dornhaus, *Anim. Behav.* **77**, 641 (2009).

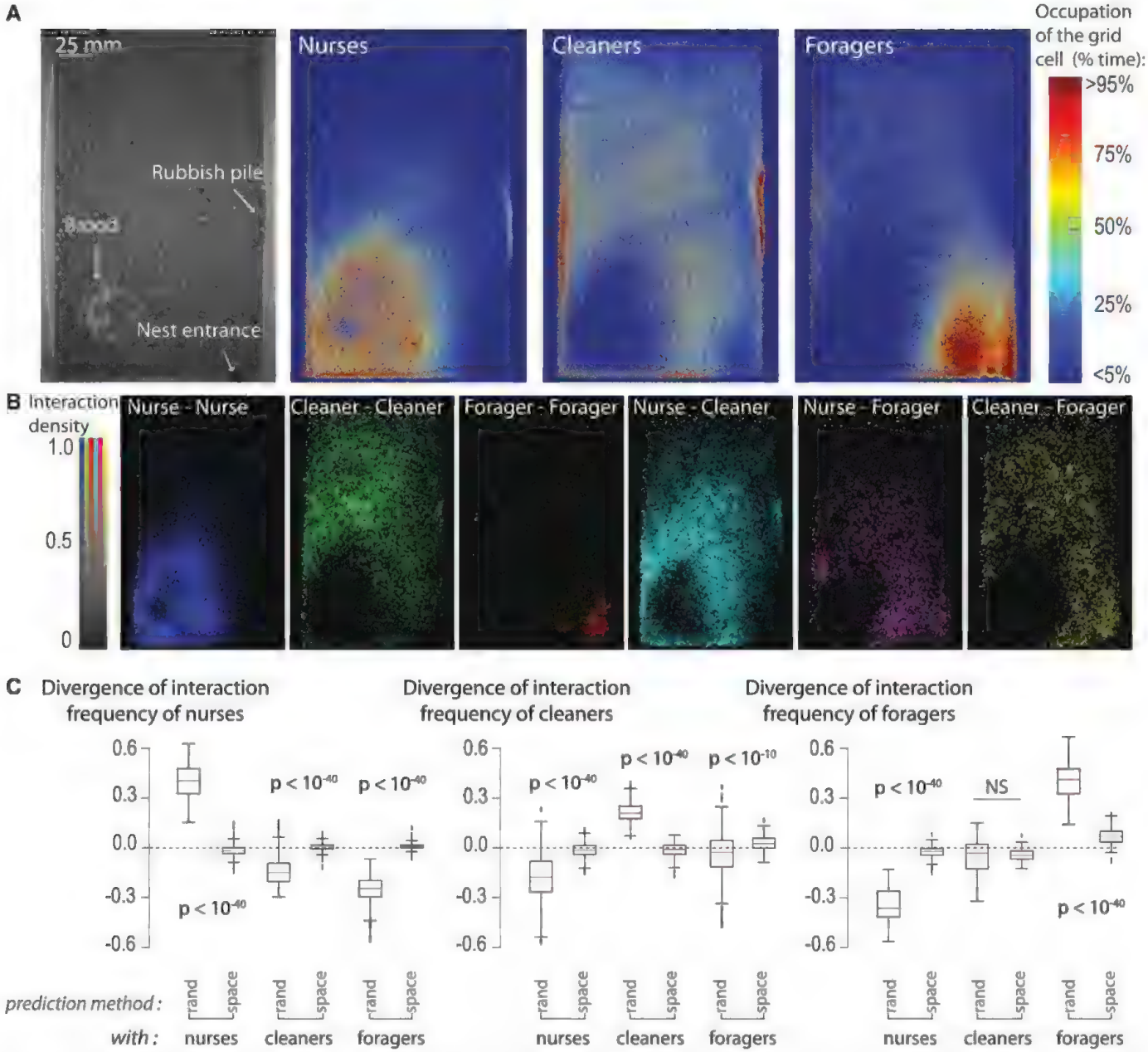

Fig. 4. Spatial segregation of social groups is best explained by the local neighborhood of the ant. (**A**) Spatial organization of a nest and spatial distribution of nurses, cleaners, and foragers. (**B**) Spatial distribution of within- and between-group interactions. (**C**) Divergence between the observed and predicted interaction frequencies. Predictions are generated by assuming random interactions and no spatial segregation among workers from the three groups (i.e., random method) or by taking into account the spatial segregation of workers (i.e., space method). A perfect correspondence between the observed and predicted interaction frequencies is indicated by zero divergence (dotted lines). *P* values were from Kruskal-Wallis tests.

7. C. R. Smith, A. L. Toth, A. V. Suarez, G. E. Robinson, *Nat. Rev. Genet.* **9**, 735 (2008).
8. B. R. Johnson, *Behav. Ecol. Sociobiol.* **62**, 777 (2008).
9. T. D. Seeley, *Behav. Ecol. Sociobiol.* **11**, 287 (1982).
10. M. Vonshak, A. Shlagman, *Isr. J. Entomol.* **39**, 165 (2009).
11. M. Fiala, "Comparing ARTag and ARToolkit Plus fiducial marker systems," *HAVE 2005*, IEEE International Workshop on Haptic Audio Visual Environments and Their Applications, Ottawa, 1 to 2 October 2005.
12. Materials and methods are available as supplementary materials on *Science* Online.
13. M. Rosvall, C. T. Bergstrom, *Proc. Natl. Acad. Sci. U.S.A.* **105**, 1118 (2008).
14. M. A. Seid, J. F. A. Traniello, *Behav. Ecol. Sociobiol.* **60**, 631 (2006).
15. A. Lenoir, *Bull. Biol. Fr. Belg.* **2–3**, 80 (1979).
16. J. Mourier, J. Vercelloni, S. Planes, *Anim. Behav.* **83**, 389 (2012).
17. D. Lusseau *et al.*, *J. Anim. Ecol.* **75**, 14 (2006).
18. B. Blonder, A. Dornhaus, *PLoS ONE* **6**, e20298 (2011).
19. P. Shannon *et al.*, *Genome Res.* **13**, 2498 (2003).

Acknowledgments: This work was funded by an advanced European Research Council grant, several grants from the Swiss National Science Foundation, the Société Académique Vaudoise, and the Fondation Erna Hamburger. We declare no conflicts of interest. We thank M. Fiala for advice on the use of the ARTag library; A. Hefetz for collecting queens; B. Hollis for help with the information spread analysis; R. James for discussions on network analysis; the Swiss Institute of Bioinformatics for data storage; and M. Chapuisat, B. Hollis, T. Kawecki, E. Lucas, N. Stroeymeyt, T. Richardson, and three anonymous reviewers for comments on the manuscript. Electronic schematics and software are available upon request. Data (social networks, behavior, spatial structure, observed and expected interaction frequencies, and information spread) that pertain to the experiments and analyses reported in this paper can be accessed at DOI: 10.5061/dryad.8d8h7.

Supplementary Materials

www.sciencemag.org/cgi/content/full/science.1234316/DC1
Materials and Methods
Supplementary Text
Figs. S1 to S18
References (*20-22*)
Movies S1 to S3

20 December 2012; accepted 28 March 2013
Published online 18 April 2013;
10.1126/science.1234316

Mechanisms of Age-Dependent Response to Winter Temperature in Perennial Flowering of *Arabis alpina*

Sara Bergonzi,[1]* Maria C. Albani,[1]* Emiel Ver Loren van Themaat,[1,2] Karl J. V. Nordström,[1]† Renhou Wang,[1]‡ Korbinian Schneeberger,[1] Perry D. Moerland,[2] George Coupland[1]§

Perennial plants live for more than 1 year and flower only after an extended vegetative phase. We used *Arabis alpina*, a perennial relative of annual *Arabidopsis thaliana*, to study how increasing age and exposure to winter cold (vernalization) coordinate to establish competence to flower. We show that the APETALA2 transcription factor, a target of microRNA miR172, prevents flowering before vernalization. Additionally, miR156 levels decline as *A. alpina* ages, causing increased production of SPL (SQUAMOSA PROMOTER BINDING PROTEIN LIKE) transcription factors and ensuring that flowering occurs in response to cold. The age at which plants respond to vernalization can be altered by manipulating miR156 levels. Although miR156 and miR172 levels are uncoupled in *A. alpina*, miR156 abundance represents the timer controlling age-dependent flowering responses to cold.

Polycarpic perennial plants live for many years and flower each year. To maintain resources and sustain multiple flowering cycles, they tightly control the extent and duration of flowering. In particular, perennials flower only when they reach a certain age and then are described as competent to flower (*1*). Environmental signals induce flowering of older plants, whereas younger plants remain vegetative under the same conditions. Other age-dependent developmental processes, such as the transition from juvenile to adult vegetative phase, are regulated by microRNAs miR156 and miR172 (*2*, *3*). As plants age, the abundance of miR156 declines while miR172 levels increase (*4*–*6*), and these opposing effects are mechanistically coupled in *Arabidopsis thaliana* (*6*). In addition, miR156 and miR172 respectively repress or promote the transition from vegetative growth to flowering (*2*). In *A. thaliana*, the targets of miR156 are the mRNAs of 11 genes encoding SQUAMOSA PROMOTER BINDING PROTEIN LIKE (SPL) transcription factors (*7*–*9*), whereas miR172 regulates six members of the APETALA2 (AP2) transcription factor family (*10*–*12*). Involvement of miR156 and miR172 in regulating age-related competence to flower is difficult to test in the model annual species *A. thaliana* because it responds to environmental cues to induce flowering soon after germination (*13*, *14*). Mutants in *SPL* genes are less sensitive to inductive photoperiods, but how this is related to age-dependent flowering is unclear (*15*). We studied these processes in the model perennial *Arabis alpina* accession Pajares that flowers only if exposed to winter cold (vernalization) when at least 5 weeks old (*16*).

To identify genes that regulate flowering and perennial traits, we first screened a mutagenized population of *A. alpina* (*17*). The *perpetual flowering 2-1* (*pep2-1*) mutant flowered without vernalization and showed perpetual flowering (Fig. 1, A and B). These phenotypes were described previously for *pep1-1*, which is caused by a mutation in the *A. alpina* ortholog of the *A. thaliana FLOWERING LOCUS C* (*FLC*) gene (*17*). The *pep2-1* mutation is not allelic to *pep1-1* (Fig. 1C), and using whole-genome sequencing as well as genetic linkage analysis, we showed that the *pep2-1* phenotype is caused by an amino acid substitution in the DNA binding domain of *A. alpina* APETALA2 (AaAP2) (fig. S1A) (*18*). Based on conservation of synteny of flanking regions, *PEP2* is the ortholog of *A. thaliana AP2* (fig. S1B). The AP2 transcription factor represses flowering and confers floral organ identity in *A. thaliana* (*19*, *20*), and *pep2-1* shows similar floral defects (*18*) (fig. S1C). Additional mutagenesis screens for enhancers of *pep1-1* identified six mutants carrying nonsynonymous changes in *AaAP2* (Fig. 1D, *pep2-2* to *pep2-7*) (*18*). These *pep2 pep1-1* double mutants flowered earlier than *pep1-1* (Fig. 1, E and F, and fig. S1D) and showed floral phenotypes similar to that of *pep2-1* (Fig. 1, G and H), supporting the idea that the *pep2-1* phenotype is due to the mutation in *AaAP2*. Although *AP2* delays flowering of *A. thaliana*, it was not previously reported to confer a vernalization requirement (*19*).

We examined whether PEP2 acts in the same molecular pathway as PEP1. *PEP1* mRNA levels were lower in 2-week-old *pep2-1* seedlings compared to wild type, whereas *PEP2* mRNA levels were not reduced in *pep1-1* mutants (Fig. 2A). PEP1 represses flowering through the *A. alpina SOC1* ortholog (*AaSOC1*) (*16*), which is a promoter of flowering in *A. thaliana* (*21*, *22*). *AaSOC1* mRNA levels were approximately twice as high in *pep2-1* seedlings compared to wild type (Fig. 2A). Therefore, PEP2 likely confers a vernalization requirement in *A. alpina* in part by increasing transcription of *PEP1*. However, PEP2 must also delay flowering by other means because *pep1-1* and *pep2* mutations have additive effects on flowering time (Fig. 1, E and F, and fig. S1, D to F). *PEP2* mRNA levels did not change during prolonged exposure to cold (fig. S2A) or as plants aged and became sensitive to vernalization (Fig. 2, B to D).

AP2 activity is regulated by miR172, and in several species the abundance of this miRNA increases as plants age (*4*, *5*, *10*, *23*, *24*). *PEP2* mRNA also contains a binding site for miR172 (Fig. 1D and fig. S2B). During vegetative growth, miR172 levels did not change, either in *A. alpina* apices (Fig. 2B) or in young plants exposed to cold for several weeks (Fig. 2E). By contrast, the abundance of miR172 increased during cold treatment of older plants that flowered in response to vernalization (Fig. 2E). This increase occurred during flower development, recognized by higher expression of *A. alpina LEAFY* (Fig. 2E) (*16*). In the inflorescence meristem, miR172 and *PEP2* showed complementary spatial expression patterns, with miR172 accumulating mainly in the center and *PEP2* mRNA in the lateral floral primordia (Fig. 2, F and G), as described in *A. thaliana* (*10*, *23*). Thus, miR172 and *PEP2* appear to have conserved roles in flower development of *A. alpina* but do not contribute to the age-dependent initiation of flowering.

To identify genes that confer age-dependent sensitivity to vernalization, we compared global gene expression patterns between apices of 2-week-old and 8-week-old *A. alpina* plants (*25*) (table S1). Expression of several genes encoding SPL transcription factors was increased in apices of older plants (table S2). In *A. alpina*, 15 genes show high sequence similarity and conserved synteny to the *A. thaliana SPL* genes (fig. S3 and table S3), and these fell into three major groups on the basis of their temporal expression patterns (Fig. 3A). The first of these groups comprised six *AaSPL* genes that were more highly expressed in apices of older plants that flower in response to vernalization.

All of the *AaSPL* genes up-regulated in apices of older *A. alpina* plants before or during vernalization contained miR156 binding sites (Fig. 3A). Therefore, we tested the abundance of miR156 at the shoot apex and found that it declined as plants aged, similarly to other species (Fig. 3, B to D). Trough levels of miR156 occurred about 5 weeks after germination, around the time *A. alpina* plants acquired sensitivity to vernalization (*16*). These results suggested that at the main shoot apex,

[1]Max Planck Institute for Plant Breeding Research, Carl-von-Linné-Weg 10, D-50829 Cologne, Germany. [2]Bioinformatics Laboratory, Department of Clinical Epidemiology, Biostatistics, and Bioinformatics, Academic Medical Center, University of Amsterdam, Post Office Box 22700, 1100 DE, Amsterdam, Netherlands.

*These authors contributed equally to this work.
†Present address: Universität des Saarlandes, FR 8.3 Biowissenschaften, Genetik/Epigenetik, Naturwissenschaftlich-Technische Fakultät III, Postfach 151150, 66041 Saarbrücken, Germany.
‡Present address: Division of Biological Sciences, University of California San Diego, 9500 Gilman Drive 0116, La Jolla, CA 92093–0116, USA.
§Corresponding author. E-mail: coupland@mpipz.mpg.de

reduction in miR156 accumulation to trough levels sets the age at which plants become sensitive to vernalization. Axillary branches attain the ability to respond to vernalization independently of the main shoot apex, and this also correlates with a reduction in miR156 levels in the axillary shoot apices (fig. S4).

Exposure of young plants to cold increases the age at which they become able to flower in response to vernalization. Two-week-old *A. alpina* seedlings exposed for more than a year to cold continued to grow but did not flower when returned to warm conditions (fig. S5, A and B). The high miR156 abundance observed in 2-week-old plants remained stably high throughout the cold treatment and declined only after a return to warm conditions (Fig. 3E). This reduction of miR156 accumulation after cold also correlated with flowering when plants were exposed to a second vernalization (Fig. 3E). The levels of miR156 declined slowly in young plants exposed

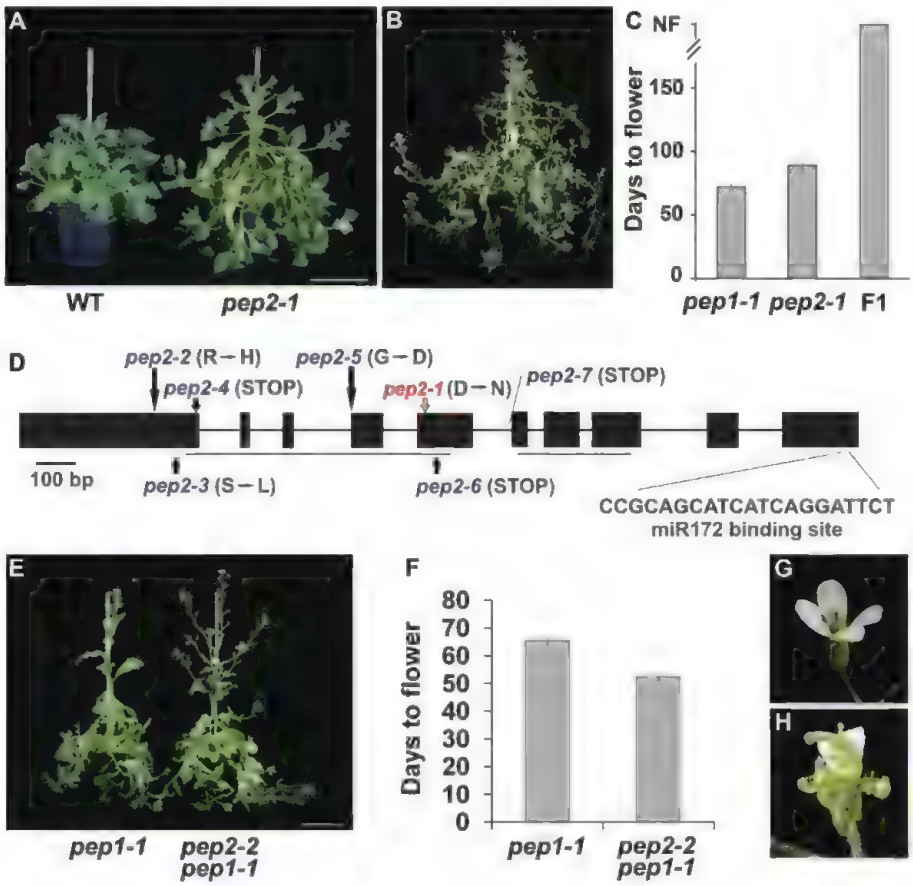

Fig. 1. *PEP2* regulates flowering in response to vernalization and is the *A. alpina* ortholog of *APETALA2*. (**A**) The *pep2-1* mutant flowers without vernalization. WT, wild-type; bar, 9 cm. (**B**) The *pep2-1* mutant flowers perpetually. (**C**) The *pep2-1* and *pep1-1* mutations are not allelic. Flowering time in long days of *pep1-1*, *pep2-1*, and F1 plants derived from crossing the mutants. NF, never flowers. (**D**) Mutations in the *A. alpina* ortholog of *APETALA 2* (*AaAP2*) in *pep2* mutants. The *pep2-1* allele (red) is in wild type whereas *pep2-2* to *pep2-7* (blue) are in *pep1-1* mutant. (**E** to **H**) Mutations in *PEP2* enhance the early flowering of *pep1-1* mutants, and the double mutants show floral homeotic conversion. The *pep1-1* and *pep2-2 pep1-1* mutants 10 weeks after germination (E); flowering time in long days (F). Flower phenotype of *pep1-1* (G) and *pep2-2 pep1-1* (H). Error bars in (C) and (F) indicate standard deviation.

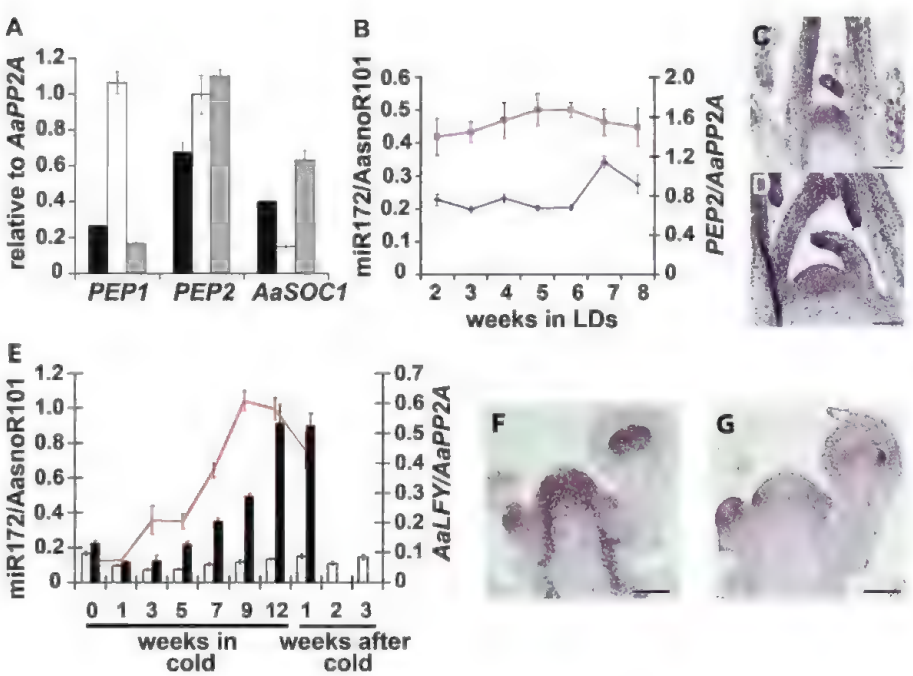

Fig. 2. *PEP2* and miR172 expression patterns and the effect of *pep2-1* on *PEP1* mRNA. (**A**) *PEP1*, *PEP2*, and *AaSOC1* mRNA levels in 2-week-old *pep2-1* (black), wild-type (white), and *pep1-1* (gray) seedlings. (**B**) miR172 (blue) and *PEP2* mRNA (purple) levels in apices of plants growing in long days (LDs). (**C** and **D**) In situ hybridization of *PEP2* mRNA in the main shoot apices of 2-week-old (C) and 8-week-old (D) plants. Bar, 100 μm. (**E**) miR172 abundance in apices of plants exposed to cold. Plants grown for 2 weeks (white) or 8 weeks (black) before exposure to cold. *AaLEAFY* mRNA level (red line) in 8-week-old plants exposed to cold. (**F** and **G**) In situ hybridization of inflorescence meristems. miR172 locked nucleic acid (LNA) probe (F) and *PEP2* mRNA probe (G) hybridized to subsequent sections of the same apex. Plants were grown for 8 weeks, exposed to cold for 12 weeks, and returned to long days for 2 weeks. Bar, 100 μm. Error bars in (A), (B), and (E) indicate standard deviation.

to cold for up to 60 weeks, suggesting that cold strongly delays but does not prevent the reduction in miR156 abundance (Fig. 3F). A similar but less extreme effect was observed in *A. thaliana* (fig. S5C). In addition, Aa pre-miR156a showed the same pattern of accumulation in cold-exposed plants as mature miR156 (fig. S5D), suggesting that transcription of *MIR156* genes is regulated by cold. Thus, young *A. alpina* plants do not respond to vernalization, even if maintained in cold for more than a year, because reduction of *MIR156* transcription is delayed.

The importance of reduced miR156 levels for the age-related response to vernalization was tested with the use of transgenic plants. First, *MIR156b* was expressed at high levels from the heterologous *CaMV35S* promoter in wild-type plants. Eight-week-old overexpressor plants failed to

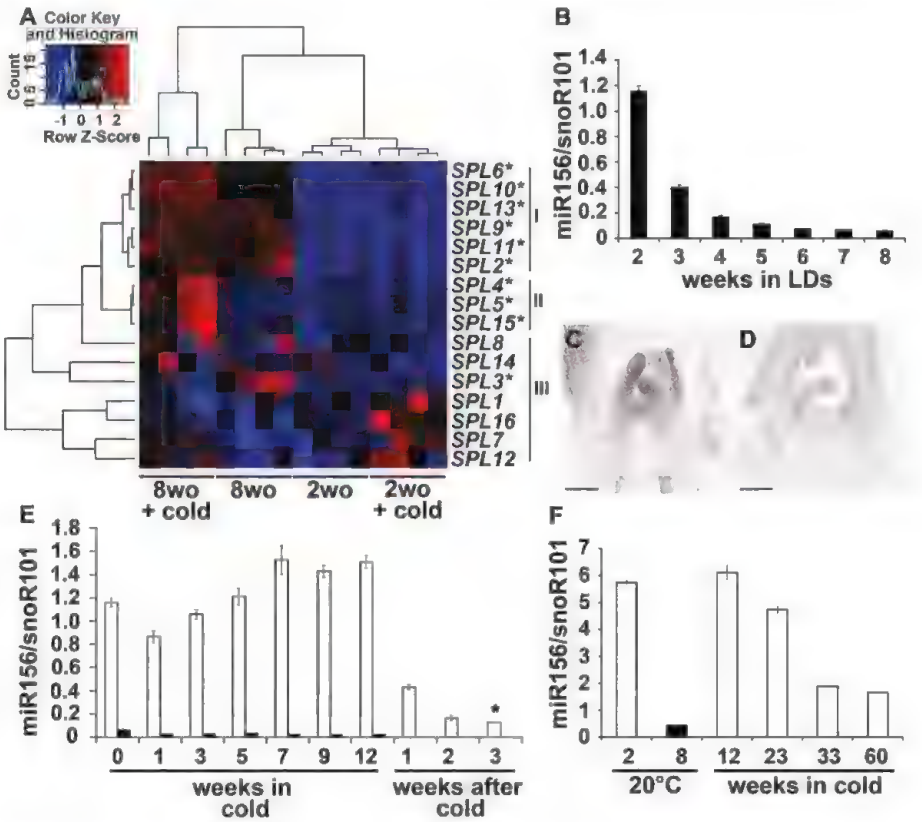

Fig. 3. miR156 abundance is reduced as *A. alpina* plants age and is regulated by cold. (**A**) Heat map of microarray hybridization levels for *SPL* genes of *A. alpina* in apices of 2-week-old (2wo) and 8-week-old (8wo) plants before and after 4 weeks at 4°C (+ cold) (*25*). *SPL* genes are placed in three groups (I, II, III) according to their expression pattern. Asterisks: *A. alpina* genes containing a miR156 binding site. (**B**) miR156 abundance in the main shoot apex of plants growing in long days (LDs). (**C** and **D**) In situ hybridization of miR156 (LNA probe) in apices of 2-week-old (C) and 8-week-old (D) plants growing in long days. Bar, 100 μm. (**E**) miR156 abundance in apices of 2-week-old (white) or 8-week-old (black) plants exposed to cold. Time points as in Fig. 2E. Asterisk: miR156 levels in plants able to flower after a second cold treatment. (**F**) miR156 abundance in apices of 2-week-old plants exposed to cold for up to 60 weeks (white) compared to levels in 8-week-old plants (black). Error bars in (B), (E), and (F) indicate standard deviation.

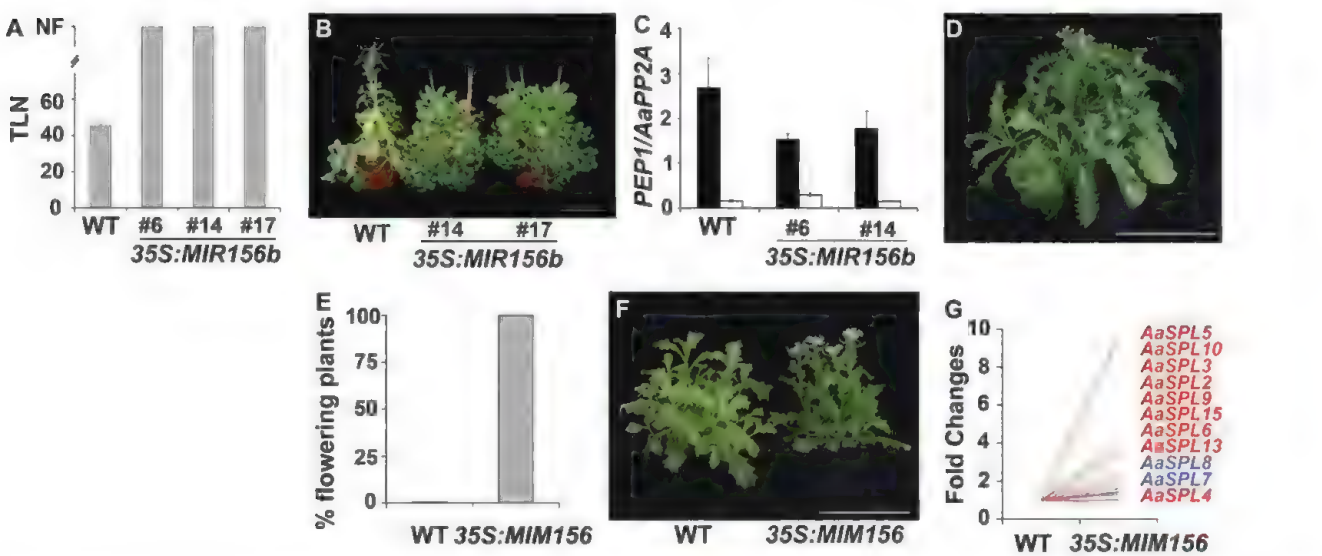

Fig. 4. Reducing miR156 levels accelerates age-related sensitivity to vernalization. (**A** and **B**) Flowering of plants overexpressing *MIR156b*. Cuttings from T1 plants grown for 8 weeks, exposed to cold for 12 weeks, and transferred back to warm long days for 5 weeks (n = 20). WT, wild type; NF, never flowers. (**C**) *PEP1* mRNA expression is down-regulated by vernalization in *35S:MIR156b* plants. *PEP1* mRNA levels after 8 weeks in long days (black) and after transfer to cold for 12 weeks (white). Plants as in (A). (**D**) Wild-type plants overexpressing *MIM156* do not flower in long days. (**E** and **F**) Wild-type plants overexpressing *MIM156* flower when exposed to cold 3 weeks after germination. n = 12. Bars, 12 cm. (**G**) mRNA levels of *AaSPL* genes 3 weeks after germination in WT and transgenic plants overexpressing *MIM156*. *AaSPL* genes targeted (red) and not targeted (blue) by miR156. Error bars in (A) and (C) indicate standard deviation.

flower when exposed to 12 weeks of vernalization, in contrast to control wild-type plants (Fig. 4, A and B). Although these transgenic plants did not flower, *PEP1* mRNA level was reduced during vernalization (Fig. 4C), so miR156 does not prevent flowering in response to vernalization through *PEP1*. The effect of miR156 overexpression was also tested in the *pep1-1* mutant, which flowers in long days without vernalization and shows a temporal pattern of miR156 accumulation similar to that of the wild type (fig. S6A) (*17*). Expression of *MIR156b* from the *CaMV35S* promoter in *pep1-1* strongly delayed flowering when the transgenic plants were grown under long days (fig. S6B). By contrast, in *A. thaliana*, *MIR156b* overexpression strongly delays flowering only in short days, whereas in long days it causes a moderate delay (*4*, *7*, *26*). To test whether lowering miR156 activity reduces the age at which plants become sensitive to vernalization, we overexpressed a mimicry construct (*MIM156*) in *A. alpina* (*27*). These transgenic plants did not flower without vernalization (Fig. 4D) but flowered when vernalized at the age of 3 weeks, whereas wild-type plants of this age did not (Fig. 4, E and F). Transcript levels of several miR156-regulated *AaSPL* genes were increased in apices of 3-week-old *35S:MIM156* lines compared to the wild type (Fig. 4G). Thus, AaSPL transcription factors are essential for the promotion of flowering in perennial *A. alpina*, and the antagonistic regulation of miR156 and *SPL* expression determines the age at which these plants can flower in response to vernalization.

Our findings indicate that miR156 and PEP2/PEP1 act in parallel repressive pathways to ensure that *A. alpina* meristems become competent to flower only if they have reached the appropriate age and have been exposed to winter temperatures (fig. S7). The floral repressor AaTFL1 also delays the acquisition of age-related response to cold (*16*), probably by setting a threshold for AaSPL activation of flowering (fig. S7). In *A. thaliana* and maize, the decrease in miR156 is coupled with an increase in miR172, but we did not observe this relationship in *A. alpina*. Maintaining miR172 at low levels during vegetative growth might allow the activity of its target PEP2 to remain high, ensuring that plants do not flower before they are exposed to cold. In the annual species *A. thaliana* flowering in response to environmental cues can occur in young plants before the decline in miR156 levels, and *SPL* activity is not essential for flowering under inductive photoperiods. Probably other flowering pathways can bypass the requirement for SPL factors in *A. thaliana* under long days, and this is likely important in conferring its rapid cycling life history. Our data illustrate how recruitment of the miR156 and miR172 regulatory modules to control environmental responses contributes to evolution of the plant life cycle and that this can occur rapidly, even among closely related species.

References and Notes

1. S. Bergonzi, M. C. Albani, *J. Exp. Bot.* **62**, 4415 (2011).
2. P. Huijser, M. Schmid, *Development* **138**, 4117 (2011).
3. R. S. Poethig, *Plant Physiol.* **154**, 541 (2010).
4. G. Wu, R. S. Poethig, *Development* **133**, 3539 (2006).
5. G. Chuck, A. M. Cigan, K. Saeteurn, S. Hake, *Nat. Genet.* **39**, 544 (2007).
6. G. Wu *et al.*, *Cell* **138**, 750 (2009).
7. R. Schwab *et al.*, *Dev. Cell* **8**, 517 (2005).
8. M. W. Rhoades *et al.*, *Cell* **110**, 513 (2002).
9. M. Gandikota *et al.*, *Plant J.* **49**, 683 (2007).
10. X. M. Chen, *Science* **303**, 2022 (2004).
11. M. Schmid *et al.*, *Development* **130**, 6001 (2003).
12. M. J. Aukerman, H. Sakai, *Plant Cell* **15**, 2730 (2003).
13. D. Mozley, B. Thomas, *J. Exp. Bot.* **46**, 173 (1995).
14. M. Koornneef, C. J. Hanhart, J. H. van der Veen, *Mol. Gen. Genet.* **229**, 57 (1991).
15. S. Schwarz, A. V. Grande, N. Bujdoso, H. Saedler, P. Huijser, *Plant Mol. Biol.* **67**, 183 (2008).
16. R. Wang *et al.*, *Plant Cell* **23**, 1307 (2011).
17. R. H. Wang *et al.*, *Nature* **459**, 423 (2009).
18. K. J. V. Nordström *et al.*, *Nat. Biotechnol.* **31**, 325 (2013).
19. L. Yant *et al.*, *Plant Cell* **22**, 2156 (2010).
20. J. L. Bowman, D. R. Smyth, E. M. Meyerowitz, *Plant Cell* **1**, 37 (1989).
21. H. Lee *et al.*, *Genes Dev.* **14**, 2366 (2000).
22. A. Samach *et al.*, *Science* **288**, 1613 (2000).
23. H. Wollmann, E. Mica, M. Todesco, J. A. Long, D. Weigel, *Development* **137**, 3633 (2010).
24. N. Tanaka *et al.*, *Plant Cell* **23**, 2143 (2011).
25. Supplementary materials are available on *Science* Online.
26. J. W. Wang, B. Czech, D. Weigel, *Cell* **138**, 738 (2009).
27. J. M. Franco-Zorrilla *et al.*, *Nat. Genet.* **39**, 1033 (2007).

Acknowledgments: We thank E. Willing, G. Velikkakam, and the "*A. alpina* genome consortium" for access to genomic information and Y. Zeng for technical support. We thank members of G.C.'s laboratory and P. Huijser for critical reading of the manuscript and D. Weigel for *MIR156* constructs and comments on the manuscript. We acknowledge funding from Deutsche Forschungsgemeinschaft SPP1530 grants to G.C. and M.C.A., the Max Planck Genome Centre, and a core grant from the Max Planck Society. GenBank accession numbers are GSE40455 (microarray data), KC815948 to KC815963 (AaSPLs), KC831439 (PEP2), and KC848668 (Aapre-miR156a). Materials described here are available from G.C. subject to a Material Transfer Agreement with the Max Planck Institute for Plant Breeding Research.

Supplementary Materials

www.sciencemag.org/cgi/content/full/340/6136/1094/DC1
Materials and Methods
Supplementary Text
Figs. S1 to S9
Tables S1 to S4
References

17 December 2012; accepted 13 March 2013
10.1126/science.1234116

Molecular Basis of Age-Dependent Vernalization in *Cardamine flexuosa*

Chuan-Miao Zhou,[1] Tian-Qi Zhang,[1,2] Xi Wang,[3] Sha Yu,[1,2] Heng Lian,[1] Hongbo Tang,[1] Zheng-Yan Feng,[1,2] Judita Zozomova-Lihová,[4] Jia-Wei Wang[1,3]*

Plants flower in response to many varied cues, such as temperature, photoperiod, and age. The floral transition of *Cardamine flexuosa*, a herbaceous biennial-to-perennial plant, requires exposure to cold temperature, a treatment known as vernalization. *C. flexuosa* younger than 5 weeks old are not fully responsive to cold treatment. We demonstrate that the levels of two age-regulated microRNAs, miR156 and miR172, regulate the timing of sensitivity in response to vernalization. Age and vernalization pathways coordinately regulate flowering through modulating the expression of *CfSOC1*, a flower-promoting MADS-box gene. The related annual *Arabidopsis thaliana*, which has both vernalization and age pathways, does not possess an age-dependent vernalization response. Thus, the recruitment of age cue in response to environmental signals contributes to the evolution of life cycle in plants.

Plants show diverse life-cycle strategies. Annual plants go from germination to death within 1 year. Biennial and perennial plants take 2 or more years to complete their life cycles. Monocarpic perennials, such as bamboo, bloom once then die, whereas polycarpic perennials preserve some meristems in the vegetative state to sustain flowering in subsequent years (*1*–*3*). In *Arabidopsis thaliana*, an annual plant, the floral transition is controlled by various exogenous and endogenous cues, such as photoperiod or day length, transient exposure to low or high temperature, hormone, and age (*4*–*7*).

We studied the molecular mechanisms that regulate flowering in the biennial-to-perennial wavy bittercress (*Cardamine flexuosa*), a herbaceous Brassicaceae widely distributed in Europe (*8*) (supplementary text). Under constant temperature (23°C) and humidity (50%) conditions, *C. flexuosa* exhibited a typical polycarpic perennial growth habit. Plants did not flower when grown continuously in long (16 hours of light) or short (8 hours of light) days (Fig. 1A and fig. S1). Exposure of 8-week-old long-day plants to short days did not induce flowering (fig. S1I). *C. flexuosa*

[1]National Key Laboratory of Plant Molecular Genetics (NKLPMG), Institute of Plant Physiology and Ecology (SIPPE), Shanghai Institutes for Biological Sciences (SIBS), Shanghai 200032, P. R. China. [2]University of Chinese Academy of Sciences (CAS), Shanghai 200032, P.R. China. [3]Department of Molecular Biology, Max Planck Institute (MPI) for Developmental Biology, D-72076 Tübingen, Germany. [4]Institute of Botany, Slovak Academy of Sciences, SK-845 23 Bratislava, Slovak Republic.

*Corresponding author. E-mail: jwwang@sibs.ac.cn

plants flowered only when exposed to cold temperature (4°C) for 2 months (Fig. 1B and fig. S1I), a treatment called vernalization. After seed maturation, all inflorescences senesced and died, whereas the rosette and axillary shoots (branches) initiated after vernalization remained alive and vegetative (Fig. 1C). A second round of flowering could be induced by another 2-month cold treatment (fig. S1H).

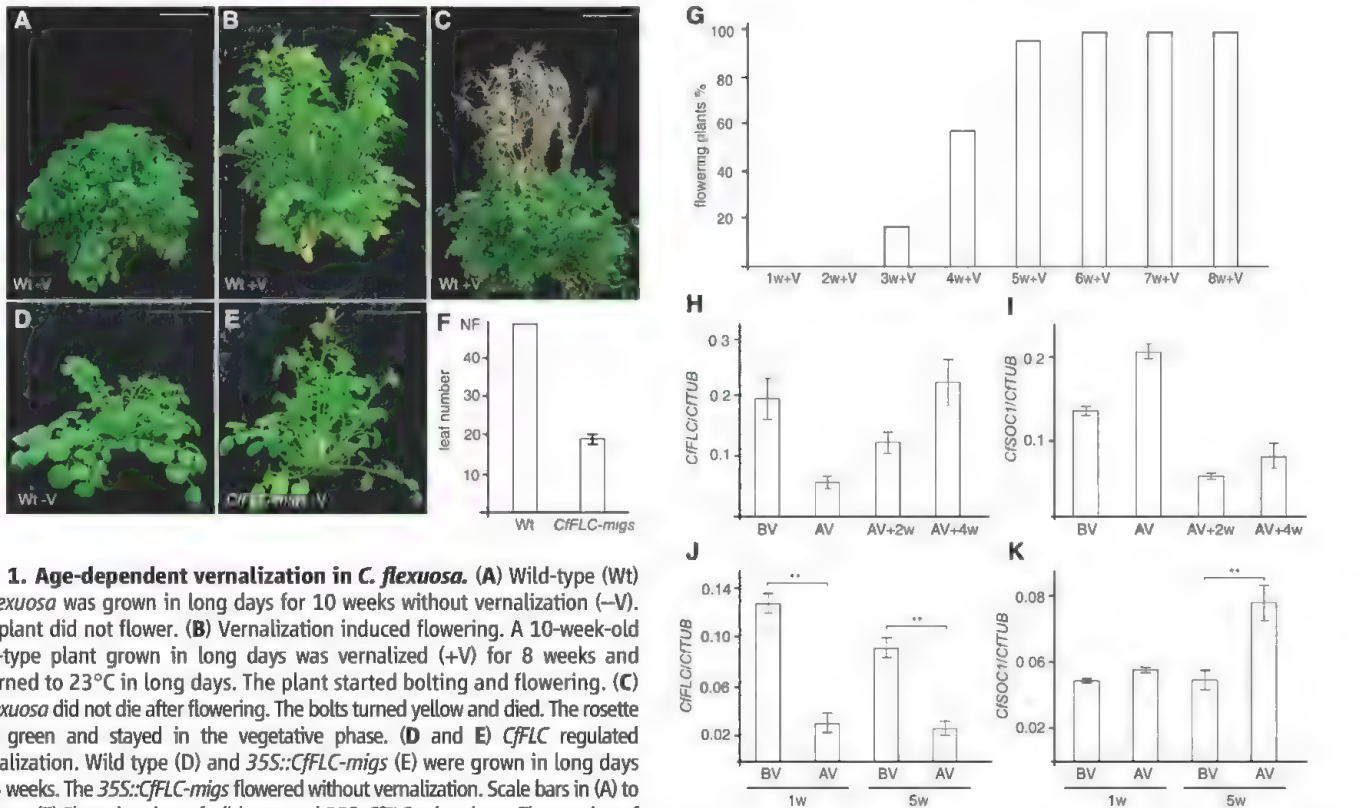

Fig. 1. Age-dependent vernalization in *C. flexuosa*. (**A**) Wild-type (Wt) *C. flexuosa* was grown in long days for 10 weeks without vernalization (–V). The plant did not flower. (**B**) Vernalization induced flowering. A 10-week-old wild-type plant grown in long days was vernalized (+V) for 8 weeks and returned to 23°C in long days. The plant started bolting and flowering. (**C**) *C. flexuosa* did not die after flowering. The bolts turned yellow and died. The rosette kept green and stayed in the vegetative phase. (**D** and **E**) *CfFLC* regulated vernalization. Wild type (D) and *35S::CfFLC-migs* (E) were grown in long days for 5 weeks. The *35S::CfFLC-migs* flowered without vernalization. Scale bars in (A) to (E), 5 cm. (**F**) Flowering time of wild-type and *35S::CfFLC-migs* plants. The number of leaves when the plants started to flower was scored. NF indicates never flowering; error bar indicates SD. $n = 13$. (**G**) Age-dependent vernalization in *C. flexuosa*. Plants of different ages (from 1 to 8 weeks old) were vernalized for 2 months and returned to 23°C long days. Number of flowered plants was scored. $n = 20$. 1w+V, plants grown for 1 week in long days and then exposed to vernalization. (**H** and **I**) Temporal expression pattern of *CfFLC* (H) and *CfSOC1* (I). Wild-type plants were grown in long days for 5 weeks before cold treatment. BV, before vernalization; AV, after a 2-month vernalization treatment; AV+2w, plants grown in long days for 2 weeks after vernalization. RNA levels in leaves were measured by real-time quantitative polymerase chain reaction (qPCR). The expression levels were normalized to that of *CfTUB*. The data presented are the means of two technical replicates; error bars indicate SD. (**J** and **K**) Expression of *CfFLC* (J) and *CfSOC1* (K) in response to vernalization and age. One- or 5-week-old *C. flexuosa* plants were subjected to vernalization treatment for 2 months. $^{**}P < 0.001$, Student's *t* test.

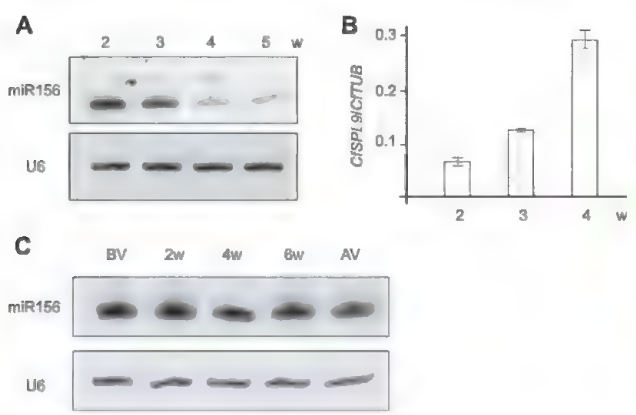

Fig. 2. miR156 contributes to age-dependent vernalization. (**A** and **B**) Expression of miR156 (A) and *CfSPL9* (B) during development. Wild-type plants of different ages (2 to 5 weeks old) were used for expression analyses. miR156 levels were monitored by small RNA blots. The level of U6 was monitored as the loading control. Error bars, SD. (**C**) Expression of miR156 during vernalization. One-week-old wild type grown in long days was vernalized for 2 months. The expression of miR156 was examined every 2 weeks during vernalization. (**D** to **G**) Vernalization response of transgenic plants. One-week-old wild-type (D), 1-week-old *35S::MIM156* (E), 5-week-old wild-type (F), and 5-week-old *35S::MIR156* (G) plants were vernalized for 2 months and returned to 23°C long days. Scale bars in (D) to (G), 5 cm. (**H**) Percentage of flowered plants after vernalization treatment. Plants of different ages (from 1 to 10 weeks old) were vernalized for 2 months and returned to 23°C long days. $n = 20$.

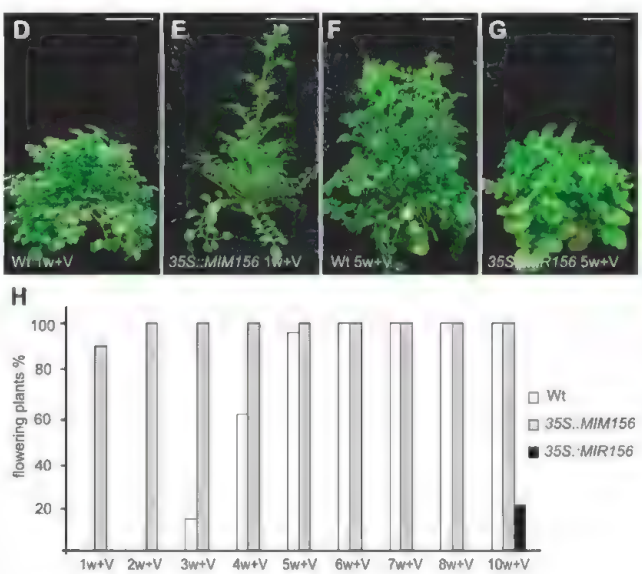

The vernalization response in the perennial Brassicaceae *Arabis alpina* is controlled by the MADS-box gene *PERPETUAL FLOWERING 1* (*PEP1*), an ortholog of *A. thaliana FLOWERING LOCUS C* (*AtFLC*) (*7*, *9*). We isolated *CfFLC*, an *AtFLC* homolog, in *C. flexuosa* (fig. S2 and supplementary text). When we overexpressed *CfFLC* in *A. thaliana*, flowering was delayed in long days (fig. S3A), indicating that CfFLC acts as a flowering repressor. To analyze the function of *CfFLC* in *C. flexuosa*, we generated *CfFLC* knockdown plants with the microRNA-induced gene silencing (MIGS) technology (*35S::CfFLC-migs*) (*10*). These plants had about fivefold less *CfFLC* expression than wild type (fig. S3B) and were able to flower without vernalization (Fig. 1, D to F). All subsequent axillary shoots were floral (fig. S3C). Thus, *CfFLC* encodes an ortholog of *A. alpina PEP1* and regulates perennial flowering in *C. flexuosa*.

Wild-type plants were grown in long days for 5 weeks and then exposed to cold temperature for 8 weeks. Cold treatment decreased the transcript levels of *CfFLC* by three-fourths (Fig. 1H). After return to 23°C long days, *CfFLC* mRNA levels gradually increased, reaching the same level as that before vernalization within 1 month (Fig. 1H). Therefore, in the perennials *C. flexuosa* and *A. alpina*, *FLC* expression is only transiently suppressed by vernalization, whereas vernalization stably represses *FLC* expression in the annual *A. thaliana* (*7*, *11*).

In *A. thaliana*, flowering time pathways are integrated by several integrator genes, including *SUPPRESSOR OF OVEREXPRESSION OF CONSTANS1* (*SOC1*) (*12*). Overexpression of *C. flexuosa SOC1* (*CfSOC1*) in *C. flexuosa* bypassed the vernalization requirement (figs. S4 and S5), suggesting that *CfSOC1* acts downstream of the vernalization pathway. The expression pattern of *CfSOC1* was opposite to that of *CfFLC*, with the expression transiently increased upon cold treatment (Fig. 1I).

We found that the ability of cold exposure to cause vernalization of *C. flexuosa* plants was age-dependent. Plants less than 5 weeks old were not fully responsive to cold treatment (Fig. 1G). The expression of *CfFLC* was repressed by vernalization in both young (1-week-old) and old (5-week-old) plants (Fig. 1J). However, cold treatment induced an increase of *CfSOC1* expression in old but not young plants (Fig. 1K). We infer that the insensitivity of young plants to cold treatment is due to a defect in activation of *CfSOC1* rather than a change in the repression of *CfFLC*.

MicroRNA156 (miR156), which targets a group of *SQUAMOSA PROMOTER BINDING–LIKE* (*SPL*) transcription factors, regulates the age-dependent developmental transitions (*13*–*16*). As in *A. thaliana*, maize, and poplar, miR156 levels correlated with age in *C. flexuosa* (*13*, *14*, *17*, *18*), being most abundant in seedlings (Fig. 2A). The miR156 target gene *CfSPL9* showed an opposite expression pattern (Fig. 2B and figs. S6 and S7). miR156 level did not decline in 1-week-old seedlings during a 2-month cold treatment (Fig. 2C).

To determine whether miR156 contributes to the age-dependent vernalization response, we generated transgenic *C. flexuosa* plants that overexpressed either miR156 (*35S::MIR156*) or a target mimicry of miR156 (*35S::MIM156*), in which miR156 activity is attenuated (*13*) (figs. S8 and S9). Neither *35S::MIM156* nor *35S::MIR156* flowered without vernalization (fig. S8D). Wild-type, *35S::MIR156*, and *35S::MIM156* plants were grown in long days for 1 week or 5 weeks and then exposed to 8 weeks of cold temperature. One-week-old wild-type plants were insensitive to cold treatment, whereas flowering was readily induced in 1-week-old *35S::MIM156* plants (Fig. 2, D, E, and H). The *35S::MIR156* plants became less insensitive to vernalization (Fig. 2, F to H), even when much older. At 10 weeks of age, only 20% of *35S::MIR156* plants responded to vernalization (Fig. 2H). These results illustrate a correlation between miR156 abundance and the sensitivity in response to vernalization.

To understand the molecular mechanism by which miR156 contributes to the process to make plants susceptible to vernalization, we examined the expression of *CfFLC* and *CfSOC1*. The response of *CfFLC* to cold treatment was independent of miR156 levels (fig. S10A). Upon cold treatment, *CfSOC1* expression was elevated in 1-week-old *35S::MIM156* plants but not in wild type at the

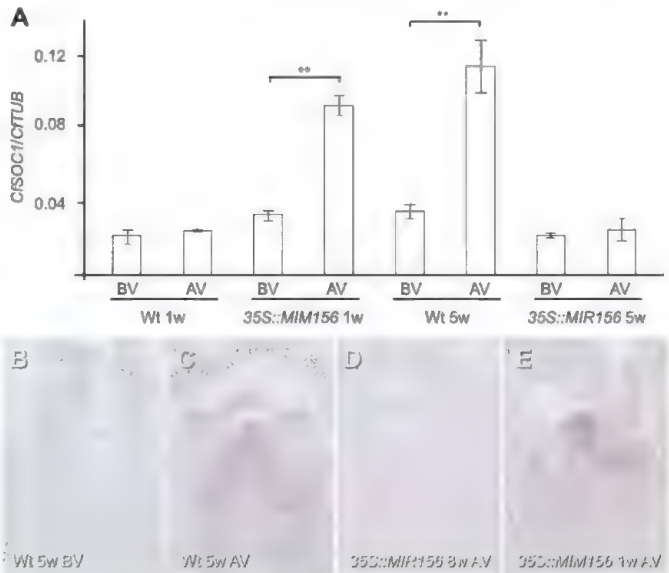

Fig. 3. *CfSOC1* acts downstream of vernalization and age pathways. (A) Expression of *CfSOC1* in the shoot apices. Wild type, *35S::MIM156*, and *35S::MIR156* plants were grown in long days for 1 or 5 weeks. The plants were then vernalized for 2 months. $^{**}P < 0.001$; Student's *t* test; error bars, SD. **(B** to **E)** Expression of *CfSOC1* in the shoot apices of 5-week-old wild type before vernalization (B), 5-week-old wild type after vernalization (C), 8-week-old *35S::MIR156* after vernalization (D), and 1-week-old *35S::MIM156* after vernalization (E). Scale bars, 50 μm.

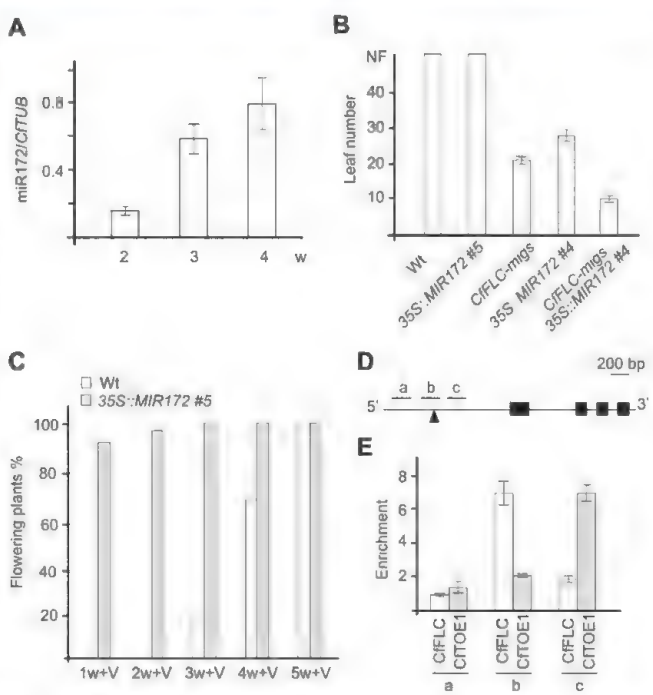

Fig. 4. Integration of age and vernalization pathways in *C. flexuosa*. (A) Expression of miR172 during development. Wild-type plants of different ages (from 2 to 4 weeks old) were used for real-time qPCR analyses. Error bars, SD. **(B)** Flowering time measurement. Plants were grown in long days. $n = 12$. **(C)** Vernalization response of wild-type and *35S::MIR172* plants (line 5). Plants of different ages (from 1 to 5 weeks old) were vernalized for 2 months and returned to 23°C long days. Wild type, $n = 10$. *35S::MIR172* (line 5), $n = 12$. **(D)** Schematic of *CfSOC1* genomic region. Solid lines, promoter or introns. Black boxes, exons. The first four exons are shown. Three regions (a to c) were chosen for qPCR analyses. The black triangle stands for CArG boxes. **(E)** ChIP analyses of *35S::CfTOE1-3xHA* and *35S::CfFLC-3xHA* plants. Crude chromatin extracts were immunoprecipitated with antibody against hemagglutinin. Purified ChIP and input DNAs were used for qPCR analyses. Error bars, SD.

same age (Fig. 3, A and E). *CfSOC1* transcripts in the shoot apical meristems were detected when 5-week-old wild type had been vernalized (Fig. 3, B and C). In *35S::MIR156* plants, *CfSOC1* was underexpressed even when 8-week-old plants were vernalized (Fig. 3D). *A. alpina TERMINAL FLOWER1* (*AaTFL1*) regulates the perennial flowering in *A. alpina* (*19*). Expression of *CfTFL1*, a homolog of *AaTFL1* in *C. flexuosa* (fig. S11), was independent of age and miR156 levels (fig. S12).

miR156 promotes the juvenile-to-adult transition through miR172, which targets *APETALA2* (*AP2*)–like genes in *A. thaliana* (*14*, *20*). The level of miR172 increased as *C. flexuosa* aged (Fig. 4A). miR172 accumulation was reduced in *35S::MIR156* and enhanced in *35S::MIM156* plants (fig. S9). Thus, as in *A. thaliana*, maize, rice, and poplar (*14*, *17*, *21*, *22*), miR172 is regulated by miR156 in *C. flexuosa*.

To understand how miR172 regulates flowering in *C. flexuosa*, we generated the transgenic plants overexpressing miR172 (*35S::MIR172*). These *35S::MIR172* plants exhibited varying degrees of vernalization response in accordance with their miR172 levels (fig. S13). Wild-type plants did not fully respond to vernalization until they were 5 weeks old. However, 1-week-old transgenic plants with a moderate miR172 level (line 5) flowered when vernalized (Fig. 4, B and C). The transgenic plants with the highest miR172 level (line 4) flowered without exposure to cold temperature (Fig. 4B and fig. S14). Expression analyses indicated that miR172 level did not change in response to cold treatment and that *CfFLC* expression was not affected by miR172 overexpression (fig. S10, B and C). Epistasis analysis further showed that miR172 promotes flowering in parallel with *CfFLC* (Fig. 4B and fig. S14).

In *A. thaliana*, FLC and miR172-targeted AP2-like proteins repress flowering through *SOC1* (*23*–*26*). We identified a homolog of *A. thaliana* miR172 target *TARGET OF EAT1* (*TOE1*), *CfTOE1*, in *C. flexuosa* (fig. S15) (*27*). The transgenic *C. flexuosa* plants that overexpressed in-frame fusions of *CfFLC* or *CfTOE1* to triple hemagglutinin epitope tags (3xHA) (*35S::CfFLC-3xHA* or *35S::CfTOE1-3xHA*) did not flower in long days after vernalization (fig. S16). Chromatin immunoprecipitation (ChIP) assays indicated that CfFLC and CfTOE1 bound to the promoter region of *CfSOC1* (Fig. 4, D and E, and supplementary text), indicating that CfFLC and CfTOE1 regulate *C. flexuosa* flowering through repressing *CfSOC1*.

We suggest that age and vernalization cues coordinate to regulate floral induction in *C. flexuosa* by removal of two repressors, CfFLC, which is repressed by vernalization, and CfTOE1, which is down-regulated by the miR156-SPL-miR172 cascade (fig. S17). In the young seedling, high levels of miR156 lead to the accumulation of CfTOE1. CfTOE1 represses *CfSOC1* expression regardless of vernalization; as the plant grows, the endogenous sugar content is elevated, resulting in a decreased level of miR156 and the concomitant increase in miR172 (*28*–*30*). As a consequence, the occupation of CfTOE1 at *CfSOC1* promoter was reduced, leading to a cold-sensitive state. Flowering can be successfully induced when *CfFLC* expression is reduced by vernalization.

The integration of age and vernalization pathways offers an advantage for the perennial growth habit by ensuring that plants do not flower until they develop axillary vegetative shoots and sufficient biomass. Although both vernalization and age pathways operate in the annual *A. thaliana*, this species does not have a pronounced age-dependent vernalization response. The relative stronger contribution of the age pathway in *C. flexuosa* suggests a scenario in which the species-specific imbalance of repressive versus inductive signals determines the life-cycle strategy of flowering plants.

References and Notes

1. R. Amasino, *Genome Biol.* **10**, 228 (2009).
2. M. C. Albani, G. Coupland, *Curr. Top. Dev. Biol.* **91**, 323 (2010).
3. S. Bergonzi, M. C. Albani, *J. Exp. Bot.* **62**, 4415 (2011).
4. I. Bäurle, C. Dean, *Cell* **125**, 655 (2006).
5. R. Amasino, *Plant J.* **61**, 1001 (2010).
6. F. Andrés, G. Coupland, *Nat. Rev. Genet.* **13**, 627 (2012).
7. J. Song, A. Angel, M. Howard, C. Dean, *J. Cell Sci.* **125**, 3723 (2012).
8. J. Lihová, K. Marhold, H. Kudoh, M. A. Koch, *Am. J. Bot.* **93**, 1206 (2006).
9. M. C. Albani *et al.*, *PLoS Genet.* **8**, e1003130 (2012).
10. F. F. de Felippes, J. W. Wang, D. Weigel, *Plant J.* **70**, 541 (2012).
11. R. Wang *et al.*, *Nature* **459**, 423 (2009).
12. A. Samach *et al.*, *Science* **288**, 1613 (2000).
13. J. W. Wang, B. Czech, D. Weigel, *Cell* **138**, 738 (2009).
14. G. Wu *et al.*, *Cell* **138**, 750 (2009).
15. R. S. Poethig, *Plant Physiol.* **154**, 541 (2010).
16. P. Huijser, M. Schmid, *Development* **138**, 4117 (2011).
17. G. Chuck, A. M. Cigan, K. Saeteurn, S. Hake, *Nat. Genet.* **39**, 544 (2007).
18. G. Wu, R. S. Poethig, *Development* **133**, 3539 (2006).
19. R. Wang *et al.*, *Plant Cell* **23**, 1307 (2011).
20. X. Chen, *Science* **303**, 2022 (2004); 10.1126/science.1088060.
21. J. W. Wang *et al.*, *PLoS Genet.* **7**, e1002012 (2011).
22. K. Xie *et al.*, *Plant Physiol.* **158**, 1382 (2012).
23. S. R. Hepworth, F. Valverde, D. Ravenscroft, A. Mouradov, G. Coupland, *EMBO J.* **21**, 4327 (2002).
24. I. Searle *et al.*, *Genes Dev.* **20**, 898 (2006).
25. D. Li *et al.*, *Dev. Cell* **15**, 110 (2008).
26. J. Mathieu, L. J. Yant, F. Mürdter, F. Küttner, M. Schmid, *PLoS Biol.* **7**, e1000148 (2009).
27. M. J. Aukerman, H. Sakai, *Plant Cell* **15**, 2730 (2003).
28. L. Yang, M. Xu, Y. Koo, J. He, R. S. Poethig, *eLife* **2**, e00260 (2013).
29. S. Yu *et al.*, *eLife* **2**, e00269 (2013).
30. V. Wahl *et al.*, *Science* **339**, 704 (2013).

Acknowledgments: We thank I. R. Somoza and D. Weigel (MPI, Tübingen) for commenting on the manuscript, S. Bergonzi and G. Coupland (MPI, Köln) for exchanging unpublished results, and Y.-L. Guo (Institute of Botany, CAS, Beijing) for suggestion on phylogenetic analyses. The early phase of the work was conducted at the MPI for Developmental Biology, where it was supported by Max Planck Society funds to D. Weigel. The majority of this work was conducted at SIPPE and supported by grants from National Natural Science Foundation of China (31222029 and 912173023), State Key Basic Research Program of China (2013CB127000), Shanghai Pujiang Program (12PJ1409900), Recruitment Program of Global Experts (China), and NKLPMG (SIPPE, SIBS) to J.-W.W., and Open Project Program of NKLPMG (SIPPE, SIBS) to X.W.

Supplementary Materials

www.sciencemag.org/cgi/content/full/340/6136/1097/DC1
Materials and Methods
Supplementary Text
Figs. S1 to S20
Table S1
References (*31*–*42*)

20 December 2012; accepted 9 April 2013
10.1126/science.1234340

A Tumor Suppressor Complex with GAP Activity for the Rag GTPases That Signal Amino Acid Sufficiency to mTORC1

Liron Bar-Peled,[1,2]* Lynne Chantranupong,[1,2]* Andrew D. Cherniack,[4] Walter W. Chen,[1,2] Kathleen A. Ottina,[1,2] Brian C. Grabiner,[1,2] Eric D. Spear,[7] Scott L. Carter,[4] Matthew Meyerson,[4,5,6] David M. Sabatini[1,2,3,4]†

The mTOR complex 1 (mTORC1) pathway promotes cell growth in response to many cues, including amino acids, which act through the Rag guanosine triphosphatases (GTPases) to promote mTORC1 translocation to the lysosomal surface, its site of activation. Although progress has been made in identifying positive regulators of the Rags, it is unknown if negative factors also exist. Here, we identify GATOR as a complex that interacts with the Rags and is composed of two subcomplexes we call GATOR1 and -2. Inhibition of GATOR1 subunits (DEPDC5, Nprl2, and Nprl3) makes mTORC1 signaling resistant to amino acid deprivation. In contrast, inhibition of GATOR2 subunits (Mios, WDR24, WDR59, Seh1L, and Sec13) suppresses mTORC1 signaling, and epistasis analysis shows that GATOR2 negatively regulates DEPDC5. GATOR1 has GTPase-activating protein (GAP) activity for RagA and RagB, and its components are mutated in human cancer. In cancer cells with inactivating mutations in GATOR1, mTORC1 is hyperactive and insensitive to amino acid starvation, and such cells are hypersensitive to rapamycin, an mTORC1 inhibitor. Thus, we identify a key negative regulator of the Rag GTPases and reveal that, like other mTORC1 regulators, Rag function can be deregulated in cancer.

The mTOR complex 1 (mTORC1) kinase is a master regulator of growth, and its deregulation is common in human disease, including cancer and diabetes (*1*). In response to a diverse set of environmental inputs, including amino acid levels, mTORC1 regulates many

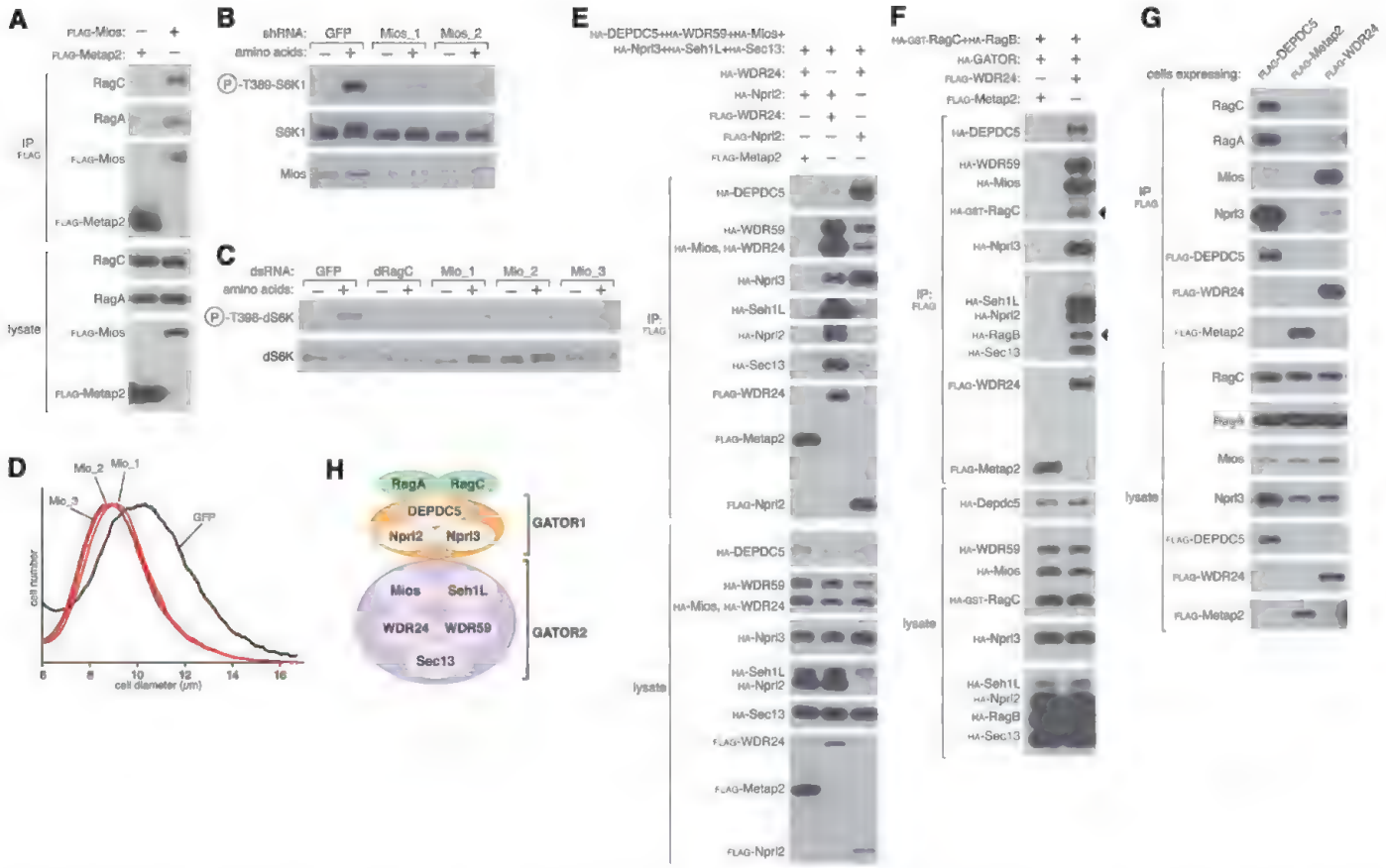

Fig. 1. GATOR is a Rag-interacting complex, whose Mios component is necessary for the activation of mTORC1 by amino acids. (**A**) Mios interacts with endogenous RagA and RagC. HEK-293T cells were transfected with the indicated cDNAs in expression vectors. Cells were treated with a cell-permeable chemical cross-linker, lysates were prepared and subjected to FLAG immunoprecipitation (IP) followed by immunoblotting for the indicated proteins. (**B**) Mios is necessary for the activation of the mTORC1 pathway by amino acids. HEK-293T cells expressing short hairpin RNAs (shRNAs) targeting GFP or Mios were starved of amino acids for 50 min or starved and then restimulated with amino acids for 10 min. Cell lysates were analyzed for the phosphorylation state of S6K1. (**C**) S2 cells treated with dsRNAs targeting Mio or GFP were starved of amino acids for 90 min or starved and restimulated with amino acids for 30 min. The indicated proteins were detected by immunoblotting. (**D**) Cell size histogram of S2 cells after dsRNA-mediated depletion of Mio. (**E** and **F**) GATOR is an octomeric complex defined by two distinct subcomplexes and interacts with the Rag GTPases. HEK-293T cells were transfected and processed as in (**A**) with the exclusion of the cross-linking reagent, and cell lysates and FLAG immunoprecipitates were subjected to immunoblotting. (**G**) HEK-293T cells stably expressing FLAG-tagged DEPDC5 or WDR24 were lysed, and cell lysates and FLAG immunoprecipitates were analyzed by immunoblotting for endogenous RagA, RagC, Mios, and Nprl3. (**H**) Schematic summarizing GATOR-Rag interactions. GATOR2 (Mios, Seh1L, WDR24, WDR59, and Sec13) interacts with GATOR1 (DEPDC5, Nprl2, and Nprl3), which likely then binds the Rags.

anabolic and catabolic processes, such as protein synthesis and autophagy (*1*, *2*). The sensing of amino acids by mTORC1 initiates from within the lysosomal lumen (*3*) and requires a signaling machine associated with the lysosomal membrane that consists of the Rag guanosine triphosphatases (GTPases) (*4*, *5*), the Ragulator complex (*6*, *7*), and the vacuolar adenosine triphosphatase (V-ATPase) (*3*). The Rag GTPases exist as obligate heterodimers of RagA or RagB, which are highly homologous, with either RagC or RagD, which are also very similar to each other (*4*, *5*, *8*). Through a poorly understood mechanism requiring the V-ATPase, luminal amino acids activate the guanine nucleotide exchange factor (GEF) activity of Ragulator toward RagA and RagB that, when guanosine triphosphate (GTP)–loaded, recruits mTORC1 to the lysosomal surface (*7*). There, mTORC1 interacts with its activator Rheb, which is regulated by many upstream signals, including growth factors (*1*). Upon amino acid withdrawal, RagA and RagB become guanosine diphosphate (GDP)–bound (*4*), and mTORC1 leaves the lysosomal surface, and that leads to its inhibition. The negative regulators that inactivate the Rag GTPases are unknown.

We suspected that important regulators of the Rags might have escaped prior identification because their interactions with the Rags are too weak to persist under standard purification conditions. Thus, to preserve unstable protein complexes (*9*), we treated human embryonic kidney–293T (HEK-293T) cells expressing FLAG-tagged RagB with a chemical cross-linker and identified via mass spectrometry proteins that coimmunoprecipitate with FLAG-RagB. This analysis revealed the presence in the immunoprecipitates of known Rag-interacting proteins, as well as Mios, a 100-kD WD40-repeat protein not previously studied (fig. S1A). Consistent with this finding, endogenous RagA and RagC coimmunoprecipitated with recombinant Mios expressed in HEK-293T cells and isolated under similar purification conditions (Fig. 1A). Suppression of Mios, by RNA interference (RNAi) in human cells, strongly inhibited the amino acid–induced activation of mTORC1,

[1]Whitehead Institute for Biomedical Research and Massachusetts Institute of Technology, Department of Biology, 9 Cambridge Center, Cambridge, MA 02142, USA. [2]Koch Institute for Integrative Cancer Research, 77 Massachusetts Avenue, Cambridge, MA 02139, USA. [3]Howard Hughes Medical Institute, Department of Biology, Massachusetts Institute of Technology, Cambridge, MA 02139, USA. [4]Broad Institute of Harvard and Massachusetts Institute of Technology, 7 Cambridge Center, Cambridge, Cambridge, MA 02142, USA. [5]Department of Medical Oncology, Dana-Farber Cancer Institute, Harvard Medical School, 450 Brookline Avenue, Boston, MA 02215, USA. [6]Department of Pathology, Harvard Medical School, 25 Shattuck Street, Boston, MA 02115, USA. [7]Department of Cell Biology, John Hopkins University School of Medicine, Baltimore, MD 21205, USA.

*These authors contributed equally to this work
†Corresponding author. E-mail: sabatini@wi.mit.edu

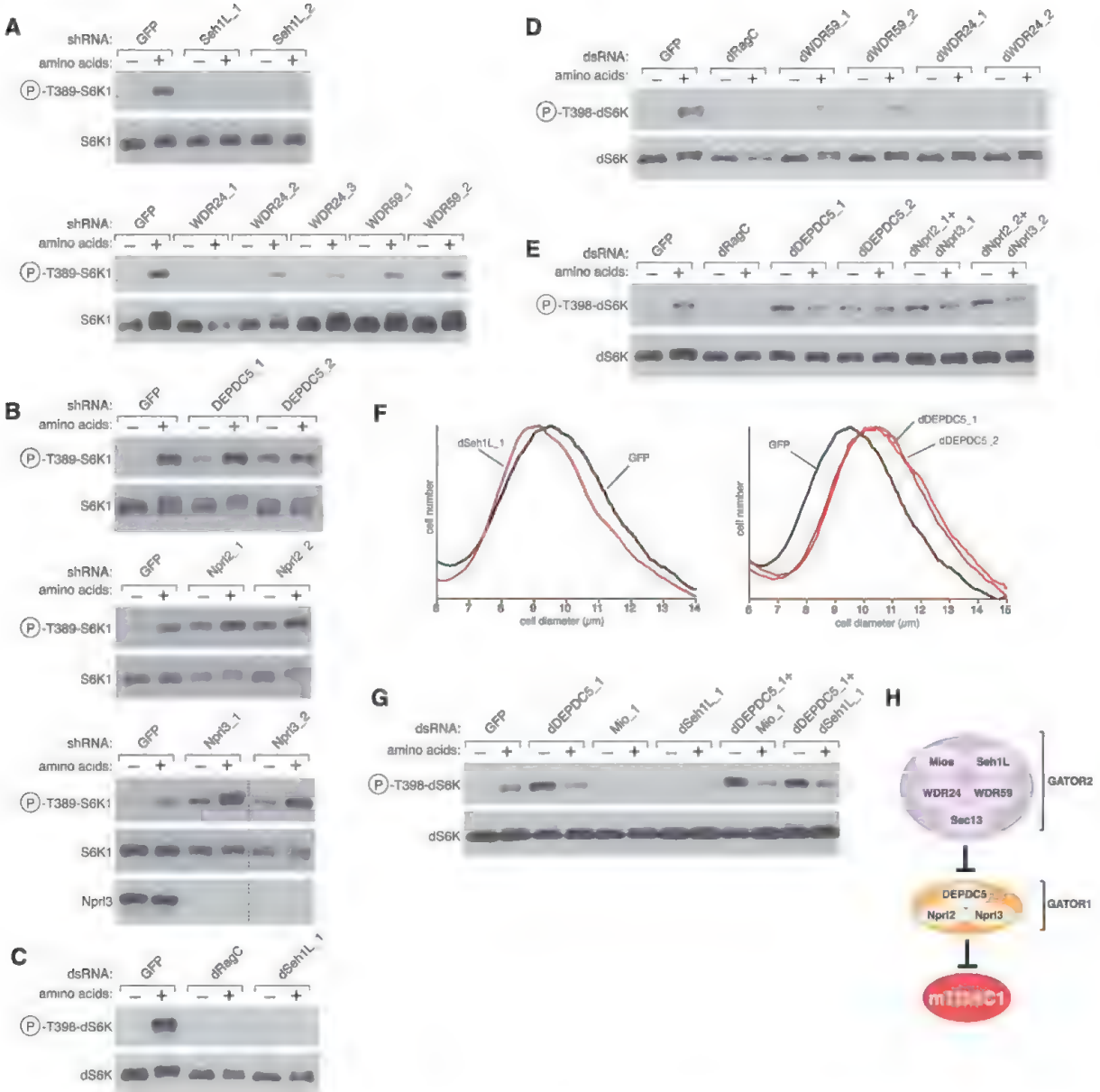

Fig. 2. The GATOR complex is required for the regulation of the TORC1 pathway by amino acids. (**A**) shRNA-mediated depletion of the GATOR2 components Seh1L, WDR24, or WDR59 in HEK-293T cells inhibits amino acid–induced S6K1 phosphorylation. (**B**) In HEK-293Ts expressing shRNAs targeting the GATOR1 components DEPDC5, Nprl2, and Nprl3, S6K1 phosphorylation is insensitive to amino acid withdrawal. In (A) and (B), cells were starved of amino acids for 50 min or starved and restimulated with amino acids for 10 min. Cell lysates were immunoblotted for the phosphorylation state of S6K1. dsRNA-mediated depletion in S2 cells of (**C**) dSeh1L; (**D**) dWDR59 and dWDR24; and (**E**) dDEPDC5, dNprl2, and dNprl3. S2 cells were treated with the indicated dsRNAs and were starved of amino acids for 90 min or starved and restimulated with amino acids for 30 min. Immunoblotting was used to detect the phosphorylation state of dS6K. (**F**) S2 cell sizes after dsRNA-mediated depletion of dSeh1L and dDEPDC5. (**G**) GATOR2 functions upstream of GATOR1. S2 cells were treated with the indicated combinations of dsRNAs and then starved and restimulated with amino acids and analyzed as in (C) to (E). (**H**) Schematic depicting the relationship between GATOR1 and GATOR2 in their regulation of mTORC1.

as detected by the phosphorylation state of its substrate S6K1 (Fig. 1B and fig. S2B). Moreover, in *Drosophila* S2 cells, double-stranded RNAs (dsRNAs) targeting Mio (*10*), the fly ortholog of Mios, ablated dTORC1 signaling and also reduced cell size (Fig. 1, C and D). Thus, in human and fly cells, Mios is necessary for amino acid signaling to TORC1.

In vitro, we failed to detect a strong interaction between purified Mios and the Rag heterodimers, which suggested that, within cells, other components exist that are needed for complex formation. Indeed, in FLAG-Mios immunoprecipitates prepared from HEK-293T cells, we detected seven additional proteins (WDR24, WDR59, Seh1L, Sec13, DEPDC5, Nprl2, and Nprl3) by mass spectrometry. The proteins varied in abundance, however, with much greater amounts of WDR24, WDR59, Seh1L, and Sec13 coimmunoprecipitating with Mios than DEPDC5, Nprl2, and Nprl3 (fig. S1B). In contrast, in FLAG-DEPDC5 immunoprecipitates, Nprl2 and Nprl3 were more abundant than Mios, WDR24, WDR59, Seh1L, and Sec13, and experiments with FLAG-Nprl2 gave analogous results (fig. S1B). These findings suggest that two subcomplexes exist, one consisting of Mios, WDR24, WDR59, Seh1L, and Sec13, and the other of DEPDC5, Nprl2, and Nprl3. To test this notion, we coexpressed FLAG-WDR24 or FLAG-Nprl2 together with hemagglutinin (HA)–tagged versions of the other seven proteins. As expected, DEPDC5 and Nprl3 coimmunoprecipitated with Nprl2 much more

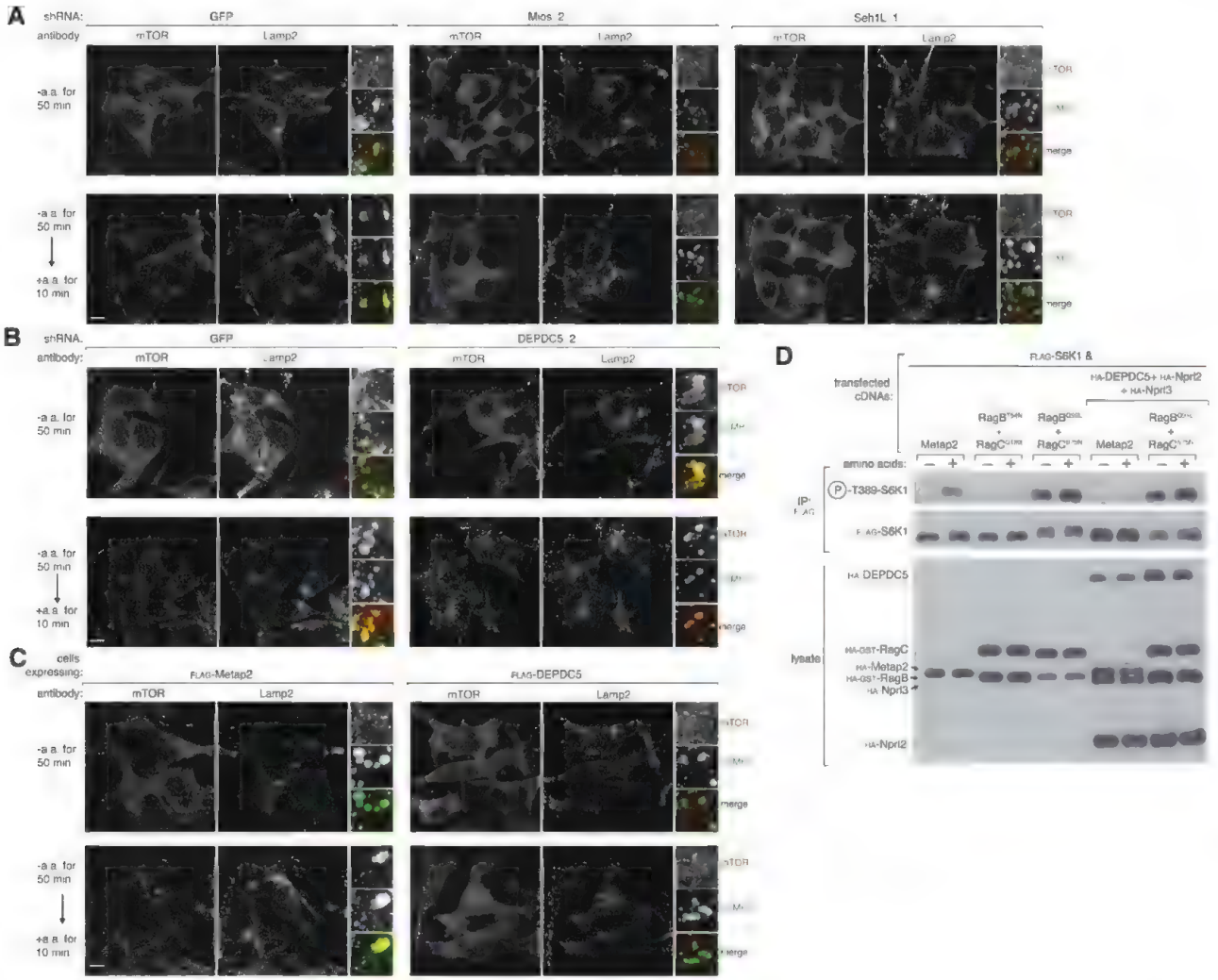

Fig. 3. GATOR regulates mTORC1 localization to the lysosomal surface and functions upstream of the Rag GTPases. (A) RNAi-mediated depletion of the GATOR2 components Mios and Seh1L prevents amino acid–induced mTOR lysosomal translocation. HEK-293T cells expressing the indicated shRNAs were starved or starved and restimulated with amino acids for the specified times before coimmunostaining for mTOR (red) and Lamp2 (green). **(B)** Reduced expression of DEPDC5 in HEK-293T cells results in constitutive mTOR localization to the lysosomal surface. HEK-293T cells treated with the indicated lentiviral shRNAs were processed as described in (A). **(C)** Images of HEK-293T cells stably expressing FLAG-DEPDC5 starved of, or starved and restimulated with, amino acids. Cells were processed as described in (A). In all images, insets show selected fields that were magnified five times and their overlays. Scale bar, 10 μM. **(D)** GATOR1 functions upstream of the nucleotide binding state of the Rags. HEK-293T cells transfected with the indicated cDNAs in expression vectors were starved of amino acids for 50 min or starved and restimulated with amino acids for 10 min. The indicated proteins were detected by immunoblotting.

strongly than with WDR24, whereas the opposite was true for Mios, WDR59, Seh1L, and Sec13 (Fig. 1E). For reasons described later, we call the eight-protein complex GATOR for GTPase-activating protein (GAP) activity toward Rags and the two subcomplexes GATOR1 (DEPDC5, Nprl2, and Nprl3) and GATOR2 (Mios, WDR24, WDR59, Seh1L, and Sec13) (Fig. 1H).

When the eight proteins were coexpressed with RagB and RagC, GATOR interacted strongly with the Rag heterodimer (Fig. 1F) and, like the Rags and Ragulator (*6*, *7*), its DEPDC5 component localized to the lysosomal surface (fig. S1E). Experiments in which single GATOR proteins were omitted revealed complex relations between the components but suggested that GATOR1 mediates the GATOR-Rag interaction (fig. S1C). Consistent with this conclusion, when stably expressed in HEK-293T cells, FLAG-DEPDC5 coimmunoprecipitated much more endogenous RagA and RagC than FLAG-WDR24, as detected by immunoblotting (Fig. 1G) and mass spectrometric analysis (fig. S1D). Amino acid starvation increased the amount of RagA and RagC that coimmunoprecipitated with DEPDC5, which suggested a regulatory role for GATOR1 (fig. S1F).

The finding that GATOR components interact with the Rag GTPases was intriguing because their likely budding yeast orthologs (IML1, NPR2, and NPR3) positively regulate autophagasome formation, a TORC1-dependent process (*11*), and, at least in certain yeast strains, also inhibit TORC1 signaling upon nitrogen starvation (*12*–*14*). Recently, the likely yeast orthologs of GATOR2 (Sea2, Sea3, Sea4, Seh1L, and Sec13) were shown to interact with IML1, NPR2, and NPR3 to form a complex that has been called SEA (*15*). However, unlike GATOR, the SEA complex does not appear to consist of two distinct subcomplexes, as its components are found in stoichiometric amounts.

We used RNAi in HEK-293T and *Drosophila* S2 cells to examine the function of each GATOR component in amino acid sensing by mTORC1 and dTORC1, respectively. We excluded Sec13 from further analysis, as it functions in several protein complexes (*16*), and so its inhibition might have effects that are difficult to interpret. Consistent with Mios being required for amino acids to activate mTORC1 (Fig. 1B), depletion of other GATOR2 components or their *Drosophila* orthologs strongly blunted amino acid–induced activation of mTORC1 and dTORC1, respectively (Fig. 2, A, C, and D; and fig. S2, A to D). It is

interesting that in contrast, loss of GATOR1 proteins had the opposite effect and prevented the inactivation of mTORC1 and dTORC1 normally caused by amino acid deprivation (Fig. 2, B and E, and fig.S2, A and D). Consistent with the opposite roles of GATOR1 and GATOR2 on dTORC1 signaling, dsRNAs targeting dSeh1L or dDEPDC5 decreased and increased, respectively, S2 cell size (Fig. 2F). To clarify the relation between GATOR1 and GATOR2, we used RNAi to inhibit dDEPDC5 at the same time as Mio or dSeh1L in S2 cells. In the background of GATOR1 inhibition, loss of GATOR2 had no effect on dTORC1 activity, which indicated that GATOR2 functions upstream of GATOR1 (Fig. 2, G and H). Thus, GATOR2 is an inhibitor of an inhibitor (GATOR1) of the amino acid–sensing branch of the TORC1 pathway.

A key step in the amino acid–induced activation of mTORC1 is its recruitment to the lysosomal surface, an event that requires known positive components of the amino acid–sensing pathway, like Ragulator (*7*) and the V-ATPase (*3*). Consistent with a positive role for GATOR2, in HEK-293T cells expressing shRNAs targeting Mios (Fig. 1B) or Seh1L (Fig. 2A), mTOR did not translocate to LAMP2-positive lysosomal membranes upon amino acid stimulation (Fig. 3A). In contrast, in cells expressing an shRNA targeting DEPDC5 (fig. S2A), mTOR localized constitutively to the lysosomal surface, regardless of amino acid availability (Fig. 3B). Moreover, just overexpression of DEPDC5 was sufficient to block the amino acid–induced translocation of mTOR to the lysosomal surface (Fig. 3C). Unlike Ragulator, which tethers the Rags to the lysosomal surface (*6*, *7*), GATOR2 is not needed for the proper Rag localization (fig. S3A). Thus, GATOR1 and GATOR2 have opposite effects on the activity and subcellular localization of mTORC1.

Consistent with the finding that GATOR1 inhibited the mTORC1 pathway, concomitant overexpression of its three components blocked the amino acid–induced activation of mTORC1 (Fig. 3D) to a similar extent as $RagB^{T54N}$-$RagC^{Q120L}$, a Rag heterodimer that is dominant negative because the $RagB^{T54N}$ mutant cannot bind GTP (*7*). In contrast, expression of the dominant active $RagB^{Q99L}$-$RagC^{S75N}$ heterodimer blocked not only amino acid deprivation but also GATOR1 overexpression from inhibiting mTORC1 signaling. Because $RagB^{Q99L}$ is constitutively bound to GTP (*17*) and $RagC^{S75N}$ cannot bind GTP (*7*), this result suggests that GATOR1 functions upstream of the regulation of the nucleotide binding state of the Rags.

To test the possibility that GATOR1 is a GEF or a GAP for the Rags, we prepared Rag heterodimers consisting of a wild-type Rag and a Rag^X mutant (see methods) (*7*). The Rag^X mutants are selective for xanthosine rather than guanine nucleotides, which allowed us to prepare heterodimers in vitro in which the wild-type Rag is loaded with radiolabeled GTP or GDP while the Rag^X partner is bound to XDP or XTP (*7*). In vitro, purified GATOR1 (fig. S4E) did not stimulate the dissociation of GDP from RagB or RagC when each was bound to its appropriate Rag^X partner (fig. S4, A and B); this ruled out its function as a GEF. In contrast, GATOR1 strongly increased, in a time- and dose-dependent manner, GTP hydrolysis by RagA or RagB within $RagC^X$-containing heterodimers, irrespective of which nucleotide $RagC^X$ was loaded with (Fig. 4, A, B, and E; and fig. S4, C and D). GATOR1 also slightly boosted GTP hydrolysis by RagC within a $RagB^X$-RagC heterodimer (Fig. 4C) but had no effect on the GTPase activity of Rap2A (Fig. 4D). Leucyl–transfer RNA synthetase (LRS), a putative GAP for RagD (*18*), did not alter the basal GTP hydrolysis by RagA, RagB, or RagC (Fig. 4, A, B, and C). Consistent with the binding preference of many GAPs for the GTP-loaded state of target GTPases, in vitro GATOR1 preferentially interacted with the $RagB^{Q99L}$-containing heterodimer (Fig. 4F). Thus, the GATOR1 complex has GAP activity for RagA and RagB, which provides a mechanism for its inhibitory role in mTORC1 signaling.

Because the pathways that convey upstream signals to mTORC1 are frequently deregulated by mutations in cancer [reviewed in (*19*)], we thought it possible that GATOR1 components might be mutated in human tumors. Indeed, previous studies identified in lung and breast cancers deletions of a 630–kilobase (kb) region of 3p21.3 that includes *NPRL2* (*20*, *21*), and one study

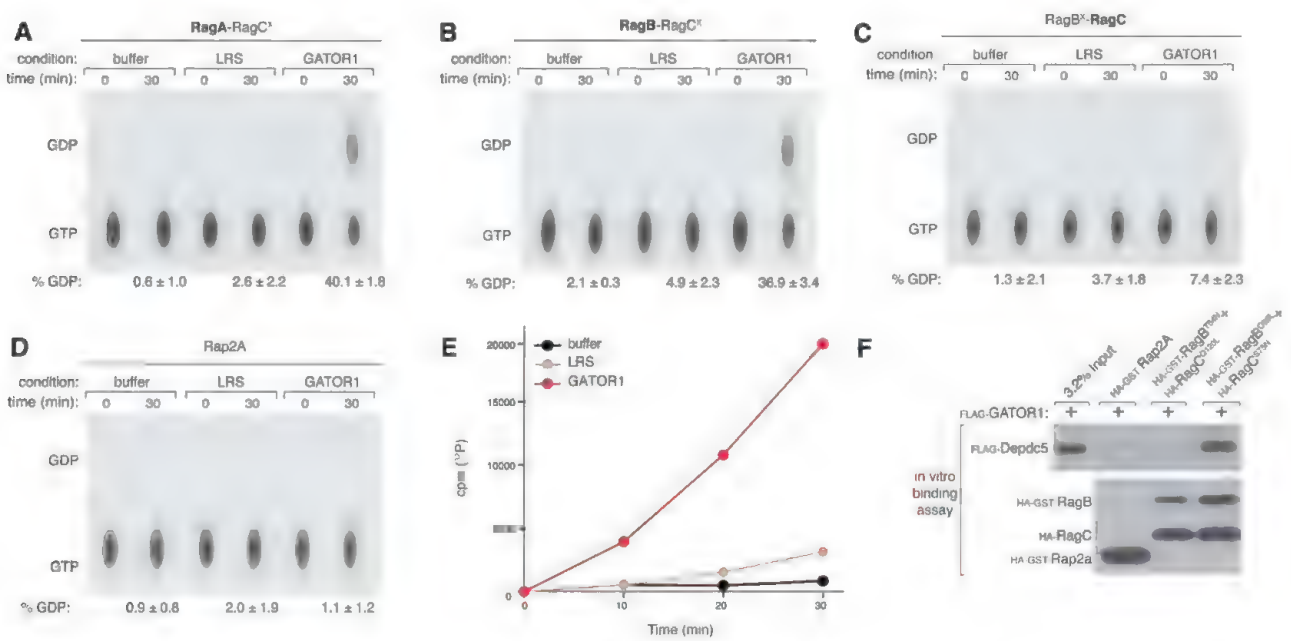

Fig. 4. GATOR1 is a GTPase-activating protein complex for RagA and RagB. (**A** to **D**) GATOR1 stimulates GTP hydrolysis by RagA and RagB. RagA-$RagC^X$, $RagB$-$RagC^X$, RagC-$RagB^X$, or the control GTPase Rap2A were loaded with [α-^{32}P]GTP and incubated with GATOR1 (20 pmol) or the control LRS (20 pmol). GTP hydrolysis was determined by thin-layer chromatography (see methods). Each value represents the normalized mean ± SD (n = 3). (**E**) GATOR1 increases GTP hydrolysis by RagB in a time-dependent manner. RagB-$RagC^X$ was loaded with [γ-^{32}P]GTP and incubated with GATOR1 or a control, and hydrolysis was determined by phosphate capture (see methods) Each value represents the normalized mean ± SD (n = 3). (**F**) GATOR1 preferentially interacts with the dominant active Rag heterodimer. In vitro binding assay in which FLAG-GATOR1 was incubated with immobilized HA–glutathione *S*-transferase (HA-GST)–tagged $RagB^{T54N}$-$RagC^{Q120L}$ (dominant negative), $RagB^{Q99L}$-$RagC^{S75N}$ (dominant active) or Rap2A. HA-GST precipitates were analyzed by immunoblotting for the levels of FLAG-GATOR1.

reported two cases of glioblastoma with deletions in a three-gene region of 22q12.2 that contains *DEPDC5* (*22*). Moreover, in cancer cells with 3p21.3 deletions, expression of Nprl2 inhibited their capacity to grow as tumor xenografts, which identified it as a tumor suppressor (*21*, *23*). Our analyses of publically available data from the Cancer Genome Atlas identified a subset of glioblastomas and ovarian cancers with nonsense or frameshift mutations or truncating deletions in *DEPDC5* or *NPRL2*. In most of these tumors, *DEPDC5* or *NPRL2* also underwent a loss of heterozygosity (LOH) event, which indicated that the tumors were unlikely to retain a functional copy of the gene products (Fig. 5, A, B, and C; and fig. S5A). In addition, in both tumor types, focal homozygous or hemizygous deletions, as well as missense mutations accompanied by LOH, were also detected in *DEPDC5* and *NPRL2* (Fig. 5A). *NPRL3* is located too proximal to the 16p telomere to adequately access copy number alterations in it using high-density microarray analysis. In aggregate, inactivating mutations in GATOR1 components are present in low single-digit percentages of glioblastomas and ovarian cancers, frequencies that may change upon better assessment of *NPRL3*.

In order to study the effects of GATOR1 loss on cancer cells, we used the Cosmic and CCLE resources (see methods) to identify human cancer cell lines with homozygous deletions in *DEPDC5*, *NPRL2*, or *NPRL3*, which we confirmed via immunoblotting or polymerase chain reaction (PCR) of genomic DNA (fig. S5, B, C, and F). In seven such lines, but not in Jurkat or HeLa cells, mTORC1 signaling was hyperactive and completely insensitive to amino acid deprivation and V-ATPase inhibition, irrespective of which GATOR1 component was lacking (Fig. 5D and fig. S5, D, E, and I). Furthermore, in GATOR1-null cells mTOR localized to the lysosomal surface even in the absence of amino acids (Fig. 5E). When DEPDC5 and Nprl2 were reintroduced into cancer cell lines lacking them, the mTORC1 pathway regained sensitivity to amino acid regulation (Fig. 5F and

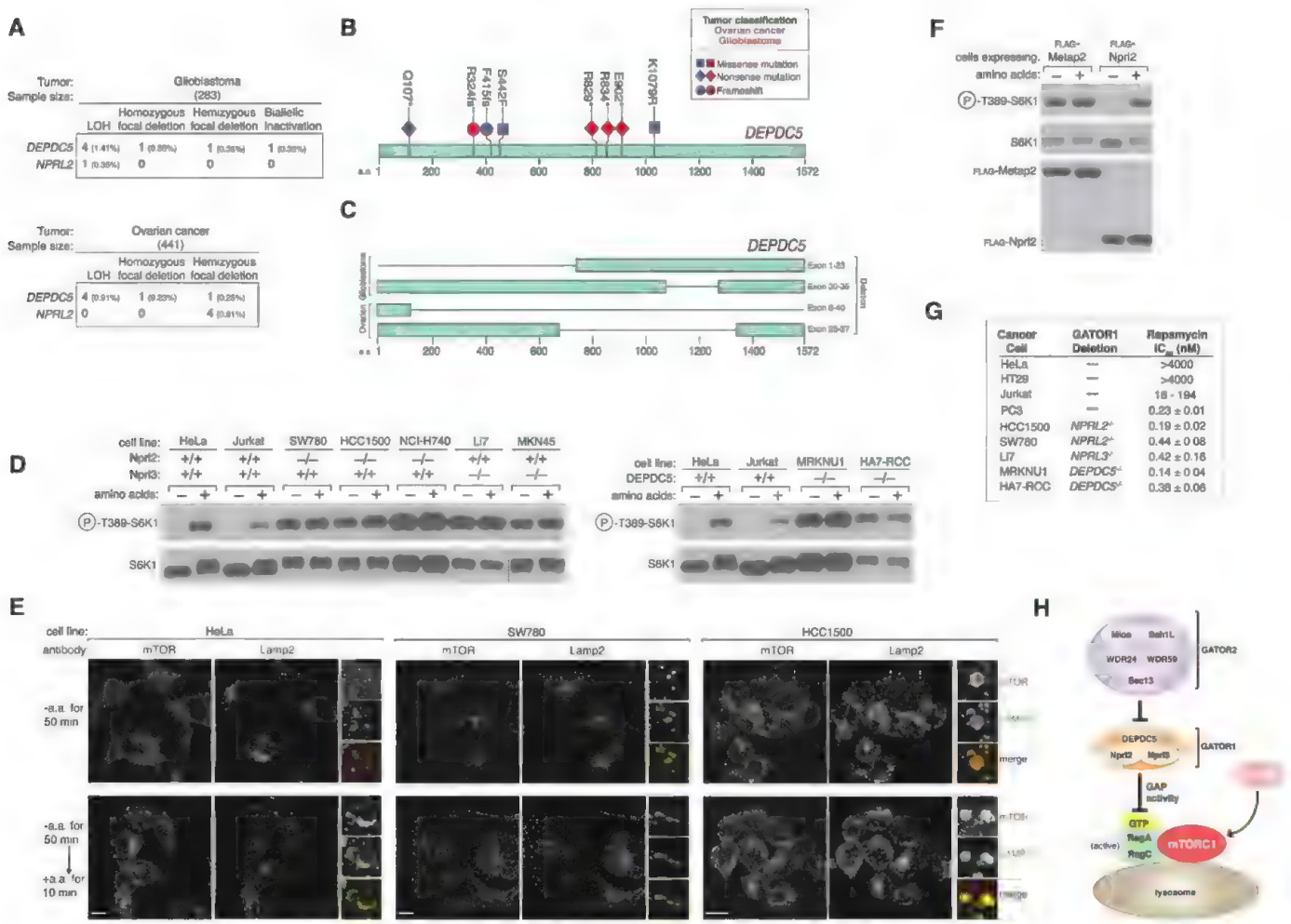

Fig. 5. GATOR1 components are mutated in cancer and GATOR1-null cancer cells are hypersensitive to the mTORC1 inhibitor rapamycin. (A) Table summarizing genomic alterations in *DEPDC5* and *NPRL2* and their frequencies in glioblastoma and ovarian cancer. The ratios of nonsense and frameshift mutations to missense mutations in *DEPDC5* ($P = 0.00015$) and *NPRL2* ($P = 0.00342$) in glioblastoma differ significantly from the ratio of all nonsense and frameshift mutations to missense mutations in glioblastoma genomes as determined by a Fisher's Exact test. **(B** and **C)** Mutations and deletions identified in *DEPDC5* in glioblastomas and ovarian cancers. **(D)** In GATOR1-null cancer cells the mTORC1 pathway is resistant to amino acid starvation. Cells were starved of amino acids for 50 min and starved or restimulated with amino acids for 10 min. Cell lysates were analyzed by immunoblotting for levels of the indicated proteins. **(E)** Cancer cells were starved or starved and restimulated with amino acids (a.a.) for the specified times before coimmunostaining for mTOR (red) and Lamp2 (green). In all images, insets show selected fields that were magnified five times and their overlays. Scale bar, 10 μM. **(F)** Reintroduction of Nprl2 into the SW780 cell line (*NPRL2*$^{-/-}$) restores amino acid–dependent regulation of mTORC1. Cells stably expressing a control protein or Nprl2 were treated and analyzed as in (D). **(G)** GATOR1-null cancer cells are hypersensitive to rapamycin. Rapamycin IC_{50} values for indicated cancer cell lines. Values are presented as means ± SD ($n = 3$). **(H)** Model for the role of the GATOR complex in the amino acid–sensing branch of the mTORC1 pathway. GATOR2 is a negative regulator of GATOR1, which inhibits the mTORC1 pathway by functioning as a GAP for RagA.

fig. S5, G, and H), which indicated that it is indeed the loss of GATOR1 proteins that is driving aberrant mTORC1 signaling in these cells.

The proliferation of the GATOR1-null cancer cells was very sensitive to the mTORC1 inhibitor rapamycin, with median inhibitory concentration (IC_{50}) values in the 0.1 to 0.4 nM range (Fig. 5G). These values are many orders of magnitude less than for cell lines that are not considered rapamycin-sensitive, like HeLa and HT29 cells, and at the low end of cancer cell lines, like PC3 and Jurkat cells, which have lost *PTEN* function (*24*–*26*), an established negative regulator of the mTORC1 pathway. In addition, the forced expression of DEPDC5 in the MRKNU1 (*DEPDC5*$^{-/-}$) cell line led to a marked reduction in its proliferation (fig. S5J).

In conclusion, we identify the octomeric GATOR complex as a critical regulator of the pathway that signals amino acid sufficiency to mTORC1 (Fig. 5G). The GATOR1 subcomplex has GAP activity for RagA and RagB and its loss makes mTORC1 signaling insensitive to amino acid deprivation. Inactivating mutations in GATOR1 are present in cancer and may help identify tumors likely to respond to clinically approved pharmacological inhibitors of mTORC1.

References and Notes

1. M. Laplante, D. M. Sabatini, *Cell* **149**, 274 (2012).
2. X. M. Ma, J. Blenis, *Nat. Rev. Mol. Cell Biol.* **10**, 307 (2009).
3. R. Zoncu *et al.*, *Science* **334**, 678 (2011).
4. Y. Sancak *et al.*, *Science* **320**, 1496 (2008).
5. E. Kim, P. Goraksha-Hicks, L. Li, T. P. Neufeld, K. L. Guan, *Nat. Cell Biol.* **10**, 935 (2008).
6. Y. Sancak *et al.*, *Cell* **141**, 290 (2010).
7. L. Bar-Peled, L. D. Schweitzer, R. Zoncu, D. M. Sabatini, *Cell* **150**, 1196 (2012).
8. T. Sekiguchi, E. Hirose, N. Nakashima, M. Ii, T. Nishimoto, *J. Biol. Chem.* **276**, 7246 (2001).
9. G. Mattson *et al.*, *Mol. Biol. Rep.* **17**, 167 (1993).
10. T. Iida, M. A. Lilly, *Development* **131**, 1029 (2004).
11. R. Loewith, M. N. Hall, *Genetics* **189**, 1177 (2011).
12. T. K. Neklesa, R. W. Davis, *PLoS Genet.* **5**, e1000515 (2009).
13. X. Wu, B. P. Tu, *Mol. Biol. Cell* **22**, 4124 (2011).
14. M. Graef, J. Nunnari, *EMBO J.* **30**, 2101 (2011).
15. S. Dokudovskaya *et al.*, *Mol. Cell. Proteomics* **10**, 006478 (2011).
16. N. C. Leksa, T. U. Schwartz, *Nucleus* **1**, 314 (2010).
17. U. Krengel *et al.*, *Cell* **62**, 539 (1990).
18. J. M. Han *et al.*, *Cell* **149**, 410 (2012).
19. D. M. Sabatini, *Nat. Rev. Cancer* **6**, 729 (2006).
20. M. I. Lerman, J. D. Minna, *Cancer Res.* **60**, 6116 (2000).
21. J. Li *et al.*, *Cancer Res.* **64**, 6438 (2004).
22. T. J. Seng *et al.*, *Genes Chromosomes Cancer* **43**, 181 (2005).
23. L. Ji *et al.*, *Cancer Res.* **62**, 2715 (2002).
24. M. S. Neshat *et al.*, *Proc. Natl. Acad. Sci. U.S.A.* **98**, 10314 (2001).
25. M. Y. Wang *et al.*, *Cancer Res.* **66**, 7864 (2006).
26. F. Meric-Bernstam *et al.*, *Clin. Cancer Res.* **18**, 1777 (2012).

Acknowledgments: We thank all members of the Sabatini lab for helpful suggestions, E. Spooner for the mass spectrometric analysis of samples, and N. Kory for technical assistance. This work was supported by grants from the NIH (CA103866 and AI47389) and Department of Defense (W81XWH-07-0448) to D.M.S. and the National Cancer Institute (NIH) (U24CA143867) to M.M. and awards from the David H. Koch Graduate Fellowship Fund to L.B.-P.; the NSF Graduate Research Fellowship Program to L.C.; the Harvard-MIT Health, Sciences, and Technology IDEA^2 program to W.W.C.; and the American Cancer Society to B.C.G. D.M.S. is an investigator of the Howard Hughes Medical Institute.

Supplementary Materials

www.sciencemag.org/cgi/content/full/340/6136/1100/DC1
Materials and Methods
Figs. S1 to S5
References (*27*–*31*)

26 October 2012; accepted 5 April 2013
10.1126/science.1232044

Impaired α-TTP-PIPs Interaction Underlies Familial Vitamin E Deficiency

Nozomu Kono,[1,2]* Umeharu Ohto,[1]* Tatsufumi Hiramatsu,[1] Michiko Urabe,[1] Yasunori Uchida,[1] Yoshinori Satow,[1] Hiroyuki Arai[1,2]†

α-Tocopherol (vitamin E) transfer protein (α-TTP) regulates the secretion of α-tocopherol from liver cells. Missense mutations of some arginine residues at the surface of α-TTP cause severe vitamin E deficiency in humans, but the role of these residues is unclear. Here, we found that wild-type α-TTP bound phosphatidylinositol phosphates (PIPs), whereas the arginine mutants did not. In addition, PIPs in the target membrane promoted the intermembrane transfer of α-tocopherol by α-TTP. The crystal structure of the α-TTP–PIPs complex revealed that the disease-related arginine residues interacted with phosphate groups of the PIPs and that the PIPs binding caused the lid of the α-tocopherol–binding pocket to open. Thus, PIPs have a role in promoting the release of a ligand from a lipid-transfer protein.

Intracellular lipid transport is required for numerous cellular events (*1*, *2*). Lipids are transported between organelles by vesicles or are delivered by lipid-transfer proteins (*3*). Some lipid-transfer proteins possess specific organellar-targeting motifs to assure precise lipid transport from donor to acceptor organelles (*1*, *2*). However, many other lipid-transfer proteins have no known organellar-targeting domains, and the molecular bases underlying intracellular lipid transport by these proteins are largely unknown.

α-Tocopherol transfer protein (α-TTP), which specifically binds α-tocopherol (α-Toc), the most abundant form of vitamin E in mammals, is expressed in the liver where it regulates the amount of α-Toc secreted into the plasma (*4*). Heritable mutations in the α-TTP–encoding gene result in ataxia with vitamin E deficiency (AVED), an autosomal recessive disorder associated with low circulating vitamin E concentrations and neurodegenerative pathology (*5*). More than 20 mutations in the α-TTP gene have been identified in AVED patients (*5*). α-TTP is a member of the Sec14-like protein family (*6*) and has a lipid-binding domain, the Sec14 domain. Because α-TTP has no known organellar-targeting domain, we focused on the mutations in AVED patients to investigate the molecular mechanism underlying α-TTP–mediated α-Toc transport in liver cells. Of the nine disease-associated missense mutations (Fig. 1A), three (R59W, R192H, and R221W) are located in one region on the α-TTP protein surface, which is distinct from the α-Toc binding site (*7*) (Fig. 1B). The R59W and R221W mutations give rise to the severe, early-onset form of the disease (*8*), indicating that these arginine residues are critical for α-TTP function.

We assessed the α-Toc binding and intermembrane transfer activities of recombinant R59W α-TTP (R59W) in vitro. α-[^{3}H]Toc comigrated with the wild type or R59W on gel filtration, and the peaks of α-Toc of R59W and the wild type were almost the same (Fig. 1C). The intermembrane α-Toc transfer activity of R59W was somewhat higher than that of the wild type (Fig. 1D). The wild type stimulated secretion of α-Toc from hepatoma cells, but R59W did not stimulate it at all (*9*) (Fig. 1E). Thus, R59W can bind and transfer α-Toc in vitro, but cannot stimulate α-Toc transport in cells.

Using beads derivatized with phosphatidylinositol 3,4-bisphosphate [$PI(3,4)P_2$], α-TTP bound $PI(3,4)P_2$ as expected (*10*), but R59W did not (Fig. 2A). Native polyacrylamide gel electrophoresis (PAGE) analysis of the α-TTP-$PI(3,4)P_2$ mixture revealed that the PIPs increased the mobility of α-TTP (Fig. 2B), which also suggests that α-TTP interacts with $PI(3,4)P_2$. The mobility shift of α-TTP was increased more by $PI(4,5)P_2$ than by $PI(3,4)P_2$. It was also slightly increased by PI(4)P and $PI(3,4,5)P_3$ (Fig. 2, C and E, and fig. S1). None of the above PIPs affected the mobility of R59W (Fig. 2, D and F, and fig. S1). Thus, α-TTP binds $PI(4,5)P_2$ and $PI(3,4)P_2$ and the disease-associated R59 is involved in the α-TTP-PIPs interaction. Gel filtration chromatography of a mixture of α-TTP and [^{3}H]$PI(4,5)P_2$ showed that $PI(4,5)P_2$ induced the formation of α-TTP tetramers (Fig. 2G).

[1]Graduate School of Pharmaceutical Sciences, University of Tokyo, 7-3-1 Hongo, Bunkyo-ku, Tokyo 113-0033, Japan. [2]Core Research for Evolutional Science and Technology, Japan Science and Technology Agency, 4-1-8 Honmachi, Kawaguchi, Saitama, 332-0012, Japan.

*These authors contributed equally to this work.
†Corresponding author. E-mail: harai@mol.f.u-tokyo.ac.jp

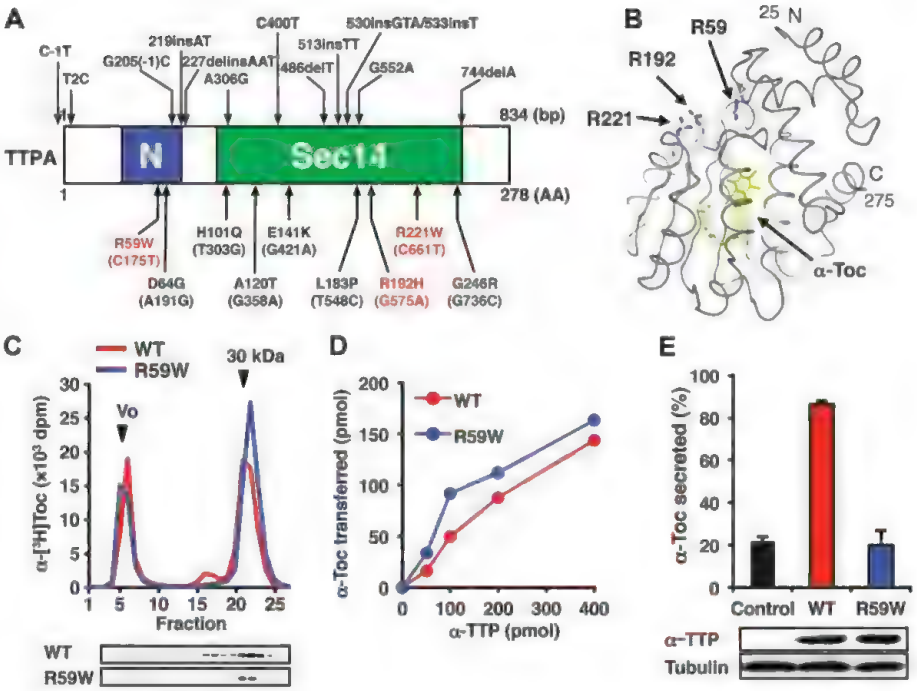

Fig. 1. R59W α-TTP mutant impairs α-Toc secretion without affecting α-Toc binding and transfer. (**A**) Distribution of α-TTP mutations. Blue and green boxes indicate CRAL_TRIO_N (N) and Sec14 domain, respectively. Missense mutations are shown below the panel, and insertions, deletions, and splicing mutations are indicated above the panel. (**B**) A loop representation of α-TTP (PDB: 1R5L). α-Toc is in yellow. The side chains of R59, R192, and R221 are depicted as stick models. (**C**) α-[^{3}H]Toc binding assay of wild type (WT) or R59W. Immunoblot of α-TTP in each fraction is also indicated. (**D**) Intermembrane α-Toc transfer activity of WT or R59W. (**E**) α-Toc secretion from McA-RH7777 cells stably transfected with WT or R59W. Protein amounts of α-TTP and α-tubulin were evaluated by immunoblot. Error bars indicate SE (n = 3 biological replicates). Abbreviations for the amino acid residues are as follows: A, Ala; C, Cys; D, Asp; E, Glu; F, Phe; G, Gly; H, His; I, Ile; K, Lys; L, Leu; M, Met; N, Asn; P, Pro; Q, Gln; R, Arg; S, Ser; T, Thr; V, Val; W, Trp; and Y, Tyr.

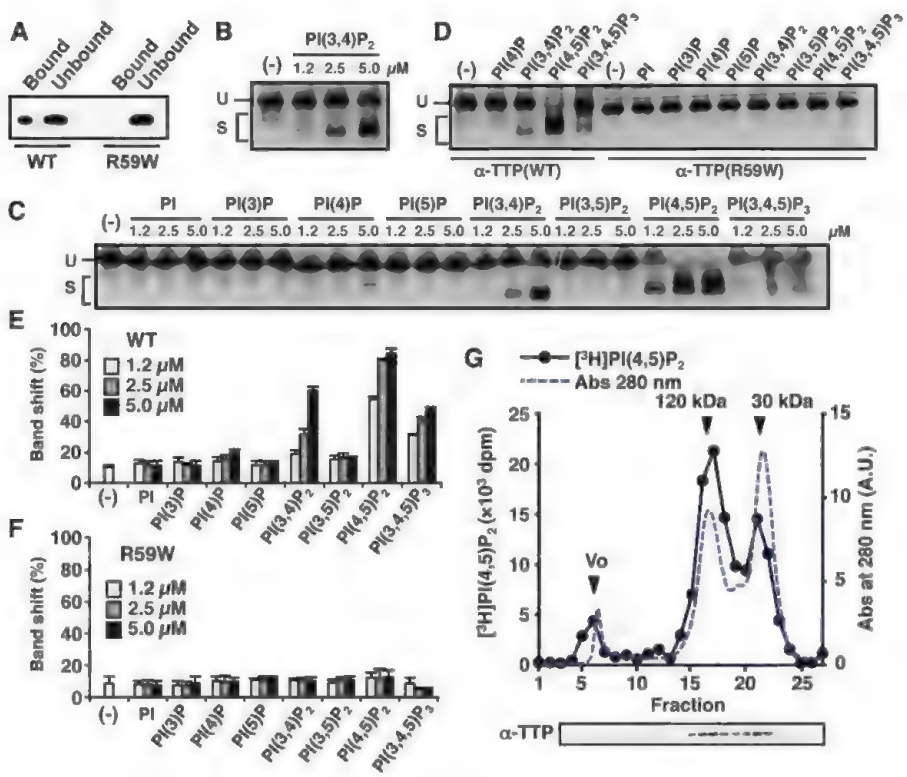

Fig. 2. R59W α-TTP mutant impairs PIPs binding. (**A**) Binding of WT and R59W to PI(3,4)P_2-derivertized beads. (**B**) Native PAGE analysis of α-TTP-PI(3,4)P_2 interaction. Gel was stained with silver. U, unshifted; S, shifted. (**C**) Same as in (B), except that PI or various PIPs were tested. (**D**) Native PAGE of WT or R59W with PI or various PIPs at a concentration of 2.5 μM. (**E**) Same as in (C), except that gels were stained with SYPRO ruby and band shifts were quantified. (**F**) Same as in (E), except that R59W was used. (**G**) [^{3}H]PI(4,5)P_2 binding assay. Immunoblot of α-TTP in each fraction was also indicated. For (E) and (F), error bars indicate SE (n = 3 independent reactions).

[^{3}H]PI(4,5)P_2 comigrated with both the monomer and the tetramer. Sedimentation velocity analysis also confirmed the tetramer formation by PI(4,5)P_2 (fig. S2). The stoichiometry between α-TTP and PI(4,5)P_2 was ~1:1.

Crystals of the ternary complex consisting of α-TTP, α-Toc, and either PI(3,4)P_2 or PI(4,5)P_2 were analyzed by x-ray crystallography at 2.6 or 2.0 Å resolution, respectively (table S1). The crystallographic asymmetric unit contained four α-TTP molecules related by noncrystallographic 222 symmetry. Each α-TTP monomer bound both α-Toc and PIPs (Fig. 3A and fig. S3A). α-Toc was located deep in the hydrophobic core of α-TTP, as expected (*7*, *11*). PIPs lay in close proximity to the bound α-Toc. The inositol phosphate (IP) head group was bound in the positively charged cleft (Fig. 3B and fig. S3B). The head groups of PI(3,4)P_2 and PI(4,5)P_2 were clearly defined in the electron density maps, whereas the diacyl moieties of the PIPs were not visible. Only the glycerol backbone and several carbon atoms of the acyl chains were visible between the hydrophobic groove formed by α9 (residues 165 to 185) and α10 (residues 198 to 221, termed the "lid") in the α-TTP-PI(3,4)P_2 complex. The positively charged cleft of α-TTP, which accommodates the negatively charged IP head group of PIPs, was composed of three distinct regions in the amino acid sequence of α-TTP (residues 58 to 68, 184 to 191, and 214 to 222; Fig. 3A and fig. S3A). The side chains of R59, R68, D185, K190, R192, T215, K217, and R221 formed the inner wall of the cavity (Fig. 3C and fig. S3C). The three disease-associated arginine residues (R59, R192, and R221) all interacted with PIPs. The side chain of R59 formed a salt bridge with D185 and

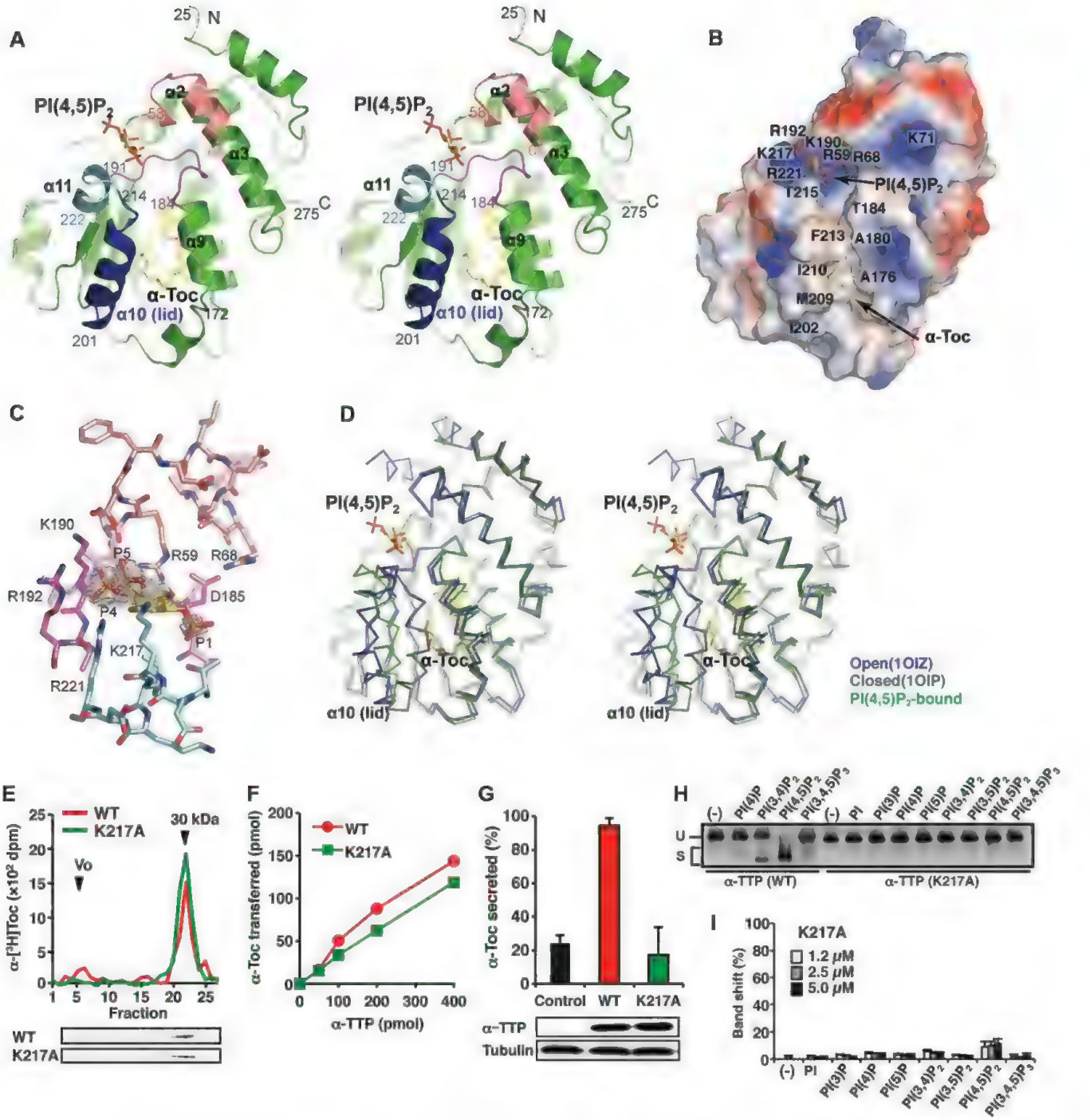

Fig. 3. Crystal structure of α-TTP-PI(4,5)P_2 complex. (**A**) Stereo view of the structure of α-TTP in complex with α-Toc and PI(4,5)P_2. PI(4,5)P_2 and α-Toc are shown as stick models: C in yellow, O in red, and P in orange. Some α helices are indicated with their labels, and some amino acid residues with their numbers. The "lid" helix is in blue, and three amino acid segments forming a positively charged cavity are differently colored: residues 58 to 68 in salmon, 184 to 191 in magenta, and 214 to 222 in cyan. (**B**) The structure of the PI(4,5)P_2 complex in electrostatic potential surface representation, and residues of interest, are indicated. Positive and negative potentials are in blue and red, respectively. (**C**) PI(4,5)P_2 and residues surrounding the head group as stick models. Carbon atoms of protein residues are colored as in (A). Residues of interest and phosphate groups of PI(4,5)P_2 are indicated. The $2F_O - F_C$ difference electron density map for PI(4,5)P_2 is contoured at 1.5σ level in gray mesh. (**D**) Superposition of the open (blue, PDB: 1OIZ), closed (gray, PDB: 1OIP), and PI(4,5)P_2-bound (green) structures is shown in Cα models. (**E**) α-[^{3}H]Toc binding assay of WT or K217A. Immunoblot of α-TTP in each fraction is shown below. (**F**) Intermembrane α-Toc transfer activity of WT or K217A. (**G**) α-Toc secretion from McA-RH7777 cells stably transfected with WT or K217A. Protein amounts of α-TTP and α-tubulin were evaluated by immunoblot. Error bars indicate SE ($n = 3$ biological replicates). (**H**) Native PAGE analysis of WT or K217A with PI or various PIPs. Gel was stained with silver. U, unshifted; S, shifted. (**I**) Same as in (H), except that gels were stained with SYPRO ruby and band shifts were quantified. Error bars indicate SE ($n = 3$ independent reactions).

attracted negatively charged phosphates of PIPs. The side chains of R192 and R221 interacted with the 4-phosphate of the PIPs. Like the side chains of R59, R192, and R221, the side chain of K217 interacted with the 5-phosphate of $PI(4,5)P_2$ or the 3-phosphate of $PI(3,4)P_2$ (Fig. 3C and fig. S3C). Substituting K217, which is not a disease-related residue, with alanine did not affect in vitro α-Toc binding and intermembrane transfer activities (Fig. 3, E and F). However, K217A mutant did not stimulate α-Toc secretion in hepatoma cells (Fig. 3G). None of the PIPs caused a significant mobility shift of K217A in native PAGE (Fig. 3, H and I, and fig. S1). Thus, as inferred from the crystal structure, K217 is also required for both PIPs binding and the cellular α-Toc transport activities of α-TTP. Taken together, α-TTP binds PIPs through the positively charged cleft where the disease-associated arginine residues are clustered and PIPs binding is required for the cellular transport of α-Toc.

In the α-TTP-$PI(4,5)P_2$ complex, the hydrophobic groove between α9 and α10 had a volume of 1147 $Å^3$, which is large enough to accommodate the acyl chains. The groove was lined with residues with hydrophobic side chains in α9 and α10 (Fig. 3B). Hence, the two acyl chains are probably confined to the groove and are in contact with these residues through van der Waals interactions. Crystal structures of α-TTP in complex with α-Toc [Protein Data Bank (PDB) ID: 1OIP and 1R5L] and in complex with Triton X-100 (PDB ID: 1OIZ) are known (*7*, *11*). In the α-TTP-α-Toc complex, bound α-Toc is isolated from the solvent by closing the lid (closed conformation). In contrast, in the α-TTP-Triton X-100 complex, α-TTP adopts a conformation with an open lid (open conformation). A superposition of the open, closed, and PIPs-bound structures of α-TTP (Fig. 3D and fig. S3D) suggests that the α-TTP-PIPs complex is intermediate between the closed and open conformations. Thus, binding of the acyl chains of PIPs to α-TTP may open the lid of the hydrophobic groove that contains α-Toc.

In vitro, addition of $PI(4,5)P_2$ or $PI(3,4)P_2$ to the acceptor liposomes increased the transfer of α-Toc by the wild type (Fig. 4A). Other negatively charged lipids such as cardiolipin or phosphatidylserine did not increase the transfer (fig. S4). The PIPs did not promote the α-Toc transfer by R59W and K217A (Fig. 4B). PIPs in the donor liposomes decreased the α-Toc transfer by the wild type (Fig. 4A). The antibiotic neomycin, which strongly binds to $PI(4,5)P_2$, suppresses $PI(4,5)P_2$-related events by masking $PI(4,5)P_2$ (*12*, *13*). Indeed, neomycin inhibited the in vitro α-TTP-$PI(4,5)P_2$ interaction (Fig. 4C). Neomycin treatment inhibited α-Toc efflux in α-TTP–expressing hepatoma cells, but did not significantly affect α-Toc efflux in the cells that did not express α-TTP (Fig. 4D), suggesting that $PI(4,5)P_2$ is involved in α-TTP–mediated α-Toc efflux from hepatocytes.

The yeast sterol transfer protein Osh4p binds PI(4)P and acts as a sterol/PI(4)P exchanger in vitro (*14*). The similarity between Osh4p and α-TTP in the mode of PIPs binding and the effect on the transfer activity is notable. Moreover, like Osh4p, α-TTP acted as an α-Toc/$PI(4,5)P_2$ exchanger: α-TTP bound α-Toc and $PI(4,5)P_2$ in a competitive manner (fig. S5) and transferred them between liposomes in the opposite direction (Fig. 4, E and F). Gel filtration analysis of α-TTP with $PI(4,5)P_2$ and α-[^{3}H]Toc showed that α-[^{3}H]Toc bound mainly to the monomer and, to a lesser extent, to the tetramer (fig. S6). Given that the tetramer consists of $PI(4,5)P_2$-bound α-TTP, the result suggests that α-TTP can bind both α-Toc and $PI(4,5)P_2$ simultaneously. The α-TTP-α-Toc-PIPs complex in the crystal structures may represent a transient intermediate between the α-Toc–bound and PIPs-bound forms. We thus suggest a potential mechanism of intracellular α-Toc transport by α-TTP: α-TTP containing α-Toc first interacts with the head group of PIPs in the target membrane through the positively charged cleft. The PIPs is then transferred to α-TTP, which leads to opening the lid of the α-Toc–binding pocket and stimulates the transfer of α-Toc to the target membrane. As a result, α-TTP exchanges α-Toc for PIPs.

PI-binding motifs have been proposed from the crystal structure of the yeast Sec14 homolog 1 (Sfh1)–PI complex (*15*) and are considered to be biologically important in humans, as well as in yeast (*16*). We have shown that the disease-associated basic residues in the motif interact with PIPs and that this interaction is essential for the function of α-TTP. Several Sec14-like proteins bind PIPs (*10*, *17*–*20*). At least three of the basic amino acid residues that interact with the phosphate groups of PIPs in α-TTP are conserved (fig. S7). R103 and R234 in cellular retinaldehyde binding protein (CRALBP) are mutated in hereditary retinopathy and are also present in the predicted PI-binding motifs (*21*). R103 and R234 of CRALBP correspond to R59 and K190 of α-TTP, respectively (fig. S7), suggesting that binding of PIPs to these amino acid residues has a role in transporting 11-cis-retinal.

In liver cells, α-TTP is thought to catalyze the transfer of endocytosed α-Toc to the plasma membrane (PM) where a transporter secretes it into the circulation (*22*). Given that α-TTP interacted preferentially with $PI(4,5)P_2$ and $PI(3,4)P_2$, both of which are concentrated in the PM, we hypothesize that α-TTP transfers α-Toc to the PM by targeting these PIPs. Thus, PIPs binding may be required for α-TTP both to target the PM and to stimulate the release of α-Toc.

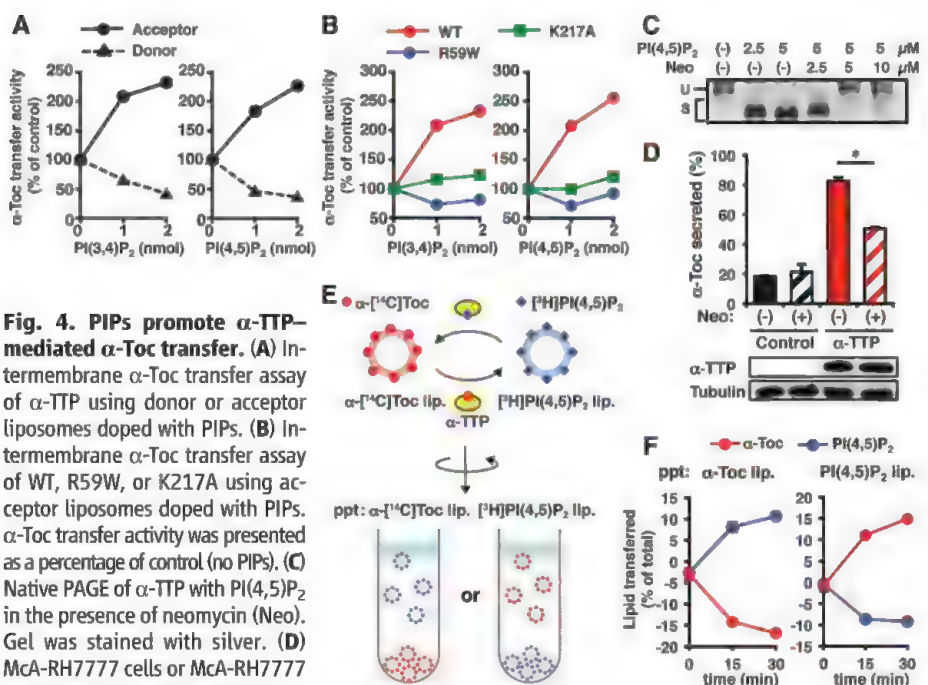

Fig. 4. PIPs promote α-TTP–mediated α-Toc transfer. (**A**) Intermembrane α-Toc transfer assay of α-TTP using donor or acceptor liposomes doped with PIPs. (**B**) Intermembrane α-Toc transfer assay of WT, R59W, or K217A using acceptor liposomes doped with PIPs. α-Toc transfer activity was presented as a percentage of control (no PIPs). (**C**) Native PAGE of α-TTP with $PI(4,5)P_2$ in the presence of neomycin (Neo). Gel was stained with silver. (**D**) McA-RH7777 cells or McA-RH7777 cells stably transfected with WT α-TTP were assayed for α-Toc secretion in the absence or presence of 10 mM neomycin. Expression levels of α-TTP and α-tubulin were evaluated by immunoblot (below). Error bars indicate SE ($n = 3$ biological replicates). *$P < 0.05$ (unpaired t test, two-tailed). (**E**) Scheme of α-Toc/$PI(4,5)P_2$ exchange assay. (**F**) α-TTP–dependent gain or loss of α-Toc and $PI(4,5)P_2$ in the precipitated liposomes. ppt, precipitate; lip., liposomes.

References and Notes

1. J. C. Holthuis, T. P. Levine, *Nat. Rev. Mol. Cell Biol.* **6**, 209 (2005).
2. S. Lev, *Nat. Rev. Mol. Cell Biol.* **11**, 739 (2010).
3. D. R. Voelker, *Experientia* **46**, 569 (1990).
4. M. G. Traber, H. Arai, *Annu. Rev. Nutr.* **19**, 343 (1999).
5. I. Di Donato, S. Bianchi, A. Federico, *Neurol. Sci.* **31**, 511 (2010).
6. K. Saito, L. Tautz, T. Mustelin, *Biochim. Biophys. Acta* **1771**, 719 (2007).
7. K. C. Min, R. A. Kovall, W. A. Hendrickson, *Proc. Natl. Acad. Sci. U.S.A.* **100**, 14713 (2003).
8. L. Cavalier *et al.*, *Am. J. Hum. Genet.* **62**, 301 (1998).
9. M. Arita, K. Nomura, H. Arai, K. Inoue, *Proc. Natl. Acad. Sci. U.S.A.* **94**, 12437 (1997).
10. S. Krugmann *et al.*, *Mol. Cell* **9**, 95 (2002).

11. R. Meier, T. Tomizaki, C. Schulze-Briese, U. Baumann, A. Stocker, *J. Mol. Biol.* **331**, 725 (2003).
12. A. Arbuzova *et al.*, *Biochim. Biophys. Acta* **1464**, 35 (2000).
13. B. C. Suh, T. J. Park, K. T. Kim, *Eur. J. Pharmacol.* **314**, 235 (1996).
14. M. de Saint-Jean *et al.*, *J. Cell Biol.* **195**, 965 (2011).
15. G. Schaaf *et al.*, *Mol. Cell* **29**, 191 (2008).
16. A. H. Nile, V. A. Bankaitis, A. Grabon, *Clin Lipidol* **5**, 867 (2010).
17. H. Huynh *et al.*, *J. Immunol.* **171**, 6661 (2003).
18. M. Merkulova *et al.*, *FEBS J.* **272**, 5595 (2005).
19. J. C. Saari, M. Nawrot, R. E. Stenkamp, D. C. Teller, G. G. Garwin, *Mol. Vis.* **15**, 844 (2009).
20. Y. Katoh *et al.*, *J. Biol. Chem.* **284**, 27646 (2009).
21. X. He, J. Lobsiger, A. Stocker, *Proc. Natl. Acad. Sci. U.S.A.* **106**, 18545 (2009).
22. T. Takada, H. Suzuki, *Mol. Nutr. Food Res.* **54**, 616 (2010).

Acknowledgments: We thank P. T. Hawkins for providing $PI(3,4)P_2$-derivatized beads; K. Yamamoto for providing *Ricinus communis* agglutinin 120; the beamline staffs at Photon Factory for their assistance with data collection; and J. Raymond for English proofreading. This work was supported by the Core Research for Evolutional Science and Technology, Japan Science and Technology Agency (CREST, JST) (to H.A.); the Program for Promotion of Basic and Applied Researches for Innovations in Bio-oriented Industry (to H.A.); Grants-in-aid from the Japanese Ministry of Education, Culture, Sports, Science, and Technology (20370045 to H.A.); and the Japanese Ministry of Health, Labor, and Welfare (to H.A.). The coordinate and structure factor data of α-TTP-$PI(3,4)P_2$ and α-TTP-$PI(4,5)P_2$ complexes have been deposited to the Protein Data Bank under the accession codes 3W67 and 3W68, respectively.

Supplementary Materials

www.sciencemag.org/cgi/content/full/science.1233508/DC1
Materials and Methods
Figs. S1 to S7
Table S1
References (*23*–*33*)

3 December 2012; accepted 27 March 2013
Published online 18 April 2013;
10.1126/science.1233508

A Conserved Mechanism for Centromeric Nucleosome Recognition by Centromere Protein CENP-C

Hidenori Kato,[1] Jiansheng Jiang,[2] Bing-Rui Zhou,[1] Marieke Rozendaal,[3] Hanqiao Feng,[1] Rodolfo Ghirlando,[4] T. Sam Xiao,[2] Aaron F. Straight,[3] Yawen Bai[1]*

Chromosome segregation during mitosis requires assembly of the kinetochore complex at the centromere. Kinetochore assembly depends on specific recognition of the histone variant CENP-A in the centromeric nucleosome by centromere protein C (CENP-C). We have defined the determinants of this recognition mechanism and discovered that CENP-C binds a hydrophobic region in the CENP-A tail and docks onto the acidic patch of histone H2A and H2B. We further found that the more broadly conserved CENP-C motif uses the same mechanism for CENP-A nucleosome recognition. Our findings reveal a conserved mechanism for protein recruitment to centromeres and a histone recognition mode whereby a disordered peptide binds the histone tail through hydrophobic interactions facilitated by nucleosome docking.

The accurate segregation of chromosomes during mitosis is essential for the reproduction and development of all organisms. Chromosome segregation is facilitated by the attachment of mitotic spindle microtubules to the kinetochore, which is assembled on the chromosomal centromere (*1*). Human centromere protein A (CENP-A) chromatin is constitutively associated with a complex of 16 centromere proteins (*2*, *3*). Among these 16 proteins, only CENP-C has been identified in all model organisms (*4*). CENP-C recognizes the carboxyl tail of CENP-A in the centromeric nucleosome (*5*, *6*). Human CENP-C consists of four functional regions (fig. S1A). The N-terminal region interacts with the Mis12 complex (*7*). The central region and the CENP-C motif are required for targeting CENP-C to the centromere (*5*, *8*–*11*). The central region directly binds to the CENP-A nucleosome, whereas the targeting mechanism for the CENP-C motif is unknown. The C-terminal region is responsible for CENP-C dimerization (*12*).

To explore how CENP-C recognizes the CENP-A nucleosome, we first investigated the central region ($CENP\text{-}C_{426–537}$) alone by nuclear magnetic resonance (NMR) spectroscopy and found that it is disordered (fig. S1, B and C). We then examined $CENP\text{-}C_{426–537}$ in complex with reconstituted *Drosophila* nucleosomes containing the $H3_{1–132}$-LEEGLG (Leu-Glu-Glu-Gly-Leu-Gly) chimera. The residues in the CENP-A nucleosome that are exposed for binding of CENP-C are essentially conserved in the *Drosophila* H3 nucleosome (*5*, *13*) (fig. S2, A and B), and $CENP\text{-}C_{426–537}$ binds to the CENP-A and *Drosophila* $H3_{1\ 132}$-LEEGLG nucleosomes with the same stoichiometry and similar affinity (fig. S2, C to E, and fig. S3). We found that residues 426 to 481 of $CENP\text{-}C_{426–537}$ remain disordered while residues 482 to 537 fold into the chimeric nucleosome core (fig. S1B).

Using methyl-based chemical shift perturbation and paramagnetic relaxation enhancement (*14*, *15*), we mapped the binding sites between $CENP\text{-}C_{426–537}$ and the chimeric nucleosome. Upon binding of $CENP\text{-}C_{426–537}$, the cross-peaks of methyl groups of residues Leu^{62} in H2A; Leu^{103} in H2B; Leu^{100}, Leu^{103}, Ile^{124}, Leu^{126}, and Ile^{130} in H3; and Ile^{50} and Leu^{58} in H4 displayed large chemical shift changes, whereas those of Leu^{64} in H2A and Val^{57}, Val^{60}, Leu^{62}, and Val^{65} in H4 disappeared (Fig. 1, A and C, and fig. S4), suggesting close contact of these residues with $CENP\text{-}C_{426–537}$. We next individually mutated each of the residues Phe^{500}, Val^{509}, Val^{517}, Ile^{523}, and Ser^{535} in $CENP\text{-}C_{484–537}$ to Cys and linked them to a paramagnetic spin label. Binding of paramagnetic spin-labeled $CENP\text{-}C_{484–537}$ reduced the peak intensities of the methyl groups in the nucleosome in accordance with their distance from the paramagnetic center. Whereas the spin labels of residues Val^{509} and Val^{517} mainly affected the methyl groups near the C-terminal region of the histone fold of H2B, the spin label of residue Ile^{523} affected methyl groups at an acidic residue–rich region (acidic patch) (Fig. 1, B and C, and fig. S5). In contrast, the spin label of residue Ser^{535} affected the methyl groups of $H3_{1–132}$-LEEGLG near the C-terminal tail (Fig. 1, B and C). These results indicate that CENP-C residues 509 to 535 bind to the histone surface, using hydrophobic residues Trp^{530}, Trp^{531}, Val^{532}, and Val^{533} to recognize the LEEGLG tail and docking the positively charged region (Arg^{521}, Arg^{522}, Arg^{525}, and Arg^{526}) on the acidic patch region (fig. S5E, fig. S6, and supplementary text). The CENP-C residues 482 to 508, which include many positively charged residues, likely bind to DNA (fig. S6). The CENP-C binding region in the core histones of the *Drosophila* H3 nucleosome has the same structure as the corresponding region of the human CENP-A nucleosome (*16*) (fig. S7), further validating the use of the chimeric nucleosome.

Deletion and isothermal titration calorimetry studies showed that CENP-C residues 520 to 537 include residues critical for binding to the chimeric nucleosome (table S1). Alanine scanning revealed that substitution of any one of the Arg^{522}, Trp^{530}, or Trp^{531} residues with Ala in $CENP\text{-}C_{444–537}$ abolished binding (Fig. 2A, fig. S8A, and table S2). Conversely, the single charge-reversal mutations $Glu^{60} \rightarrow Lys$, $Glu^{63} \rightarrow Lys$, and the neutralizing mutation $Glu^{90} \rightarrow Thr$ in H2A each essentially abolished the binding (fig. S8A and table S2). Individual substitution of the two Leu residues in the C terminus of $H3_{1–132}$-LEEGLG with Ala increased the dissociation equilibrium constant (K_d) by factors of ~3 and

[1]Laboratory of Biochemistry and Molecular Biology, National Cancer Institute, Bethesda, MD 20892, USA. [2]Laboratory of Immunology, National Institute of Allergy and Infectious Diseases, Bethesda, MD 20892, USA. [3]Department of Biochemistry, Stanford University School of Medicine, Stanford, CA 94305, USA. [4]Laboratory of Molecular Biology, National Institute of Diabetes and Digestive and Kidney Diseases, Bethesda, MD 20892, USA.

*Corresponding author. E-mail: yawen@helix.nih.gov

~4, respectively (fig. S8A and table S2). In contrast, Ala substitution of the two Glu residues decreased K_d by factors of ~3 and ~10, respectively (table S2), indicating that the CENP-A C-terminal tails have not evolved for high-affinity binding with CENP-C. Mutation of CENP-C central region residues Arg^{522}, Trp^{530}, or Trp^{531} to Ala also substantially decreased the localization of GFP-fused CENP-$C_{1–537}$ to centromeres in human cells, whereas the Ser^{520} → Ala and Ser^{524} → Ala mutations had smaller effects (Fig. 2B and fig. S8B). Mutation of the two acidic patch residues Glu^{61} and Glu^{64} residues in H2A to either Ala or positively charged Lys inhibited the recruitment of CENP-C from the *Xenopus* egg extract to the reconstituted CENP-A nucleosome array (Fig. 2C and fig. S8C) (*6*). Neutralization of the acidic patch by the mutations did not disrupt the formation of condensed CENP-A nucleosome arrays (fig. S9).

The central region of CENP-C is conserved in most mammals, whereas the CENP-C motif is conserved from budding yeast to human (fig. S10A). Residues Arg^{522}, Trp^{530}, and Trp^{531}, which are most important for the binding of the CENP-C central region to the chimeric nucleosome, are essentially conserved in the CENP-C motif and correspond to residues Arg^{742}, Tyr^{750}, and Trp^{751}; this finding suggests that the human CENP-C motif may also bind to CENP-A and $H3_{1–132}$-LEEGLG nucleosomes. Indeed, chemical shift perturbation studies indicate that the CENP-C motif and the CENP-C central region bind to similar sites on the core histones in the $H3_{1–132}$-LEEGLG nucleosome (Fig. 3A and fig. S11). Furthermore, binding of the CENP-C motifs from human, rat, fission yeast, and budding yeast to the H3 chimeric nucleosomes containing

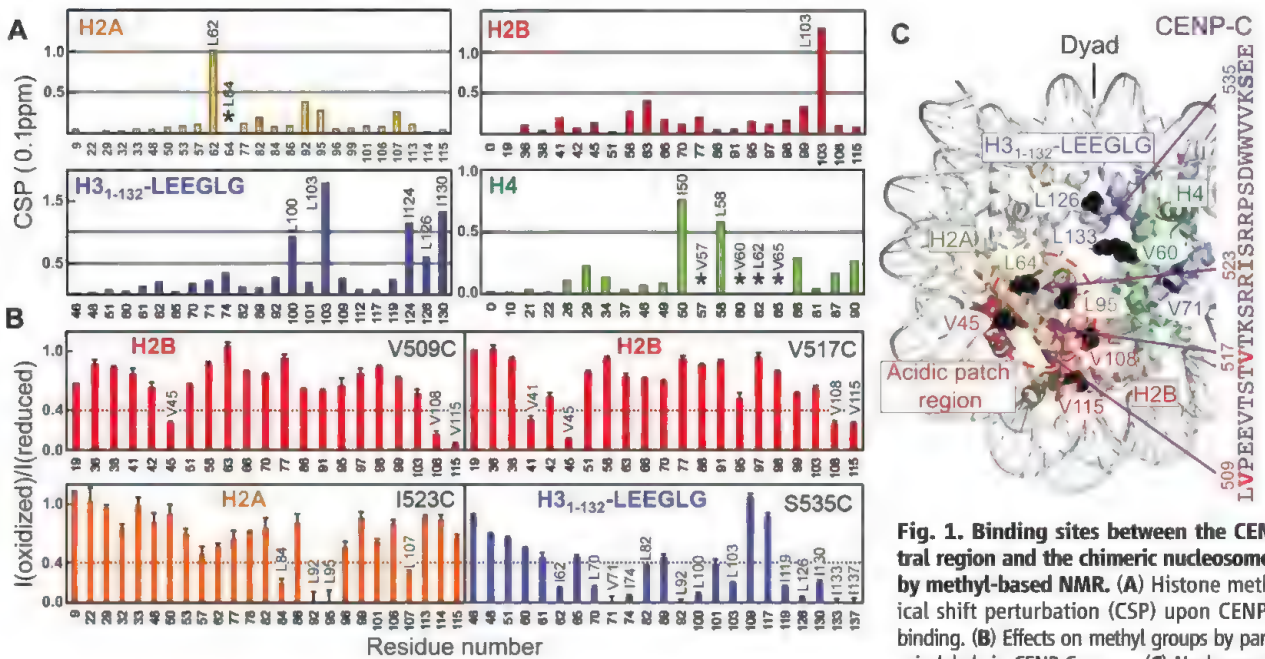

Fig. 1. Binding sites between the CENP-C central region and the chimeric nucleosome mapped by methyl-based NMR. (**A**) Histone methyl chemical shift perturbation (CSP) upon CENP-$C_{426–537}$ binding. (**B**) Effects on methyl groups by paramagnetic spin labels in CENP-$C_{484–537}$. (**C**) Nucleosome structure showing representative side chains (black balls) whose methyl groups display large changes in (A) or (B), as well as approximate locations of CENP-C residues (arrows). Glu^{133} in H3 is used to represent Leu^{133} in $H3_{1–132}$-LEEGLG. Single-letter abbreviations for amino acid residues: C, Cys; D, Asp; E, Glu; G, Gly; I, Ile; K, Lys; L, Leu; P, Pro; R, Arg; S, Ser; T, Thr; V, Val; W, Trp. The histones in the front side of the nucleosome are colored orange (H2A), salmon (H2B), blue (H3), and green (H4), respectively. DNA and the histones in the back of the nucleosome are shown in light gray.

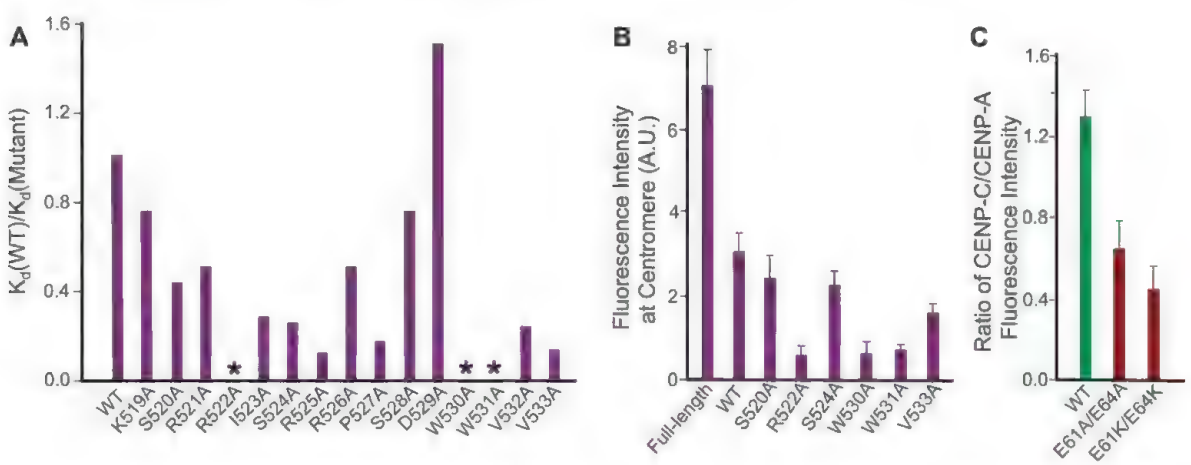

Fig. 2. Residues important for binding of the central region of CENP-C and the chimeric nucleosome. (**A**) Effects of mutations in CENP-$C_{444–537}$ on its binding to the $H3_{1–132}$-LEEGLG nucleosome. Asterisk indicates no detectable binding. (**B**) Effect of CENP-$C_{1–537}$ mutations on centromere targeting in human cells (fig. S8B). Error bars denote SEM; $n = 4$, Student's t probability $P \leq 0.02$ for all mutants. (**C**) Effect of H2A acidic patch mutations on localization of CENP-C to the CENP-A nucleosome arrays (fig. S8C). Error bars denote SEM; $n = 4$, Student's t probability $P \leq 0.05$ for both mutants.

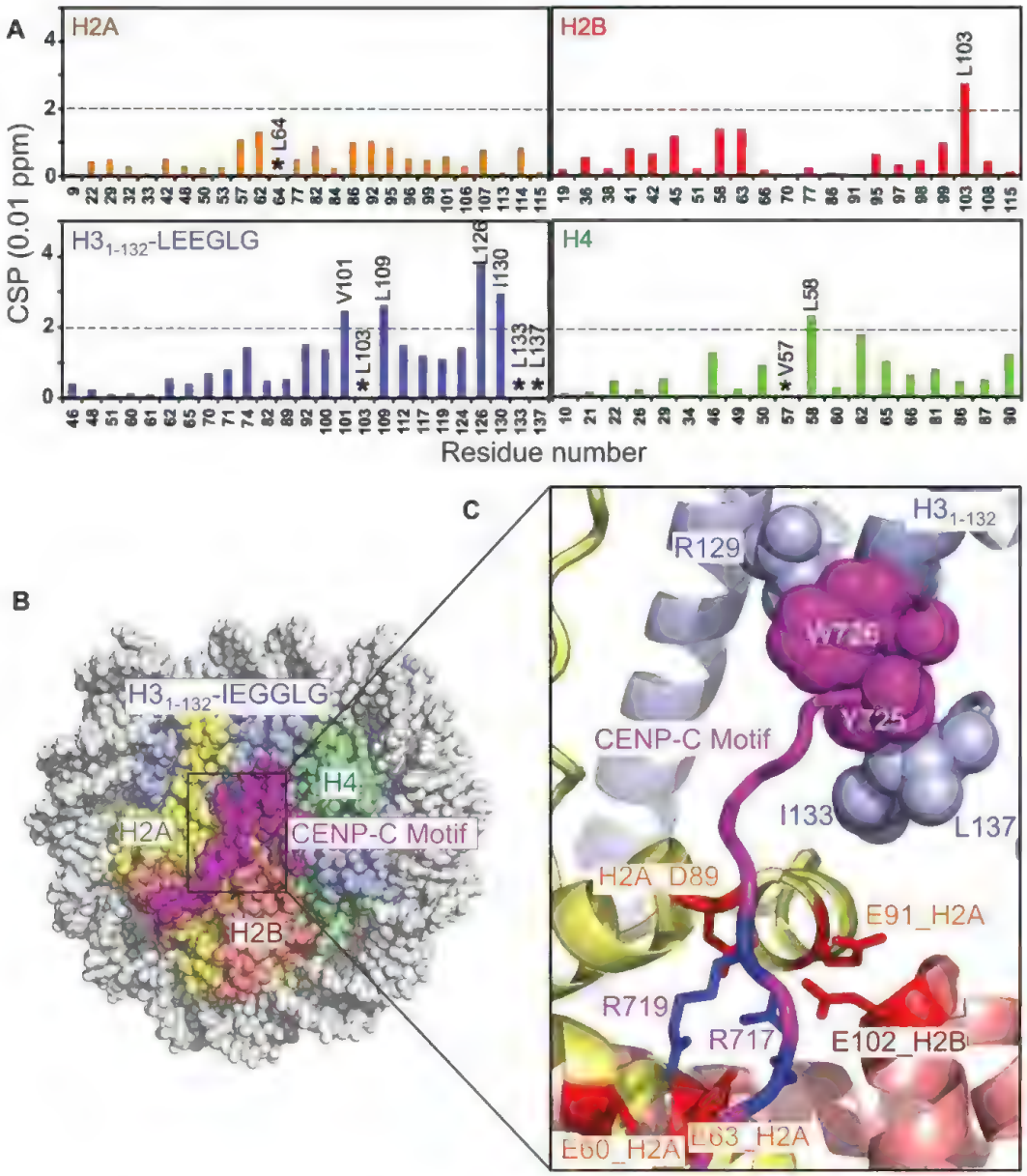

Fig. 3. Broadly conserved CENP-C motifs bind to the H3 nucleosome chimera containing CENP-A C-terminal tails. (**A**) Nucleosome methyl CSP upon binding of the human CENP-C motif. (**B**) The structure of the rat CENP-C motif in complex with the $H3_{1–132}$-IEGGLG nucleosome. (**C**) Enlarged region showing hydrophobic and electrostatic interactions.

the corresponding C-terminal residues of the CENP-A homolog displayed reasonably strong affinities, with K_d values of 1.4, 0.1, 1.4, and 0.3 μm, respectively (fig. S12 and table S3). Charge reversal mutation of a single acidic residue in the acidic patch (Glu^{60} → Lys or Glu^{63} → Lys) abolished the binding of the CENP-C motif (table S3). Furthermore, mutation of the conserved sites within the rat CENP-C motif (Arg^{717} → Ala, Tyr^{725} → Ala, or Trp^{726} → Ala) substantially decreased the binding affinity (fig. S12 and table S4). Mutation of the residues corresponding to Arg^{717} in frog, fly, and fission yeast prevented targeting of CENP-C to the centromere (*9*–*11*).

We determined the crystal structure of the rat CENP-C motif in complex with the corresponding $H3_{1–132}$-IEGGLG (Ile-Glu-Gly-Gly-Leu-Gly) nucleosome at 3.5 Å resolution (Fig. 3B, fig. S13, and table S5). In the structure, the conserved CENP-C motif residue Tyr^{725} recognizes the residues Ile^{133} and Leu^{137} in the IEGGLG tail through hydrophobic interactions, inducing the IEGGLG tail to fold into a turn structure and promoting intramolecular hydrophobic interactions between Ile^{133} and Leu^{137}. CENP-C residue Trp^{726} forms intramolecular hydrophobic interactions with CENP-C residue Tyr^{725}, in addition to interacting with the hydrophobic region of the side chain of residue Arg^{129} in $H3_{1–132}$. CENP-C residues Arg^{717} and Arg^{719} form electrostatic interactions with the acidic patch residues Glu^{60}, Glu^{63}, Asp^{89}, and Glu^{91} of H2A and Glu^{102} of H2B. Binding to the acidic patch was similarly found in structures of LANA (*17*), RCC1 (*18*), and the Sir3 BAH domain (*19*) in complex with the nucleosome.

Whereas CENP-C motifs are well conserved among all species, the C-terminal tails of CENP-As are not (fig. S10B). We observed a common feature in the C-terminal tails of CENP-As: They are more hydrophobic than those of corresponding H3. In particular, the C-terminal tails of CENP-As have at least one bulky hydrophobic residue such as Ile, Leu, Val, or aromatic residues (with the exception of fission yeast), which are absent in the C-terminal tails of H3. In addition, nucleosomes containing chimeric $H3_{1–132}$-QFI (C-terminal tail of CENP-A in budding yeast) bound to the central region and the CENP-C motif of human CENP-C with affinity similar to that of nucleosomes containing $H3_{1–132}$-LEEGLG (Fig. 4 and table S3). Thus, the higher hydrophobicity of the C-terminal tail of CENP-A, rather than a specific amino acid sequence, is the key determinant for specific recognition by CENP-C.

Our findings can explain diverse experimental results in the literature. In human cells, the

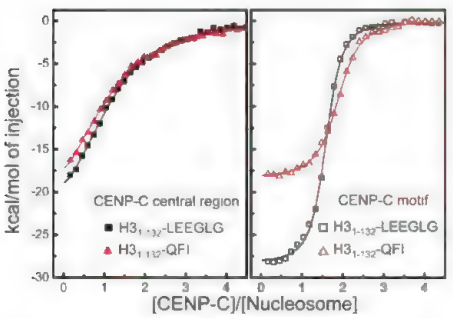

Fig. 4. Hydrophobicity of the CENP-A tail is the primary determinant for recognition of the CENP-A nucleosome by CENP-C. Isothermal titration calorimetric curves are shown for binding of the human CENP-C central region (CENP-$C_{444–537}$) and the CENP-C motif (CENP-$C_{727–767}$) to nucleosomes containing $H3_{1–132}$-LEEGLG (human) and $H3_{1–132}$-QFI (budding yeast), respectively.

CENP-$C_{638–943}$ fragment, which contains the CENP-C motif and the dimerization domain, is capable of being targeted to the centromere when overexpressed (*20*). In *Xenopus*, chromatin in which H2A/H2B is replaced by protamines does not support CENP-C localization to the centromere of sperm (*9*, *21*). However, CENP-C colocalizes with CENP-A upon addition of egg extract, because the histone chaperone nucleoplasmin catalyzes the eviction of protamines and the incorporation of H2A/H2B dimers into the sperm chromatin (*21*). The function of human CENP-A can be complemented by the budding yeast *Saccharomyces cerevisiae* homolog Cse4 (*22*) (Fig. 4). Our study also suggests that CENP-C can recognize CENP-A chromatin through multivalent interactions, allowing it to associate more strongly and selectively (figs. S14 and S15) (*20*, *23*). In addition, our results have implications for various structural models of the centromeric nucleosome, a widely discussed and controversial topic (*24*). The finding that the broadly conserved CENP-C motif in a dimeric CENP-C could bind to two H2A/H2B and two CENP-A/H4 molecules constrains these models because CENP-C is constitutively associated with the centromeric nucleosome. Our study provides the structural basis for the recognition of the CENP-A octameric nucleosome by CENP-C. Further understanding of how it engages chromatin should provide important insight into favored compositions of CENP-A nucleosomes.

Our finding that the widely conserved CENP-C motif binds to the centromeric nucleosome, along with the recent identification of the budding yeast homologs of the vertebrate centromere proteins CENP-T and CENP-W (*25*, *26*), supports a conserved mechanism of centromere targeting by the kinetochore. Furthermore, our study has revealed a histone recognition mode whereby an intrinsically disordered peptide binds to the histone tail through hydrophobic interactions facilitated by nucleosome docking; this broadens the repertoire of the cell to "read" histone variations (*27*, *28*), not only at the centromere but possibly also in other contexts.

References and Notes

1. S. Henikoff, K. Ahmad, H. S. Malik, *Science* **293**, 1098 (2001).
2. J. S. Verdaasdonk, K. Bloom, *Nat. Rev. Mol. Cell Biol.* **12**, 320 (2011).
3. T. Hori *et al.*, *Cell* **135**, 1039 (2008).
4. M. R. Przewloka *et al.*, *Curr. Biol.* **21**, 399 (2011).
5. C. W. Carroll, K. J. Milks, A. F. Straight, *J. Cell Biol.* **189**, 1143 (2010).
6. A. Guse, C. W. Carroll, B. Moree, C. J. Fuller, A. F. Straight, *Nature* **477**, 354 (2011).
7. E. Screpanti *et al.*, *Curr. Biol.* **21**, 391 (2011).
8. K. Song, B. Gronemeyer, W. Lu, E. Eugster, J. E. Tomkiel, *Exp. Cell Res.* **275**, 81 (2002).
9. K. J. Milks, B. Moree, A. F. Straight, *Mol. Biol. Cell* **20**, 4246 (2009).
10. K. Tanaka, H. L. Chang, A. Kagami, Y. Watanabe, *Dev. Cell* **17**, 334 (2009).
11. S. Heeger *et al.*, *Genes Dev.* **19**, 2041 (2005).
12. R. L. Cohen *et al.*, *Mol. Biol. Cell* **19**, 4480 (2008).
13. C. W. Carroll, M. C. Silva, K. M. Godek, L. E. Jansen, A. F. Straight, *Nat. Cell Biol.* **11**, 896 (2009).
14. V. Tugarinov, V. Kanelis, L. E. Kay, *Nat. Protoc.* **1**, 749 (2006).
15. H. Kato *et al.*, *Proc. Natl. Acad. Sci. U.S.A.* **108**, 12283 (2011).
16. H. Tachiwana *et al.*, *Nature* **476**, 232 (2011).
17. A. J. Barbera *et al.*, *Science* **311**, 856 (2006).
18. R. D. Makde, J. R. England, H. P. Yennawar, S. Tan, *Nature* **467**, 562 (2010).
19. K. J. Armache, J. D. Garlick, D. Canzio, G. J. Narlikar, R. E. Kingston, *Science* **334**, 977 (2011).
20. S. Trazzi *et al.*, *J. Struct. Biol.* **140**, 39 (2002).
21. A. Philpott, G. H. Leno, *Cell* **69**, 759 (1992).
22. G. Wieland, S. Orthaus, S. Ohndorf, S. Diekmann, P. Hemmerich, *Mol. Cell. Biol.* **24**, 6620 (2004).
23. S. Ando, H. Yang, N. Nozaki, T. Okazaki, K. Yoda, *Mol. Cell. Biol.* **22**, 2229 (2002).
24. B. E. Black, D. W. Cleveland, *Cell* **144**, 471 (2011).
25. L. J. Bock *et al.*, *Nat. Cell Biol.* **14**, 614 (2012).
26. A. Schleiffer *et al.*, *Nat. Cell Biol.* **14**, 604 (2012).
27. S. Khorasanizadeh, *Curr. Opin. Struct. Biol.* **21**, 744 (2011).
28. C. A. Musselman, M. E. Lalonde, J. Côté, T. G. Kutateladze, *Nat. Struct. Mol. Biol.* **19**, 1218 (2012).

Acknowledgments: We thank the staff at the Advanced Photon Source (APS) (23-ID beamline) for technical support; C. Carroll for initial participation of the project; J. Barrowman for manuscript editing; A. Kelly, C. Wu, and C. Klee for comments; H. Kurumizaka and K. Morikawa for human histone plasmids and advice for CENP-A nucleosome reconstitution; and S. Tan for the 601 DNA plasmid. Supported by the intramural programs of the National Cancer Institute (H.K., H.F., B.-R.Z., and Y.B.); the National Institute of Allergy and Infectious Diseases (J.J. and T.S.X.); the National Institute of Diabetes and Digestive and Kidney Diseases (R.G.); NIH grant R01 GM074728 (M.R. and A.F.S.); and National Cancer Institute grant Y1-CO-1020, National Institute of General Medical Sciences grant Y1-GM-1104, and U.S. Department of Energy grant DE-AC02-06CH11357 (APS). The structure PDB ID is 4INM.

Supplementary Materials

www.sciencemag.org/cgi/content/full/340/6136/1110/DC1
Materials and Methods
Figs. S1 to S15
Tables S1 to S5
References (*29–45*)

23 January 2013; accepted 8 April 2013
10.1126/science.1235532

Structure of RSV Fusion Glycoprotein Trimer Bound to a Prefusion-Specific Neutralizing Antibody

Jason S. McLellan,[1]* Man Chen,[1] Sherman Leung,[1] Kevin W. Graepel,[1] Xiulian Du,[1] Yongping Yang,[1] Tongqing Zhou,[1] Ulrich Baxa,[2] Etsuko Yasuda,[3] Tim Beaumont,[3] Azad Kumar,[1] Kayvon Modjarrad,[1] Zizheng Zheng,[4] Min Zhao,[4] Ningshao Xia,[4] Peter D. Kwong,[1]* Barney S. Graham[1]

The prefusion state of respiratory syncytial virus (RSV) fusion (F) glycoprotein is the target of most RSV-neutralizing activity in human sera, but its metastability has hindered characterization. To overcome this obstacle, we identified prefusion-specific antibodies that were substantially more potent than the prophylactic antibody palivizumab. The cocrystal structure for one of these antibodies, D25, in complex with the F glycoprotein revealed D25 to lock F in its prefusion state by binding to a quaternary epitope at the trimer apex. Electron microscopy showed that two other antibodies, AM22 and 5C4, also bound to the newly identified site of vulnerability, which we named antigenic site Ø. These studies should enable design of improved vaccine antigens and define new targets for passive prevention of RSV-induced disease.

Respiratory syncytial virus (RSV) infects nearly all children by 3 years of age (*1*) and is a leading cause of infant hospitalization and childhood wheezing (*2*, *3*). Globally, RSV accounts for 6.7% of deaths among infants 1 month to 1 year old—more than any other single pathogen except malaria (*4*). The only intervention is passive administration of the licensed monoclonal antibody palivizumab (Synagis), which recognizes the RSV fusion (F) glycoprotein (*5*, *6*) and reduces incidence of severe disease (*7*). Clinical evidence that RSV F-specific antibodies can protect against disease has prompted a search for better antibodies (*8–10*) and a concerted effort to develop an effective vaccine (*11*).

RSV F is a type I fusion protein (*12*) that rearranges from a metastable prefusion conformation to a highly stable postfusion structure.

Three previously described antigenic sites (I, II, and IV) associated with neutralizing activity (*13*–*15*) exist on the postfusion form of F (*16*, *17*). Absorption of human sera with postfusion F, however, fails to remove most of the F-specific neutralizing activity, suggesting that there are neutralizing antigenic sites unique to the prefusion form (*18*). Thus, determining the prefusion RSV F structure and identifying antibodies that bind prefusion-specific antigenic sites have become converging priorities for developing new antibodies and vaccines to prevent RSV infection.

From mice immunized with gene-based vectors expressing the F protein (*19*), we isolated an antibody, 5C4, that was 50 times as potent as palivizumab (Fig. 1A) and did not bind to a soluble form of RSV F stabilized in the postfusion conformation (*16*) (Fig. 1B). We determined that 5C4 shared these properties with two recently isolated human antibodies, D25 and AM22 (*10*, *20*, *21*) (Fig. 1, A and B), and we hypothesized that these antibodies recognized the metastable prefusion conformation (*22*).

We focused our structural efforts on the human antibodies by first screening their binding to a panel of RSV F glycoprotein variants (*23*). We observed D25 and AM22 antibody binding to a construct, RSV F(+) Fd, comprising residues 1 to 513 fused to a C-terminal fibritin trimerization domain (*24*). However, we failed to form complexes by mixing purified RSV F(+) Fd with purified D25 or AM22, suggesting that F was triggered during purification (*25*). To capture F in its prefusion state, RSV F(+) Fd was expressed as a complex with D25. Optimal expression was obtained from cotransfection of DNA encoding D25 Fab with DNA encoding RSV F(+) Fd (fig. S1). X-ray diffraction data to 3.6 Å resolution were obtained on crystals of this complex, and the structure was solved by molecular replacement using the unbound D25 Fab structure (table S1) and portions of the postfusion RSV F structure (*16*, *17*) as search models. The structure was refined to R_{cryst}/R_{free} of 21.3/26.7% (Fig. 1C and table S1).

The D25-bound RSV F structure resembled the prefusion structure of the related parainfluenza virus 5 (PIV5) F glycoprotein (*26*, *27*), indicating that D25 binding stabilizes RSV F in the prefusion conformation (fig. S2). Comparison with the postfusion RSV F glycoprotein structure (*16*, *17*) revealed that most of the secondary and tertiary structure was preserved in both pre- and postfusion states, with 215 residues showing less than 2 Å Cα deviation between the two structures (Fig. 2). In contrast, regions at the N and C termini of the F_1 subunit showed marked conformational changes. The fusion peptide, located at the N terminus of F_1, and five secondary-structure elements (α2, α3, α4, and the β3/β4 hairpin) rearrange and fuse with the α5 helix to form a single extended postfusion helix ($\alpha5_{post}$) of >100 Å in length (fig. S3). At the C terminus of F_1, the sole parallel strand (β22) unravels, allowing the prefusion α10 helix to move toward the $\alpha5_{post}$ helix. Similar rearrangements are observed in the comparison of prefusion PIV5 and postfusion parainfluenza virus 3 (PIV3) F glycoprotein structures (*27*), indicating that F glycoproteins from both the *Paramyxovirinae* (PIV5/PIV3) and *Pneumovirinae* (RSV) subfamilies undergo similar conformational rearrangements to facilitate membrane fusion.

Despite overall similarities between the PIV5 and RSV F prefusion structures, there are distinct differences important for function and antigenicity. In the prefusion RSV F structure, the helix-loop-helix (α6 and α7) motif that constitutes antigenic site II is located further away from the three-fold trimer axis than is the homologous region in PIV5 F (fig. S4). This repositioning exposes the face of the helix-loop-helix bound by palivizumab and motavizumab, allowing these antibodies to bind prefusion RSV F without first requiring a conformational rearrangement to occur as originally suggested on the basis of modeling with the PIV5 F structure (*28*).

Another difference is that the RSV F fusion peptide is buried in the center of the trimer cavity, with its N terminus located more than 40 Å away from the last visible F_2 residue (Fig. 2). In contrast, the PIV5 F fusion peptide lies in a surface groove between subunits, is partially exposed to solvent (*27*), and undergoes minimal movement after protease cleavage (*26*). This suggests that in RSV F, a substantial structural rearrangement of the fusion peptide occurs after the F_0 precursor is cleaved by the furin-like host protease to produce F_1 and F_2 subunits (*29*). In comparison to other structures of cleaved, type I fusion proteins (*26*, *30*, *31*), the location of the RSV F fusion peptide is most similar to that of influenza hemagglutinin (*31*) (fig. S5), which is surprising

[1]Vaccine Research Center, National Institute of Allergy and Infectious Diseases, National Institutes of Health, Bethesda, MD 20892, USA. [2]Electron Microscopy Laboratory, Advanced Technology Program, SAIC-Frederick, Inc, Frederick National Laboratory for Cancer Research, Frederick, MD 21702, USA. [3]AIMM Therapeutics, Academic Medical Center, Amsterdam, Netherlands. [4]National Institute of Diagnostics and Vaccine Development in Infectious Diseases, Xiamen University, Xiamen, China, 361005.

*Corresponding author. E-mail: mclellanja@niaid.nih.gov (J.S.M.); pdkwong@nih.gov (P.D.K.)

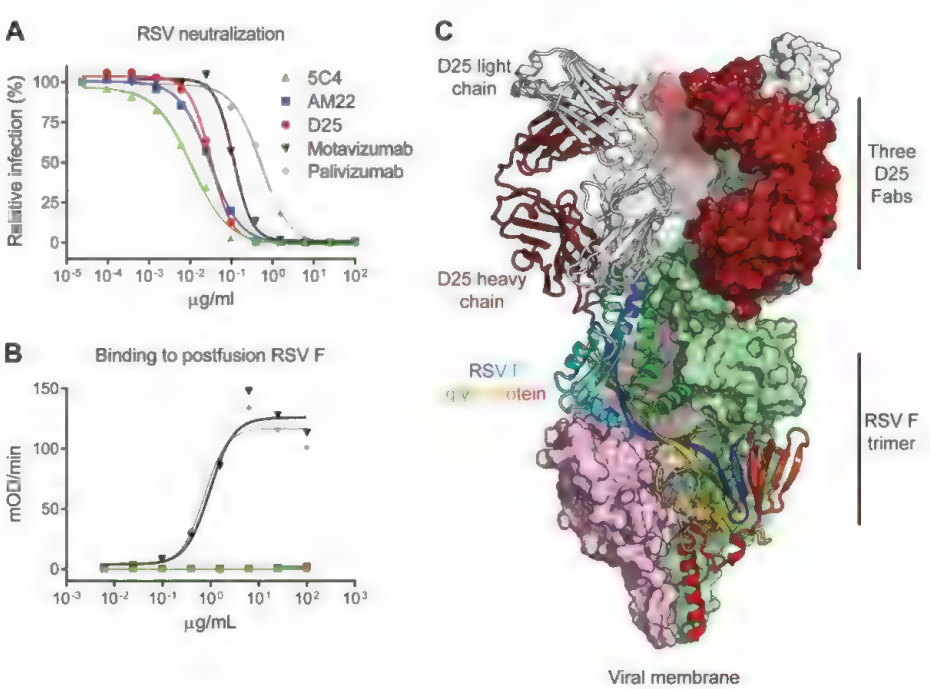

Fig. 1. RSV neutralization, F glycoprotein recognition, and crystal structure of human antibody D25 in complex with the prefusion RSV F trimer. The prefusion conformation of RSV F is metastable, and when expressed in a soluble form readily adopts the postfusion state; a number of potent antibodies, including D25, bind to a newly revealed antigenic site at the top of the prefusion F glycoprotein. **(A)** RSV neutralization by antibodies. Palivizumab is the U.S. Food and Drug Administration (FDA)–approved prophylactic antibody that prevents severe RSV disease. **(B)** Enzyme-linked immunosorbent assay measuring antibody binding to postfusion F glycoprotein. For (A) and (B), data are representative of multiple independent experiments. **(C)** D25-RSV F trimer crystal structure in ribbon and molecular surface representations. One protomer of the F glycoprotein trimer is shown as ribbons and colored as a rainbow from blue to red, N terminus of F_2 to C terminus of F_1, respectively. Molecular surfaces are shown for the other two F protomers, colored pink and green. The D25 Fab bound to the F protomer shown in ribbons is also displayed in ribbon representation, with the heavy chain colored red and light chain colored gray. The other D25 Fabs are colored the same, but shown in surface representation.

given that hemagglutinin is triggered by acidic pH in the endosome, whereas RSV F triggering is pH-independent and thought to occur at the cell surface (*32*).

In the RSV F prefusion trimer, the C-terminal helices (α10) form an inverted pyramid (fig. S4). In contrast, the C-terminal helices in the PIV5 F trimer form a coiled-coil, which was stabilized by a coiled-coil GCN4-trimerization motif (*27*). The addition of this motif was sufficient to stabilize PIV5 and human metapneumovirus (hMPV) F proteins in the prefusion state (*27*, *33*). The inverted pyramid conformation observed in the RSV F structure may explain why RSV F could not be expressed with the GCN4 motif, but could be expressed with the fibritin trimerization domain (*24*). The addition of the fibritin domain was not, however, sufficient to stabilize RSV F in the prefusion state, suggesting that it is not an optimal substitute for the native transmembrane domains that normally stabilize F in the viral membrane (*34*). The binding of antibody D25 was thus required to stabilize the prefusion trimer.

D25 recognizes a quaternary epitope at the membrane-distal apex of the RSV F glycoprotein (Fig. 1C). The D25 heavy chain interacts with one protomer (involving 638 $Å^2$ of interactive surface area on F), and the D25 light chain binds to the same protomer (373 $Å^2$) and a neighboring protomer (112 $Å^2$) (Fig. 3A). D25 contacts RSV F with five of its six complementarity-determining regions (CDRs), with the heavy-chain third CDR interacting with the α4 helix (F_1 residues 196 to 210) and forming intermolecular hydrogen bonds with F_2 residues 63, 65, 66, and 68 in the loop between strand β2 and helix α1. Whereas the secondary structure of the D25 epitope remains mostly unchanged in pre- and postfusion conformations, the tertiary structure changes substantially, with helix α4 pivoting ~180° relative to strand β2 (Fig. 3B). This explains the failure of D25 to bind postfusion F and suggests that D25 neutralizes RSV by fixing F in its prefusion conformation.

D25 binds the least conserved region on the F glycoprotein (Fig. 3C). Although F proteins from human RSV A and B subtypes are highly related in sequence (447 of 472 or 94.7% of the amino acids comprising the mature F_2/F_1 ectodomain are identical), six naturally observed sequence variations are located in the region bound by D25 (Fig. 3D). Similarly, of the 56 amino acids in bovine RSV F that are not identical to the mature ectodomain of human RSV F subtype A, 13 are found in this same region (Fig. 3D). Thus, the D25 epitope, at the apex of the prefusion RSV F structure, may be under immune pressure and serve as a determinant of subtype-specific immunity (*35*, *36*).

To investigate whether AM22 and 5C4 bind the D25 epitope, we performed competition binding and electron microscopy (EM) experiments. We determined that D25 binding to RSV-infected cells was competed by AM22 and 5C4 (Fig. 4A). In addition, negative-stain EM images of Fab D25-RSV F complexes resembled the EM images of Fab AM22-RSV F and Fab 5C4-RSV F complexes (Fig. 4B). Together, these results suggest that antibodies D25, AM22, and 5C4 recognize the same or a highly related epitope, which we named "antigenic site Ø." In addition to their extraordinary potency and prefusion specificity (Fig. 1A), all three antibodies strongly inhibited fusion when added after attachment (Fig. 4C), and all three were unable to block cell-surface attachment (Fig. 4D), suggesting that the putative RSV F receptor binds to a region on F not blocked by these antibodies. AM22 and D25 antibodies also neutralized similarly in both Fab and immunoglobulin contexts (fig. S6), indicating that avidity was not required for potent neutralization, in contrast to what was previously observed for some influenza-virus antibodies (*37*). Thus, antigenic site Ø–specific antibodies are distinct from neutralizing antibodies to other known antigenic sites on RSV F because of their exclusive recognition of the prefusion F structure and extremely high potency (fig. S7).

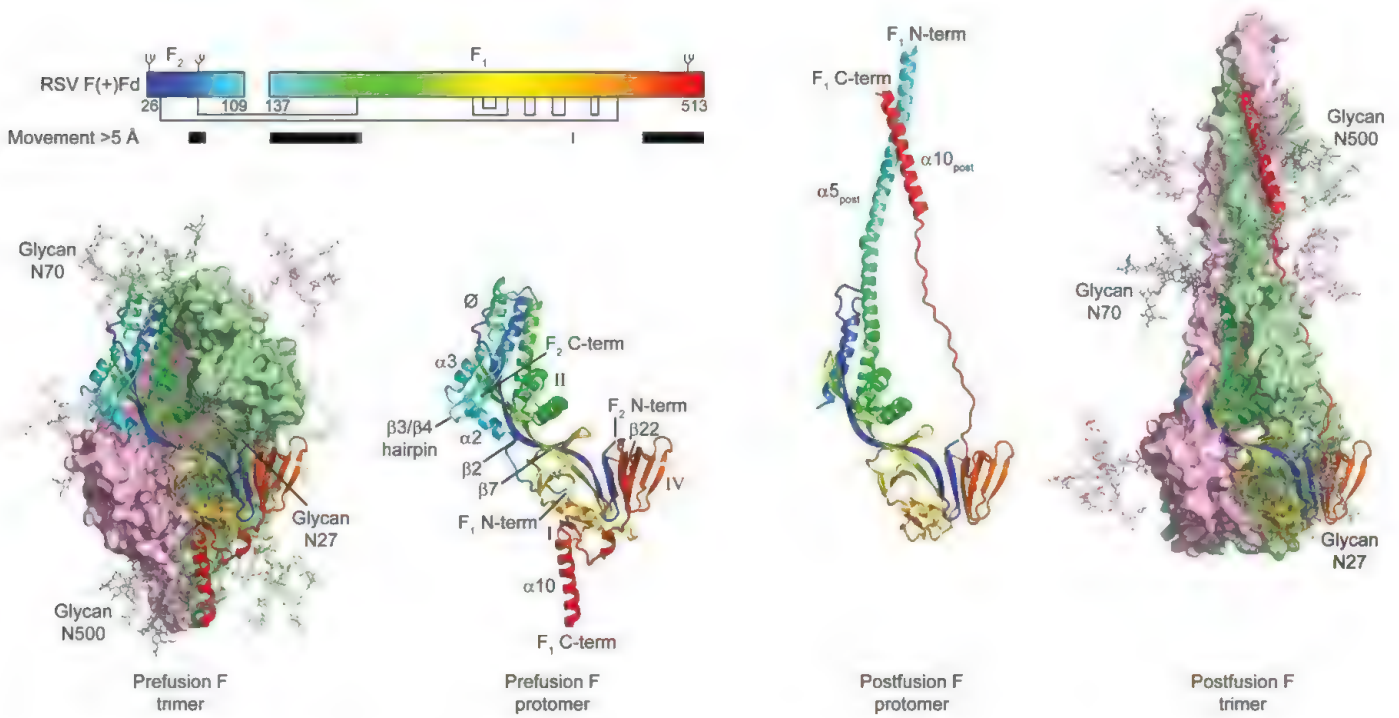

Fig. 2. Structural rearrangement of RSV F. To mediate virus-cell entry, the RSV F glycoprotein transitions from a metastable prefusion conformation to a stable postfusion conformation. Outer images display prefusion (left) and postfusion (right) trimeric structures, colored the same as in Fig. 1C. A complex glycan, shown as sticks, is modeled at each of the three *N*-linked glycosylation sites found in the mature protein. Inner images display a single RSV F protomer in ribbon representation, colored as a rainbow from blue to red, N terminus of F_2 to C terminus of F_1, respectively. Select secondary-structure elements are labeled (correspondence with amino acid sequence in pre- and postfusion conformations is shown in fig. S3). Inset: Schematic of the mature RSV F protein in the RSV F(+) Fd construct. The rainbow coloring of the boxes representing the F_2 and F_1 subunits matches that in the structures. Glycans are shown as branches on top of the boxes, and disulfide bonds are shown as black lines under the boxes. Amino acids that move more than 5 Å in the pre- and postfusion conformations are indicated by black bars.

Antigenic site Ø, located at the apex of the prefusion F trimer, should be readily accessible even on the crowded virion surface, which may explain the observation that most neutralizing activity in human sera induced by natural RSV infection is directed against the prefusion form of RSV F (*18*). That the three antibodies described in this study recognize antigenic site Ø at different angles (Fig. 4B) and share low sequence

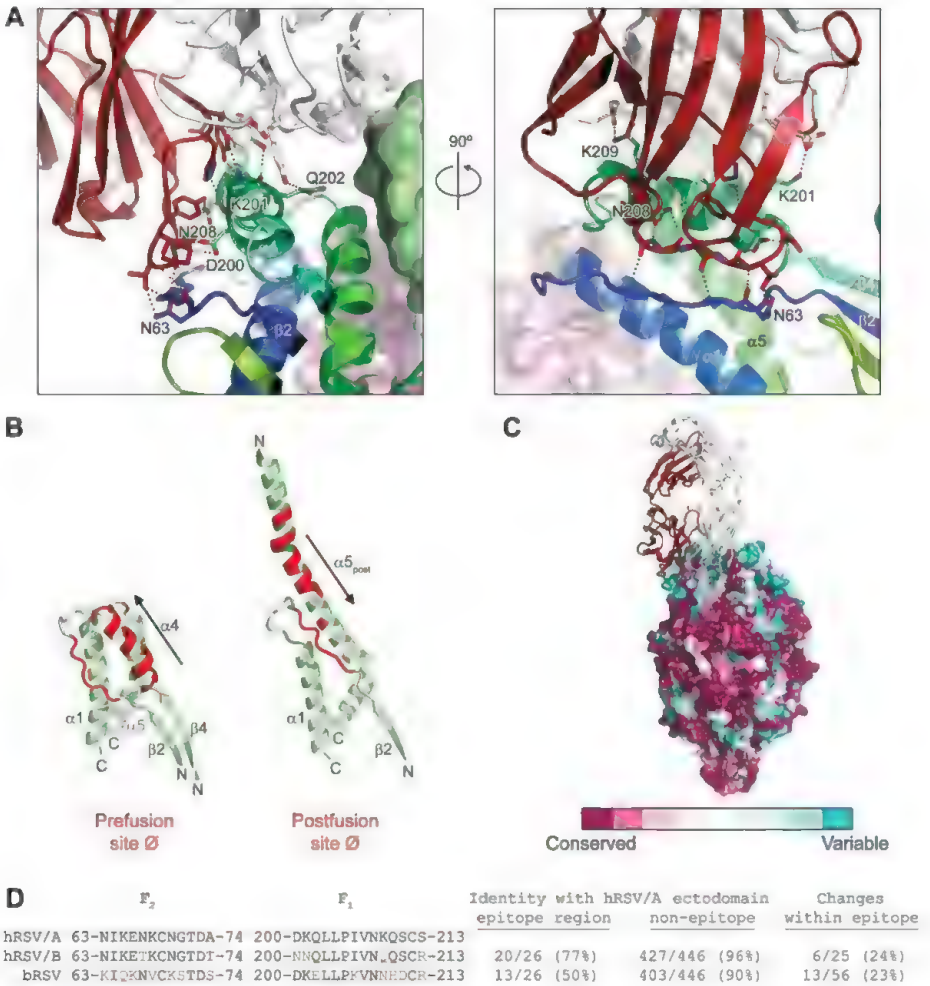

Fig. 3. RSV F interface with D25. Antibody D25 binds a quaternary epitope spanning two protomers at the apex of the prefusion F trimer. (**A**) Close-up of the interface between D25 and RSV F. Side chains of F residues interacting with D25 are labeled and shown as sticks. Oxygen atoms are colored red and nitrogen atoms are colored blue. Hydrogen bonds are depicted as dotted lines. The two images are related by a 90° rotation about the vertical axis. (**B**) Position and conformation of the D25 epitope on the prefusion and postfusion F molecules. RSV F residues at the D25 interface are colored red; polarity of α4 and $\alpha5_{post}$ is indicated with arrows, with fragment N and C termini indicated. (**C**) Surface representation of RSV F colored according to sequence conservation. Coloring was generated with the ConSurf server (*40*) using 178 F glycoprotein sequences from human RSV subtype A and B, as well as bovine RSV. (**D**) Sequence conservation of F residues in regions recognized by D25. Amino acids in human RSV subtype B (hRSV/B) or in bovine RSV (bRSV) that differ from hRSV/A are colored red. Ectodomain is defined as F residues 26 to 109 and 137 to 524. Abbreviations for the amino acid residues are as follows: A, Ala; C, Cys; D, Asp; E, Glu; G, Gly; H, His; I, Ile; K, Lys; L, Leu; N, Asn; P, Pro; Q, Gln; R, Arg; S, Ser; T, Thr; and V, Val.

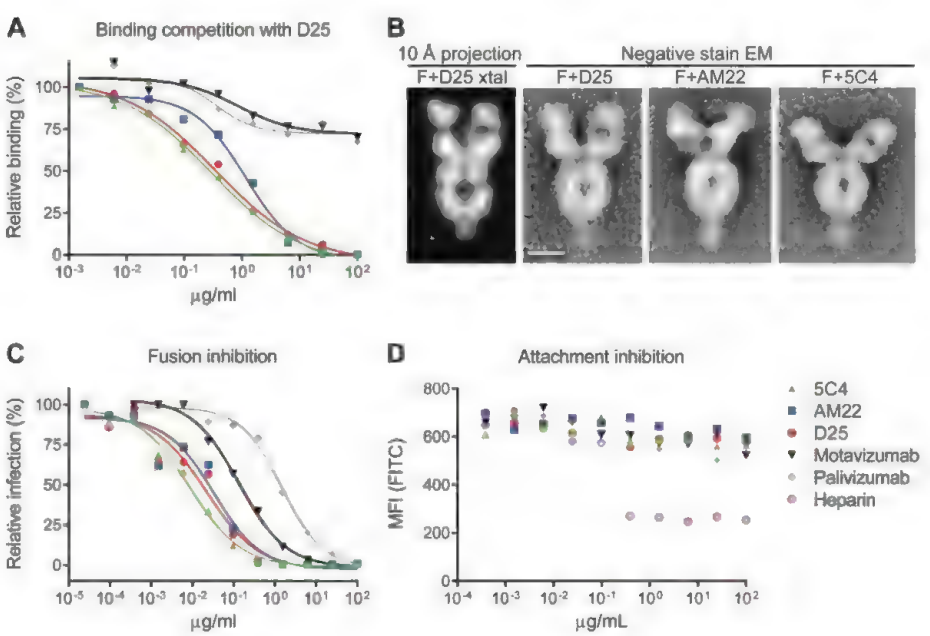

Fig. 4. Antigenic site Ø. Highly effective RSV-neutralizing antibodies target a site at the membrane-distal apex of the prefusion F trimer. (**A**) The ability of antibodies to block D25 binding to RSV-infected cells was measured as a function of antibody concentration. (**B**) Analysis of RSV F-Fab complexes by negative-stain electron microscopy (EM): Reprojection of a 12 Å slice through the crystal structure of RSV F + D25 Fab filtered to 10 Å resolution (left). A slice was used to emphasize visibility of the F glycoprotein cavity. Aligned average of 263 particles of RSV F + D25 Fab (middle left). Aligned average of 550 particles of RSV F + AM22 Fab (middle right). Aligned average of 171 particles of RSV F + 5C4 Fab (right). Scale bar, 50 Å. (**C**) Fusion inhibition and (**D**) attachment inhibition activity for antibodies targeting antigenic site Ø and F-specific antibodies targeting other antigenic sites. For the attachment-inhibition assay, heparin was used as a positive control. Data in (A), (C), and (D) are representative of multiple independent experiments.

homology suggests that there may be many other antibodies within the repertoire capable of recognizing this prominent epitope. The high potency of antibodies against antigenic site Ø suggests that they could be developed for passive prophylaxis of RSV-induced disease in neonates. Notably, the immunogen-elicited 5C4 antibody provides proof-of-principle that antibodies against antigenic site Ø can be induced by gene-based immunization presenting the native form of F. Vaccine antigens stabilized in the prefusion conformation, perhaps facilitated by linking mobile and immobile portions of F with disulfide bonds, may further improve elicitation of antibodies to antigenic site Ø. Definition of the D25-RSV F structure thus provides the basis for new approaches to prevent RSV-induced disease.

References and Notes

1. W. P. Glezen, L. H. Taber, A. L. Frank, J. A. Kasel, *Am. J. Dis. Child.* **140**, 543 (1986).
2. D. K. Shay *et al.*, *JAMA* **282**, 1440 (1999).
3. C. B. Hall *et al.*, *N. Engl. J. Med.* **360**, 588 (2009).
4. R. Lozano *et al.*, *Lancet* **380**, 2095 (2012).
5. S. Johnson *et al.*, *J. Infect. Dis.* **176**, 1215 (1997).
6. J. A. Beeler, K. van Wyke Coelingh, *J. Virol.* **63**, 2941 (1989).
7. The IMpact-RSV Study Group, *Pediatrics* **102**, 531 (1998).
8. E. J. Collarini *et al.*, *J. Immunol.* **183**, 6338 (2009).
9. H. Wu *et al.*, *J. Mol. Biol.* **368**, 652 (2007).
10. M. J. Kwakkenbos *et al.*, *Nat. Med.* **16**, 123 (2010).
11. B. S. Graham, *Immunol. Rev.* **239**, 149 (2011).
12. E. E. Walsh, J. Hruska, *J. Virol.* **47**, 171 (1983).
13. J. Arbiza *et al.*, *J. Gen. Virol.* **73**, 2225 (1992).
14. J. A. López *et al.*, *J. Virol.* **72**, 6922 (1998).
15. J. A. López, C. Peñas, B. García-Barreno, J. A. Melero, A. Portela, *J. Virol.* **64**, 927 (1990).
16. J. S. McLellan, Y. Yang, B. S. Graham, P. D. Kwong, *J. Virol.* **85**, 7788 (2011).
17. K. A. Swanson *et al.*, *Proc. Natl. Acad. Sci. U.S.A.* **108**, 9619 (2011).
18. M. Magro *et al.*, *Proc. Natl. Acad. Sci. U.S.A.* **109**, 3089 (2012).
19. Information on materials and methods is available on *Science* Online.
20. H. Spits, T. Beaumont, RSV-specific binding molecules and means for producing them. Patent Application 12/600,950 (2010).
21. T. Beaumont, A. Q. Bakker, E. Yasuda, RSV specific binding molecule. Patent application 12/898,325 (2012).
22. Approximately 100-fold greater potency of AM22 and D25 relative to palivizumab was observed by Beaumont and colleagues in a plaque assay; in our flow-based neutralization assay, we observed a 15-fold improvement over palivizumab and a 3-fold improvement over motavizumab.
23. M. Pancera *et al.*, *PLoS ONE* **8**, e55701 (2013).
24. S. Frank *et al.*, *J. Mol. Biol.* **308**, 1081 (2001).
25. S. Chaiwatpongsakorn, R. F. Epand, P. L. Collins, R. M. Epand, M. E. Peeples, *J. Virol.* **85**, 3968 (2011).
26. B. D. Welch *et al.*, *Proc. Natl. Acad. Sci. U.S.A.* **109**, 16672 (2012).
27. H. S. Yin, X. Wen, R. G. Paterson, R. A. Lamb, T. S. Jardetzky, *Nature* **439**, 38 (2006).
28. J. S. McLellan *et al.*, *Nat. Struct. Mol. Biol.* **17**, 248 (2010).
29. RSV F has the shortest fusion peptide of all paramyxoviruses, which may allow it to move from an initially exposed position to the central cavity of the trimer.
30. J. E. Lee *et al.*, *Nature* **454**, 177 (2008).
31. I. A. Wilson, J. J. Skehel, D. C. Wiley, *Nature* **289**, 366 (1981).
32. The fusion peptide is connected to the surface-exposed α2 and α3 helices through a cylindrical opening between the protomers that is roughly 10 Å in diameter; this opening may be used as an exit path for the fusion peptide during triggering.
33. X. Wen *et al.*, *Nat. Struct. Mol. Biol.* **19**, 461 (2012).
34. "Breathing" of the F_1 C terminus could potentially trigger the F protein because the region near residue 461 is in contact with the fusion peptide of a neighboring protomer. During the transition to the postfusion state, F_1 residues 461 to 513 move at least 8 Å, which could destabilize the fusion peptide and lead to triggering.
35. P. Chambers, C. R. Pringle, A. J. Easton, *J. Gen. Virol.* **73**, 1717 (1992).
36. On the basis of sequence analysis, a loop region in F glycoproteins was hypothesized to exist within the Paramyxoviridae family that might be under immune pressure (*35*). It has been demonstrated that binding of RSV subgroup-specific monoclonal antibodies can be affected by site-directed mutations between F_1 residues 200 and 216 (*38*) and that a peptide comprising F_1 residues 205 to 225 could elicit neutralizing activity in rabbits, although a specific epitope was not defined (*39*).
37. D. C. Ekiert *et al.*, *Nature* **489**, 526 (2012).
38. A. L. Connor, D. J. Bevitt, G. L. Toms, *J. Med. Virol.* **63**, 168 (2001).
39. C. Corvaisier, C. Bourgeois, P. Pothier, *Arch. Virol.* **142**, 1073 (1997).
40. H. Ashkenazy, E. Erez, E. Martz, T. Pupko, N. Ben-Tal, *Nucleic Acids Res.* **38**, (Web Server), W529 (2010).

Acknowledgments: We thank members of the Structural Biology Section, Structural Bioinformatics Core Section, and Viral Pathogenesis Laboratory at the Vaccine Research Center for helpful comments, and J. Chrzas, J. Gonczy, U. Chinte, and staff at SER-CAT (Southeast Regional Collaborative Access Team) for help with x-ray diffraction data collection. The data presented in this manuscript are tabulated in the main paper and supplementary materials. Atomic coordinates and structure factors of the reported crystal structures have been deposited in the Protein Data Bank under accession codes 4JHA and 4JHW. Support for this work was provided by the Intramural Research Program (National Institute of Allergy and Infectious Diseases) and the National Natural Science Foundation of China (81161120419). Use of insertion device 22 (SER-CAT) at the Advanced Photon Source was supported by the U.S. Department of Energy, Basic Energy Sciences, Office of Science, under contract W-31-109-Eng-38. T.B. is an inventor on an international patent application describing the technology used to isolate D25 and AM22 (Means and methods for influencing the stability of antibody producing cells, WO2007067046A1). E.Y. and T.B. are inventors on international patent applications for antibody D25 (RSV-specific binding molecules and means for producing them, WO2008147196A2) and antibody AM22 (RSV-specific binding molecule, WO2011043643A1). J.S.M., P.D.K, and B.S.G. are inventors on a U.S. patent application describing the use of prefusion-stabilized RSV F glycoproteins as vaccine antigens (Prefusion RSV F proteins and their use, 61/798,389). J.S.M, M.C., Z.Z., M.Z., N.X., and B.S.G. are inventors on a Chinese patent application for antibody 5C4 and its epitope (Anti-RSV high neutralization antibody and the peptide can be used for prevention of RSV infection and related disease, 201310082338.1).

Supplementary Materials

www.sciencemag.org/cgi/content/full/science.1234914/DC1
Materials and Methods
Figs. S1 to S7
Table S1
References (*41*–*58*)

8 January 2013; accepted 25 March 2013
Published online 25 April 2013;
10.1126/science.1234914

Stem Cell Lawsuit Finally Over. Russian Team Retrieves First Sample from Lake Vostok. Surprise Choices Mark New Leadership on U.S. House Science Panel. India Unveils Ambitious Science Policy.

Now, more than ever, developments in the lab are directly connected to decisions made in the halls of government.

*Science*Insider, the policy blog from the journal *Science*, is your source for news from the intersection of science and policy. From budget debates in the United States Congress, to climate change agreements at the United Nations, *Science*Insider covers the issues that have an impact on your work, your field, and your world.

Keep up to date and keep informed. Go inside the issues at **www.ScienceInsider.org**

*Science*Insider

Breaking news and analysis from the world of science policy

Science

AAAS

Produced by the *Science*/AAAS Custom Publishing Office

Mass Spec Imaging: From Bench to Bedside

There's a lot of high [illegible] and histology stains are sharing bench [illegible]ce with flow cytometers and microfluidic processors, DNA sequencers, and microarray readers [illegible] and mass spectrometers. Long the province [illegible] more recently [illegible]stablished itself as a bona fide clinical tool. Now a new application is heading to the clinic, m[illegible]pec imaging.

By Jeffrey M. Perkel

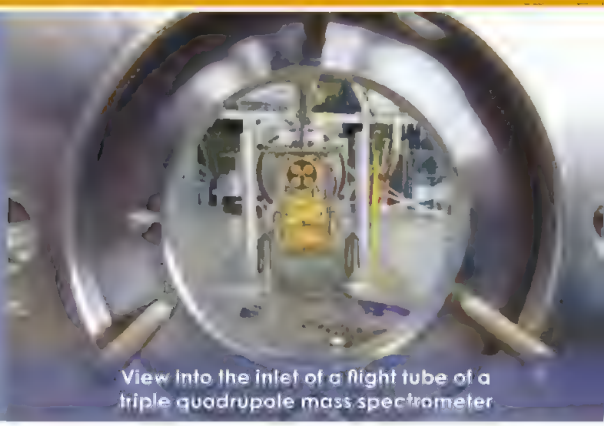

View into the inlet of a flight tube of a triple quadrupole mass spectrometer

"We human beings are built to gather a tremendous amount of information visually," says Richard Caprioli, the Stanford Moore Chair of Biochemistry and director of the Mass Spectrometry Research Center at **Vanderbilt University School of Medicine.** "We love patterns, we love pictures, and we get a great deal of information by looking at a simple picture."

That, Caprioli says, explains in part the growing popularity of mass spec imaging (MSI): It plays into the expertise that histologists, in particular, spend years developing. "The fact that it's in molecular dimensions rather than a color dimension, is less important, as long as that molecular dimension is more informative," he says.

MSI is like a high throughput form of immunohistochemistry, but without the antibodies. Instead of proactively staining tissue sections for specific markers, MSI uses the mass spec to pick out and map the spatial arrangement of hundreds or thousands of molecular species at once. The technique can do that without the researcher knowing a priori what molecules might be important, and do so quickly. "We have lasers now on our instruments that can do 5,000 mass spectra per second," Caprioli says—fast enough to scan an entire tissue microarray, containing hundreds of patient biopsies, in under an hour.

On the other hand, MSI also presents significant hurdles. Imaging resolution improves with decreasing spot size, for instance, but at the cost of decreasing ionized material yield. With no prefractionation steps, MSI tends to sample only the most abundant molecules. And on the computational side, figuring out how to work with those data, and especially making sense of them, is particularly challenging. Nevertheless, researchers are now using MSI to localize drug metabolites in tissue sections with subcellular resolution, pin down disease biomarkers, and identify tumor boundaries, among other applications. They are even taking the technique into the clinic—or at least, just outside of it.

MSI STRATEGIES

So just what is MSI? Picture a standard digital photograph. The colors in digital images are built by overlaying three color channels, red, green, and blue, with the color of any pixel given by the intensity of those colors in its tiny slice of screen real-estate.

Now imagine an image with thousands of color channels. That's exactly what MSI does, Caprioli says, devoting one channel to each particular molecular species—or mass spectral peak you wish to represent. By overlaying those different channels, researchers can produce a Technicolor map of a tissue's molecular makeup and spatial distribution, whether of proteins, neuropeptides, metabolites, or increasingly, lipids.

Researchers have devised dozens of strategies for doing MSI, but as described in a 2012 review (*J. Proteomics,* 75:4883, 2012) three are the most common. Caprioli's approach, matrix-assisted laser desorption ionization (MALDI) MSI, builds an image by rastering an ultraviolet laser over a matrix-coated tissue slice. Pixel size in this technique is typically on the order of 1 to 10 µm or so, meaning it can achieve subcellular resolution. But because it requires deposition of a MALDI matrix and vacuum conditions, MALDI-MSI is incompatible with living samples. Also, the matrix, which serves to absorb the laser energy and transfer it to the sample itself, can be difficult to apply and produces an abundance of small molecular weight ions, which can obscure the metabolite region of the resulting spectra.

Nick Winograd, the Evan Pugh Professor of Chemistry at **Pennsylvania State University,** uses a second approach, secondary ion mass spectrometry (SIMS). SIMS induces sample ionization by "sputtering" a sample surface with an ion beam (for instance, charged C60 or argon cluster beams from U.K.-based Ionoptika) rather than a laser, an approach that offers two advantages, Winograd says. The first is resolution: SIMS can produce pixels on the order of 300 nm or so, compared to, at best, 1 mm with MALDI. The other is molecular depth profiling, continued>

MSI uses the mass spec to pick out and map the spatial arrangement of hundreds or thousands of molecular species at once.

Upcoming Features

Data Management: Cloud-Based—June 14
Separation Techniques—July 12
Genomics—October 11

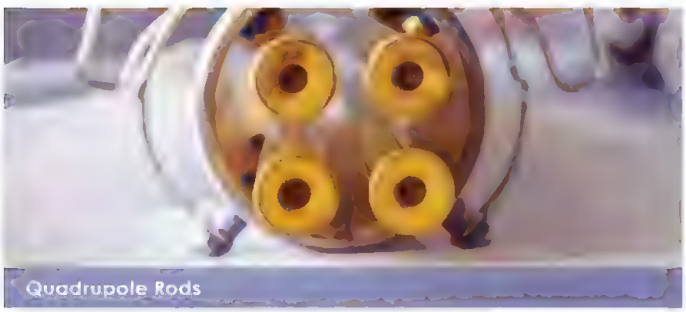
Quadrupole Rods

which allows researchers to use the collision-induced craters to "dig into" a sample and map its molecular composition in three dimensions.

The third strategy is DESI (desorption electrospray ionization), an ambient (that is, non-vacuum) ionization method in which a stream of solvent is sprayed at an untreated tissue surface, where it pools and extracts surface molecules. Additional droplets splash that extracted material into the mass spectrometer, where it is ionized and analyzed. (DESI has been commercialized by Prosolia, a company cofounded by R. Graham Cooks, the Purdue University chemist who developed the technique.)

DESI, MALDI, SIMS, and their variants all operate in what Ron Heeren of the **FOM-Institute AMOLF** in Amsterdam calls a "microprobe" mode, in which resolution increases with decreasing pixel size. The challenge there is to maximize sample ionization from the smallest possible spot. But smaller spots mean fewer ions to detect, not to mention longer imaging times (as there are more pixels).

Heeren favors an alternative "microscopy" mode, which actually uses de focused pixels for faster imaging, plus a pixelated detector, like a CCD, to effectively capture 262,144 (512x512) spectra at once.

"It's like a photo camera," Heeren explains. "The only thing is, we make molecular flash photographs."

Key to this "mass microscope," as Heeren calls it, is the Timepix detector, which essentially is a cross between a CCD and a time-of-flight mass analyzer. (Timepix is available from Omics2Image, a company Heeren cofounded.) Most mass spec detectors, he explains, treat the detector as one large pixel, integrating all ion collisions over the surface into a single signal; Timepix splits that signal into 262,000 spatially resolved ones, such that the spatial orientation of molecules on the imaged surface is maintained and recorded as they strike the detector, producing an ultrafast image.

How fast? A MALDI-MSI instrument capable of one-micron resolution and one second per pixel would take 2.7 hours to image the 10,000 pixels in a 100x100 mm area, Heeren says. Using the mass microscope and a Timepix detector, "We get the same information in a second."

The rest of the microscope is a Physical Electronics TRIFT SIMS-TOF system tricked out with a second MALDI source, which Heeren's team recently used to explore the biological changes underlying osteoarthritis. "We could actually show that both on the protein level, the lipid-metabolite level, as well as the mineralization of the cartilage combined lead to the loss of mechanical strength in the cartilage," he says.

AMBIENT MSI

Ambient ionization methods like DESI and LAESI, a laser-based alternative commercialized by Protea Biosciences, offer several advantages over MALDI and SIMS. Most significantly, they require no sample preparation, and operate in ambient air rather than a vacuum. Thus, they can be applied to live samples, or even a human patient.

That's a goal Cooks has been working towards for decades. "Doing mass spectrometry without doing sample workup has actually been a personal, lifelong quest," he says.

Ultimately, if MSI is to reach the clinic it must expand beyond the mass spec cognoscenti and into the hands of those who will be using it.

As a graduate student, Cooks worked to extract and determine the structure of plant alkaloids. After a frustratingly long time, during which he extracted only "a little bit of impure alkaloid and was making no progress on the structure," an encounter with a visiting speaker, Carl Djerassi of **Stanford University,** opened his eyes. Djerassi, Cooks says, took a sample of his material back to the lab, collected mass spectra, and 10 days later returned its structure. "That convinced me of the power of mass spectrometry," Cooks says. "And, at the same time, I was convinced of the limitations of the extraction methodologies."

Since then, he has worked steadily to decouple mass spectrometry from some of its less-biologically friendly technical limitations, developing several ambient ionization methods, most notably DESI. In 2011, a team led jointly by Cooks and Nathalie Agar at **Harvard Medical School** applied DESI-MS to banked brain cancer tissues, using the resulting lipid profiles to teach a computer how to differentiate different forms and histopathologic grades of glioma (a brain tumor).

Lipids might seem an odd choice for such an analysis. Indeed, their popularity among MSI practitioners is something of a lemonade-from-lemons situation. In standard cellular analyses, researchers can fractionate cell extracts to remove unwanted components, often including lipids. But in MSI and other in situ applications, researchers must image what's in front of them. And what's in front of them, for the most part, is lipids. Fortunately, lipids are not only abundant—and exceptionally ionizable—they also are highly informative.

"If you are looking at just lipids, the histological specificity is much better than looking at proteins," says Zoltán Takáts, a reader in Medical Mass Spectrometry at **Imperial College London.**

More recently, Cooks and Agar applied their approach to 32 surgical specimens taken from five brain cancer patients currently under treatment. Pixel-by-pixel, the system reported the tumor subtype, grade, and fraction of cancerous cells. Using those data, the team could resolve specific regions of different histopathologic grade, complementing MRI data in mapping tumor boundaries, Cooks says. And they did all that, he emphasizes, using "bottom-of-the-line" mass spectrometry, a unit-resolution single- (as opposed to tandem) stage Thermo Fisher LTQ ion trap.

Still, this was a research project; the team could not communicate those findings to the surgeons in real time, Agar notes, as the samples were collected in Boston but imaged in Indiana. Since then, her team has installed a DESI-enabled Bruker amaZon Speed ion trap in Brigham and Women's AMIGO (Advanced Multimodality Image Guided Operating) surgical suite, part of the hospital's National Center for Image Guided Therapy, and tested it on brain tumor cases. Breast cancer testing could come soon, but the team still cannot guide the surgeons actually doing the cutting, Agar says; the methodology first must be validated, "which will eventually need a clinical trial to do so."

SIMPLIFYING DATA ANALYSIS

Ultimately, if MSI is to reach the clinic it must expand beyond the mass spec cognoscenti and into the hands of those who will be using it. Yet few

Featured Participants

Brigham and Women's Hospital
www.brighamandwomens.org

FOM Institute AMOLF
www.amolf.nl

Harvard Medical School
hms.harvard.edu

Imperial College London
www3.imperial.ac.uk

Lawrence Berkeley National Laboratory
www.lbl.gov

Omics2Image
www.omics2image.com

Pennsylvania State University
www.psu.edu

Prosolia
www.prosolia.com

Purdue University
www.purdue.edu

Vanderbilt University Mass Spectrometry Research Center
www.mc.vanderbilt.edu/root/vumc.php?site=msrc

Additional Resources

Bruker
www.bruker.com

Ionoptika
www.ionoptika.com

MediMass
medimass.com

NERSC
www.nersc.gov

Physical Electronics
www.phi.com

Protea Biosciences
proteabio.com

Sequenom
www.sequenom.com

Thermo Fisher Scientific
www.thermoscientific.com

clinicians are well versed in the nuances of MSI technology, data handling, and informatics, and even fewer likely have the time to become so. The technology cannot spread if it requires "extremely expensive and delicate and Ph.D.-run mass spectrometry," Cooks says. "It's got to all be automated and the instrument's got to be rugged and reliable and relatively simple."

For typical histopathology applications that shouldn't be much of a problem, as the systems can be configured as turnkey boxes programmed to look for specific biomarkers. Non-imaging mass specs already are used routinely in clinical laboratories worldwide, including Bruker's MALDI Biotyper and Sequenom's MassARRAY. Caprioli imagines arming histologists and pathologists with under-the-desk MSIs that behave like microscopes. The lab techs simply need to be taught how to prepare sample and operate the machine, and the software can take care of the rest.

But more complex applications like biomarker identification are another matter. "The datasets in mass spec imaging scale with the number of pixels in the image and the resolution of the mass spectrometer, and in recent years those are the two things that have drastically changed," says Ben Bowen, a research scientist at **Lawrence Berkeley National Laboratory,** who develops MS imaging data analysis software.

Pixels have been shrinking while resolving power has increased. At the same time, researchers performing discovery mode experiments don't know a priori which molecules are important, so they have to consider all of them, running countless pairwise comparisons on thousands upon thousands of color channels.

All those pixels add up. Bowen's colleague Trent Northen, who uses MS imaging in his own work, has collected terabytes of data over the years, he says. For newbies, just opening the datafiles can be challenging, making them reliant on more knowledgeable experts. "You can understand why this leaves a bad taste in a scientist's mouth," Bowen says.

To mitigate that problem, Northen and Bowen worked with Berkeley Lab data visualization scientist, Oliver Ruebel to develop a cloud-based platform called OpenMSI, which allows users to view and manipulate cloud-based MS imaging data directly in a web browser. The system derives its power from the U.S. Department of Energy-funded National Energy Research Scientific Computing Center (NERSC) supercomputer, Bowen says, reducing processing time from days to minutes.

Bowen says one of his and Northen's collaborators was able to use OpenMSI to traverse a 50 gigabyte dataset she had collected a year-and-a-half earlier but had never been able to access. "Now she's doing it in [Google] Chrome," he says—viewing the RGB images, examining the underlying spectra, and sharing the data with colleagues. "All the things that you would expect in the 21st century that the Internet offers, we've made that possible for MS imaging through OpenMSI."

MASS SPEC IN THE OR

But for the ultimate in clinical translatability, researchers may have to shed the imaging part of MSI altogether. That's what Imperial College London's Takáts has done.

Takáts, Cooks' former postdoc and lead author on the paper first describing DESI, developed and is testing a new ambient ionization technique called rapid evaporative ionization mass spectrometry (REIMS) and a device called the 'Intelligent Knife' (iKnife), which enables surgeons to assess the histology and histopathology of tissue in situ, right in the operating room.

"The final device is very simple," Takáts explains, and relies on electrosurgery, a cutting technique that uses electrical current to vaporize tissue. That process releases smoke, a combination of tar, particulates and ionized lipids, which the iKnife continuously samples through an attached Teflon tube coupled to a mass spec inlet.

Over the past several years, Takáts has built up a database of some 200,000 lipid profiles of human cancers and healthy tissue, and using those data, he has identified the lipid biomarkers that can distinguish one from the other. As a result, his system can, using the ionized lipid profiles arising during electrosurgical procedures, determine essentially in real time whether the tissue under the iKnife is healthy or cancerous, as well as its histologic state.

To be clear, this isn't imaging. "The answer that comes out is histology level identification," Takáts says. "The system would say that this is a non-small-cell lung cancer, grade 2 something like that."

The iKnife (being developed by MediMass and Imperial College) has already been tested in the course of more than 500 interventions to date in Hungary, Germany, and the United Kingdom, producing "in most of the cases close to 100% correct classification," Takáts says. That's over a range of tumors including gastrointestinal, liver, lung, breast, and brain. In some cases, the technique revealed that what surgeons thought were tumors actually were something else, such as benign tissue or inflammatory disease. Now Takáts is working on a new system to perform similar assessments of growths for endoscopy.

Ultimately, says Takáts, such applications could make MSI "meaningful" not only as a research tool but as a routine clinical technique. Histopathologists, he notes, will likely be reluctant to adopt such a comparatively slow and expensive technology. But speed and cost will improve, he says. If the technology enables physicians to make a diagnosis in seconds, and in vivo, that previously took at best a half-an-hour after dissection, uptake of the technology could grow.

"It gives an advantage to this bundle which histopathology cannot compete with," he says.

Jeffrey M. Perkel is a freelance science writer based in Pocatello, Idaho.

DOI: 10.1126/science.opms.p1300076

SAMPLE PREP AND LC SYSTEM

The Prelude SPLC sample preparation and liquid chromatography system has been developed to make analysis of target compounds in complex biological matrices routine for clinical research and forensic toxicology laboratories. LC-MS/MS offers significant advantages in selectivity and quantitative accuracy over immunoassays and other analytical techniques. The Prelude SPLC sample preparation and liquid chromatography system is designed to work seamlessly with Thermo Scientific mass spectrometers. The Prelude SPLC system is designed to enhance the cost effectiveness of LC-MS/MS instrumentation by automating sample preparation and increasing mass spectrometer throughput. Automation can minimize variability inherent in manual sample preparation procedures while also reducing sample preparation time and effort. Innovative TurboFlow technology is designed to negate problems caused by sample matrix interference while capturing analytes of interest. This level of sample clean up can enhance MS quantitative analysis by reducing ion suppression.

Thermo Fisher Scientific

For info: 800-532-4752 | www.thermoscientific.com/prelude

PROTEIN PROTEOLYSIS

Trypsin/Lys-C Mix, Mass Spectrometry Grade, is a unique combination of Trypsin Gold and rLys-C proteases. The new mix increases peptide generation with in-solution protein digestion and works with even difficult-to-digest proteins. Enhanced proteolytic activity achieved through the use of Trypsin/Lys-C Mix can result in a 20%–40% increase in the number of peptides generated, enabling a higher number of proteins to be identified. Trypsin/Lys-C Mix is also tolerant to Trypsin-inhibiting contaminants, enabling researchers to generate mass spectrometry data from poor quality sample material such as FFPE sections. Many proteins are resistant to trypsin due to tight conformation, and although protein denaturation enables proteolysis, trypsin is inactive under these conditions. The Trypsin/Lys-C Mix overcomes this barrier as it remains active even under strong denaturing conditions, enabling digestion of even proteolytically resistant proteins.

Promega

For info: 608-274-4330 | www.promega.com/tryplys

HEAT-STABILIZATION SYSTEM

A heat-stabilization system has been demonstrated to be compatible with MALDI imaging analysis. The preservation of sample components prior to MALDI imaging analysis is crucial to accurately measure the distribution and abundance of biological molecules in organs. During downstream analysis, the presence of metabolites, drug compounds, and endogenous peptides, which exist at very low levels in the tissue sample, is often difficult to detect due to rapid degradation of the molecule of interest or masking by protein fragments generated from normal degradation processes. Utilization of Denator's Stabilizor system has been shown to stop degradation from the moment of sampling. This leads to increased accuracy and quality of analytical results. This development ensures that researchers who heat-stabilize tissues upstream achieve the best possible analytical results downstream.

Denator AB

For info : +46-(0)-70-771-59-67 | www.denator.com

MASS SPECTROMETRY INSTRUMENT

The Microsaic 4000 MiD represents the culmination of over a decade of research, bringing together two high-tech fields—chemical analysis and silicon microengineering—to make possible a transformative capability in detection. The mass spectrometry instrument is easily accommodated in a standard fume hood and, unlike any conventional system, does not require a cumbersome floor pump or separate PC. The 4000 MiD is readily integrated with existing chromatography equipment, and is ideally suited to reaction and process monitoring. Consuming only a fraction of the power demanded by conventional instruments, the Microsaic 4000 MiD is also in tune with modern green laboratory working practices. Its low operating cost and small footprint make the instrument deployable in a wide range of applications that mass spectrometry has not been able to reach—until now. The core technologies are chip-scale versions of traditional mass spec components which can be interchanged rapidly by the user.

Microsaic Systems

For info: +44-(0)-1483-751577 | www.microsaic.com

MYCOBACTERIAL LIBRARY

The MALDI Biotyper (MBT) system allows for an instantaneous identification of colonies from a plate and covers a broad range of more than 4,600 microbial isolates from gram-negative bacteria, gram-positive bacteria, yeasts, multicellular fungi, and mycobacteria. Microbial identification with the MALDI Biotyper is done using a proteomic fingerprint. This unique species-specific pattern is automatically compared with reference spectra in the MALDI Biotyper library. In addition, the MALDI Biotyper supports the Open Microbiology Concept which allows customers to generate their own database entries from regional isolates via a push-button storage in a customer-specific sub-library. The new second edition of the MBT Mycobacteria Library adds another 140 isolates from 37 new species. The library is fully compatible with all standard cultivation media for mycobacteria, such as solid Löwenstein-Jensen medium or in liquid culture using the MGIT system from Becton Dickinson. With these added capabilities the MALDI Biotyper covers now more than 130 species of mycobacteria.

Bruker Corporation

For info: +49-42-12205-270 | www.bruker.com

Electronically submit your new product description or product literature information! Go to **www.sciencemag.org/products/newproducts.dtl** for more information.

Newly offered instrumentation, apparatus, and laboratory materials of interest to researchers in all disciplines in academic, industrial, and governmental organizations are featured in this space. Emphasis is given to purpose, chief characteristics, and availability of products and materials. Endorsement by *Science* or AAAS of any products or materials mentioned is not implied. Additional information may be obtained from the manufacturer or supplier.

POSITIONS OPEN

PROFESSOR AND HEAD
DEPARTMENT OF PATHOBIOLOGY
College of Veterinary Medicine
Auburn University

The College of Veterinary Medicine, Auburn University, invites applications and nominations for the position of Professor and Head of the Department of Pathobiology. The Department of Pathobiology is seeking a dedicated, enthusiastic Department Head to lead a diverse and progressive faculty of over 45 tenure-track, clinical/research track, adjunct, and affiliate members in the development of its scholarly programs devoted to excellence in research, teaching, and diagnostic service. Review of applications will begin August 1, 2013, and continue until the position is filled. For a complete description of the position, please see **website: http://www.vetmed.auburn.edu/pathobiology.**

Auburn University is an Affirmative Action/Equal Employment Opportunity Employer and educational institution. Women and minorities are encouraged to apply.

UNIVERSITY OF HAWAII
AT MANOA CANCER CENTER

ASSISTANT/ASSOCIATE/FULL RESEARCHER (Cancer Biology Program), **Position #85911**, Tenure-track, Continuous – application review begins May 31, 2013. Refer to **website: http://www.pers.hawaii.edu/wuh/** for complete information. *The University of Hawaii is an Equal Opportunity/Affirmative Action Institution. Women and minorities are encouraged to apply.*

Hiring Vice President at South University of Science and Technology (SUSTC)Shenzhen, China

The South University of Science and Technology, China (SUSTC) invites applications and nominations for Vice President (Academic Affairs) and Vice President (Education). SUSTC is committed to **excellence in teaching and research**; therefore, it offers internationally competitive salaries, fringe benefits, retirement and housing subsidy to the Vice Presidents. The modern campus also offers pleasant working conditions.

About SUSTC

SUSTC is a public institution funded by the municipal of Shenzhen, a special economic zone city in southern China. The University receives full financial support from the municipal. Set on five hundred acres of wooded landscape in the picturesque Nanshan (South Mountain) area, the campus offers an idyllic environment suitable for learning and scholarship. SUSTC engages in basic and problem-solving research of lasting impact to benefit society and mankind. Key research areas of the university include but not limited to: *Neural and Cognitive Sciences, Biology and Gene Engineering, Modern Physics, Control and Modification of Materials, Nanoscience and Nanotechnology, Mathematics and Applied Mathematics, Molecular Chemistry and Catalysis, Large-Scale Computational Research, Robotics and Artificial Intelligence, Information Systems and Electronic Engineering, Modern Cities and future developments, Energy Sciences and technology, Environmental Sciences, Financial Mathematics and Engineering.*

The Vice President (Academic Affairs, VPAA) and Vice President (Education, VPE) report directly to the president. The **VPAA** provides strategic leadership in the development and implementation of academic and research programs. The **VPE** provides strategic leadership in student education and whole person development. Successful candidates are expected to be internationally renowned scholars with administrative experience and good communication skills. Excellent leadership and organizational skills are also important.

The teaching language at SUSTC is English or Putonghua. As we expect an international faculty, the majority of teaching materials and reference books will be in English and many classes will be conducted in English. With a very high faculty-to-student ratio, SUSTC is committed to delivering a student-centered education. Students at junior and senior years are expected to participate in research in Research Centers.

Send nominations, inquiries or applications to: hiring@sustc.edu.cn. All applications should include a detailed CV and a list of publications. Additional information on SUSTC is available on the University homepage **http://www.sustc.edu.cn**

AAAS is here – helping scientists achieve career success.

Every month, over 400,000 students and scientists visit ScienceCareers.org in search of the information, advice, and opportunities they need to take the next step in their careers.

A complete career resource, free to the public, *Science* Careers offers a suite of tools and services developed specifically for scientists. With hundreds of career development articles, webinars and downloadable booklets filled with practical advice, a community forum providing answers to career questions, and thousands of job listings in academia, government, and industry, *Science* Careers has helped countless individuals prepare themselves for successful careers.

As a AAAS member, your dues help AAAS make this service freely available to the scientific community. If you're not a member, join us. Together we can make a difference.

To learn more, visit **aaas.org/plusyou/sciencecareers**

AAAS + U = Δ

University of Zurich[UZH]

Faculty of Science

The Faculty of Science at the University of Zurich invites applications for a

Professorship in Molecular Design and Synthesis

The Department of Chemistry wishes to appoint a new full professor with research interests in the broad area of molecular design and the art of organic synthesis. We seek an outstanding and innovative chemist who is familiar with the broad field of synthetic organic chemistry, and who can contribute to teaching in this area at Bachelor, Master and PhD level in English or German. The successful candidate will already have an outstanding track record in his/her chosen field of research. Examples can be found in diverse areas such as chemical biology, supramolecular chemistry and organic materials.

The University of Zurich provides generous research support and competitive start-up packages. The town of Zurich offers a stimulating scientific environment, with many opportunities for collaborations with research groups at the Faculties of Science and Medicine as well as at other neighboring institutions.

Application packages should include a cover letter, complete curriculum vitae, statement of current and future research plans, and the names and addresses of three potential
referees. The documents should be addressed to Prof. Dr. Michael O. Hengartner, Dean of the Faculty of Science, University of Zurich, and submitted as a single PDF file at www.mnf.uzh.ch/mds at the latest by 31 August 2013. Further information can be obtained by contacting Prof. Dr. John Robinson, Department of Chemistry, at robinson@oci.uzh.ch, and by visiting the new Department web-site at www.chem.uzh.ch, or www.oci.uzh.ch

The University of Zurich is an equal opportunities employer. Applications from women are particularly encouraged.

University of Zurich[UZH]

Faculty of Science

The Faculty of Science at the University of Zurich invites applications for a

Professorship in Environmental Science / Ecology

at the Institute of Evolutionary Biology and Environmental Studies. The Institute conducts research in the fields of ecology, evolution, behaviour and the environment. We seek an outstanding and innovative ecologist who is familiar with evolutionary concepts. Examples of areas of interest are animal ecology, community ecology, conservation biology, and functional ecology.

The successful candidate will have a record of excellent research for their career stage. She or he will develop a strong, independent program of empirical research on animals or animal-plant interactions, and will contribute to graduate and undergraduate teaching (in English or German) in environmental science and ecology.

The position will be filled preferentially at the level of associate or tenure-track assistant professor.

The University of Zurich provides generous research support, including earmarked funds for personnel and running expenses, and competitive start-up packages. Zurich offers a stimulating scientific environment, and extensive opportunities for collaborations. Switzerland provides excellent opportunities for external funding of research.

Application packages should include a cover letter, a full curriculum vitae (see http://www.ieu.uzh.ch/static/documents/ for guidelines), a vision statement of research interests and the names and addresses of three potential referees. Applications should be addressed to Prof. Dr. Michael O. Hengartner, Dean of the Faculty of Science, University of Zurich, and submitted as a single PDF document at www.mnf.uzh.ch/ese by 20 June 2013. For further information, please contact Prof. Dr. Barbara König, Institute of Evolutionary Biology and Environmental Studies, at barbara.koenig@ieu.uzh.ch, or visit the homepage at www.ieu.uzh.ch.

The University of Zurich is an equal opportunities employer. Applications from women are particularly encouraged.

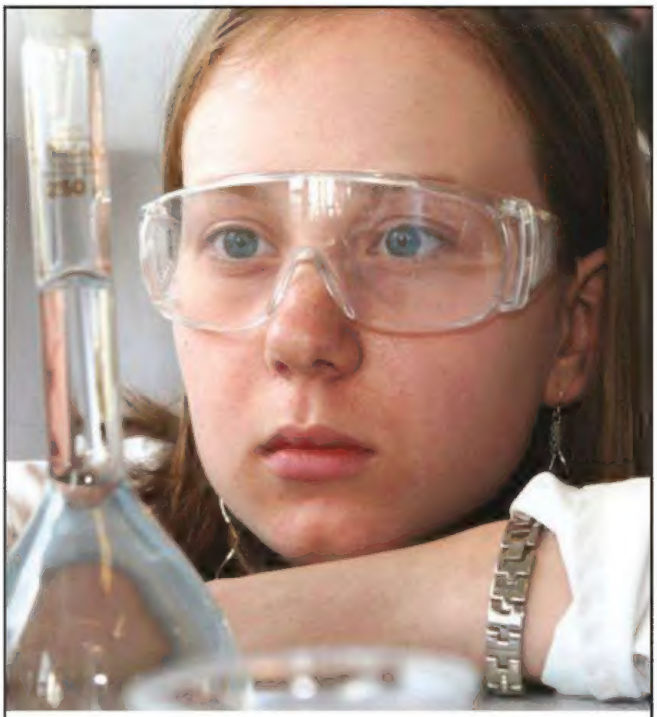

WEBINAR

A Traveler's Guide to Next Generation Sequencing

Navigating the Sea of Genetic Variants

Wednesday, June 26, 2013

12 noon Eastern, 9 a.m. Pacific, 5 p.m. UK, 6 p.m. Central Europe

Recent advances in technology and cost effectiveness of next generation sequencing has led to its progressively wider implementation in both research and clinical settings. The amount of data it produces, however, can be overwhelming—typically over three million variants per genome. The challenges for many researchers today are how to make sense of this huge volume of data in the context of the scientific question being asked, and how to identify those variants that provide meaningful and relevant information. In this webinar we will discuss current approaches to variant analysis and how they can be most effectively integrated into the next generation sequencing pipeline.

DURING THE WEBINAR, VIEWERS WILL:

- Learn about various methods for analyzing and comparing variants, including tips and pitfalls
- Gain a fuller understanding of the importance of accurate and robust variant analysis
- Receive advice on managing and manipulating large data sets
- Have the opportunity to put their questions to our panel of experts!

Speakers

Ruthild Weber, M.D.
Hannover Medical School
Hannover, Germany

Scott D. Kahn, Ph.D.
Illumina
San Diego, CA

REGISTER NOW!
webinar.sciencemag.org

Webinar sponsored by

BIOBASE
BIOLOGICAL DATABASES

Brought to you by the *Science*/AAAS Custom Publishing Office

Science
AAAS

Promega

FuGENE® HD
Illuminate Real Biology

Don't let old toxic transfection technology get in the way of your science. FuGENE® HD provides the power to transfect virtually any cell type while maintaining biologically relevant cell signaling responses.

Key applications:

- Cancer Biology
- Stem Cell Research
- Developmental Biology
- Neurobiology
- Immunobiology
- Lentivirus Production
- CHO Cell Protein Production

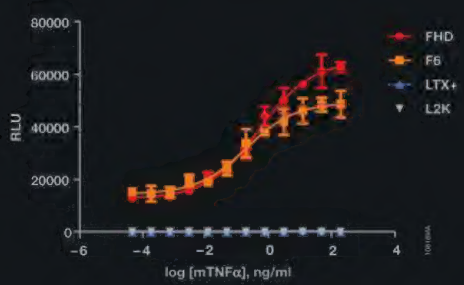

In this BaF3 cell model of NF-kB luciferase induction, only FuGENE® HD and FuGENE® 6 are able to create a usable assay.

To discover the power of FuGENE® HD for your biology, request a free sample at
www.promega.com/pathwaybiology